Analysis of Thermodynamic Behaviour of Valuable Elements and Slag Structure during E-Waste Processing through Copper Smelting

By

Mohammad Al Hossaini Shuva (B.Sc.Eng., M.Sc.Eng.)

A Thesis
Submitted to the Faculty of Science, Engineering and Technology
for the Degree of
Doctor of Philosophy

Swinburne University of Technology
Melbourne, Australia
September 2017

Abstract

Waste of electronics and electrical equipment (WEEE or e-waste) and other end-of-life (eol) high technology products can be viewed as resources for metals, as they do not only contain the common metals like iron (Fe), aluminium (Al), lead (Pb) and copper (Cu) but also trace valuable and rare elements such as gold (Au), silver (Ag), tin (Sn), selenium (Se), tellurium (Te), platinum (Pt), palladium (Pd), tantalum (Ta), cobalt (Co) and indium (In). The recovery of these trace elements is vital, not just because it has high commercial values, but also for resources efficiency. One of the existing industrial routes for processing of e-waste is through the primary and secondary copper smelting processes. During these processes, the trace elements are distributed in different phases, i.e., in metal/matte, slag and gas. Different elements have different thermodynamic properties that govern the partitioning behaviour during the process. There has been a number of studies on the distribution behaviour of the trace elements relevant to primary copper smelting (extraction of metals from virgin ores). However, there are only limited thermodynamic data relevant to secondary copper smelting (extraction of metals from secondary/recycled sources).

The main purpose of the present study is to investigate the thermodynamic behaviour of germanium (Ge), palladium (Pd) and tantalum (Ta) metals and determine their distribution-ratio in slag-metal equilibrium reaction during black copper processing. A secondary aim is to examine the FeO_x-CaO-SiO_2-MgO and FeO_x-CaO-SiO_2-MgO-Cu_2O-(GeO_2/PdO) slag using vibrational spectroscopy (i.e., Fourier Transform Infrared) to understand the effect of experimental parameters on the silicate slag structure. Furthermore, a correlation between the degree of polymerization and distribution-ratio was developed using multiple regression analysis.

The distribution-ratio of germanium (Ge), $L_{Ge}^{s/m}$, during equilibrium reactions between magnesia saturated FeO_x-CaO-SiO_2 (FCS) slag and molten copper was measured using vertical tube furnace. The results showed that the Ge distribution-ratio increases with increasing oxygen partial pressure, and with decreasing temperature. It was also observed that the distribution-ratio is strongly dependant on the slag basicity. At fixed CaO concentration (in the slag), the distribution-ratio was found to increase with increasing Fe/SiO_2 ratio, tending to a plateau at $L_{Ge}^{s/m} = 0.8$. This result, together with the assessment of ionic bond fraction carried out in this study, suggested the acidic nature of germanium oxide

(GeO_2) in the slag system. The characterisation results of the quenched slag suggested that Ge is present in the FeO_x-CaO-SiO_2-MgO slag predominantly as GeO_2. At 1300°C (1573 K) and $p_{O_2} = 10^{-8}$ atm, the activity coefficient of GeO_2 in the slag was calculated to be in the range of 0.24 to 1.50. The results from the present study suggested that less-basic slag, high operating temperature, and low oxygen partial pressure promote a low Ge distribution-ratio.

The slag-to-metal distribution-ratio of palladium (Pd), $L_{Pd}^{s/m}$, in the range of oxygen partial pressure (p_{O_2}) from 10^{-10} to 10^{-7} atm at 1473 to 1623K (1200 to 1350°C) was investigated. The results showed that $L_{Pd}^{s/m}$ increased with increasing p_{O_2} and with decreasing temperature. It was also observed that the $L_{Pd}^{s/m}$ is strongly dependant on slag basicity, i.e., as defined using the mass ratio of (CaO+MgO)/SiO_2 or optical basicity. The present results suggested that Pd is present in the FeO_x-CaO-SiO_2-MgO slag predominantly as Pd^{2+}. The activity coefficient of PdO in the slag at 1573K (1300°C) and $p_{O_2} = 10^{-8}$ atm was calculated and found between the range of 3.89×10^{-3} to 2.63×10^{-2}. The results from the Pd study suggested that to promote the recovery of palladium from Pd-containing e-waste during a secondary copper smelting process, a slag with lower silica content, high temperature with reducing atmosphere, are highly desired.

This study also examined the distribution-ratio of tantalum (Ta), $L_{Ta}^{s/m}$, in the range of oxygen partial pressure (p_{O_2}) from 10^{-16} to 10^{-12} atm at 1673 and 1873K (1400°C and 1600°C). It was found that Ta mostly partitions to slag phase and very small amount of Ta is found in liquid copper at high temperature and reduced condition.

The slag structure study focused on the structure of silicate units in the FeO_x-CaO-SiO_2-MgO and FeO_x-CaO-SiO_2-MgO-Cu_2O-(GeO_2/PdO) slags. It was found that the slags structure is affected by the experimental parameters and slag compositions. The present results suggested that the degree of polymerization Q^3/Q^2 is strongly related with thermophysical and thermodynamic properties of the slag melt. A correlation based on experimental results was suggested between distribution-ratio and the degree of polymerization is presented as follows:

$$L_{Ge}^{S/m} = \frac{181}{75}\log p_{O_2} + \frac{61422}{T} - \frac{365}{36}\ {}^{Q^3}\!/_{Q^2} - \frac{115}{8}$$

$$L_{Pd}^{S/m} = \frac{74}{9999}\log p_{O_2} - \frac{724}{T} + \frac{8}{21}\ {}^{Q^3}\!/_{Q^2} + \frac{2}{5}$$

The novel aspect of the present study is that the distribution behaviour of valuable metals (Ge, Pd, Ta) between copper and FCS slags has been determined. The oxidation state and activity coefficient of these valuable metals oxide (GeO_2, PdO) in the FeO_x-CaO-SiO_2 system and their acid/base character have also been determined. The thermodynamic data generated from this study can be used for process modelling purposes to improve the recovery of valuable metals in primary and secondary copper smelting processes. These data can further be used to update the database of thermochemical software. It was recommended from the slag structure analysis that, Q^3/Q^2 is a good candidate for practical measurement of the degree of networking that relates slag structure to thermodynamics and properties.

Acknowledgements

I would like to express sincere gratitude to my principle supervisor Associate Professor M Akbar Rhamdhani for his continuous support throughout the period of my doctoral study. He has excellent knowledge in the field of process metallurgy, and his right guidance helped me all the time of research and thesis writing. His sincere devotion to research and tremendous patience of reading my thesis helped me to produce this thesis. He was very friendly in discussion and supportive in case of social aspects. I could not have imagined someone in replacement of Akbar, and I always feel proud to become his student.

I would like to acknowledge the support and guidance received from other members of my supervisor team. I am grateful to Professor Geoffrey Brooks for his encouragement, guidance and support during my study. His valuable suggestion helped me to improve my research and analytical skills. I am also thankful to Professor Syed Masood for his precious advice and support.

I would also thankful to my associate supervisor Professor Markus Reuter (Director, Helmholtz Institute Freiberg for Resource Technology, Freiberg, Germany), for his valuable support and guidance. It is an honour to work with him and his guidance helped me a lot.

I wish to thank Dr James Wang and Dr Deming Zhu for their assistance in performing XRD and Raman at Swinburne. My sincere thankfulness goes to technical staffs at Faculty of Science, Engineering and Technology: Walter Chetcuti, Yeannette Lizama, Savithri Galappathie and Aidan O'Keefee. I wish to acknowledge Mr Bernard Hedger from Spectrometer Service Pty Ltd, for assisting me in ICP-AES analysis.

I would like to acknowledge the Swinburne University Postgraduate Research Award (SUPRA) support. The author would like to also recognise the support of the *Wealth from Waste Research Cluster*, a collaborative program between the Australian CSIRO (Commonwealth Scientific Industrial Research Organisation); University of Technology, Sydney; The University of Queensland, Swinburne University of Technology, Monash University and Yale University, USA.

I would like to thank my research fellows of high temperature processing (HTP) group: Dr Reiza Mukhlis, Dr Sazzad Ahmed, Dr Saiful Islam, Dr Mehedi Mohammed, Jaefer Yenus, Muhamad Firdaus, Bapin Kumar Route, and Epma Lupita Putri. I would like to specially thank Dr Sazzad, Jaefer, Bapin and Firdaus for their all discussion and sharing of knowledge.

My profound love and appreciation go to my parents, parents-in-law, sisters and brothers for their support. I would like to honestly thankful to my wife, Nasrin Akter Shipon. She was very patience throughout my study and her on going encouragement and care helped me to finish this PhD journey.

This thesis is dedicated

to

my lovely wife and my entire family

Declaration

The author declares that this thesis on the "**Analysis of Thermodynamic Behaviour of Valuable Elements and Slag Structure during E-Waste Processing through Copper Smelting**",

is produced from my own work which contains no material that has been accepted for the award to the candidate of any other degree or diploma where due reference is made in the text of this thesis.

The results presented in this thesis have been published in different journals and conferences. The papers published from this study are listed below:

- **Shuva, M.A.H.**, Rhamdhani, M.A., Brooks, G. A, Masood, S., and Reuter, M.A, "Thermodynamics of palladium (Pd) and tantalum (Ta) relevant to secondary copper smelting", *Metallurgical and Material Transactions B*, 48 (1) (2017), 317-327.
- **Shuva, M.A.H.**, Rhamdhani, M.A., Brooks, G.A, Masood, S., and Reuter, M.A, "Thermodynamics behaviour of germanium during equilibrium reactions between FeO_x-CaO-SiO_2-MgO slag and molten Copper," *Metallurgical and Material Transactions B,* 47 (5) (2016), 2889-2903.
- **Shuva, M.A.H.**, Rhamdhani, M.A., Brooks, G.A, Masood, S., and Reuter, M.A, "Thermodynamics data of valuable elements relevant to e-waste processing through primary and secondary copper production: a review," *Journal of Cleaner Production* 131 (2016), 795-809.
- **Shuva, M.A.H.**, Rhamdhani, M.A., Brooks, G.A, Masood, S., and Reuter, M.A., "Analysis for optimum conditions for recovery of valuable metals from e-waste through black copper smelting" *8th International Symposium on High Temperature Metallurgical Processing (TMS)*, Part VII , 2017, San Diego, USA, 419-427.
- **Shuva, M.A.H.**, Rhamdhani, M.A., Brooks, G.A, Masood, S., and Reuter, M.A., "Partitioning of germanium during secondary copper smelting process: a preliminary study", *World Resource Forum (WRF) Asia Pacific*, 2015 Sydney, Australia.
- Rhamdhani, M.A., **Shuva, M.A.H.**, Ahmad, S., Islam, M.S., Khaliq, A., Brooks, G.A, and Masood, S., "Challenges of materials recovery from low grade and urban

ores for resource efficiency", *High Temperature Processing Symposium (HTPS)*, 2015, Melbourne, Australia.

I, Mohammad Al Hossaini Shuva, the undersigned, hereby declare that the information stated above is true to the fullest of my knowledge.

(Mohommad Al Hossaini Shuva)

Table of Contents

List of Figures

List of Tables

Chapter 1 Introduction

1.1 Motivation of the work

The growing demand for electrical and electronics products in recent decades has significantly impacted promotion of new technology and high demands of raw materials including the precious and rare earth metals. As the demand increases, it has resulted in the high generation of WEEE (Waste Electrical and Electronic Equipment or simply E-waste) worldwide. The volume of e-waste generated was estimated to be about 40-50 million tonnes per annum worldwide (Awasthi and Li, 2017). The generation rate of e-waste affects the environment mainly in two ways; firstly, in terms of volume of discarded products generated annually and secondly, in extraction of natural materials to supply the demand of the current industry. However, a continuous depletion of this primary resource has diverted us to recycle metals from non-primary sources such as from industrial wastes, consumer wastes and e-waste (Worrell and Reuter, 2014).

E-waste is defined as a broad and growing range of electronic devices ranging from large household equipment, such as refrigerators, air conditioners, personal stereos and consumer electronics to cell phones and computers which have been discarded by their user (Puckett et al., 2002). In addition to the common metals such as iron (Fe), copper (Cu), aluminium (Al), nickel (Ni), e-waste also contains traces of precious and rare elements, like gold (Au), silver (Ag), platinum (Pt), palladium (Pd), cadmium (Cd), selenium (Se), arsenic (As), cobalt (Co), tellurium (Te), tantalum (Ta), ruthenium (Ru), germanium (Ge), gallium (Ga), rhenium (Rh), tin (Sn), lead (Pb), and bismuth (Bi) (Cui and Zhang, 2008, Lehner, 2003). As, Bi and Pb are considered to be hazardous elements, while Au, Ag, Sn, Pt, Pd, Ge, Rh, Co and other rare elements have high commercial values. To put it into perspective, one tonne of end-of-life mobile phones contain approximately 200g of Au, 3kg of Ag and 100kg of Cu; while one tonne of computer scraps contain more gold than seventeen tonnes of gold ores (Australian Bureau of Statistics, 2013, Doran, 2014). The metals and their concentration vary from one type of e-waste to another and also vary with time as the technology changes. One possible solution to handle e-waste is recycling. One major driving force of recycling e-waste is the decline in the grade of the primary ore resources. Besides that, the concentration of valuable metals in e-waste is also much higher compared to their ores or mines.

It is mentioned earlier that one possible solution to handle e-waste can be recycling. Through recycling, we can recover the valuable metals from the e-waste. Recycling and utilisation of e-waste and other urban ores as alternative resources are important for resource efficiency (Worrell and Reuter, 2014, Reuter and Kojo, 2014). Nevertheless, there is still a gap in the knowledge, and there are technical and non-technical challenges that prevent the use of these resources efficiently. There are a number of systematic studies on the analysis of e-waste collection, benefits of e-waste recycling and various proposed solution to e-waste problems (Chi et al., 2014, Menikpura et al., 2014, Nelen et al., 2014, Zeng et al., 2015) which are mainly intended to reduce the environmental challenges. Reuter et al. (2013) described the opportunities and limits of metal recycling from e-waste. A number of studies have also pointed out that recycling of the rare earth metals from e-waste is important to build a green economy (Binnemans et al., 2013) and reduce the supply chain risk (Binnemans et al., 2015).

Currently, one of the existing industrial routes for processing of e-waste is through metallurgical processes embedded in primary and secondary base metals productions, such as through copper smelting. It is a great challenge for metal industries to develop and design optimal smelting processes utilising e-waste (Götze and Rotter, 2012, Khaliq et al., 2014). The elements found (and their concentrations) in e-waste are significantly different than those found in common primary ore concentrates. Smelting operations are optimized over many years through a combination of fundamental studies and industry best practises. A large database of information, in particular, the solution thermodynamic data in the primary copper processing has accumulated over the years, but the information is limited to a number of elements (such as In, Te, Se, Co, Pd, Pt and Rh) behaving in copper/matte/slag systems. There are limited published data available which focus on the trace elements distribution in secondary copper processing. The composition of the slag, oxygen partial pressure and temperature has significant control on the distribution of the trace elements in the smelting process. There is still some gaps in the information for the separation of the combination of elements in e-waste particularly in the operating conditions beyond those commonly used in the existing processes. This requires a rethinking of traditional processing techniques, which must be based on knowledge of how these unusual trace elements distribute between phases during smelting.

Metallurgical slag plays a vital role to purify the liquid hot metal in the ferrous and non-ferrous metals production processes. In the present study, magnesia saturated FeO_x-

CaO-SiO_2 (FCS) slag is used to conduct the equilibrium experiment. Yazawa et al. (1999) reported that FCS slag would have the ability to remove more impurities including acidic, basics and neutral oxide. The composition of slag mainly controls the absorbance capacity of impurities from the liquid metal. Kaur et al. (2009) also compared the distribution behaviour of minor metals and found that FCS slag was more effective than calcium silicate and iron silicate slag. It was also suggested that the overall properties of FCS slag are acceptable for process requirements in industry.

The slag composition also has a dramatic influence on the thermophysical and the thermodynamic properties such as viscosity, surface tension, molar volume, sulphide capacity and mixing free energy of silicates melt (Park, 2013a, Halter and Mysen, 2004). They also determined that the thermodynamic and thermophysical properties are affected by slag structure units, particularly with the degree of polymerization. The structure-properties relationship of silicate slags system has been investigated extensively using spectroscopic techniques by a number of investigators (Park, 2013b, Park and Min, 1999, Park et al., 2002, Mysen and Richet, 2005). But, the information on the structure of FeO_x-CaO-SiO_2-MgO is not studied very well. The effect of reducing condition (at low p_{O_2}) on the structure is not studied properly and no information is found on the relationship between the degree of polymerization and distribution-ratio of valuable elements. Therefore, understanding the inter-relationship between composition, structure and properties is vital.

There are different types of recycling technology and process routes practised in industries for recycling of end-of-life consumer goods including e-waste. However, the existing processes applied in industry for recovering all valuable metals are far from optimized. To recover all valuable metals, understanding the underlying knowledge of thermodynamics relevant to each metal in e-waste is vital. The current study will focus on the distribution-ratio of valuable metals to understand their thermodynamic behaviour in one of secondary copper processing routes (i.e., black copper smelting) and on the analysis of the slag structure to find their correlations.

1.2 Aim of the thesis

The aim of this thesis is to understand the thermodynamic behaviour of trace valuable elements, particularly germanium, palladium and tantalum in systems and conditions relevant to black copper smelting. This study also investigates the structure of anionic species and estimates the chemical speciation of oxygen in the FeO_x-CaO-SiO_2-MgO. Furthermore, a correlation between the degree of polymerization and distribution-ratio is developed.

1.3 Objective of this thesis

The objectives of this research project are to:

- Determine the time required to reach the equilibrium state of relevant slag-metal reactions at high temperature
- Analyse the effect of oxygen partial pressure and temperature on the distribution-ratio
- Determine the oxidation state of valuable metals (i.e., Ge, Pd, Ta) in the slag
- Analyse the effect of slag composition on the distribution-ratio
- Determine the activity coefficient of oxide in the slag and analyse the effect of temperature and basicity on the activity coefficient of oxide
- Propose a conceptual route of multi-stage black copper smelting for e-waste recycling
- Analyse the effect of oxygen partial pressure, temperature and slag composition on the slag structure units
- Determine a relationship between the degree of polymerization and distribution-ratio
- Calculate the viscosity of slag using FactSage and the oxygen species in the slag

1.4 About the thesis

This thesis consists of eight chapters. The background and objectives of the study of the research are explained in Chapter 1. Chapter 2 provides a brief description of primary and secondary copper processing. It also provides scenario of electronic waste (e-waste) generation and overview of existing techniques available for recycling e-waste.

It also includes structural details of silicate slag and different techniques to analyse of the slag structure. Chapter 3 focuses on a comprehensive and systematic review of thermodynamic data of valuable metals associated with primary and secondary copper smelting. Particularly, identifying the distribution-ratio data of valuable metals during copper smelting process relevant to e-waste processing. This chapter then highlights the gaps in knowledge required for the improvement and optimization of current industrial processes. The implication for the metal recycling industry, as well as the challenges for future research and improvement of industrial processes, are also described. Chapter 4 describes the thermodynamic assessment approach, selection of database and also discusses the limitation of databases for the thermodynamic calculation. This chapter also further explains the experimental methodology including materials used, calibration of thermocouple and oxygen sensor, preparation of master alloys and slags, experimental techniques, post experimental samples analysis and characterization techniques. Chapter 5 mainly focuses on distribution behaviour of Ge in FeO_x-CaO-SiO_2-MgO slag and molten copper under conditions relevant to the black copper smelting. It includes the calculation of the activity coefficient of germanium oxide and the determination of the oxidation state of germanium in the slag. Chapter 6 focuses on the examination thermodynamic behaviour of Pd and Ta in FeO_x-CaO-SiO_2-MgO slag and liquid copper at conditions pertinent to the black copper smelting; including the calculation of the activity coefficient of palladium oxide and the oxidation state of Pd in the slag. Chapter 7 analyses the slag structure using FTIR to investigate the effect of slag compositions, p_{O_2} and temperature on the degree of polymerization. It also provides a relationship between the distribution-ratio with the degree of depolymerization of slag melt. Finally, Chapter 8 includes a summary of the work from the present study and conclusions.

To enhance the flow of the thesis, the supplementary information is included in several Appendices:

A: Temperature Profile and Picture of Vertical Tube Furnace

B: Flow Rate Calculation and Calibration

C: Curve Fitting on IR Spectra of Slags

D: Error Analysis

Chapter 2 Literature Review

2.1 Introduction

A literature review to provide a context for the current research topic is presented briefly in this Chapter 2 (while a more detailed review on the thermodynamics of valuable elements is presented in Chapter 3). This Chapter 2 includes a description of primary and secondary copper processing. It also provides information about electronic waste (e-waste) generation and overview of existing industrial practises for recycling e-waste. Furthermore, it also describes briefly the theory about silicate slag structure and different techniques to analyse the slag structure.

2.2 Primary copper processing

Copper is mostly present in the earth's crust as copper containing minerals and gangue minerals. Chalcopyrite ($CuFeS_2$), Bornite ($CuFeS_4$) and Chalcocite (Cu_5FeS_4) are the common copper-iron-sulphur ores in the earth's crust; which commonly used as precursors to produce pure copper. Most of these ores have 0.5 (in open pit mines) to 1 or 2 wt% (in underground mines) copper concentration. In addition to these ores, some oxidized minerals of copper like as carbonates, oxides, silicates and sulphates are also present but are less commonly used as source of copper.

Currently, about 80% of the copper is produced using pyrometallurgical techniques from sulphide type copper ores which are treated through smelting and converting to make blister copper. The sulphide bearing copper ores contain many other gangue minerals. Therefore, prior to smelting of these ores some other operations are required to increase the concentration of copper in the ores. The overall process flow of primary copper is shown in Figure 2.1.

Comminution is the first step where large ores lumps are crushed in jaw or gyratory crushers and wet grinding in rod and ball mills (Schlesinger et al., 2011). The gangue of the copper minerals also liberates during comminution. The next step is froth flotation, where ores are suspended in water and air bubbles which adhere to the copper minerals. Frothing agent is used to help to bring up the copper sulphide minerals to the surface. The mineral-laden froth is then removed and the wet product is dewatered in large thickeners (Schlesinger et al., 2011).

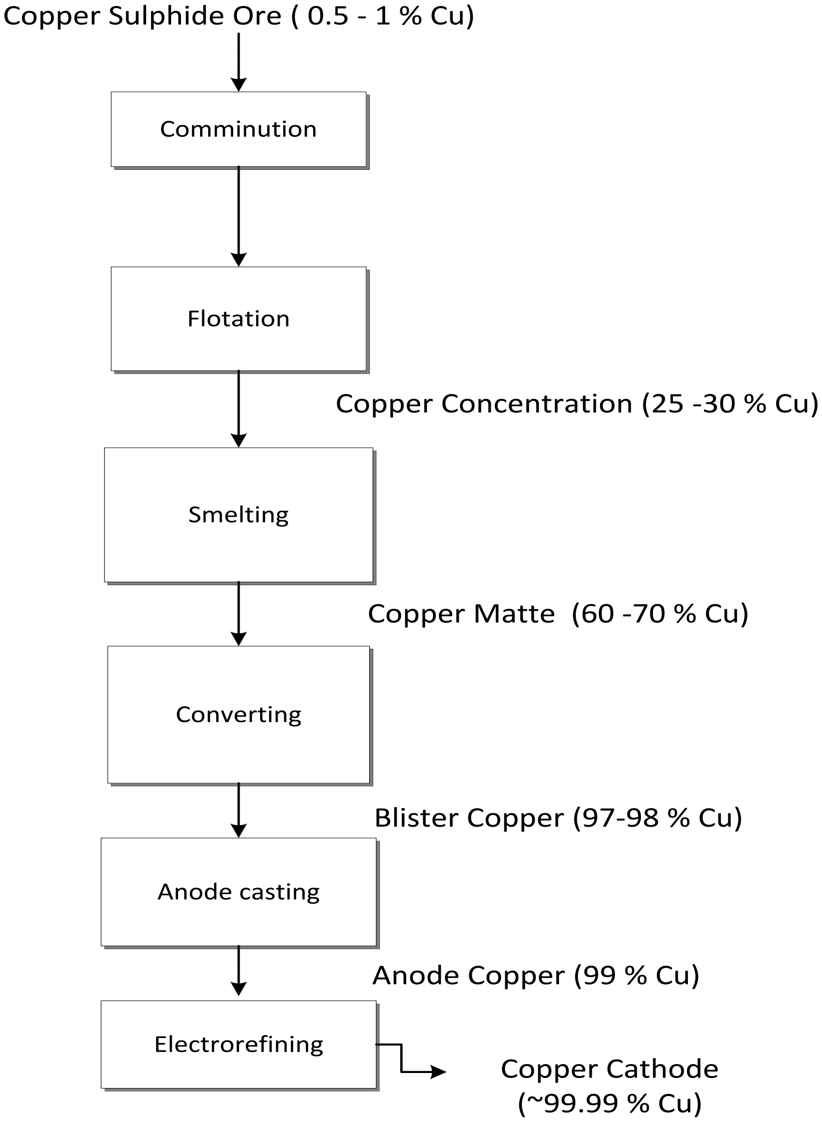

Figure 2.1: Flow sheet of primary copper production through pyrometallurgy.

Roasting is a process where copper sulphide concentrates are partially oxidized with the help of air. In roasting, the charge is dried and heated in order to increase the copper grade concentration for the following smelting process. During the roasting operation some sulphur is oxidized to sulphur dioxide. The process is autogenous where the high temperature is maintained from the heat of oxidation. When the desired temperature is not attained, e.g., due to the insufficient heat of oxidation, then some fuel i.e., natural gas, fuel or coal can be added. After roasting, some impurities like sulphur is eliminated resulting in higher copper sulphide concentration (Biswas and Davenport, 2013). The stoichiometry of the reaction which occurs is:

$$2\ CuFeS_{2\,(s)} + 4\ O_{2\,(g)} \rightarrow 2\ FeO_{(l)} + Cu_2S_{(l)} + 3\ SO_{2\,(g)} \tag{2.1}$$

Copper smelting is the next process after roasting where the concentrated copper sulphide is separated into two particular liquid phases, i.e., as matte phase (which contains majority of copper) and slag phase. At temperature 1200°C, the slag can be formed by adding silica flux. When the slag is saturated with silica, immiscibility will be maximum and silica, iron oxides, other minor oxides, and lime form the molten slag.

Copper sulphide, iron sulphide and the precious metals form the matte phase. The density of slag is lighter than the matte so it is easier to tap off the molten slag from the top. In case of excessive oxidizing condition, magnetite could form. The presence of magnetite is undesirable as it will make the slag more viscous and create difficulties for the separation of matte from slag. The product of the smelting process contains 60-70 mass pct of copper. The molten slag also takes away little amount of copper, thus the slag is further treated for copper recovery (Biswas and Davenport, 2013)

Roasting and smelting can be carried out in the same furnace in modern copper pyrometallurgical processes. Combined roasting and smelting are beneficial in terms of energy saving because it allows the utilisation of the heat released by oxidation during roasting for smelting. In addition, the sulphur dioxide can also be treated in one furnace facilitating better collectioned/capture without leakage to the environment.

Copper converting is the final step in producing blister copper, where the matte from the previous smelting step is further oxidized. Air is blown into the matte in order to remove iron, sulphur, and other impurities, resulting in the production of blister copper (~ 98 mass pct Cu). The stoichiometry of the reaction which occurs in converting is:

$$2\ Cu_2S_{(l)} + 3\ O_{2\,(g)} \rightarrow 2\ Cu_2O_{(l)} + 2\ SO_{2\,(g)} \tag{2.2}$$

$$Cu_2S_{(l)} + O_{2\,(g)} \rightarrow 2\ Cu_{(l)} + SO_{2(g)} \tag{2.3}$$

Blister copper is then subjected to further operation in anode furnace to increase its purity by removing the remaining sulphur and oxygen. This creates at about 99% pure copper. These anode products are further electrorefined where it is dissolved in an aqueous solution and applying electrical potential. The copper migrates to deposit in cathode and other noble as well as precious metal remains at the bottom of cell as anode slime. The purity of cathode copper is 99.99%.

Hydrometallurgy is another route for primary copper production and about 20% of the copper produce by these processes. Firstly, copper ores are leached in a leaching agent to produce pregnant leach solution (PLS) which is carried over into the solvent extraction (SX) circuit. During solvent extraction the PLS is further purified. The final purified solvent extraction product is then reduced to pure copper metal by subsequent electrowinning process.

2.3 Copper processing technology

The processes used in copper pyrometallurgy may be distinguished based on whether they copper concentrations are smelted or converted and subdivided based on whether the oxidation reactions take place within the molten bath or in the gas phase. There are different types of technologies used for smelting and converting. They are classified mainly into two broad categories based on oxidation reaction (i.e., Bath and Flash Processes).

In bath process, oxidation reactions take place within a molten pool contains both matte and slag, while flash process employs oxidation reaction within gas phase. Bath processes have the ability to accept variety of feed materials and generate small quality of dust. However, flash processes only treat dry particles in the charge, which react faster and settle less quickly. Therefore, considerable quantity of dust generates in the flash processes and requires a dust controlling unit. As a result, the capital cost also increases. Different types of bath and flash processes use in the copper processing are listed in Table 2.1.

Table 2.1: Different types of processes for copper processing

	Smelting Processes	**Converting Processes**
Bath Process	Reverberatory Furnace Noranda Reactor Mitsubishi Smelter Vanyukov Process El Teniente Process ISASMELT/Outotec Process	Peirce-Smith Batch Converting Noranda Continuous Converting Mitsubishi Converting Outotec Semi-Batch Converting
Flash Process	Outotec Flash Smelting INCO Flash Smelting	Kennecott-Outotec Flash Converting

In modern copper making processes, simultaneous smelting and converting are carried out in the same furnace (Moskalyk and Alfantazi, 2003). This combination of process is implemented to maximise the recovery of copper and also to produce high grade of copper. Continuous copper converting has also been introduced in the early 1980s and has brought with it many process benefits. These benefits include the direct converting of copper concentrates into blister copper within the same vessel and more energy efficient. In addition, a short residence time in the vessel decreases product cost. It also produces off gases rich in SO_2. However, the off gases flows continuously through a waste heat boiler for energy recovery, then into gas cleaning followed by sulphur recovery in the acid plant (George, 2002).

2.4 Secondary copper processing

Up to one-third of consumed copper metal is produced through recycling from secondary copper resources in which is commonly called secondary copper processing (Goonan, 2010). A wide range of copper bearing scraps including electronic wastes can be inputted into secondary copper smelters for the recovery of various contained metals in these resources. Depending on the characteristics of the feeds, the secondary copper smelting operations can be distinguished into two groups (Davenport et al., 2002). The first one relates to processing of high-grade copper scraps, while the second is called black copper route, which treats low-grade scraps with large proportion of metal impurities. In the black copper route, two groups of elements can be found (Anindya et al., 2013). The first group is oxidized easily compared to copper and this constitutes of Fe, Pb, Sn, and Zn. The second group of metals is difficult to remove by oxidation, this includes Ni, Ag, Au and platinum group metals.

In general, multi-stage black copper smelting can be carried out through a number of process routes (reduction followed by oxidation; or vice versa) depending on the type and composition of feeds, as can be seen from the Figure 2.2. The key points from the black copper smelting process are to:

- Use copper as the metal collector for valuable metals such as In, Sn, Ge, Pd, Au, Ag, and others.
- Separate the volatile valuable metals from copper/slag phases to the gaseous phase (Zn, Pb and some other valuable metals that have large partitioning to

the gas phase) and condensed them to allow further processing for their recovery.

- Produce a clean slag (typically contain oxides of Fe, Mg, Si, Ca, Al) so that it can be discarded or re-use for other applications (such as concrete and road mix).

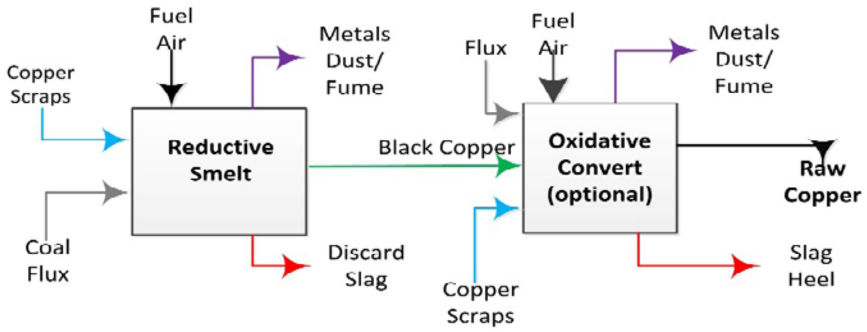

Flow Sheet 1: Reductive Smelt/ Oxidative Convert

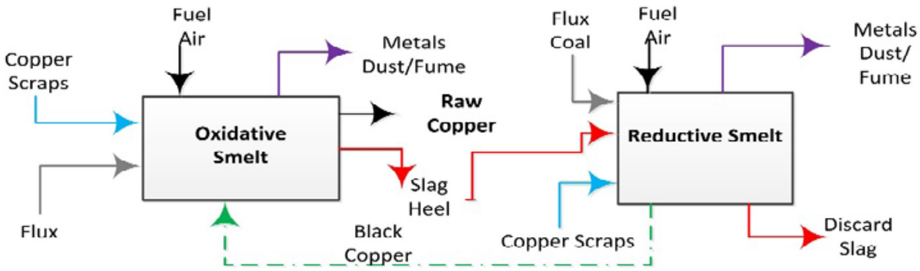

Flow Sheet 2: Oxidative Smelt/ Reductive Smelt

Figure 2.2: Variation of black copper smelting process routes depending on the type/composition of feed (Worrell and Reuter, 2014).

In case of low-grade secondary copper resources, the reductive-oxidative smelting route is more suitable. The reductive-oxidative black copper smelting for e-waste recycling (and other secondary Cu sources) is schematically shown in Figure 2.3. The first step of processing the e-waste and other secondary low-grade copper resources is carried out in a reduction furnace where the black copper is produced. From this process some metals (mainly Zn) also partition into the gaseous phase as Zn-rich fume. The typical operating conditions of this reduction process are at temperatures 1250°C (1523 K) to 1300°C (1573 K) and oxygen partial pressures of 10^{-2} to 10^{-6} atm. The black copper produced is then oxidized in an oxidation furnace to convert Zn, Sn, and Pb into oxide fumes (Khaliq et al., 2014, Wood et al., 2011). This produces a higher purity copper, which is then further refined in an anode furnace through a combination of oxidation and reduction depending on the composition. Alloyed copper scraps of higher purity can be added in the oxidation furnace or in the anode furnace. Further impurities removal occurs during the process in the anode furnace. Anode copper produced in anode furnace is then electrorefined to increase the purity and the remaining materials are deposited at the bottom in the electrorefining reactor, known as anode sludge. The precious metals coming from the feed (for example Ag and Au from the e-waste) mainly proceed to anode sludge which is processed further using hydrometallurgical techniques to recover the precious metals. Other valuable trace metals partition in either the copper, the slag or to the gaseous phases.

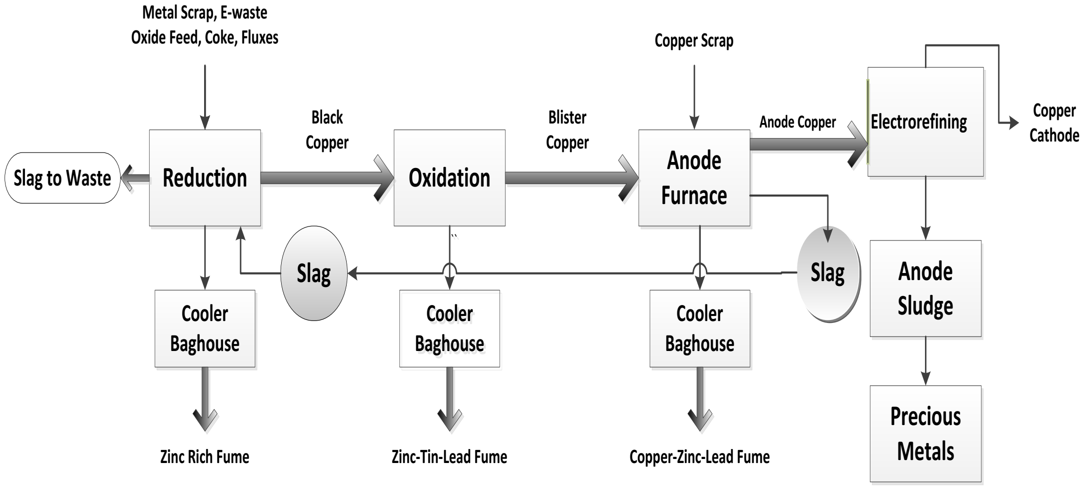

Figure 2.3: Simplified flow sheet of the reductive-oxidative black copper smelting process for e-waste processing.

2.5 E-waste

E-waste or electronic waste is defined as relinquished electrical or electronic device and equipment which have been discarded.

E-waste is a term used to consider almost any types of electrical and equipment which has or could enter the waste steam. It encompasses almost any home or commercial appliances such as TVs, computers, mobile phones, white goods (e.g., fridges, washing machines, dryers), home entertainment and stereo systems, toys, toasters, kettles which have the circuitry components with power or battery supply (StEp-Initiative, 2014).

The European Waste Electrical and Electronic Equipment (WEEE) Directives define e-waste as electrical or electronic equipment which is waste including all components, subassemblies and consumables, which are parts of the product at the time of discarding. Directive 2002/96/EC, Article 1(a) defines “waste” as any substance or object, which the holder disposes of or is required to dispose of pursuant to the provisions of the national law in force (EU, E-waste Directive, 2003). The European WEEE Directives has divided e-waste in ten categories as shown in Table 2.2. Among the 95% of the e-waste generated from first four categories and these are counted by most of the countries to consider the total volume of e-waste they generate.

Table 2.2: E-waste separate in ten categories by the European Directives on WEEE (EU, E-Waste Directive, 2002, 2012)

No.	Category	Indication
1	Large household appliances	Large HH
2	Small household appliances	Small HH
3	IT and telecommunications equipment	ICT
4	Consumer equipment	CE
5	Lighting equipment	Lighting
6	Electrical and electronic tools (with the exceptional of large –scale stationary industrial tools)	E & E tools
7	Toys, leisure and sport equipment	Toys
8	Medical devices (with the exception of all implanted and infected products)	Medical Equipment
9	Monitoring and control instruments	M & C
10	Automatic dispensers	Dispensers

Another important subclass of e-waste is printed circuit boards (PCBs) which are found in mostly in televisions, computer, mobile phones and laptops. FR-4 and FR-2 are the types of PCBs which are used in mobile phones and personal computers. These FR-4 and FR-2 types of PCBS are made of fiber glass layer coated with copper. In general, PCBs are composed of 40% metals, 30% plastics and 30% ceramics.

2.5.1 Scenario of e-waste

The demand of electrical and electronics products has been increased significantly in recent decades. As the demand increases, it has resulted the high generation of e-waste in worldwide. The generated high volume of e-waste has affected the environment in number of ways.

It was estimated that the volume of e-waste generated is about 40-50 million tonnes annually, which is approximately 5 percent of solid waste generated worldwide (Awasthi and Li, 2017). Robinson (2009) reported that most e-waste is generated in the United

States and Europe; although the generation of e-waste becoming large in China, Eastern Europe, Australia, Latin America and India. It is also estimated by Robinson (2009) that most of e-waste generated from computers, mobiles and television sets. According to Computer Industry Almanac, the number of computers in use worldwide had increased approximately from 553 million to 2000 million in last 15 years (Veit and Bernardes, 2015). Another type of e-waste is discarded mobile phone, and the number of discarded mobile phone is approximately 125 million that is equivalent to 65000 tonnes of e-waste (Veit and Bernardes, 2015).

The technology throughout the world changes rapidly, and new technology is now replacing older devices. Therefore, the generation rate of e-waste increases significantly day by day.

2.5.2 Recycling of e-waste

Recycling of e-waste can be classified into three major steps such as a) disassembly, b) upgrading and c) metal recovery. The first two steps are the pre-treatment of e-waste. Numerous research have been carried out for the investigation of this pre-treatment (Cui and Zhang, 2008). In the third step, metals are recovered from e-waste through metallurgical processes, such pyrometallurgy, hydrometallurgy, electrometallurgy and biometallurgy.

Pyrometallurgy is a method using a high temperature to recover non-ferrous and precious metals where the crushed electronic wastes are melted in a furnace or molten bath. Hydrometallurgical processing consists of acid or caustic leaching of solid material to extract selective elements. The leaching solution then subjective to further separation and purification methods such precipitation, solvent extractive and ion-exchange to separate the fraction of the metals of interest. Biometallurgy has two main areas for recovery of metals, namely bioleaching and biosorption. But, there is very limited knowledge for recover the precious metals from e-waste. Electrometallurgy is a technique that uses to produce metals by electrolysis. Usually, it is the last stage in the metal production followed by pyrometallurgical or hydrometallurgical processes.

2.6 Recycling of metals from e-waste practised in industries

Incineration, sintering, melting and smelting in arc furnace, blast furnace or other reactors are the common pyrometallurgy methods used in the last 20 years for processing secondary non-ferrous metals, including e-waste. During a smelting process, crushed scrap is fed into a furnace or a molten bath to melt it and also to separate the refractory oxides which make a slag phase. The underlying liquid metal which includes some soluble valuable metal is then subsequently subjected to a number of operations for refining and recovery of the metals.

In the Noranda process at Quebec, Canada, e-waste is processed through a primary copper smelting process route. As reported by Veldbuizen and Sippel (1994), about 14% of e-waste is added to mined copper concentrates in the smelter and these materials are supercharged with oxygen-enriched air (containing 39% oxygen). The precious metal containing copper matte is upgraded in a converter furnace, and finally refined in an anode furnace and cast with a purity of 99.1%. The rest of the compositions (0.9%) include the precious metals, such as gold, silver, platinum and palladium, along with other recoverable metals such as selenium, tellurium and nickel. By subsequent electrorefining of cast anode, these elements are segregated to anode sludge which is then further processed for their recovery.

The smelter of Rönnskår in Sweden also processes e-waste (Lehner, 1998). There are usually two particular routes for treating the scrap. The scrap containing high grade copper is fed directly into a converting process while the low grade is fed into an Kaldo furnace. It was reported that they process scrap, including e-waste, about 100,000 tonnes annually. In the process, the temperature of the off-gases is about 1200^{o}C (1473 K) which then subjected to surplus combustion air and the heat is recovered by a steam network of gas handling unit. A mixed copper alloy is produced in the Kaldo furnace which is then sent to copper converting process for recovery of metals, such as Cu, Ag, Au, Pd, Ni, Se and Zn. The dust, containing Pb, Sb, In and Cd, are processed to recover the metals through other operations (Lehner, 1998).

Umicore processes different industrial wastes as well as by-products from the non-ferrous industries, spent industrial catalysts, car exhaust catalysts and printed circuit boards (PCBs). They take an integrated approach of smelting and refining processes for the recovery of precious and other valuable metals. In the plant at Hoboken Belgium (Hageluken, 2006), an integrated process that include pyrometallurgical, hydrometallurgical and electrochemical processes is used not only to recover the base metals but also the platinum group metals and specials metals (Hagelüken, 2006).

Annually, Umicore processes 250,000 tonnes of the above wastes in which about 10% feed are e-waste. An IsaSmelt furnace is used to smelt the wastes in the first stage of the precious metals operations (PMO). The precious metals are separated into the copper bullion and while the other metals concentrate into slag which is the by-product of the PMO. The slag is further treated in the Base Metals Operations (BMO). For the copper bullion, leaching and electrowinning are performed to recover copper and lastly the precious metals are recovered in the precious metal refinery. The special metals residues containing indium, selenium, and tellurium are generated in BMO which are further refined in the special metals refinery.

Dowa Mining in Kosaka Japan uses an Top Submerged Lance (TSL) furnace to process approximately 150,000 tonnes of secondary copper feed annually (Wood et al., 2011, Worrell and Reuter, 2014). The operations combine, in different stages, both oxidation and reduction processes to produce high grade copper product and to recover valuable elements in refining process such as PGMs, Ni, Zn and Pd. LS Nikko's Global Resources & Material (GRM) in Danyang, Korea also uses TSL furnace and they operate it under reducing conditions to produce black copper (Wood et al., 2011). The black copper is refined by an oxidation process followed by electrolytic refining. The sludge from the electrolytic refining process is then further processed for the recovery of the precious metals.

In summary, there are different types of recycling technology and process routes practised in industry for recycling of secondary copper products and end-of-life consumer goods. Depending on the type of waste/secondary input, concentration and composition, suitable methods and technologies must be incorporated with optimized operating conditions. These wide variations in operating conditions require detailed thermodynamic information for optimization of those processes.

2.7 Structure of silicate base slag

Slag is a melt of an oxy-compound of silicon, aluminium, calcium and iron (among others) and has an important role from in process metallurgy. In both ferrous and non-ferrous metallurgical processes, silica have been one of the key components of slag melt. The role of slag melts have a vital role that affect the performance and productivity of processes in the both industries. The slag also contains other components such as alkali oxides (Na_2O), alkaline earth oxide (CaO or MgO), amphoteric oxide (Al_2O_3) etc. The composition of the slag melts have comprehensive effect on the thermophysical and thermochemical properties. For example, viscosity is a thermophysical property of slag melt that is controlled by the composition, which has direct impact on the metal-slag reaction kinetics, separation and heat transfer. The impact of slag melts can be accommodated through optimization of the overall slag melt composition.

In silica, four oxygen atoms are bonded with each silicon and each oxygen atom is bonded with two silicon atoms. In such a way, each of the tetrahedral linked with one another to create a three dimensional (3D) network in the silicate base slag.

The chemical components of the silicate slag melts can be classified according to the nature of components within the slag system. It can be either acidic or basic component. When alkali or alkaline earth metal oxides (e.g. Na_2O, CaO, MgO) are added to silica containing slags, such oxides can provide free oxygen ions (O^{2-}) in the silicate melt which reacts with bridged oxygen (O^0) and then produce a non-bridged oxygen (O^-). The non-bridged oxygen (O^-), therefore, reduces the degree polymerization of the slag network structure. However, acidic oxides (e.g.P_2O_5) do not react to provide free oxygen ions (O^{2-}) rather produces bridged oxygen (O^0) which can enhance the formation of more complex slag structure through polymerization. The behaviour of amphoteric oxides (e.g. Al_2O_3) actually depend on the oxides presence in the slag. They can behave either acidic oxides that increase the polymerization by producing bridged oxygen (O^0) or basic oxides which depolymerize the structure by producing more free oxygen ions (O^{2-}) in the silicate melt.

Some of the features are outlined to understand the factors affecting the structure of silicate melts as following (Mills, 1993, Mysen and Richet, 2005):

- The silicate melt contains anionic units, e.g.,SiO_2, $Si_2O_5^{2-}$, $Si_2O_6^{4-}$, $Si_2O_7^{6-}$ and SiO_4^{4-}.The anionic unit contain 3-6 atoms and these atoms can arrange themselves in different forms, i.e., chain, rings and sheets. The nature of anionic units are not affected by the addition of network breaking ion, i.e., Ca^{2+}, Mg^{2+}. However, it affects the quantity of anionic units and increases the rate of depolymerization.
- The degree of polymerization (DOP) of silicate slag is favoured with smaller radii (r) and higher valency (z), e.g., Ca^{2+} ($r_{ca^{2+}}$= 0.1 nm) favour the formation

of more depolymerize unit (e.g. SiO_4^{4-}) than Na^+ (r_{Na^+}= 0.102 nm).

- There are some cations, which can fit into the 3-D silicate units and contribute to the overall polymerization of the melt, such as Al^{3+}, $Fe^{3+,}$ Ti^{4+} and P^{5+}. Some of tetrahedra ions such as (AlO_4^{5-}) have a different charge than silicon tetrahedral, and therefore electrical charge balancing of cations are required.
- Fe^{3+} act as both network former and breaker, and can adopt two coordinations (i.e., four-fold and six-fold coordination) depending on the concentration. It has been reported that the range of Fe^{3+}/Fe_T ratios to act network modifier and breaker are > 0.5, and <0.3, respectively(Mysen, 1990b, Mills, 1993). In steelmaking slags, Fe^{3+} acts as network breaker
- PO_4^{3-} tetrahedra form when P_2O_5 is present in the silicate slag, and complex P-O-Si bonds are formed with silicate melt and increase the rate of polymerization. However, P_2O_5 also has an affinity for cations, e.g., Al^{3+}, Na^+ than silicon tetrahedra to form complex phosphate.

2.8 Techniques for analysis of silicate structure

Understanding of the inter-relationship between the slag structure, to its composition and thermophysical properties is vital for designing a suitable slag for particular metallurgical process. Mysen (1990b) previously performed studies in the geological science field. There is a similarity between nature of magmatic melts in geophysics and metallurgical slag. Magmatic liquid contains network forming and breaking cations and it requires charge-balancing as well. In addition, the physical and chemical properties of maganitc liquids govern by the composition and structure of magmatic liquid (Mysen, 1990c).

Silicate melts structure for binary system that include chains and rings, is very complex. Multicomponent silicate slags will have a more complex structure. In addition, the polymerized structures of multicomponent slag systems have yet to be elucidated with different non-destructive techniques. Broader knowledge of silicate melts structure analysed using more rigorous analysis technique such as spectroscopic methods are required for further understanding. There has been a number of studies that attempt to determine the slag structure of quenched sample using different spectroscopic methods such as Fourier transform infrared (FTIR) spectroscopy, Raman spectroscopy, X-ray photoelectron spectroscopy (XPS) and nuclear magnetic resonance (NMR) Spectroscopy. However, it is suggested that the extrapolation of structural model derived from silicate glasses at room temperature using spectroscopic technique, and from the silicate melts of high temperature must have similar molecular structure of glasses and melts (Mysen and Frantz, 1992, Mysen et al., 1980, Mysen, 1990b).

Raman spectroscopy is a light scattering technique to extract the information about the bond and structure of materials. It differentiates the elastic Rayleigh and inelastic Raman scattering from the scattering of the radiation at the point of collision between incident monochromatic light and the molecules. The energy of inelastic Raman scattering is affected by the interaction between incident light and molecules. However, the frequency of Rayleigh scattering does not change after the collision. The frequency of Raman scattering is shifted up or down which provides the information about the vibrational state of molecules. This concept is used for quantitative measurements of silicate tetrahedra units in silicate structure based through deconvolution procedure of the Raman spectra. Mysen et al. (1980), McMillan (1984) and Furukawa et al. (1981) determined the semi-quantitative band intensities of complex silicate structures using Raman spectroscopy as shown in Table 2.3. The associated structures of the different silicate units are shown in Figure 2.4. They also demonstrated the effect compositions on slag structure which have been employed to characterize the possible relationship between the slag structure and properties.

Fourier Transform Infrared (FTIR) is similar technique like Raman spectroscopy. The measurement is based on the molecular vibration and dipole moment change of the sample (Rouessac and Rouessac, 2013). When infrared radiation (IR) is passed through a sample, the molecules absorb or transmit the IR. The spectra that is resulted from that absorption or transmission of sample represent the fingerprint of the sample. Park et al. (2002) Sun et al. (2015), and Eom et al. (2016) analysed different types of slag structure using FTIR to understand the structural aspects of slag based on slag compositions. They reported about the change of slag structure and how it can be correlated with the physicochemical properties in relation to FTIR measurement. The wavenumbers of the anionic units in silicate are found similar to that from the Raman measurement as mentioned in Table 2.3 (Sohn and Min, 2012).

Table 2.3: Raman shift with vibration mode for different silicate structure units

NBO/T (Q^n)	**Unit**	**Frequency (cm^{-1})**	**Mode**	**Ref.**
0 (Q^4)	SiO_2	1200, 1190	Asymmetric stretch	(Mysen et al., 1980)
1 (Q^3)	$Si_2O_5^{2-}$	1100-1050	Symmetric stretch	(Mysen et al., 1980)
2 (Q^2)	$Si_2O_6^{4-}$	980-950	Symmetric stretch	(Mysen et al., 1980)
3(Q^1)	$Si_2O_7^{6-}$	920-900	Symmetric stretch	(Mysen et al., 1980)
4 (Q^0)	SiO_4^{4-}	880-850	Symmetric stretch	(Mysen et al., 1980)
-	$Si-O-Si$	800-780	Asymmetric bending	(McMillan, 1984)
-	$Si-O-Si$	650-500	Symmetric bending	(McMillan, 1984)
-	$Si-O-Si$	480-440	Rocking	(McMillan, 1984)

Nuclear Magnetic Resonance (NMR) spectroscopy is a technique where a sample in placed in magnetic field. The present of the magnetic field around a nucleus of the sample allow it to transfer the energy into the molecules. Due to the transfer of energy, chemical shifts are found from NMR spectroscopy. This chemical shift is used to investigate the structural information. NMR spectroscopy is a dominant method for the organic compound. However, it is used for analysis of slag structure. An investigation was carried out by Sun et al. (2015) using NMR spectroscopy to identify the roles of phosphorous (P) in the network. They found that PO_4 tetrahedra units in the CaO-SiO_2-P_2O_5 as Q^o (P) and Q^1 (P). It was also observed the fraction of Q^o (P) and Q^1 (P) decreases with increasing P_2O_5 which suggested of an acid-base equilibrium reaction. They also validated their results with other spectroscopy techniques (i.e., FTIR, Raman).

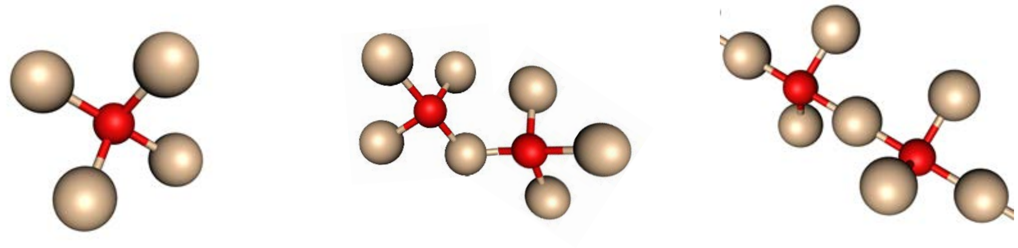

SiO_4^{4-} (monomer), Q^0 $Si_2O_7^{6-}$ (dimer), Q^1 $Si_2O_6^{4-}$ (chain), Q^2

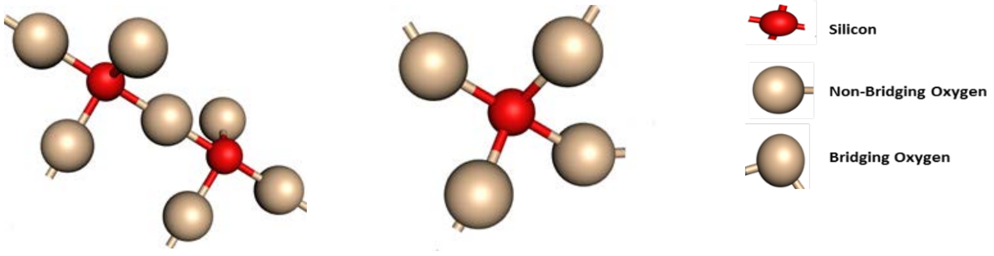

$Si_2O_5^{2-}$ (branch/sheet), Q^3 SiO_2 (3D network), Q^4

Figure 2.4: Structure of different silicate tetrahedral units in silicate glass melt.

X-ray photoelectron spectroscopy (XPS) is another technique where X-rays incidents on the sample. The present of energy excited the electrons which are emitted. During XPS analysis the energy of emitted electrons and energy level are determined which could be used to identify the valence state and coordination number of sample. It can be used for the surface structure analysis of silicate melts (Sohn and Min, 2012). Kim and Sohn (2011) investigated the effect of CaF_2 and Li_2O on the structure of CaO-SiO_2-Na_2O using XPS and correlated with the oxygen species (bridged oxygen (O^0), non-bridged oxygen (O^-), free oxygen ions (O^{2-}). The results suggested that the role of network modifier of CaF_2 and Li_2O in CaO-SiO_2-Na_2O slag was found up to 8 mass% of CaF_2, and 2 mass% of Li_2O beyond that composition it does not show any significant effect on the physical properties.

Mössbauer spectroscopy is a technique which has been used to examine the distribution of iron cations in silicate melt. It can also be used to characterize the change of proportion of phase, coordination and oxidation state of iron. The effect of

Table 2.4: Summary of previous studies on slag structure analysis using vibrational spectroscopy

Investigators	Slag System	Temperature, °C	Technique	Comments
Mysen et al. (1980)	Na_2O-SiO_2, CaO-SiO_2, CaO-MgO-SiO_2, Na_2O-Al_2O_3-SiO_2	1200 -1650	Raman Spectroscopy	Investigate the structure–properties relationship, and it was suggested that the change of structure affects the viscosity and activation energy
McMillan (1984)	CaO-SiO_2-MgO	2000-2500	Raman Spectroscopy	The role of metal cations on the silicate structure units were investigated
Mysen (1990b)	(Li_2O/Na_2O/K_2O)-Al_2O_3-SiO_2	1400	Raman Spectroscopy	The effect of slag composition on the relative fraction of silicate tetrahedra units was determined
Chaskar et al. (1993)	Fe_xO-Al_2O_3, Fe_xO- Al_2O_3-SiO_2	1400	Mössbauer Spectroscopy	Quantified the effect of Fe^{2+} and Fe^{3+} on the degree of polymerization
Mysen and Frantz (1992)	(Li_2O/Na_2O/K_2O)-Al_2O_3-SiO_2	25-1475	Raman Spectroscopy	Spectra of different slag systems were investigated at different temperature and was found that abundance of structure units affect by temperature
Park et al. (2002)	CaO-SiO_2, CaO-SiO_2-CaF_2	1500-1550	FTIR Spectroscopy	The effect of slag compositions on the binary and ternary slag system structure was investigated and also reported about the network modifier role of fluorine ion
Lee et al. (2004)	CaO-SiO_2-Al_2O_3-MgO-FeO	1400-1450	FTIR Spectroscopy	The effect of the slag composition on the DOP and viscosity was reported
Park (2012)	CaO-SiO_2-MnO	1600	Raman Spectroscopy	Developed relationships with thermophysical properties and degree of polymerization
Park et al. (2012)	CaF_2-CaO-SiO_2-FeO_x	1550	FTIR and Raman Spectroscopy	The mechanism of hydrogen dissolution (i.e., hydroxyl ion and free hydroxyl) in acidic and basic slag have been elucidated
Park (2013b)	CaO-SiO_2-MgO	1600	Raman Spectroscopy	Predicted relationships with thermophysical properties and degree of polymerization and also determine the effect of slag composition on slag structure
Gao et al. (2014)	SiO_2 -CaO-MgO-Al_2O	1450-1500	FTIR Spectroscopy	Effect of MgO content to depolymerize the complex structure was determined, and a correlation between viscosity and slag structure was reported.
Sun et al. (2015)	CaO-SiO_2-P_2O_5, CaO-SiO_2-TiO_2-P_2O_5	1500	FTIR, Raman and NMR spectroscopy	The of role P_2O_5 and TiO_2 on the slag structure were identified
Řeháčková et al. (2015)	CaO-SiO_2-Al_2O_3	1400-1600	FTIR Spectroscopy	The effect of the internal structure of slag on viscosity was studied by FTIR
Mohassab and Sohn (2015)	CaO-SiO_2-MgO-MnO-Al_2O_3-FeO-FeS-$Ca_2P_2O_7$	1550	FTIR and Raman Spectroscopy	Effect of water vapour in the gas mixtures was investigated
Eom et al. (2016)	Cao-SiO_2-MnO	1500	FTIR Spectroscopy	Determined the role of Mn and effect of free oxygen on the activity coefficient of MnO in slag from the slag structure analysis
Wang et al. (2017)	CaO-SiO_2-$CaCl_2$	1550	Raman Spectroscopy	Studied the role of Chlorine as network modifier and its effect on the degree of polymerization

the gas mixture (CO +CO_2) on iron coordination in quenched Fe_xO-Al_2O_3, Fe_xO-Al_2O_3-SiO_2 and Fe_xO-Al_2O_3-CaO slag at 1400°C (1673 K) were carried out by Chaskar et al. (1993) and McCammon et al. (1991). They found that concentration of Fe^{2+} increases in Fe_xO-Al_2O_3 at reducing conditions because of increasing free O^{2-} ions. They also revealed that in Fe_xO-Al_2O_3-SiO_2 slag both Fe^{2+} and Fe^{3+} decrease with increasing the gas mixture and silica, therefore increases the degree of polymerization. However, opposite results found in Fe_xO-Al_2O_3-CaO slag; Fe^{3+} increases with the increasing during reducing conditions and affects the degree of polymerization. Finally, it was concluded that the behaviour of iron oxide during reduction is very complex and depend on the slag composition, and therefore the degree of polymerization is affected.

Numerous research have been carried out to study the structure of silicate melts particularly correlating between the structure and properties of silicates using spectroscopic techniques (Virgo et al., 1980, Mysen and Dubinsky, 2004, McMillan et al., 1992, Park and Min, 1999, Mysen et al., 1980, Mysen, 1990b, Park, 2013a, Park et al., 2002, Park, 2012, Park, 2013b, Eom et al., 2016). The identification of the structure of oxide melts will evaluate the structure and properties of slag melts and provides information required in the metallurgical process. The spectroscopic methods to determine the relative fraction of silicate tetrahedral have been adopted by many researchers to understand the slag structure and determined the degree of polymerization of the melt. The information existing in the literature have been collected and listed for different slag systems as shown in Table 2.4. The detailed literature review of slag structure and structure-properties relationship will be discussed in Section 7.2.

2.9 Summary

Declining the grade of primary resources and increasing the high demand of valuable metals have diverted us to recover metals from non-primary sources. Black copper smelting route can be used to recover copper and valuable metal using non-primary sources (i.e., e-waste). Thermodynamics of valuable metal plays the significant role to use this route potentially. It is required to understand thermodynamics information available in the literature relevant to copper smelting and extend the knowledge of other valuable metals which will be discussed in the following chapters. Further to this, slag structure is strongly affected by slag composition and parameters in the metallurgical processes. Therefore, the effect of experimental parameters relevant to black copper smelting on the slag structure is inevitabel to study. The slags used in the present study will be investigated using vibrational spectroscopy.

Chapter 3 Thermodynamics Data of Minor Elements Relevant to E-waste Processing through Primary and Secondary Copper Production

3.1 Introduction

E-waste and other urban ores are vital for resource efficiency (Reuter and Kojo, 2014; Worrell and Reuter, 2014). A number of studies have been pointed out about the hazardous impact of e-waste on environment and also benefits of e-waste recycling (Chi et al., 2014; Menikpura et al., 2014; Nelen et al., 2014; Zeng et al., 2015). However, there are some technical challenges that also prevent to the utilisation of these resources efficiently.

It has been mentioned in the earlier Chapter 2 that one of the existing industrial routes for processing of e-waste to overcome the technical challenges is through metallurgical processes embedded in primary and secondary base metals productions, such as through copper smelting. This is mainly due to the flexibility of the process in which different variety of copper bearing resources (including e-waste) can be inputted into the process. But, the metals and their concentration vary from one type of e-waste to another and also vary with time as the technology changes. A summary of selected metals and their concentration in different types of e-wastes is shown in Table 3.1. The elements found (and their concentrations) in e-waste are significantly different than those found in common primary ore concentrates. It is a great challenge for metal industries to develop and design optimal smelting processes utilising e-waste (Götze and Rotter, 2012, Khaliq et al., 2014).

One of the key enablers of processing e-waste using pyrometallurgical route is understanding the fundamental thermodynamics of all the minor elements. The underlying thermodynamics knowledge governs the important role to recover these precious metals using a carrier metal production route. Smelting operations are optimized over many years through a combination of fundamental studies and industry best practises. A large database of information, in particular, the solution thermodynamic data in the primary copper processing has accumulated over the years but the information is limited to a number of elements (such as In, Te, Se, Co, Pd, Pt and Rh) behaving in copper/matte/slag systems. There are limited published data available which focus on the trace elements distribution in secondary copper processing. The composition of the slag, oxygen partial pressure and temperature has significant control on the distribution of the trace elements in the smelting process. There is still some gap in the information for the separation of the combination of elements in e-waste particularly in the operating conditions beyond those commonly used in the existing processes. This requires a rethinking of traditional processing techniques, which must be based on knowledge of how these unusual trace elements distribute between phases during copper smelting route.

The aim of this chapter is to review the available thermodynamic data on trace valuable elements, particularly those associated with e-waste, in systems relevant to primary and secondary copper pyrometallurgical processes by a systematic way.

3.2 Methods

The current study presented in this chapter, focuses on a comprehensive and systematic review of thermodynamic data of valuable metals associated with primary and secondary copper smelting. Particularly, identifying the distribution-ratio data of valuable metals during copper smelting process relevant to e-waste processing, available in the environmental, metallurgical and chemical literature. This chapter then highlights the gaps in knowledge required for the improvement and optimization of current industrial processes. The implication for the metal recycling industry, as well as the challenges for future research and improvement of industrial processes, are also described. It is hoped that the finding presented in this chapter helps the development of ideas for further research on the thermodynamic behaviour of valuable elements to promote metals resource efficiency and also useful for the industry and scientific community.

Table 3.1: Different types of selected metals content in end of life electronic equipment (Oguchi et al., 2011)

Equipment Type	**No of Data**	**Typical Metal content of printed circuit board (mg/kg)**														
		Common Metal						**Precious Metal**			**Less Common Metal**					
		Al	**Cu**	**Fe**	**Pb**	**Sn**	**Zn**	**Ag**	**Au**	**Pd**	**Ba**	**Bi**	**Co**	**Ga**	**Sr**	**Ta**
Refrigeration	1	16,000	170,000	21,000	21,000	83,000	17,000	42	44	–	82	480	120	–	51	–
Washing	1	1000	70,000	95,000	2200	9100	2400	51	17	–	65	51	16	–	9	–
Air conditioner	1	6900	75,000	20,000	5800	19,000	4900	58	15	–	320	–	29	–	26	–
CRT TV	5	62,000	72,000	34,000	14,000	18,000	5300	120	5	20	2400	280	36	–	550	–
PDP TV	2	38,000	210,000	20,000	7100	15,000	12,000	400	300	–	3900	100	–	–	650	100
LCD TV	1	63,000	180,000	49,000	17,000	29,000	20,000	600	200	–	3000	–	–	–	300	–
Desktop PC	8	18,000	200,000	13,000	23,000	18,000	2700	570	240	150	1900	50	48	11	380	7
Notebook PC	2	18,000	190,000	37,000	9800	16,000	16,000	1100	630	200	5600	120	80	10	380	5800
VCR	2	35,000	160,000	38,000	20,000	18,000	16,000	210	23	50	1200	–	47	9	27	23
DVD	3	54,000	220,000	11,000	12,000	22,000	26,000	710	150	20	4300	85	110	9	400	77
Radio cassette	2	61,000	140,000	58,000	17,000	24,000	11,000	170	26	34	1400	230	8	12	120	9
Facsimile	1	37,000	120,000	11,000	19,000	7400	7700	69	35	110	4300	–	420	–	95	–
Printer	2	180,000	140,000	17,000	10,000	16,000	4200	70	38	21	3000	9	39	3	170	–
Mobile Phone	19	15,000	330,000	18,000	13,000	35,000	5000	3800	1500	300	19,000	440	280	140	430	2600
Digital Camera	10	24,000	270,000	30,000	17,000	39,000	8800	3200	780	200	16,000	230	140	15	440	7900
Camcorder	8	29,000	210,000	45,000	30,000	38,000	13,000	5000	530	970	18,000	240	180	52	610	8000
Portable CD	2	68,000	200,000	46,000	12,000	50,000	20,000	3700	370	10	8600	1100	80	–	230	670
Portable MD	2	27,000	330,000	45,000	9300	48,000	11,000	3400	940	550	19,000	660	150	–	340	9600
Video game	6	40,000	190,000	77,000	13,000	26,000	12,000	740	230	43	5100	260	100	16	400	83

3.3 Thermodynamics behaviour of valuable elements in copper

During pyrometallurgical processing of primary and secondary copper, valuable elements distribute themselves into different phases (slag, matte, copper, gas, depending on the process). Understanding the distribution behaviour, which is governed by the thermodynamics, is vital from fundamental perspective and improvement of industrial operation. Such information provides the basic knowledge for developing optimum conditions to recover the precious metals and to eliminate the deleterious elements during the processing.

The equilibrium reaction of a solute element 'M' between liquid metal and slag having a valence of $2v$ can be described by Eq.(3.1)

$$[\mathrm{M}] + \frac{v}{2}\mathrm{O}_2 = (\mathrm{MO}_v) \tag{3.1}$$

The equilibrium constant K for the above reaction is expressed by the activities of metal oxide and metal distribution as follows

$$K = \frac{a_{\mathrm{MO}_v}}{a_{\mathrm{M}}\, p_{\mathrm{O}_2}^{v/2}} \tag{3.2}$$

The distribution-ratio of 'M' in slag and metal can be defined as

$$\mathrm{L}_{\mathrm{M}}^{\mathrm{s/m}} = \frac{(pct\ \mathrm{M})}{[pct\ \mathrm{M}]} \tag{3.3}$$

Where the parentheses ( ) and [ ] denote the concentration of the element in slag and metal phases respectively. It was shown that the distribution-ratio can be represented as (Takeda et al., 1983, Yazawa and Takeda, 1982)

$$\mathrm{L}_{\mathrm{M}}^{\mathrm{s/m}} = \frac{K\,(n_T)[\,\gamma_{\mathrm{M}}]p_{O_2}^{v/2}}{[\,n_T](\,\gamma_{\mathrm{MO}_v}\,)} \tag{3.4}$$

Where K is the equilibrium constant for Reaction (3.1), n_T is the total number of moles in constituents in the relevant phases, γ_{M} is the activity coefficient of M in the metal, γ_{MO_v} is the activity coefficient of metal oxide MO_v in the slag and p_{O_2} is the oxygen partial pressure. There are some data available in the open literature for γ_{M} in the Cu-M binary system. In an infinite dilute solution, the activity coefficient of solute elements in liquid metal and its oxide in slag does not change significantly and sometime can be assumed to be constant. It was reported that monocation form of oxides show constant activity coefficient over a large

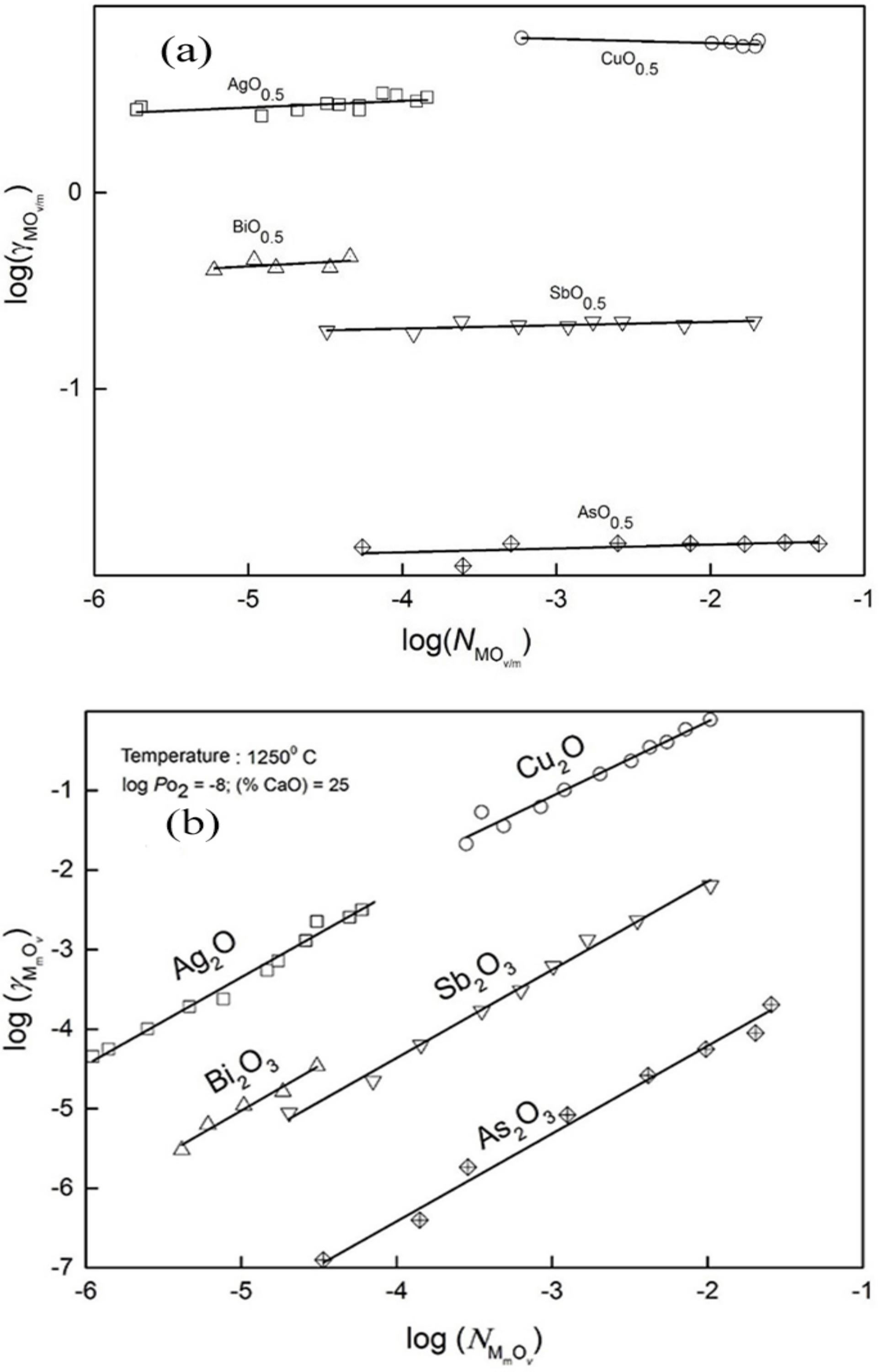

Figure 3.1: Relationship between the activity coefficient of oxides and the mole fraction of oxides in calcium ferrite slag at 1250°C,(reproduced from Takeda et al., 1983, Yazawa et al., 1968).

range of composition (Takeda et al., 1983, Yazawa and Takeda, 1982, Yazawa et al., 1968). As shown in Figure 3.1, the activity coefficient of oxides in the slag is a function of mole fraction. It can be seen from Figure 3.1(a) that mono-nuclear atom base oxides such as $CuO_{0.5}$, $AsO_{1.5}$, etc., showing constant activity value throughout the concentration range. However, the activity coefficients of multi-nuclear atom base expression such Cu_2O, As_2O_3 etc., as shown in Figure 3.1(b) do not show constant values against the concentration. It was also reported that the value of the total number of moles of species in non-ferrous smelting slag systems (such as in $FeO_{1.5}$-$CuO_{0.5}$-CaO-MgO-$MO_{v/m}$ slag systems) is similar when all the constitutes were expressed in mono-nuclear atom base, i.e. the number of moles (n_T) is 1.45 per 100 g of slag phase, and 1.57 per 100g of metal phase (Takeda et al., 1983). For a particular temperature, all the terms on the right side of Eq.(3.4) are constant, with the exception of oxygen partial pressure. Therefore, the following relationship can be established:

$$\log \mathrm{L}_{\mathrm{M}}^{\mathrm{s/m}} = \log B + \left(\frac{v}{2}\right) \log p_{\mathrm{O}_2} \qquad (3.5)$$

Takeda et al. (1983) described how to determine the value of v and also measured the value of $\log \mathrm{L}_{\mathrm{M}}^{\mathrm{s/m}}$, as a function of oxygen partial pressure at constant temperature. From the slope of the linear relationship between $\log \mathrm{L}_{\mathrm{M}}^{\mathrm{s/m}}$ and $\log p_{\mathrm{O}_2}$, the degree of oxidation of solute element $\frac{v}{2}$ in the slag can be determined. Moreover, the activity coefficient of MO_v in the slag can also be calculated by using Eq.(3.4) if the activity coefficient in of element M in liquid metal phase, γ_{M}, is known. Takeda et al. (1983) extensively studied the distribution-ratio of selected solute metal elements as a function of oxygen partial pressure as shown in Figure 3.2.

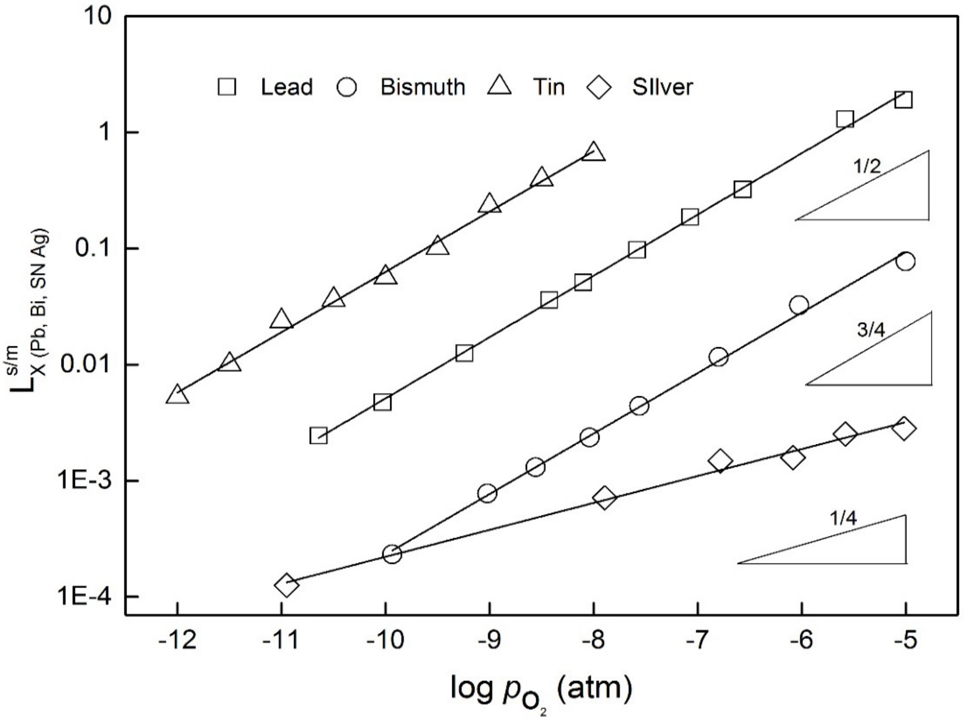

Figure 3.2: Distribution-ratios of Pb, Bi, Sn and Ag between slag and liquid copper systems at 1250ºC, (reproduced from Takeda et al., 1983, Yazawa et al., 1968).

In the primary copper processing (smelting and converting), we deal with sulphide and oxides systems. Yazawa (1974) described that the trace elements behaviour in primary copper processing can be represented by the following two reactions:

$$[\mathrm{M}]_{(s,l)} + \frac{1}{2}\,\mathrm{S}_2 = (\mathrm{MS})_{(s,l)} \tag{3.6}$$

$$[\mathrm{M}]_{(s,l)} + \frac{1}{2}\,\mathrm{O}_2 = (\mathrm{MO})_{(s,l)} \tag{3.7}$$

The logarithmic equilibrium constants, $\log K_1$ and $\log K_2$ of Reactions (3.6) and (3.7) were calculated respectively for the various elements found in primary copper smelting at 1300°C (1573 K), and is shown in Table 3.2. In addition, the activity coefficient (γ^0_{M}) at infinite dilute solution of elements and the distribution coefficient, $\mathrm{L_M}$, in molten copper and white metal are also given in the Table 3.2. From Table 3.2, the stability of various elements during the copper smelting can be evaluated. The solute elements of gold, silver, selenium and tellurium are stable among other elements and difficult to be removed by oxidation. Some other elements can be removed in the oxide or sub oxide forms. Because of the limited basic data, it is difficult to predict the optimum conditions at different range of oxygen potential and temperature.

Table 3.2: Thermodynamic data of minor elements in primary copper smelting at 1300°C (Yazawa, 1974, Yazawa and Azakami, 1969)

	Cu	**Au**	**Ag**	**Pb**	**Bi**	**As**	**Sb**	**Sn**	**Ni**	**Co**	**Fe**	**Zn**	**Se**	**Te**
$\mathbf{L_M}$	-	172	2.4	11.5	8.1	9.0	13.6	9.3	3.1	1.12	0.20	0.97	0.074	0.118
$\boldsymbol{\gamma_M^o}$	1	0.36	2.9	5.1	2.5	0.0008	0.017	0.13	2.6	8.6	12.6	0.13	0.0034	0.004
$\mathbf{\log K_1}$	2.88	-	0.94	1.12	-1.3	-	-0.2	1.35	1.34	1.15	2.39	3.27	-	-
$\mathbf{\log K_2}$	2.01	-4.63	-2.23	2.42	1.68	3.525	3.49	4.00	3.18	3.90	5.40	6.16	-1.24	0.04

Yazawa and Azakami (1969) suggested two mechanisms for handling solute elements during the primary copper smelting. First is through oxidation immediately after slagging and the second one is through volatilization. They had considered the following Reaction (3.8) to describe the removal of impurities during the copper converting:

$$\mathrm{Cu_2O}\ (l) + [\mathrm{M}]_{(s,l)} = 2\mathrm{Cu} + (\mathrm{MO})_{(s,l)} \qquad (3.8)$$

They utilised available experimental and thermodynamic data of the behaviour of solute elements at 1200°C (1473 K) as listed in Table 3.3. It was pointed out that gold to tellurium metals in Table 3.3, which have a small K (equilibrium constant) value, are difficult to oxidize. These Group 1 metals, however, have a high economic value and could be recovered from the anode slime at later stage of the copper processing. The second group of metals (Group 2) cannot be removed by oxidation but can be removed by volatilisation, particularly zinc and cadmium because of their high activity coefficient and partial vapour pressure. It should be noted that selenium, tellurium and arsenide have large partial pressure but their activity coefficient are very low (Yazawa, 1974, Yazawa and Azakami, 1969). On the contrary, the Group 3 metals have large K values and most of them are easily oxidized and very little amount may be found as inclusions. In copper smelting some impurities have value which can be recovered but deleterious elements which cannot be recovered either in converting or electrolytic refining stages should be removed as much as possible before the smelting process.

Nagamori and Mackey (1978) conducted a thermodynamic assessment of minor elements and their distribution in copper, matte and fayalite slags based on the available thermochemical data. They simplified the distribution of minor elements into three feasible models and considered equilibrium systems for high grade matte as well as fayalite slag for all these models. Au, Ag, Bi, Sb and As were categorised in the first model where their distributions depend only on the temperature. The second model represented elements whose distribution varies with temperature and partial pressure of oxygen and sulphur, which include Pb, Zn, Ni, Co and Sn. While Te and Se were in the third model where their distribution depends on the temperature and oxygen partial pressure only. The assessment established feasible physicochemical models for different minor elements in the fayalite slag. It was mentioned that these models need to be verified with experimental work and more fundamental data would be needed for an improved thermodynamic prediction (Nagamori et al., 1975a, Nagamori and Mackey, 1978).Table 3.4 shows the distribution of some elements in copper making and their relation with the partial pressure of oxygen and sulphur at 1250°C (1523 K) and Table 3.5 shows the Gibbs energy data of minor elements in copper.

Table 3.3: Thermodynamic data of minor elements in liquid copper at 1200°C (Group 1 represent the most stable metal, Group 2 represent most of the volatile metals and Group 3 represent metals who are oxidized readily) (Yazawa, 1974, Yazawa and Azakami, 1969)

Element	**Content (%)**	**Equilibrium Constant (*K*)**	γ_{M}^{0}	
Gold	0.003	1.2×10^{-7}	0.34	Group 1
Mercury	-	2.5×10^{-5}	-	
Silver	0.1	3.5×10^{-5}	4.8	
Platinum	-	5.2×10^{-5}	0.03	
Palladium	-	6.2×10^{-4}	0.06	
Selenium	0.04	5.6×10^{-4}	<<1	
Tellurium	0.01	7.7×10^{-2}	0.01	
Bismuth	0.009	0.64	2.7	Group 2
Copper	~99	-	1	
Lead	0.2	3.8	5.7	
Nickel	0.2	25	2.8	
Cadmium	-	31	0.73	
Antimony	0.04	50	0.013	
Arsenide	0.04	50	0.0005	
Cobalt	0.001	1.4×10^{2}	10	
Germanium	-	3.2×10^{2}	-	
Tin	0.005	4.4×10^{2}	0.11	
Indium	-	8.2×10^{2}	0.32	
Iron	0.01	4.5×10^{3}	15	Group 3
Zinc	0.007	4.7×10^{4}	0.11	
Sodium	-	1.1×10^{5}	-	
Chromium	-	5.2×10^{6}	-	
Manganese	-	3.5×10^{7}	0.80	
Silicon	0.002	5.6×10^{8}	0.1	
Titanium	-	5.8×10^{9}	-	
Aluminium	0.005	8.8×10^{11}	0.008	
Barium	-	3.3×10^{12}	-	
Magnesium	-	1.4×10^{13}	0.067	
Beryllium	-	5.4×10^{13}	-	
Calcium	-	4.3×10^{14}	-	

Table 3.4: Distribution value of minor elements in copper processing at 1250°C (Nagamori and Mackey, 1978)

Element	Relationship & Dependency	$L_{\mathrm{M}}^{s/m}$ (calculated*)
Ag	1000 (estimated), Independent to p_{O_2} and p_{S_2}	1000
As	30±10 (1200-1300°C), Independent to p_{O_2} and p_{S_2}	30
Au	2.5× 10^5, Independent to p_{O_2} and p_{S_2}	2.5× 10^5
Bi	15±5, Independent to p_{O_2} and p_{S_2}	15
Fe	Dependent on p_{O_2} and p_{S_2}	~10^{-4}
Ni	Dependent on p_{O_2} and p_{S_2}	1.38
Pb	Dependent on p_{O_2} and p_{S_2}	0.013
Sb	15±5, Independent to p_{O_2} and p_{S_2}	15
Se	$\frac{1}{L_{Se}^{S/m}} = (7+2t) \times 10^{-7} p_{O_2}{}^{-1/2} + 0.027 + 0.018t,$ Independent to p_{S_2}, t = 0.01(T-1523),	35.2
Sn	p_{O_2} and p_{S_2}	1.8
Te	$\frac{1}{L_{Te}^{S/m}} = (8+4t) \times 10^{-8} p_{O_2}{}^{-1/2} + 0.029 +$ $0.006t,$ Independent to p_{S_2}, t = 0.01(T-1523)	34.2
Zn	Dependent on p_{O_2} and p_{S_2}	6.33× 10^{-4}

* $p_{S_2} = 2.22 \times 10^{-6}$atm, $p_{O_2} = 2.41 \times 10^{-7}$atm

Nakajima et al. (2011) proposed that the precious metals such as Au, Pd, Ag, Pt and other metals such as Se, Te, Bi, and Sb remain in molten metal phase and these metals can be recovered or removed by the further processing such as electrorefining or hydrometallurgical processes. Some elements are also distributed in slag and metal, for example, In, Ni, Sn and Pb. A distribution-ratio chart of different phases in the copper converter of the copper processing is shown in Figure 3.3. It was reported that the distribution of minor elements largely depends on the operating temperature and oxygen partial pressure. The effect of temperature and oxygen potential on In, Ni, Pb, Sn distribution-ratio is shown in Figure 3.4. It actually indicates that higher temperature and lower oxygen pressure are beneficial to remove elements in a solvent metal. In addition, the slag composition also plays an important role in recovering or removing elements from the copper. It was also reported that copper scrap from e-waste was mixed with platinum group metals can be recovered from anode slime (Lu et al., 2012, Nakajima et al., 2011).

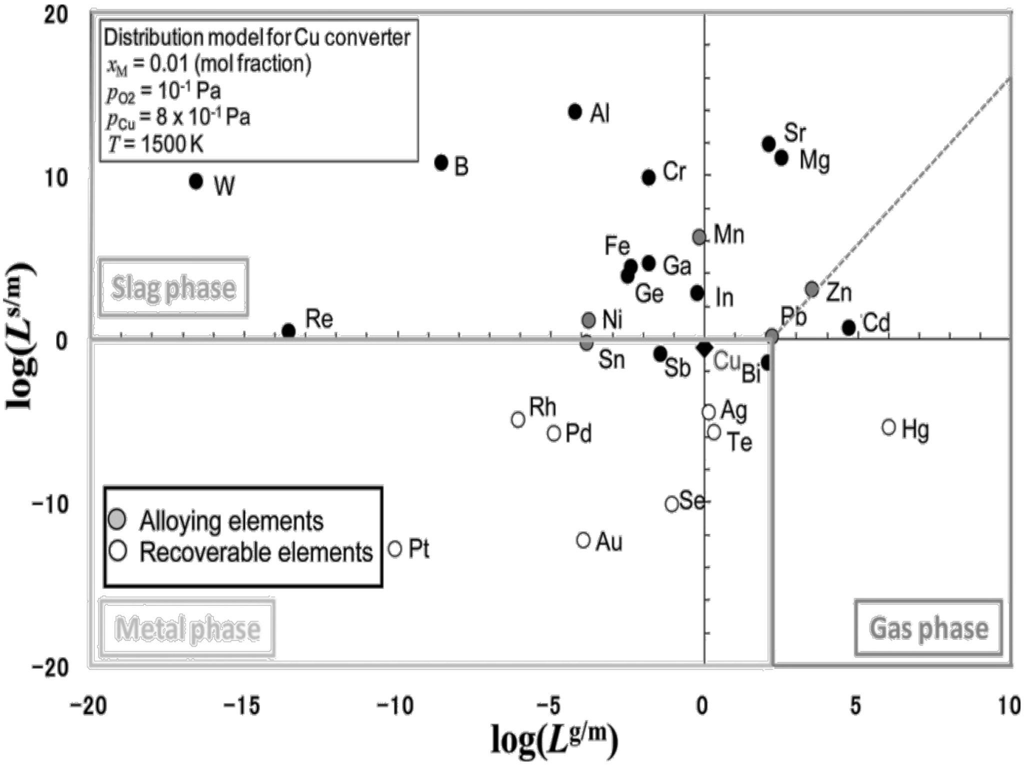

Figure 3.3: Metal distribution in different phases of the converter of the copper smelting in the certain atmosphere (Reprinted with permission from Nakajima et al., 2011).

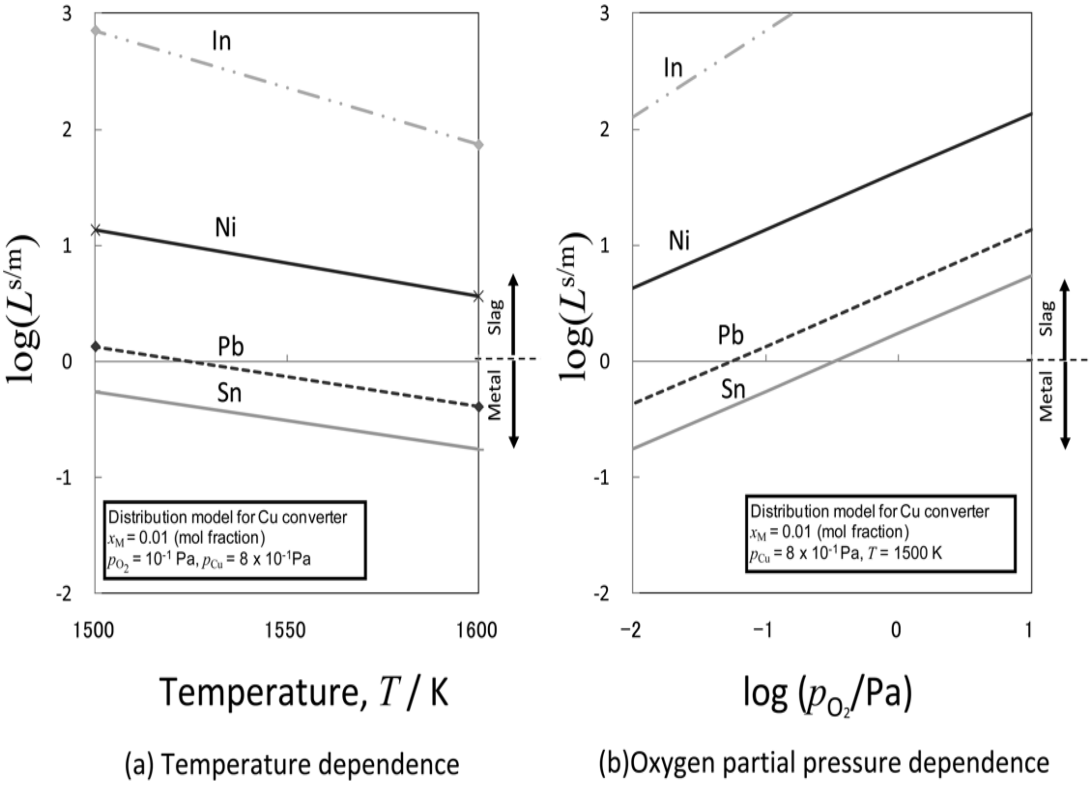

(a) Temperature dependence

(b)Oxygen partial pressure dependence

Figure 3.4: Effect of temperature and oxygen potential on the distribution-ratio of elements in a copper converter (Reprinted with permission from Nakajima et al., 2011).

Table 3.5: Gibbs energy data and activity coefficient of minor elements in copper

Reaction	**ΔG^o (J/mole)** **$\Delta G^o = \Delta H^0 - T\Delta S^0 = -RT\ln K$**	γ_M^0	**Reference**
$Cu\ (l) + \frac{1}{4} O_2(g) = CuO_{0.5}(l)$	-58800+19.55T	1	(Takeda et al., 1983, Yazawa, 1980)
$Ag\ (l) + \frac{1}{4} O_2(g) = AgO_{0.5}(s)$	-26020+40.00T	3.1	(Takeda et al., 1983, Yazawa, 1980)
$Co\ (l) + \frac{1}{2} O_2(g) = CoO\ (l)$	-235480+71.55T	14	(Takeda et al., 1983, Yazawa, 1980, Azakami and Yazawa, 1976)
$Sn\ (l) + \frac{1}{2} O_2(g) = SnO\ (l)$	-262290+86.57T	0.12	(Takeda et al., 1983, Yazawa et al., 1968)
$Sn\ (l) + \frac{1}{2} O_2(g) = SnO_2(s)$	-584090+212.55T		
$Pb\ (l) + \frac{1}{2} O_2(g) = PbO\ (l)$	-195100+77.7T	4.8	(Takeda et al., 1983, Yazawa, 1980)
$As\ (l) + \frac{3}{4} O_2(g) = AsO_{1.5}(l)$	-330620+115.39T	0.006 ~ 0.06	(Takeda et al., 1983, Hultgren et al., 1973)
$Sb\ (l) + \frac{3}{4} O_2(g) = SbO_{1.5}(l)$	-334820+114.23T	0.15 ~ 0.6	(Azakami and Yazawa, 1976, Takeda et al., 1983)
$Bi\ (l) + \frac{3}{4} O_2(g) = BiO_{1.5}(l)$	-284300+133.05T	0.1 ~ 1	(Azakami and Yazawa, 1976, Takeda et al., 1983)
$Te\ (l) + \frac{1}{2} O_2(g) = TeO_2(l)$	-315470+176.15T	0.033	(Sigworth and Elliott, 1974, Nagamori and Mackey, 1977, Mackey, 1982, Choi and Cho, 1997)
$Fe\ (\alpha) + \frac{1}{2} Te_2 = FeTe\ (s$	-46929+80.79T		
$Se\ (l) + \frac{1}{2} O_2(g) = SeO_2(s)$	-229870+189.74T	0.002	(Sigworth and Elliott, 1974, Nagamori and Mackey, 1977, Mackey, 1982, Choi and Cho, 1997)
$Fe\ (\alpha) + \frac{1}{2} Se_2 = FeSe\ (s)$	-148603+79.95T		

3.3.1 Distribution of tin in copper and slag

Tin is one of the common impurity elements found in the primary and secondary copper smelting processes. Tin is widely used in many electronic devices as a component of solder for joining on printed circuit board and as a protective coating on other metals. Tin is a relatively scarce element as its average concentration in the earth's crust is about 2 ppm (Emsley, 2001). However, in a personal computer about 1 mass pct of tin is found (Australian Bureau of Statistics, 2013). In copper smelting, it is expected that tin can be distributed between gaseous, metal and slag phases. At particular oxygen partial pressures (between 10^{-9} to 10^{-6} atm) tin remains as involatile SnO_2. As the partial pressure of oxygen decreases, for example when coke is added, SnO_2 is reduced to a volatile SnO which can segregate to off gas. The distribution-ratio data of tin in different slag system of copper smelting reported by previous researchers is shown in Figure 3.5 and the activity coefficient data of tin oxide in copper and various slag systems is presented in Table 3.6.

Takeda et al. (1983) and Yazawa et al. (1968) described the distribution-ratio of tin between slag and copper as a function of oxygen partial pressure. The authors pointed out that at high oxygen pressure, tin was found as a tetra-valent in a calcium ferrite (CaO-FeO_x) slag. However, it was not observed in an iron silicate (FeO_x-SiO_2) slag. It was also reported by Nagamori and Mackey (1977) that tin is present in the slag as SnO at oxygen partial pressures below 10^{-9} MPa (10^{-8} atm). In their work, they used alumina bearing iron silicate (FeO-Fe_2O_3-SiO_2-Al_2O_3) slag and copper reacted at 1200°C (1473 K) and 1300°C (1573 K). They also found that the presence of alumina in the slag had little effect on the tin distribution-ratio. Both Takeda et al. (1983) and Nagamori and Mackey (1977) observed a similar trend of tin distribution-ratio. Yazawa et al. (1999) also investigated distribution-ratio of tin between copper and ferrous calcium silica (FeO_x-CaO-SiO_2) (FCS) slag at oxygen partial pressure 10^{-12} to 10^{-9} atm at 1300°C (1573 K), where they found tin as SnO in slag and higher activity coefficient tin oxide in slag than that in calcium ferrite and iron silicate slag.

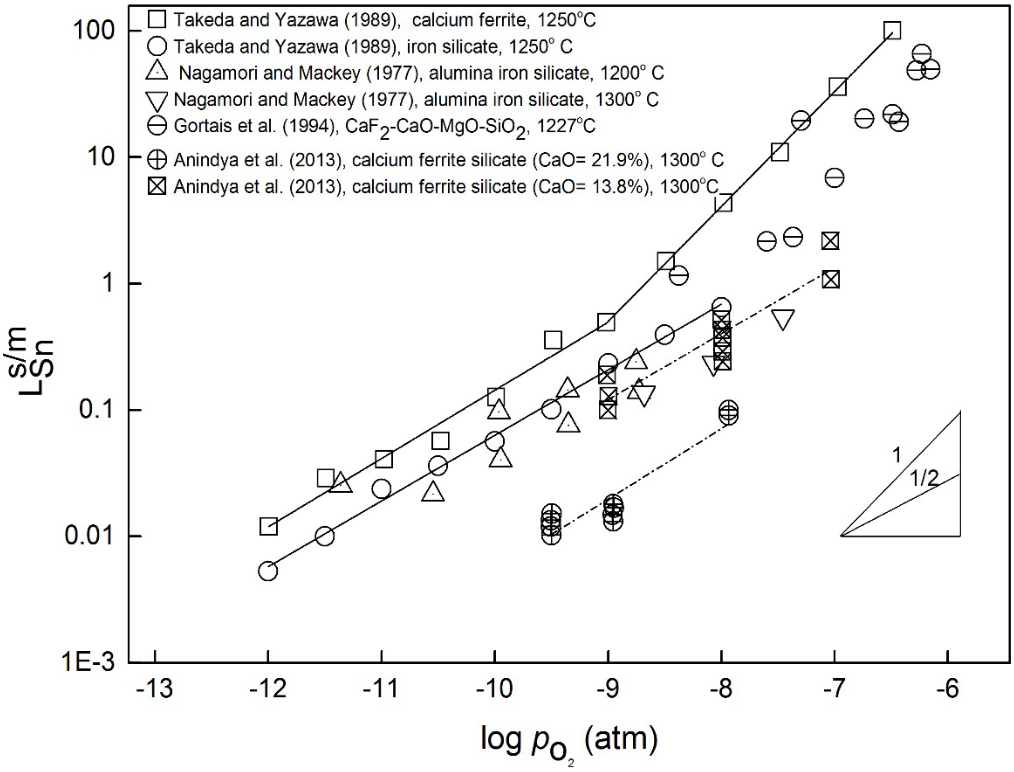

Figure 3.5: Published data summarised in the present study for tin distribution-ratio as a function of oxygen partial pressure in different slag systems and temperatures.

Gortais et al. (1994) carried out equilibrium experiments for Sn at 1227°C (1500 K) using CaO rich slag (CaF_2-CaO-MgO-SiO_2) in a magnesia crucibles. During oxidation and equilibration experiments, air and argon were used, respectively. They conducted the experiments with pure metal or Cu-based master alloys and calculated the activity coefficient of the oxides using the analytical results. It was confirmed from the investigation that tin is present as SnO_2 at high oxygen partial pressure.

Louey et al. (1999) investigated the distribution-ratio of minor elements between matte and fayalite slag at 1250°C (1523 K) using a muffle furnace. The experiments were conducted in magnesia crucible and at low oxygen partial pressure ($10^{-11.5}$ atm). It was found that tin behaved as SnO rather than SnO_2 and the distribution-ratio of tin was found to be of the value of 2.8±0.3. The value was close to the value reported by Koike and Yazawa (1994) and Yazawa et al. (1968).

Anindya et al. (2013) studied the distribution-ratio of tin between copper and ferrous calcium silica (FeO_x-CaO-SiO_2) slag at oxygen partial pressure below 10^{-10} MPa (10^{-9} atm) and at 1300°C (1573 K). The authors employed vertical tube furnace fitted with Pt/Pt-13 wt-%Rh thermocouples and magnesia crucible to conduct the experiments where oxygen partial pressure was controlled by mixing $CO/CO_2/N_2$ gas. The tin oxide was found in the form of monocation oxide in the slag as confirmed from the slope of the variation of tin distribution-ratio with partial pressure of oxygen as shown in Figure 3.5 (two sets of data at the lower part of the graph), which was also reported by Takeda et al. (1983), Yazawa et al. (1968) and Nagamori and Mackey (1977). They also found much lower distribution-ratio of tin in FCS slag and copper compared to previous studies (Takeda et al., 1983, Yazawa et al., 1968, Nagamori and Mackey, 1977, Takeda and Yazawa, 1989, Gortais et al., 1994).

It was also reported by Anindya et al. (2013) that the distribution-ratio of tin and copper decreases with increasing CaO concentration in the slag as shown in Figure 3.5. They attributed this to the increase of activity coefficient of tin oxide in slag with the increase of CaO. A relationship between γ_{CaO} and optical basicity (Λ) was also reported by Allibert (1995) as given in Eq.(3.9). From the correlation, it can be said that the distribution-ratio decreases with increasing CaO content in slag.

$$\log \gamma_{\mathrm{CaO}} = 12.5\Lambda - 10 \tag{3.9}$$

Table 3.6: Published data summarised in the present study of activity coefficient of tin oxide in various slags system

Investigators	p_{O_2} (atm)	Temperature [°C (K)]	γ_{SnO}
Iron Silicate Slag			
Nagamori and Mackey (1977)	$10^{-11} – 10^{-6}$	1200 (1473)	1.9±0.3
		1300 (1573)	0.8±0.1
Takeda et al. (1983)	10^{-9}	1250 (1523)	1.5
Takeda and Yazawa (1989)	$10^{-12} – 10^{-9}$	1300 (1573)	1.8
Louey et al. (1999)	$10^{-11.5}$	1250 (1523)	-
Calcium Ferrite Slag			
Takeda et al. (1983)	10^{-9}	1250 (1523)	0.9
Takeda and Yazawa (1989)	$10^{-12} – 10^{-9}$	1300 (1573)	1.2
Ferrous Calcium Slag			
Yazawa et al. (1999)	$10^{-12} – 10^{-9}$	1300 (1573)	5 – 6.2
Anindya et al. (2013)	$10^{-12} – 10^{-8.5}$	1300 (1573)	0.9 – 3
CaF_2-CaO-MgO-SiO_2			
Gortais et al. (1994)	-	1227 (1500)	-

Street et al. (2001) investigated the tin solubility in CaO bearing slag ($CaO-Al_2O_3-SiO_2$) at 1600°C (1873 K) and also studied the effect of oxygen partial pressure and slag composition. It was reported that solubility of tin is independent of oxygen potential in the range of p_{O_2} $10^{-19.5}$ to $10^{-15.5}$ atm. However, solubility of tin in slag was increased with increasing p_{O_2} in the higher oxygen potentials, because of tin oxide dissolution in slag.

An attempt was also taken by Li et al. (2009) to determine the thermodynamic properties of the Cu-Sn system and calculated the phase diagram. Lu et al. (2012) evaluated the thermodynamic data studied by many researchers and calculated the activity coefficient of tin in liquid Cu using interaction parameters and found good agreement with previously calculated value (Yazawa and Azakami, 1969).

Beyond the copper system, there are a number of studies on the thermodynamics of tin removal from steel scrap. Sano et al. (1998) and Kim et al. (2011) studied the recovery of tin from steel scrap. Wang et al. (1991) determined the activity of tin in liquid Fe-S alloy saturated with carbon and silver to understand the distribution behaviour and fundamental of thermodynamic.

The relationships of tin distribution-ratio in different slag systems with oxygen potential have been investigated by many researchers, but the effect of additive like Al_2O_3, MgO or mix thereof was not extensively studied. The effect of temperature has not been investigated in a wide range of oxygen partial pressure to understand the behaviour of tin in slags particularly to calculate the γ_{SnO} in slag.

3.3.2 Distribution of silver in copper and slag

Silver has long been valued as a precious metal, used in currency coins, to make ornaments, high-value tableware and utensils. The principle sources of silver are the ores of copper, copper-nickel and lead-copper. Silver is generally produced as a by-product in the electrolytic refining process of copper, gold, zinc and lead.

Takeda et al. (1983) and Yazawa et al. (1968) showed that the distribution-ratio of silver to the slag is very small because it is difficult to oxidize. Their experiments were carried out using calcium ferrite slag (25 mass pct CaO) at 1250°C (1523 K) under a current of the $CO-CO_2$ gas mixture (Takeda et al., 1983). Liquid copper containing up to 99 mass pct silver was equilibrated with the slag in a magnesia crucible. The dissolution of silver in calcium ferrite slag had not shown any dependency on the content of silver in copper. It is seen in Figure 3.6 that the distribution-ratio of silver depends on the oxygen potential.

Moreover, silver was primarily dissolved as a monovalent oxide such as $AgO_{0.5}$ at high oxygen pressure. They used basic slag in their experiment, but the effect of slag basicity or acidity on silver distribution-ratio was not reported.

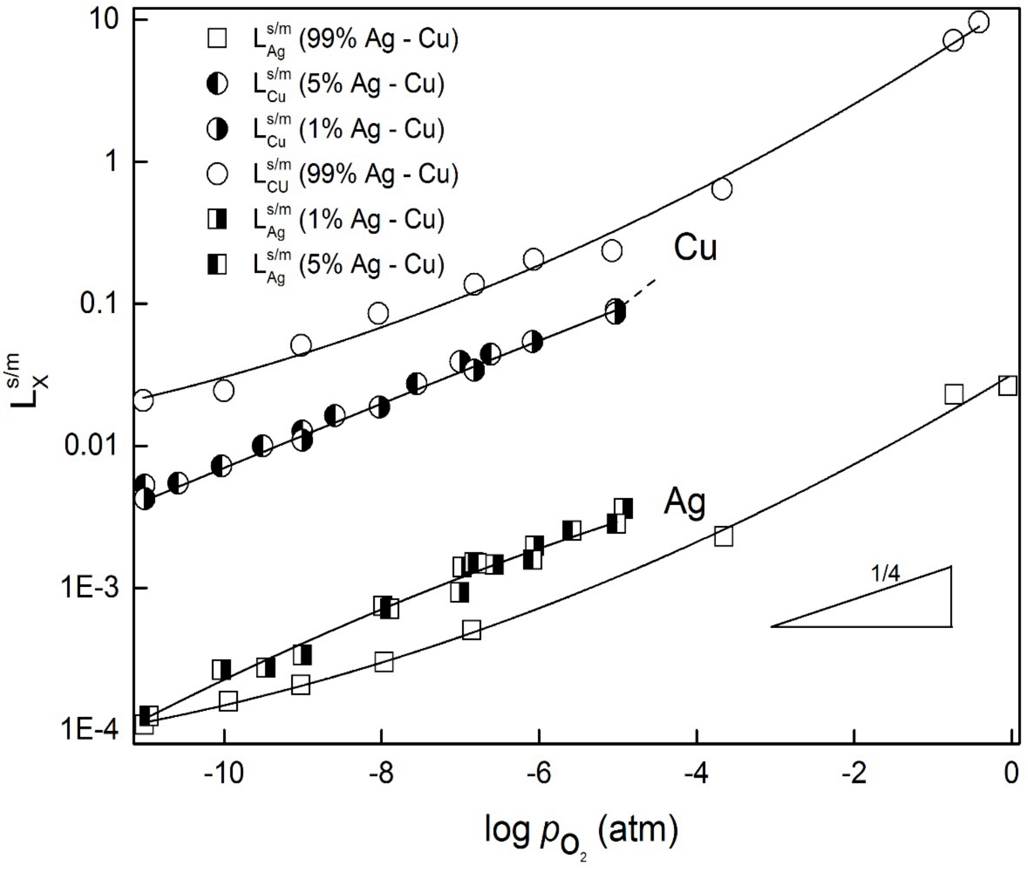

Figure 3.6: Distribution-ratio of copper and silver in matte and slag as function of log p_{O_2}, (reproduced from Takeda et al., 1983, Yazawa et al., 1968).

Louey et al. (1999) investigated the distribution-ratio of silver between copper matte and fayalite slag (FeO_x-SiO_2) at 1250°C (1523 K). The experiments were conducted in a magnesia crucible at a very low oxygen partial pressure ($10^{-11.5}$ atm). The silver matte/slag distribution-ratio was found to be 120±40 which is in agreement with previous results (Roghani et al., 1997a, Roghani et al., 1997b, Takeda and Roghani, 1993). However, Louey et al. (1999) found a discrepancy between the measured and the calculated distribution-ratio of silver, because the silver was present in slag as oxide rather than silver metal. They used a fixed oxygen potential rather than a range of oxygen partial pressure, therefore the oxidation state of silver in slag was not reported.

Kashima et al. (1978) carried out an investigation on the distribution-ratio of silver in copper, matte and an iron silicate (FeO_x-SiO_2) slag at 1300°C (1573 K) under controlled SO_2 partial pressure. A considerably scattered data was observed, therefore no conclusion was drawn on the effect of SO_2 potential. It was assumed that metallic silver dissolute in slag.

Avarmaa et al. (2015) investigated the equilibrium distribution-ratio of silver between iron silicate (FeO_x-SiO_2) slag and copper matte at 1250 to1350°C (1523 to 1623 K) under p_{O_2}, p_{S_2} and p_{SO_2}. The author reported that distribution-ratio of silver slightly increases with increasing of grade of copper matte. Apart from this, the effect of temperature on the solubility of silver in slag was very large, as volatilization of silver occurred at high temperature. Scatter was found in experimental results of the silver solubility in slag.

Schlitt and Richards (1975) determined the silver distribution-ratio in metal and matte systems at temperature 1150 to 1250°C (1423 to 1523 K) under CO_2-SO_2 and N_2 atmosphere. They had not found any dependency on temperature, oxygen and SO_2 partial pressure. It was pointed out that silver exhibits Henrian's behaviour, could be existed in monatomic state in metal and matte.

The solubility of silver in different slags was investigated (Park and Min, 2000, Park and Min, 1999) at high temperature and dissolution mechanism also examined in Na_2O-B_2O_3, CaO-B_2O_3 and BaO-B_2O_3 slags. It was suggested that solubility of silver decreases with increasing basic oxides content in the slag. In another study, the mechanism of silver loss in borosilicate slag was studied (Pickles et al., 2011). The ionic reaction of silver in MO-B_2O_3 (MO = CaO, Na_2O, BaO) slags at higher oxygen potential pressure is shown in following reaction (Park and Min, 2000):

$$\mathrm{Ag\ (l)} + \frac{1}{2}\mathrm{O_2\ (g)} + \mathrm{O^{2-}\ (slag)} = \mathrm{AgO}\,{}^{2-}_{2}\mathrm{(slag)} \tag{3.10}$$

The partitioning of silver metal is enhanced with the grade of copper matte, but the solubility of silver in slag can be increased with high operating temperature and high oxygen pressure. Therefore, low temperature is preferable for silver partitioning during smelting operation. Thermodynamic data on different slag system and the effect of slag additive have not been studied to understand the behaviour of silver in slags.

3.3.3 Distribution of indium in copper and slag

Indium is a relatively scarce element and the earth's crust average indium content is about 0.072 ppm. Indium is a critical metal and fifty percent of the amount produced being mainly used in LCD monitor and television as an oxide thin film, and also as a semiconductor material. Despite the amount of indium in these products is very small, the indium will be lost from material cycles if the discarded product is landfilled. Therefore, it is important to recycle indium-bearing materials.

There are very limited published studies on the distribution-ratio of indium in slag and molten copper metal. Some published data of distribution-ratio of indium in between lead or copper metal and slag system is shown in Figure 3.7.

Johnson (1983) carried out a study on the distribution-ratio of indium in $FeO-SiO_2-Al_2O_3-CaO-MgO-PbO$ slag and molten lead at temperature 1200°C (1473 K) and oxygen partial pressure at 10^{-12} atm. He studied the distribution behaviour of indium at a fixed oxygen pressure; therefore, the oxidation state of indium in slag was not assessed. The authors suggested that indium distribution-ratio was independent of Fe/SiO_2 ratio, and observed a declining trend when slag basicity is increased.

Hoang and Swinbourne (2007) measured the partitioning of indium in lead and FeO_x-SiO_2-CaO slag under oxygen partial pressure from 10^{-12} to 10^{-10} atm at 1200ºC (1473 K) using alumina crucible leading to the dissolution about 8 mass pct of alumina in the slag. They found that indium distribution-ratio increases with the increase of Fe/SiO_2 ratio of slag, but independent to CaO/SiO_2 ratio. Besides, highest distribution-ratio was found at most FeO-rich slag. It was reported that indium was present in slag as InO, however, evaluation of its Gibbs energy of formation suggests a formation of unstable indium oxide (Hoang and Swinbourne, 2007). The dissolution mechanism was not established from the study.

Anindya et al. (2014) determined the indium distribution-ratio in copper and $FeO_x-CaO-SiO_2$ slag at 1300°C (1573 K) under oxygen partial pressure from 10^{-6} to 10^{-8} atm. Magnesia crucibles were used to perform the experiments in the furnace leading to the dissolution of up to 6.5 mass pct of MgO in the slag. Indium was found to be in the form of $InO_{1.5}$ in slag due to the instability of InO. A similar result was also found by Henao et al. (2010), where they used a different analysis method, i.e., EPMA (Electron probe X-ray microanalysis) to avoid the systematic errors due to lead entrainment. Ionic fraction of indium oxide was calculated by Anindya et al. (2014) to investigate the acid-base characteristic and it was found that $InO_{1.5}$ behaves as neutral metal oxide in slag. The authors had not pointed out any particular mechanism or compound formation with the addition of lime in slag, but it was found that distribution of indium in metal increases with increasing of CaO in slag. Moreover, it was also suggested during the reduction stage of black copper smelting route that a high percentage of CaO could reduce indium loss to the slag (Anindya et al., 2014).

It was reported that indium solubility in slag changes with the basicity of slag (Ko and Park, 2011, Ko and Park, 2012). Ko and Park (2011) also determined that the indium solubility increases with increasing of silica content in slag, and it was reported that indium did not behave like neutral oxide. The dissolution mechanism of indium in CaO-SiO_2-Al_2O_3 slag was constructed in the following reaction (Ko and Park, 2012):

$$\mathrm{In\ (s)} + \frac{1}{4}\mathrm{O_2\ (g)} = \mathrm{In^+} + \frac{1}{2}(\mathrm{O^{2-}}) \tag{3.11}$$

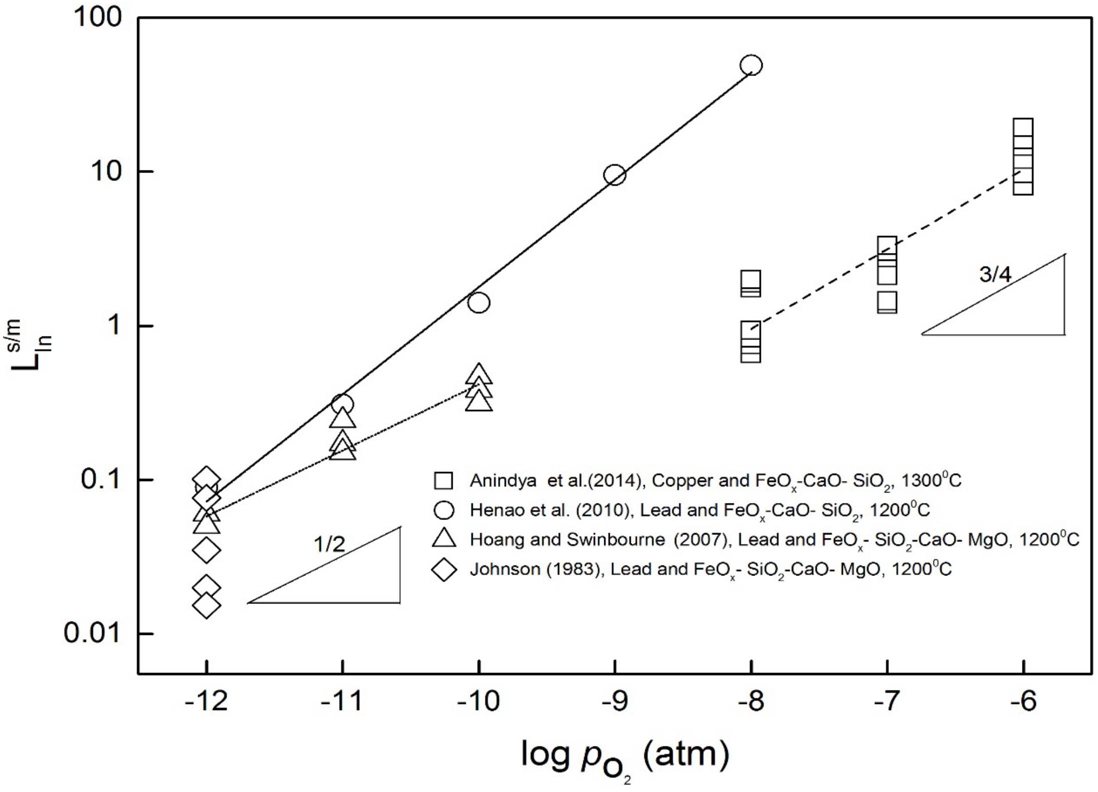

Figure 3.7: Published data summarised in the present study for indium distribution-ratio as a function of oxygen partial pressure.

Han and Park (2015) measured the indium solubility in FeO-SiO_2-Al_2O_3-5CaO-MgO_{sat} slag at 1300°C (1573 K) and oxygen potential 10^{-12} to 10^{-11} atm. They found that indium solubility increases with increasing oxygen potential in FeO-SiO_2-Al_2O_3-5CaO-MgO slag. The solubility of indium was found much lower in CaO-SiO_2-Al_2O_3 slag compared to FeO-bearing slag. It was found that dissolution of indium in FeO-SiO_2-Al_2O_3-5CaO MgO_{sat} decreases with increasing temperature, which indicates the exothermic nature of indium oxide (In_2O) in slag, and the species of indium oxide (In_2O) was found different than previous finding (Anindya et al., 2014, Hoang and Swinbourne, 2007). Nakajima et al. (2011) also reported that indium distribution-ratio mostly depends on temperature and oxygen partial pressure which has shown earlier in Figure 3.4. The presence of alumina in slag also affected the indium dissolution as it affects the basicity of slag. The acidic slag had more influence on the partitioning of indium over basic slag. The partitioning of indium to metal is enhanced in the presence of lime. It was suggested that a high temperature reducing atmosphere with low silica content in calcium aluminosilicate slag is a conducive condition for pyro-recycling of indium-bearing materials (Han and Park, 2015). The effect of slag additive have been investigated to understand the behaviour of indium in slags, but the dissolution mechanism of indium oxide in slags is still not fully understood.

3.3.4 Distribution of selenium and tellurium in copper and slag

Tellurium and selenium are commonly found in copper sulphide concentrates. Selenium has high affinity to copper and affects the softening properties of copper. Both of these elements have high value in electronic industries. Minor elements are required to be removed during the final refining step of copper production. The concentration of these minor elements in the anode copper has been increasing due to depletion of high-grade ores or the use of secondary resources (such as e-waste).

Nagamori and Mackey (1977) measured the solubility of selenium and tellurium in fayalite slag ($FeO-Fe_2O_3-SiO_2-Al_2O_3$) and metallic copper where they observed that the partitioning of selenium to slag decreases with increasing oxygen partial pressure. They investigated the distribution-ratio of Se and Te in metallic copper and alumina-containing fayalite slag at temperatures 1200°C (1473 K) and 1300°C (1573 K) in oxygen partial pressure between 10^{-11} to 10^{-6} atm and used $CO-CO_2$ gases to control the oxygen partial pressure inside the furnace. The effect of slag additive on the thermodynamic properties and activity coefficient of Se and Te was not investigated in their study. It was reported by Nagamori and Mackey (1977) that selenium and tellurium can be dissolved in slag both in elemental (Se^0, Te^0) and molecular (SeO, SeO_2, FeSe, TeO, TeO_2, FeTe) form and at low oxygen partial pressure in addition to atomic dissolution, they were dissolved as stable iron selenide and iron telluride. The distribution-ratio of Se was found increasing with lowering of the oxygen partial pressure. They found a constant relationship for tellurium with oxygen partial pressure. Alvear et al. (1994) reported that the distribution-ratios of Se and Te decrease with increasing oxygen partial pressure during reduction and opposite trend was found in oxidation in Na_2CO_3 slag system. The slag used by Alvear et al. (1994) in their investigation was not a common system used in industry. The activity of tellurium oxide and selenium oxide were reported to decrease with decreasing of the molar fraction of $NaO_{0.5}$

in $NaO_{0.5}$-CO_2-TeO_2 and $NaO_{0.5}$-CO_2-SeO_2 system which is also the indication of high partitioning ratio of Se and Te in metal for Na_2CO_3 slag system (Alvear et al., 1994).

The behaviour of selenium in iron silicate (FeO_x-SiO_2) slag was investigated by Fang and Lynch (1987). They equilibrated iron silicate (FeO_x-SiO_2) slag with a Cu-Se alloy at 1185°C (1458 K) and 1250°C (1523 K). They found that the nature of selenium species in the slag is in agreement with Nagamori and Mackey (1977). Fang and Lynch (1987) conducted their experiments in N_2 gas atmosphere and found that solubility of selenium was largely affected with Fe^{2+}/Fe^{3+} ratio and almost zero at very low ratio. But, the solubility of selenium had not been investigated in the reducing condition.

The distribution-ratios of selenium and tellurium between calcium ferrite slag saturated with magnesia (CaO-FeO-Fe_2O_3-MgO) and copper in oxygen partial pressures 10^{-9} to $10^{-0.68}$ atm at 1473 (1200°C) to 1673 K (1400°C) were investigated by Johnston et al. (2007). A negative correlation was found between the distribution-ratios of selenium and tellurium with oxygen partial pressure. In their study, pre-reduction of slag was carried out in a vertical tube furnace to reduce the equilibrium time. Magnesia was introduced in the slag from the crucible, and the gas mixture of CO_2/CO was used to control the oxygen partial pressure in the furnace. The results are shown in Figure 3.8 and Figure 3.9 compared with the result of Nagamori and Mackey (1977). Selenium and tellurium dissolve into the CaO-FeO-Fe_2O_3-MgO slag according to following ionic reaction (Johnston et al., 2007):

$$\mathrm{Se\ (s)} + \frac{1}{2}\mathrm{O_2\ (g)} = \mathrm{Se^{2+}} + (\mathrm{O^{2-}}) \tag{3.12}$$

$$\mathrm{Te\ (s)} + \frac{1}{2}\mathrm{O_2\ (g)} = \mathrm{Te^{2+}} + (\mathrm{O^{2-}}) \tag{3.13}$$

It was found that distribution-ratios of Se and Te are higher in magnesia saturated calcium ferrite slag compared to alumina bearing iron silicate slag. This was mainly due to higher activity of Se and Te in magnesia saturated calcium ferrite slag and that also increases with increasing temperature. It was reported that Se and Te enter into slag as a complex of calcium ($CaSeO_2$ and $CaTeO_2$) which are more stable thermodynamically with increasing temperature than iron compounds (Johnston et al., 2010, Johnston et al., 2007).

Johnston et al. (2007) also pointed out that the partitioning of Se and Te increases with increasing temperature. The effect of temperature and oxygen partial pressure on the Se and Te partitioning is also shown in Figure 3.8 and Figure 3.9, respectively. Nagamori and Mackey (1977), Nagamori et al. (1975b) and Takeda et al. (1983) agreed that the slag/copper distributions ratio of Se and Te increase with increasing temperature, therefore more Se and Te report to slag. Swinbourne et al. (1998) investigated tellurium distribution-ratio in copper anode slimes smelting at 1100ºC (1373 K) and found that lower smelting temperature and low oxygen partial pressure were preferable for tellurium elimination in anode furnace.

Zhao and Irons (1997) showed that selenium could be reduced using calcium carbide and sodium carbonate from molten copper at temperature 1300°C (1573 K) and they performed an experiment in MgO crucible. They used carbon to generate reducing conditions inside the furnace. They also developed a mathematical model and good agreement was found between the model and experimental results.

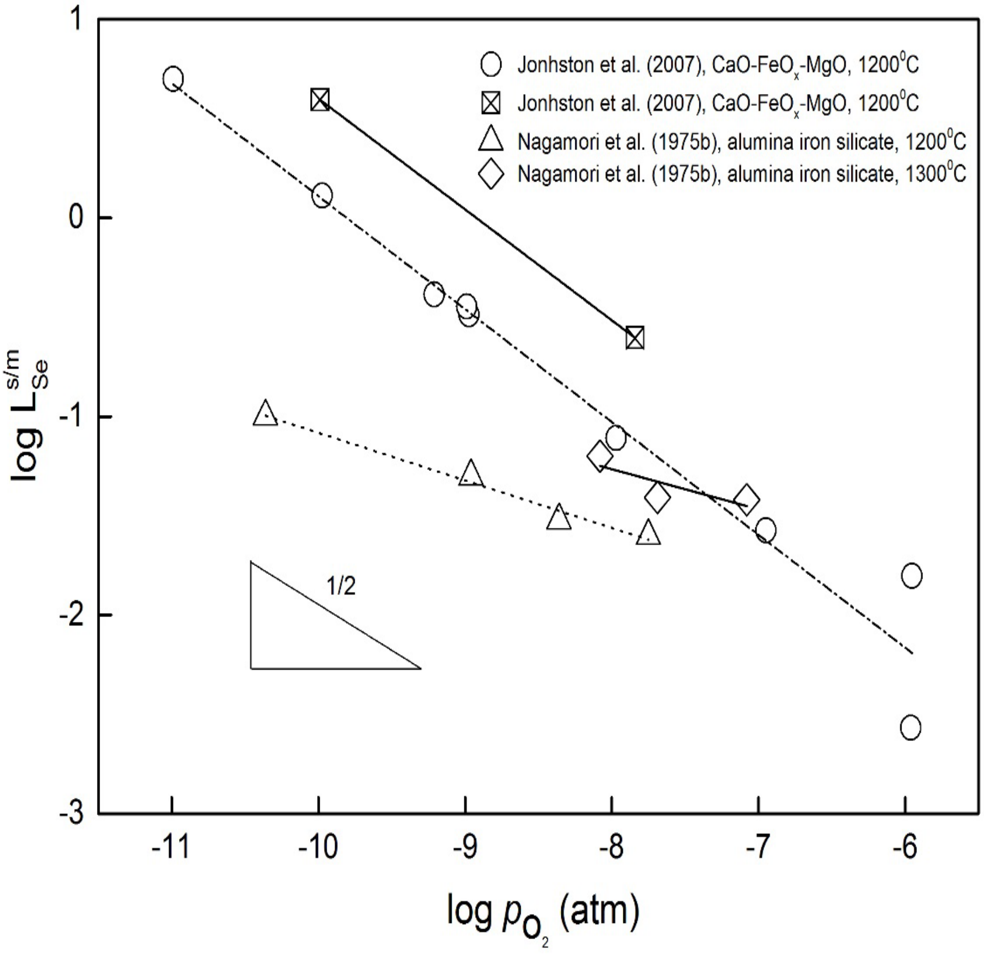

Figure 3.8: Published data summarised in the present study for selenium distribution-ratio in the slag and copper as a function of p_{O_2}.

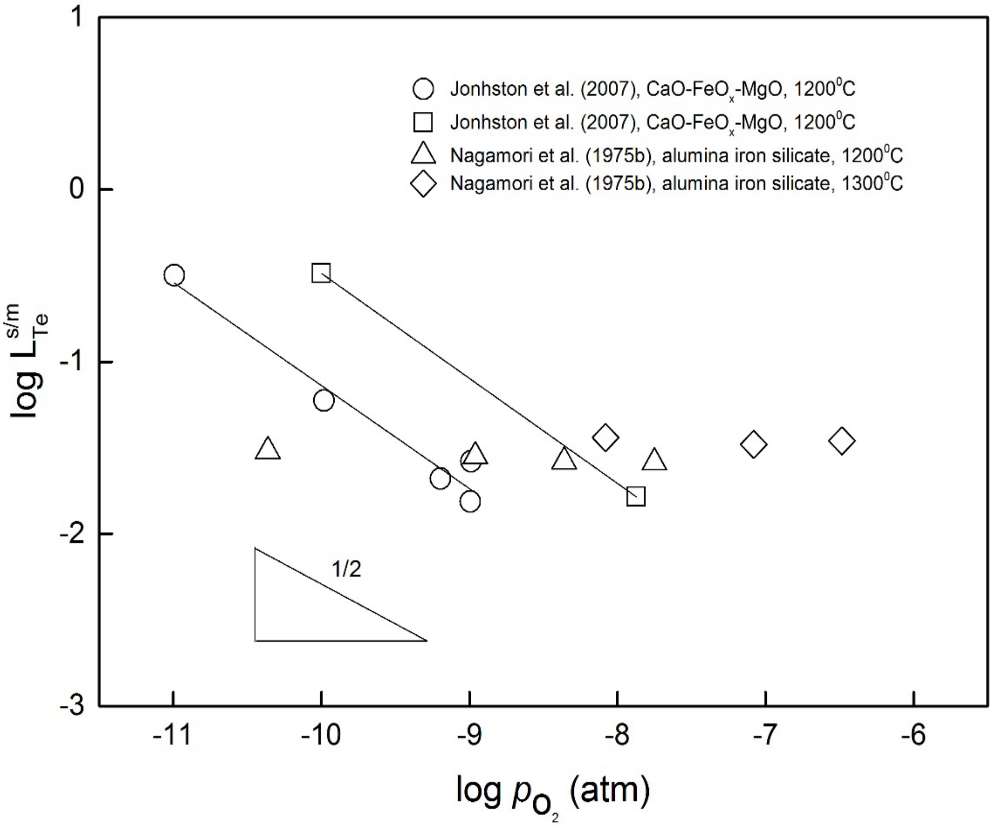

Figure 3.9: Published data summarised in the present study for tellurium distribution-ratio in the slag and copper as a function of p_{O_2}.

In summary, the partitioning of Se and Te to slag is enhanced in the presence of lime through the formation of complex calcium. In the presence of iron, iron selenide and iron telluride could form and also decrease the activity coefficient of Te and Se in slag. The effect of slag additive in iron silicate slag on the behaviour of selenium and tellurium has not been thoroughly investigated, therefore further study is required.

3.3.5 Distribution of platinum, palladium, gold and rhodium in copper and slag

The concentration of platinum group metals in the virgin ore is low (3-20 ppm), therefore most of them are recovered as by-products during nickel and copper smelting (Cabri, 1992, Graedel et al., 2002, Saurat and Bringezu, 2008). The trace concentration of platinum (Pt) in the end of life electronic and electrical products is 0.1-5 ppm. The platinum group metals (PGMs) are favourably recovered using current copper making circuits (Reuter and Kojo, 2014). Therefore, it is necessary to improve the knowledge in the behaviour of PGMs in different phases during copper smelting and converting.

An attempt was taken (Yamaguchi, 2010, Yamaguchi, 2013) to investigate PGM partitioning between copper and slag. A vertical tube furnace was used to determine the distribution-ratios of platinum and palladium in copper alloy and FeO_x-CaO slag and a mixture of CO-CO_2 gases were used to control the oxygen partial pressure inside the furnace. The experiments were carried out at 1300°C (1573 K) and in the range of oxygen partial pressure 10^{-9} to 10^{-5} atm in magnesia crucible with the nearly equal amount of FeO_x-CaO slag and copper alloy. Yamaguchi (2013) reported that the distribution-ratios of Pt and Pd in slag and liquid copper were increased with increasing partial pressure of oxygen (shown in Figure 3.10) and a small quantity of PGMs like palladium and platinum were lost in slag during the oxidation process. The effect of temperature and slag composition on activity coefficient of precious metal was not investigated in their work.

Henao et al. (2006) measured the distribution-ratios of platinum, palladium and rhodium between copper matte and iron silicate (FeO_x-SiO_2) slag in magnesia crucible at 1300°C (1573 K) under fixed partial pressure of SO2. It was found that distribution-ratios are constant up to 60 mass pct copper in matte and then increases with increasing matte grade. Henao et al. (2006) also reported that the distribution-ratios $L_x^{matte/slag}$ were found to be 1000 for palladium and 100 for platinum.

Recently, Avarmaa et al. (2015) investigated the equilibrium distribution-ratio of platinum, palladium and rhodium between iron silicate (FeO_x-SiO_2) slag and copper matte at 1250 to 1350°C (1523 to 1623 K) under controlled oxygen and sulphur pressure and fixed partial pressure of SO_2. It was found that distribution-ratios of platinum, palladium and rhodium increase with increasing matte grade (Avarmaa et al., 2015). The distribution-ratio $L_x^{matte/slag}$ were 3000 for palladium, 6000 for platinum, and 10000 for rhodium in a matte grade of 65 mass pct copper, respectively (Avarmaa et al., 2015). They also reported that the effect of temperature on the distribution-ratios was very small and the solubility of platinum and palladium in slag were increased with increasing matte grade. The solubility of platinum and palladium were also increased with increasing temperature and oxygen partial pressure (Avarmaa et al., 2015, Yamaguchi, 2010), as both platinum and palladium exhibit deviation from Raoultian behaviour in the dilute Cu-Pd and Cu-Pt system (Li et al., 2008, Abe et al., 2006).

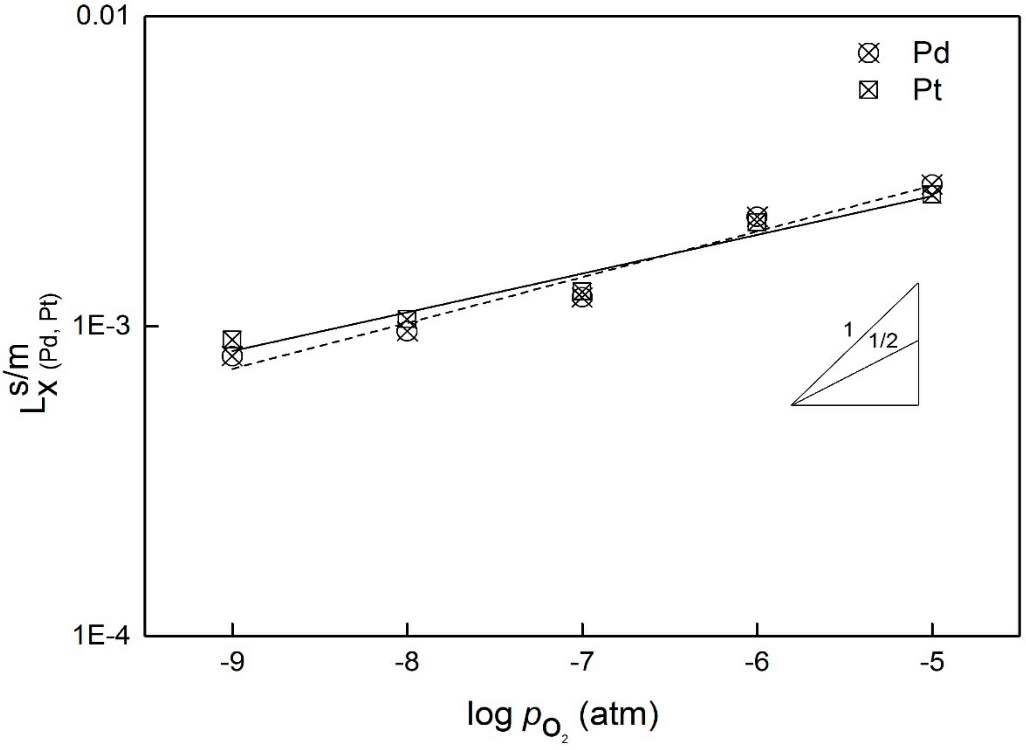

Figure 3.10: Distribution-ratio of platinum and palladium between FeO_x-CaO slag and copper alloy at 1300°C, (reproduced from Yamaguchi, 2013).

The solubility of gold in slags is very low. Nagamori and Mackey (1978) stated that gold dissolves as neutral atom in slag without any experimental evidence. Swinbourne et al. (2005) investigated gold solubility in metallurgical slag and it was found that solubility of gold in lead slag is higher compared to iron silicate and calcium silicate slag. Therefore, it is important to understand the behaviour of precious metal in slag. Recently, dissolution behaviour of precious metals like platinum (Nakamura et al., 1998, Nakamura and Sano, 1997, Wiraseranee et al., 2014), rhodium (Wiraseranee et al., 2013a, Wiraseranee et al., 2013b) and gold (Swinbourne et al., 2005, Schlitt and Richards, 1975, Han et al., 2015) have been studied to understand the dissolution reaction in slags. The ionic reactions of platinum in CaO-Al_2O_3 slag (Nakamura and Sano, 1997), gold in CaO-SiO_2-Al_2O_3-MgO_{sat} slag (Han et al., 2015) and rhodium in CaO-SiO_2 slag (Wiraseranee et al., 2013a) were suggested to follow these reactions:

$$\mathrm{Pt\ (s)} + \frac{1}{2}\mathrm{O_2\ (g)} + \mathrm{O^{2-}\ (slag)} = \mathrm{PtO_2^{2-} (slag)} \tag{3.14}$$

$$\mathrm{Rh\ (s)} + \frac{3}{4}\mathrm{O_2\ (g)} + \frac{1}{2}\mathrm{O^{2-}\ (slag)} = \mathrm{RhO_2^{-} (slag)} \tag{3.15}$$

$$\mathrm{Au\ (s)} + \frac{1}{4}\mathrm{O_2\ (g)} + \frac{1}{2}\mathrm{O^{2-}\ (slag)} = \mathrm{AuO^{-}\ (slag)} \tag{3.16}$$

$$\mathrm{Au\ (s)} + \frac{1}{4}\mathrm{O_2\ (g)} + \frac{3}{2}\mathrm{O^{2-}\ (slag)} = \mathrm{AuO}{}_{2}^{3-}\mathrm{(slag)} \tag{3.17}$$

The partitioning of platinum, palladium, gold and rhodium to metal is enhanced within the grade of copper matte up to 60 mass pct. However, the solubility of platinum and palladium in slag can be lower at a low operating temperature and low oxygen pressure. No detailed information has been found available on the effect of slag additive on the behaviour of PGM in slags.

3.3.6 Distribution of lead in copper and slag

Lead is one of the elements which is found abundantly in copper sulphide ores. It has no significant effect on electrical or heat conductivity of copper and its alloy. The presence of lead in copper can improve the machinability. Besides that, lead increases the volume of anode slime during electrorefining process and it is always practised to eliminate the lead during the copper smelting process. The summary of published data of lead distribution in copper and different slags is shown in Figure 3.11.

Takeda et al. (1983) and Yazawa et al. (1968) measured the lead partitioning between slag (calcium ferrite, FeO_x-CaO and iron silicate, FeO_x-SiO_2) and liquid copper under a CO-CO_2 atmosphere at 1250°C (1523 K). It was reported that lead exists in slag as PbO and partitioning to slag is higher in iron silicate (FeO_x-SiO_2) slag compared to calcium ferrite (FeO_x-CaO) slag. The activity coefficient of lead oxide was found to increase with increasing CaO content in slag. Takeda et al. (1983) reported the stability of lead oxide in slag increases with decreasing temperature.

Nagamori et al. (1975a) investigated the equilibration of lead in alumina bearing fayalite slag (FeO-Fe_2O_3-SiO_2-Al_2O_3-$CuO_{0.5}$) and metallic copper at 1200°C (1473 K) and 1300°C (1573 K) at oxygen partial pressure 10^{-11} to 10^{-6} atm under CO-CO_2 atmosphere. It was found that distribution-ratio of lead depends on oxygen partial pressure, and γ_{PbO} also increases with increasing Al_2O_3 content in the slag. The activity of lead oxide in slag was found to be 0.07, which was independent of oxygen partial and temperature (Nagamori et al., 1975a). It implies that lead dissolved in slag as oxide (PbO) was not in molecular form at all.

An attempt was taken by Kim and Sohn (1998) to measure the distribution behaviour of lead in copper and silica saturated iron silicate ($Fe0_x$-SiO_2) slag at 1250°C (1523 K) and

p_{O_2} of 10^{-12} to 10^{-6} atm. It was found that the distribution behaviour depends on oxygen partial pressure, slag basicity and FeO_n/SiO_2 ratio. It was observed similarly with previous finding (Takeda et al., 1983, Nagamori et al., 1975a). They also found that the activity coefficient of PbO and the partitioning of lead to slag and metal were not remarkably affected by the addition of Al_2O_3, CaO, MgO or a mixture thereof. Due to the addition of additive in slag, Pb^{2+} was replaced to decrease its proportion in slag by Ca^{2+}, Mg^{2+} and Al^{3+}, which was also reported by Takeda and Yazawa (1989).

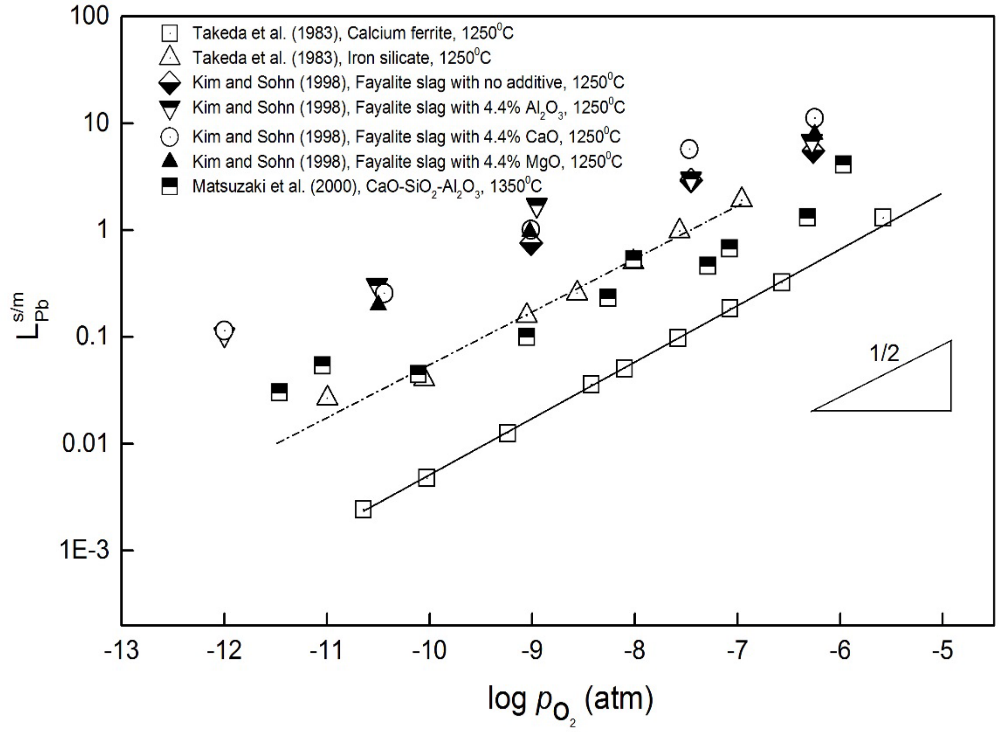

Figure 3.11: Published data summarised in the present study for lead distribution-ratio as a function of oxygen partial pressure in different slag systems.

It was proposed by Acuna and Yazawa (1987) that the distribution-ratio of lead was highest for iron silicate slag (FeO_x-SiO_2), followed by barium ferrite (FeO_x-BaO) and calcium ferrite (FeO_x-CaO) slags. They conducted the experiments in the Ar-SO_2 atmosphere at 1250°C (1523 K) for calcium ferrite and at 1300°C (1573 K) for barium ferrite considering the minimum melting point of Fe_2O_3-CaO and Fe_2O_3-BaO binaries (Acuna and Yazawa, 1987).

Matsuzaki et al. (2000) measured the distribution-ratio of lead between $CaO-SiO_2-Al_2O_3$ and liquid copper at 1350°C (1623 K) under H_2-CO_2 atmosphere. It was reported that the partitioning of lead was affected by oxygen partial pressure, temperature and slag basicity. The slag system was considered as a regular solution by Matsuzaki et al. (2000) to calculate γ_{PbO} and they found similar results indicated by Takeda and Yazawa (1989). It was also mentioned by Matsuzaki et al. (2000) that γ_{PbO} was decreased, as CaO was replaced with SiO_2 at a fixed Al_2O_3. In the study of Kim and Sohn (1998), it was also found that γ_{PbO} has a linear correlation with oxygen partial pressure.

Heo et al. (2012) investigated the distribution behaviour of lead between Fe_xO- SiO_2 - (CaO, Al_2O_3) and molten copper at 1200°C (1473 K) and 10^{-10} atm under CO_2-CO atmosphere. They found that lead partitioning decreases with increasing CaO and Al_2O_3 content in the slag. It represents very good agreement with Takeda et al. (1983) and Nagamori et al. (1975a). It was also proposed that due to the increase of alumina content, the activity of FeO decreases from about 0.45 to 0.25 which promotes the dissolution of lead into the slag (Heo et al., 2012). Furthermore, a good linear relationship was found between the lead partitioning with the lead capacity and activity of FeO.

Recently Kaur et al. (2009) measured the lead distribution-ratio between copper and ferrous calcium silicate (FeO_x-CaO-SiO_2) slag at 1300°C (1573 K) and oxygen partial pressure of 10^{-6} atm. The results showed that the lead partitioning in calcium ferrite slag (FCS) is better compared to in iron silicate slag. It was suggested by Kaur et al. (2009) to using FCS slag in the copper converter. The effect of slag basicity and oxygen partial pressure were not reported.

Degterov and Pelton (1999) optimized the thermodynamic database for equilibrium calculation of lead which relates to the copper production at temperature range 1150 to 1350°C (1423 to 1623 K) and oxygen partial pressure 10^{-10} to 10^{-6} atm. They reported that the distribution of lead is affected by slag basicity and Fe/SiO_2 ratio. The database was incorporated using modified quasichemical model to determine the lead distribution-ratio in different phase during copper production process.

Lead oxide (PbO) is an amphoteric oxide, it behaves as a strong basic oxide in the conditions of copper processing (Kim and Sohn, 1998, Matsuzaki et al., 2000, Heo et al., 2012). The partitioning of lead to slag is affected by basicity which can be increased by adding lime or alumina in slag. Moreover, high temperature and low oxygen potential also play important role in terms of lead recovery or elimination.

3.3.7 Distribution of cobalt in copper and slag

Cobalt is mostly found in nickel, silver, lead, copper and also in iron ores and it is recovered as a by-product. However, it is mostly associated with copper as sulphide concentrate. The distribution behaviour of cobalt is important to understand their partitioning during copper smelting.

The distribution-ratio of cobalt was investigated by Yazawa et al. (1968) between liquid copper and calcium ferrite (CaO-FeO_x) or iron silicate (SiO_2-FeO_x) slag at 1250°C (1523 K) under CO-CO_2 atmosphere and the result is shown in Figure 3.12. It was found that the distribution-ratio decreases with the lowering oxygen partial pressure. It was also reported that under oxidative smelting condition cobalt goes to slag and is then difficult to recover for a matte grade approximately above 80 mass pct Cu.

Kho et al. (2006) conducted two series of experiments with synthetic copper matte and synthetic magnesia saturated iron silicate (FeO_x-SiO_2-MgO) slag at 1250°C (1523 K) in a vertical tube furnace under a nitrogen atmosphere. In the first series, CoO was added to the slag and in the second series, CoS was added to matte. The distribution-ratio of cobalt in both series was found to be 4.3±0.9. There was a good agreement with the previous experimental results of Mwema et al. (1995). The distribution-ratio of cobalt was higher than the results of Yazawa et al. (1968). Furthermore, the experimental method of Kho et al. (2006) was different compared to previous studies.

Derin and Yücel (2002) studied the solubility of cobalt between Co-Cu and Al_2O_3-FeO- Fe_2O_3-SiO_2 slags at temperature 1350°C (1623 K) and oxygen partial pressure 10^{-10} to 10^{-8} atm. They found that γ_{CoO} increases with decreasing oxygen partial pressure or increasing solubility of cobalt. The Eq. (3.18) shows an equation for the activity coefficient of cobalt oxide in silica saturated fayalite slag with solubility of cobalt. It shows that γ_{CoO} increases with cobalt solubility in slag (Grimsey and Toguri, 1988). No information had been found about the effect of slag composition on the solubility of cobalt in other types of slag.

$$\gamma_{\mathrm{CoO}} = 1.94 + 0.123\ [\text{mass pct Co}] \tag{3.18}$$

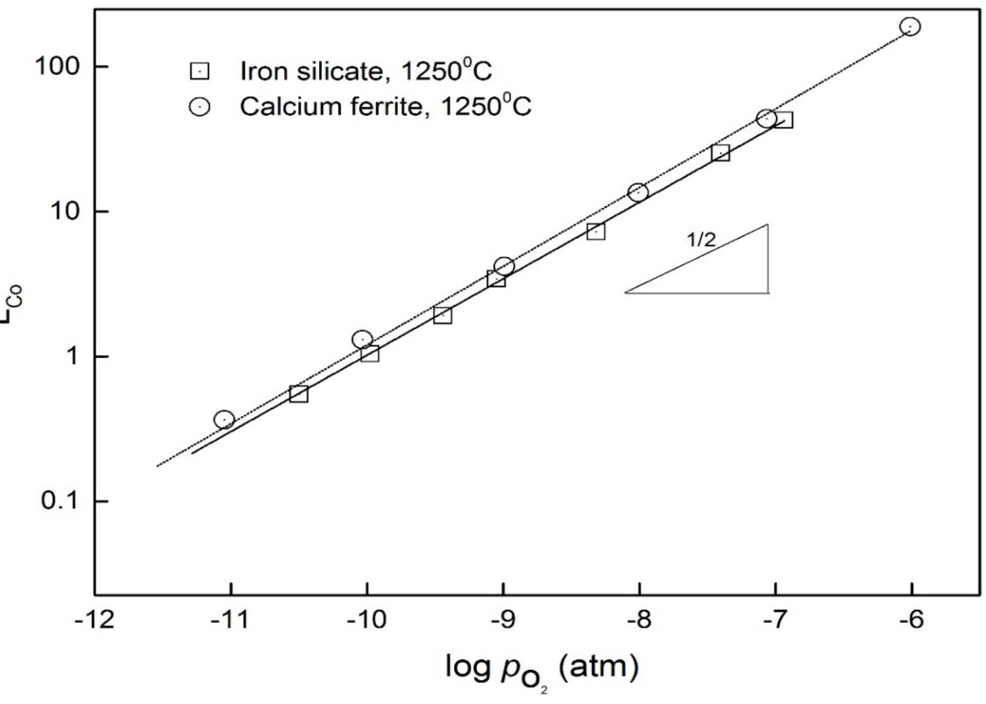

Figure 3.12: Published data for cobalt distribution-ratio as a function of oxygen partial pressure in different slag systems, (reproduced from Yazawa et al., 1968, Takeda et al., 1983).

Reddy and Healy (1981) investigated the distribution-ratio of cobalt in Cu-Co alloy and Cu_2O-CoO-SiO_2 slag in the temperature range 1200°C to 1300°C (1473 to 1573 K) under argon atmosphere, where they found that distribution-ratio of cobalt increases with decreasing temperature which is also in accordance with increase in cobalt solubility in slag with increasing Cu_2O/SiO_2 ratio. They proposed a relationship of distribution-ratio of cobalt as a function of temperature as shown in Eq. (3.19).

$$\log L_{Co}^{s/m} = {}^{2090}/_{T} + 1.26 \tag{3.19}$$

Grimsey and Liu (1997) measured the effect of additive in iron silicate slag (FeO_x-SiO_2) on the activity coefficient of cobalt oxide at an oxygen pressure of 10^{-9} to 10^{-10} at 1200°C (1573 K). They found that γ_{CoO} increases with increasing alumina, magnesia and calcia and decreases with increasing silica content in slag. According to Teague et al. (2001), γ_{CoO} increases with SiO_2 content in the slag, but above 4 mass pct SiO_2, it decreases due to precipitation of spinel crystals from the slag. Chen et al. (2004) reproduced the experimental data by model calculation for silica content up to 20 mass pct in slag. It was found that the presence of silica in calcium ferrite slag induces a strong interaction between CaO and SiO_2, thus lowering the interaction between CoO and CaO and resulting in the decrease of γ_{CoO} in slag (Chen et al., 2004).

Kubišta and Vřešt'ál (2000) determined the thermodynamic properties of Co-Cu system and calculated the phase diagram. They found very good agreement with the previous findings. Later, Lu et al. (2012) calculated the activity coefficient of Co in liquid Cu using interaction parameter determined by Kubišta and Vřešt'ál (2000).

The partitioning of Co to metal is enhanced in the presence of lime, magnesia or alumina in slag, as these increase the CoO activity in slag and the oxygen potential also plays important role in term of cobalt recovery (Grimsey and Liu, 1997, Eerola et al., 1984).

3.3.8 Distribution of arsenic, bismuth and antimony in copper and slag

Thermodynamic data play an important role to understand the behaviour of impurities usually found in copper smelting and converting processes. Arsenic, bismuth and antimony are harmful elements; therefore, it is practised to eliminate them during earlier processes. The summary of published data of distribution-ratio of arsenic, bismuth and antimony in different slag system in shown in Figures 3.13, 3.14, and 3.15, respectively and dissolution form of these metals in various slag systems is shown in Table 3.7.

Nagamori et al. (1975b) studied the distribution-ratio of arsenic, bismuth and antimony between slag (FeO-Fe_2O_3-SiO_2-Al_2O_3.$CuO_{0.5}$) and metallic copper at 1200°C (1473 K) and 1300°C (1573 K) at oxygen partial pressures 10^{-11} to 10^{-6} atm under CO-CO_2 atmosphere. It was found that distribution-ratios of Sb and Bi decrease with increasing temperature. This means that more bismuth and antimony goes to metal phase at higher temperatures. They could not determine the distribution-ratio of arsenic because of its low concentration in the slag. The distribution-ratios of Bi and Sb were found to be constant and independent of oxygen partial pressure and therefore dissolution of oxide species was ruled out. It was suggested that bismuth and antimony dissolved as an atomic form in slag. This was in good agreement with Jimbo et al. (1984).

Yazawa et al. (1968) and Takeda et al. (1983) measured the As, Bi and Sb partitioning between calcium ferrite (FeO_x-CaO) and iron silicate (FeO_x-SiO_2) slags and liquid copper under CO-CO_2 atmosphere at 1250°C (1523 K). It was reported that Bi, As, Sb dissolved through oxidic dissolution such as $BiO_{1.5}$, $AsO_{1.5,}$ $SbO_{1.5}$ respectively, which was in contrary to Nagamori et al. (1975b). Takeda et al. (1983) found a linear relationship between these metals partitioning and oxygen potential in iron silicate slag. It was also noticed that partitioning of arsenic and antimony was lower in iron silicate (FeO_x-SiO_2) slag compared to calcium ferrite (FeO_x-CaO) slag (Takeda et al., 1983), as shown in Figure 3.13 and Figure 3.15. Antimony and arsenic oxide are acidic which tend to form an oxide with basic flux.

Thus, the activity coefficient of $\gamma_{AsO_{1.5}}$ and $\gamma_{SbO_{1.5}}$ decrease with increasing CaO, which was also the reason of higher distribution-ratio of arsenic and antimony in calcium ferrite slag.

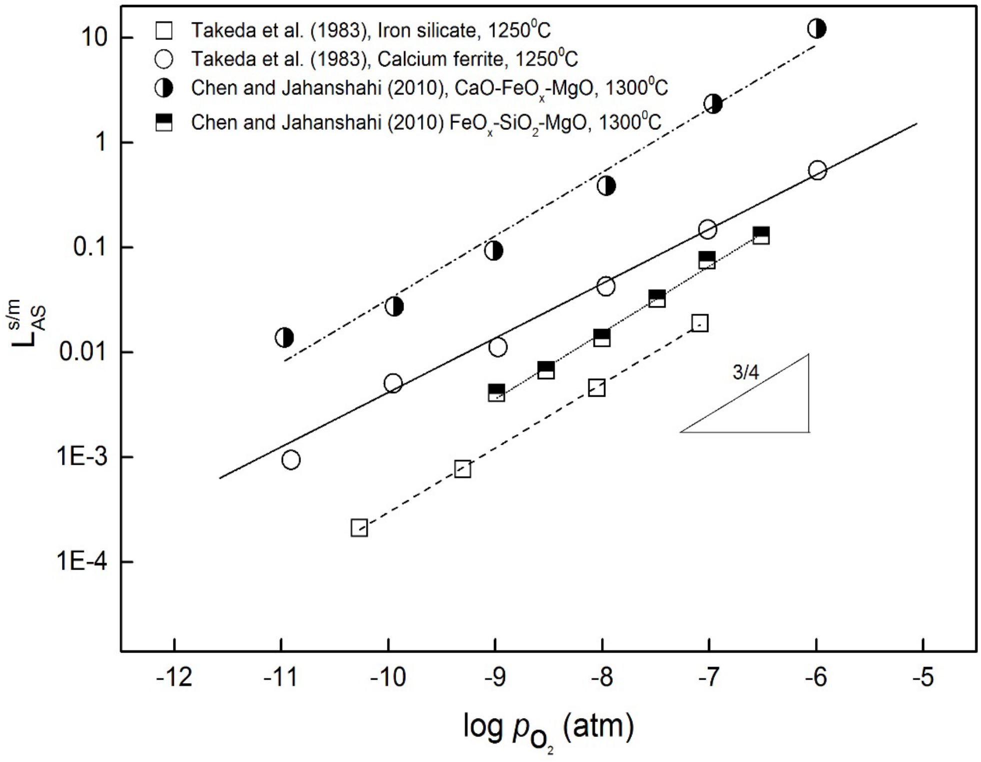

Figure 3.13: Published data summarised in the present study for arsenic distribution-ratio as a function of oxygen partial pressure in different slag systems.

An attempt was made by Kim and Sohn (1998) to examine the distribution behaviour of Bi, Sb and As in copper and silica saturated iron silicate (FeO_x-SiO_2) slag at 1250°C (1523 K) and p_{O_2} of 10^{-12} to 10^{-6} atm. It was reported that their distribution behaviour is independent of oxygen partial pressure which showed a good agreement with results from Nagamori et al. (1975b). They proposed that Bi, As and Sb dissolve as atomic form rather than as oxide in the slag and they found very small effect of Al_2O_3, CaO, MgO or a mixture thereof on the distribution-ratio. The effect of slag additives on the dissolution mechanism was not proposed in terms of ionic fraction because of limited information on ionic bonding.

Table 3.7: Dissolution form of bismuth, antimony and arsenic in slag according to literature

Investigators	**p_{O_2} (atm)**	**Temperature [°C (K)]**	**Results**
Iron Silicate Slag			
Nagamori et al. (1975b)	10^{-11} - 10^{-6}	1200 (1473) and 1300 (1573)	atomic dissolution (Bi,Sb,As)
Takeda et al. (1983)	10^{-11} - 10^{-6}	1250 (1523)	oxidic dissolution ($BiO_{1.5}$, $SbO_{1.5}$, $AsO_{1.5}$)
Jimbo et al. (1984)	10^{-11} - 10^{-7}	1200 (1473) and 1300 (1573)	oxidic dissolution (BiO, SbO, AsO)
Kim and Sohn (1998)	10^{-11} - 10^{-6}	1250 (1523)	atomic dissolution (Bi,Sb,As)
Chen and Jahanshahi (2010)	10^{-11} - 10^{-6}	1300 (1573)	oxidic dissolution ($AsO_{1.5}$)
Calcium Ferrite Slag			
Takeda et al. (1983)	10^{-11} - 10^{-6}	1250 (1523)	oxidic dissolution ($BiO_{1.5}$, $SbO_{1.5}$, $AsO_{1.5}$)
Eerola et al. (1984)	10^{-11} - 10^{-5}	1250 (1523)	oxidic dissolution ($BiO_{1.5}$, $SbO_{1.5}$, $AsO_{1.5}$)
Chen and Jahanshahi (2010)	10^{-11} - 10^{-6}	1300 (1573)	oxidic dissolution ($AsO_{1.5}$)
Ferrous Calcium Slag			
Paulina et al. (2013)	10^{-6}	1300 (1573)	oxidic dissolution ($BiO_{1.5}$)
Chen and Jahanshahi (2010)	10^{-11} - 10^{-6}	1300 (1573)	oxidic dissolution ($AsO_{1.5}$)
Kaur et al. (2011)	10^{-6}	1300 (1573)	oxidic dissolution ($SbO_{1.5}$)

Acuna and Yazawa (1987) studied the distribution-ratio of arsenic and antimony between matte and barium ferrite (FeO_x-BaO) slag at 1300°C (1573 K), and between matte and calcium ferrite (FeO_x-CaO) slag at 1250°C (1523 K). They found that distribution-ratio of arsenic and antimony decreases with increasing matte grade up to 70 mass pct. The distribution-ratio of arsenic and antimony were the highest for barium ferrite (FeO_x-BaO) and followed by calcium ferrite (FeO_x-CaO) and iron silicate slag (FeO_x-SiO_2).

Roghani et al. (1996) investigated the distribution-ratio of As, Bi and Sb between calcium ferrite slag and copper matte at 1250°C (1523 K) under high partial pressure of SO_2 and found that the distribution-ratio decreases with increasing partial pressure of SO_2. According to Roghani et al. (1996), As and Sb were stable in matte phase, therefore constant ratio of $L_{As}^{s/m}$ and $L_{Bi}^{s/m}$ were found against matte grade in low region. However, $L_{As}^{s/m}$ and $L_{sb}^{s/m}$ were found to increase with increasing mass pct Ca in the slag, whereas $L_{Bi}^{s/m}$ showed constant value. The results were in good agreement with a previous finding (Takeda et al., 1983). Roghani et al. (1996) proposed the oxidic dissolution of As, Bi and Sb in slag similar to Yazawa et al. (1968), but oxidation state was not reported.

Riveros et al. (1987) determined the distribution-ratio of arsenic and antimony between Na_2CO_3-Na_2O-SiO_2 and molten copper at 1250°C (1523 K). They found that higher valence species are more stable with an increase of oxygen potential and basicity. The most stable oxide species of arsenic was found to be $AsO_{2.5}$ which was in disagreement with earlier results (Takeda et al., 1983, Kim and Sohn, 1998, Roghani et al., 1996).

Yazawa et al. (1999) first reported the use of ferrous calcium silicate (FCS) slag in copper smelting and converting because the slag was not caused remarkable damage to refectories and also has high viscosity than traditional slag. There had been no other reports found in the literature on distribution-ratio of antimony, arsenic and bismuth in ferrous calcium silicate slag (FeO_x-CaO-SiO_2) and copper. Recently, Kaur et al. (2011), Chen and Jahanshahi (2010) and Paulina et al. (2013) studied the distribution-ratio of antimony, arsenic and bismuth in ferrous calcium silicate slag (FeO_x-CaO-SiO_2) and molten metal (copper or silver) at 1300°C (1573 K)

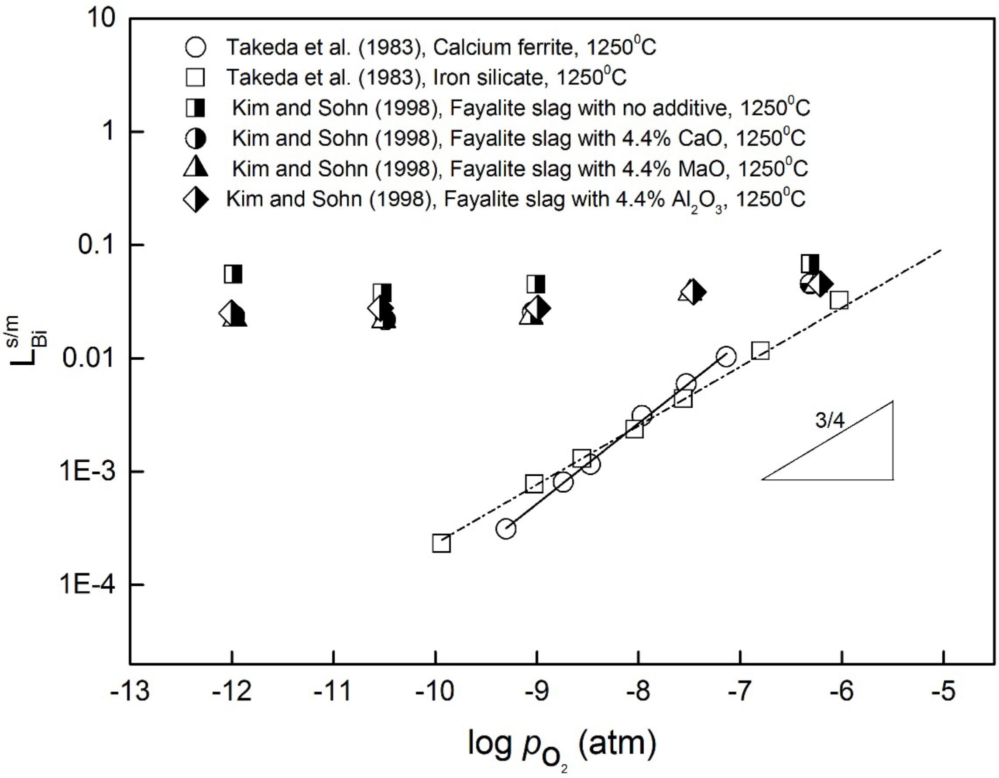

Figure 3.14: Published data summarised in the present study for bismuth distribution-ratio as a function of oxygen partial pressure in different slag systems.

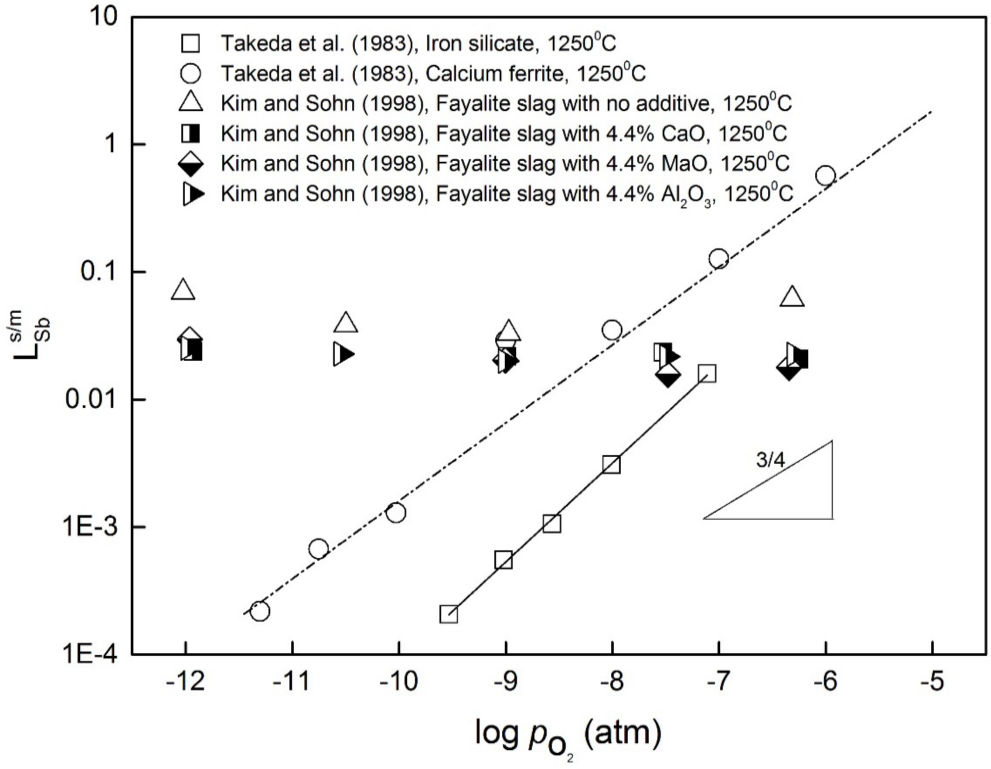

Figure 3.15: Published data summarised in the present study antimony distribution-ratio as a function of oxygen partial pressure in different slag systems.

It was proposed by Kaur et al. (2011) that antimony dissolves in ferrous calcium silicate slag (FeO_x-CaO-SiO_2) as $SbO_{1.5}$. The experiments were performed in a vertical tube furnace using magnesia crucible at a fixed oxygen partial pressure 10^{-6} atm rather than a range of oxygen partial pressure to confirm the oxidation state of arsenic in the slag. The distribution-ratio of arsenic was found to be lower than the calcium ferrite slag.

Paulina et al. (2013) determined the distribution-ratio of bismuth ferrous calcium silicate slag (FeO_x-CaO-SiO_2) and copper at a fixed oxygen partial pressure 10^{-6} atm. The distribution-ratio of bismuth was affected by the CaO content in slag, which is also shown by Takeda et al. (1983), but independent of Fe/SiO_2 ratio. Paulina et al. (2013) compared the distribution-ratio of bismuth with previous results (Takeda et al., 1983, Gortais et al., 1994) and it was predicted that bismuth dissolves in ferrous calcium silicate slag (FeO_x-CaO-SiO_2) as $BiO_{1.5}$. Furthermore, it was also shown using previous data (Nagamori et al., 1975b, Teppo et al., 1990) that activity coefficient of bismuth in liquid copper decreases with increasing temperature.

Chen and Jahanshahi (2010) measured the distribution-ratio of arsenic between magnesia saturated ferrous calcium silicate (FeO_x-CaO-SiO_2-MgO and silver using classical metal-slag-gas equilibrium technique at 1300°C (1573 K) and oxygen partial pressure = $10^{-11} - 10^{-6}$ atm. The oxide species of silver ($AgO_{0.5}$) was unstable and the solubility of silver was very low, therefore silver-arsenic alloys were used in their experiment to understand the effect of oxygen partial pressure, where they found that $\mathrm{L}_{\mathrm{As}}^{\mathrm{s/m}}$ was strongly affected by the p_{O_2}, and it was considered that arsenic dissolves in slag as $AsO_{1.5}$. Distribution-ratio of arsenic in calcium ferrite slag was one magnitude higher than in iron silicate slag, which is also consistent with the results of Takeda et al. (1983). Chen and Jahanshahi (2010) also studied the effect of slag composition on distribution-ratio of arsenic, where they found that $\mathrm{L}_{\mathrm{As}}^{\mathrm{s/m}}$ decreases with increasing silica content in the slag. According to them, oxygen partial pressure also affected the activity coefficient of arsenic oxide ($\gamma_{AsO1.5}$) and it was found that $\gamma_{AsO1.5}$ in iron silicate slag was 40 times higher than that in calcium ferrite slag. Magnesia was also found to dissolve from the crucible up to 12 mass pct but the effect of basicity due to magnesia content in the slag on $\mathrm{L}_{\mathrm{As}}^{\mathrm{s/m}}$ and $\gamma_{AsO1.5}$ were not reported.

Wypartowicz (1995) re-examined thermodynamic properties of Cu-As liquid solution within the temperature range 950°C to 1175°C (1223 to 1448 K), where they found that the activity of arsenic in copper decreases with increasing temperature. However, relation of the activity coefficient of arsenic and arsenic oxide with temperature were not studied extensively.

In summary, basic slag has an influence on the partitioning of antimony and arsenic, whereas acidic slag influences the partitioning of bismuth. Temperature and oxygen potential also play an important role on the distribution behaviour. There is gap in knowledge regarding the effect of temperature and slag composition on the distribution behaviour of antimony, arsenic and bismuth in FCS slag.

3.4 Acid-base nature of oxides of trace valuable elements

According to the ionic theory of slag, acidic slags such as silicates melt have a long chain structure, while basic slags have free cations and O^{2-} ions which can disrupt the acidic slags chain. Understanding the acid-base nature of the slags and the oxides of the trace valuable elements can provide a basis for understanding the behaviour of the elements partitioning between slag and other phases. It was described by Gilchrist (1989) that the acid- base nature of metal oxide has some relation to the electrostatic bond strength which represented by a ratio z/a^2 where 'z' is the charge of metal ion and 'a' is the sum of ionic radii of two ions (r_{cation} + r_{anion}). It was proposed the ratio range of 0.1 - 0.35 is for basic oxides, 0.39 - 0.90 is for intermediate oxides and greater than 1 is for acidic oxides.

There are also other concepts that are commonly used to characterize the acid-base nature of liquid oxides and to provide a measure of thermodynamic activity of free oxygen ion. A simple "V-ratio", which is a weight ratio of CaO to SiO_2, is widely used by engineers in steelmaking industries to provide a practical measure of basicity. Another method of comparing the basic strength of oxides is through the decomposition behaviour of the specific as carbonates and sulphates (Chipman and Chang, 1949).

In the early 1970's Duffy and Ingram (1976) introduced an optical basicity concept, which is mainly a measure of oxygen donation power relative to CaO, which has been used widely to evaluate the influence of slag composition on the thermochemical and thermophysical properties. The optical basicity also relates to another measure of the structure of glass such as the number of non-bridging oxygen per tetrahedron (NBO/T) (Lide, 2003). Moreover, the overall average state of oxygen in a particular slag system can be determined from the optical basicity.

The calculated values of z/a^2 and optical basicity of selected oxides of interest, as a mean to characterize their acid-base nature, are shown in Table 3.8. The information can help understand the behaviour of the oxides of the trace valuable elements in the slag systems, particularly on their general partitioning behaviour. For example, one would expect that partitioning of Pb into an acidic slag would be higher compared to a basic slag, as the oxide of Pb (PbO) tends to show basic nature. It is also worth to notice some disagreements in the relative order of the oxides represented by the calculated electrostatic bond strength and optical basicity in Table 3.8, which highlights that currently there is no universal approach in expressing the ionic nature of liquid slags/oxides.

There is only limited work have been done that tries to relate optical basicity to the distribution behaviour of valuable elements (associated with e-waste) in metallurgical slag systems (Han et al., 2015, Han and Park, 2015). Anindya et al. (2014) found a good agreement on the nature of indium oxide from the theoretical and experimental point of view and reported that the nature of indium oxide found in FCS slag is neutral.

Table 3.8: Calculated optical basicity and electrostatic bond strength $\left({z}/{a^2}\right)$ of oxides of trace valuable elements (Gilchrist, 1989, Duffy and Ingram, 1976, Rodriguez et al., 2011)

Trace elements	**Oxide**	**Calculated Optical Basicity**	${z}/{a^2}$	**Characteristics of oxide**[*]
Ag	Ag_2O	0.91	0.15	Basic
Pb	PbO	1.19	0.30	
Ca	CaO	1.0	0.35	
Pd	PdO	1.18	0.39	Intermediate (neutral)
Co	CoO	0.98	0.43	
Sn	SnO_2	0.85	0.46	
Bi	Bi_2O_3	1.19	0.51	
In	In_2O_3	1.06	0.62	
Sb	Sb_2O_3	1.18	0.64	
Te	TeO_2	0.93	0.71	
Ga	Ga_2O_3	0.76	0.74	
Al	Al_2O_3	0.60	0.80	
As	As_2O_3	1.01	0.87	
Ge	GeO_2	0.61	1.07	Acid
Se	SeO_2	0.95	1.11	
Si	SiO_2	0.48	1.23	

* Characteristics of the nature of oxides on the basis of ${z}/{a^2}$, where z = cation charge, a = sum of ionic radii of ions proposed by Gilchrist (1989)

3.5 Gaps in knowledge

E-waste is a heterogeneous mixture of non-metallic and metallic materials and it contains 13% nonferrous metals (Anindya et al., 2013). Among these non-ferrous metals have some valuable elements like Au, Ag, Sn, In, Pt, Ga, Rh, Co and Ge. The distribution-ratio and partitioning behaviour of common elements such as Au, Ag, Se, Te, Sn, Pb, Bi, As, and Sb in the conditions relevant to primary copper processing have been studied by a number of researchers. However, limited data were found for the elements Pt, Pd, Rh, In and Co and no data were found for Ge, Ta and Ga. Black copper route has always been used to recover tin and indium, and it has been found that during indium processing, it reports to gas phase as In_2O_3 (Anindya et al., 2014, Anindya et al., 2013). The increasing interest in precious metals have heightened the need for further studies to understand the behaviour of all of these metals found in e-waste during black copper processing. Unfortunately, the information and data on the distribution behaviour of these elements in the conditions relevant to secondary copper processing are not available except for Sn and In. The summary of previous studies of valuable elements distribution is shown in Table 3.9. It can be seen from the Table 3.9, that the majority of the thermodynamic data existed are relevant to primary rather than secondary copper processing.

The concentration of the trace valuable elements in the copper is very small and it may be considered that they obey Henry's Law and behave like dilute solution (Nagamori et al., 1975a). Nevertheless, the presence of multi-solute elements in a solution can affect each other thermodynamic behaviours. One important aspect that needs to be mentioned is the fact that the majority of the previous partitioning behaviour studies focused on selected individual trace elements and assuming that the influence of one trace element in copper on the activity of other trace elements is negligible, such as in the study by Nagamori et al. (1975a). But, in real systems when there is more than one trace element, such as in processing of e-waste via copper smelting, it is necessary to consider the trace elements confluence effect, which usually represented by interaction parameters (Sigworth and Elliott, 1974). To fully understand the distribution behaviour the interaction parameters will need to be taken into consideration for complex systems.

Resource efficiency and metal recycling are inter-connected to Circular Economy (CE). Therefore, the present study lies at the heart of realizing a CE (EU, 2015) and the key role of this work plays in a CE have also been reported by Reuter and Kojo (2014).

Table 3.9: Summary of previous work of trace valuable elements distribution in primary and secondary copper smelting

Metal	**Primary Copper Processing**	**Ref.**	**Secondary Copper Processing**	**Ref.**
Ag	Data available	(Takeda et al., 1983, Yazawa et al., 1968, Nagamori and Mackey, 1978, Mackey, 1982, Fountain et al., 1991, Louey et al., 1999, Schlitt and Richards, 1975, Takeda and Roghani, 1993, Gortais et al., 1994, Yazawa, 1974, Yazawa and Takeda, 1982, Avarmaa et al., 2015, Kashima et al., 1978)	No data available	-
Au	Limited data available	(Han et al., 2015, Swinbourne et al., 2005, Schlitt and Richards, 1975, Nagamori and Mackey, 1978)	No data available	-
Pt	Limited data available (matte-slag system)	(Avarmaa et al., 2015, Henao et al., 2006, Yamaguchi, 2010, Yamaguchi, 2013, Schlitt and Richards, 1975)	No data available	-
Pd				
Rh	Limited data available (matte-slag system)	(Avarmaa et al., 2015, Henao et al., 2006)	No data available	-
Se	Data available	(Nagamori et al., 1975b, Nagamori and Mackey, 1978, Nagamori and Mackey, 1977, Alvear et al., 1994, Johnston et al., 2010, Johnston et al., 2007, Choi and Cho, 1997, Fang and Lynch, 1987, Zhao and Irons, 1997, Swinbourne et al., 1998)	No data available	-
Te				
Sn	Data available	(Takeda et al., 1983, Takeda and Yazawa, 1989, Yazawa and Takeda, 1982, Yazawa et al., 1968, Nagamori and Mackey, 1977, Louey et al., 1999, Mackey, 1982, Nakazawa and Takeda, 1983, Fountain et al., 1991, Gortais et al., 1994, Roghani et al., 1997b, Roghani et al., 1997a)	One data available	(Anindya et al., 2013)

In	Very limited data available	Nakajima et al. (2011)	Two data available	(Anindya et al., 2014, Han and Park, 2015)
Pb	Data available	(Nakazawa and Takeda, 1983, Takeda et al., 1983, Takeda and Yazawa, 1989, Yazawa et al., 1999, Yazawa et al., 1968, Nagamori et al., 1975a, Nagamori and Mackey, 1978, Acuna and Yazawa, 1987, Degterov and Pelton, 1999, Kaur et al., 2009, Kim and Sohn, 1998, Matsuzaki et al., 2000)	No data available	-
Bi	Data available	(Nakazawa and Takeda, 1983, Takeda et al., 1983, Yazawa and Takeda, 1982, Yazawa et al., 1968, Nagamori et al., 1975a, Nagamori et al., 1975b, Nagamori and Mackey, 1978, Mackey, 1982, Paulina et al., 2013, Kaur et al., 2009, Kaur et al., 2011, Chen and Jahanshahi, 2010, Roghani et al., 1996, Jimbo et al., 1984, Riveros et al., 1987, Kim and Sohn, 1998)	No data available	-
As				
Sb				
Co	Data available	(Choi and Cho, 1997, Derin and Yücel, 2002, Grimsey and Toguri, 1988, Kho et al., 2006, Mwema et al., 1995, Teague et al., 2001)	No data available	-
Ge	No data available	-	No data available	-
Ga	No data available	-	No data available	-

3.6 Implication for metal recycling industry

The valuable elements found in e-waste could be considered as resources as opposed to waste in the overall materials flow if these can be recovered using feasible routes. It has been demonstrated in industry that valuable elements can be recovered using pyrometallurgy, hydrometallurgy, and their combinations. It may be possible to recover most of these valuable elements if the conditions favourable for partitioning them into appropriate phases are identified. For this thermodynamic data and their understanding are essential. It can be seen from the present review study that most researchers have conducted their study in the temperature range 1250-1350°C (1523 to 1623 K) which is mainly driven by the current industrial practise in the primary and secondary processing of copper. There are also other parameters such as oxygen partial pressure, the activity of these valuable metals in slag and metal and the composition of slag (which relates to slag physicochemical properties favourable for operation) to consider for the control of the distribution of valuable elements in different phases. The information on the existing thermodynamic data and distribution behaviour of the valuable elements in the literature have been collected, and listed and classified by operating parameters (temperature and partial pressure of oxygen) and slag systems as shown in Table 3.10. Nevertheless, the table provides information about the typical slags, temperatures and oxygen partial pressure range previously investigated to understand the behaviour of valuable elements distribution in industrial copper smelting processes.

A systematic research is required to understand and determine the thermodynamic data, particularly the interaction parameters and partitioning of other valuable metals in wider conditions relevant to both primary and secondary copper processing. On the basis of more comprehensive thermodynamic information, further optimization and improvement of the existing processes can be carried out to maximise recovery of most if not all the valuable metals. These can also induce the development of novel processes for better recovery of the metals from other urban ores or wastes.

Table 3.10: Different experimental conditions in various slag systems for minor elements distribution in molten metal

Equilibrium System	Slag System	p_{O_2}(atm)	Temperature (°C)	Minor Elements	Ref.
Iron silicate slag					
Slag – Cu alloy	FeO_x-SiO_2	10^{-12} – 10^{-6}	1250	Ag, Sn, Pb, As, Sb, Bi, Co	(Nakazawa and Takeda, 1983, Takeda et al., 1983, Yazawa et al., 1999, Yazawa et al., 1968)
Slag – Cu alloy	FeO-Fe_2O_3-SiO_2-Al_2O_3	10^{-11} – 10^{-6}	1200 and 1300	Sn, Te, Se, Bi, As, Pb, Sb, Co	(Nagamori et al., 1975a, Nagamori et al., 1975b, Nagamori and Mackey, 1977, Derin and Yücel, 2002)
Slag – Cu matte	FeO_x-SiO_2	$10^{-11.5}$	1250	Ag, Sn	(Louey et al., 1999)
Slag – Cu matte	FeO_x-SiO_2	–	1250 and 1300	Ag, Pb, Bi, Sb	(Roghani et al., 1997b, Roghani et al., 1997a, Takeda and Roghani, 1993, Kashima et al., 1978)
Slag – Cu matte	FeO_x-SiO_2	$10^{-8.4}$ – $10^{-7.3}$	1250 to 1350	Au, Ag, Pt, Pd, Rh	(Avarmaa et al., 2015)
Matte – Cu alloy	–	–	1150 to 1250	Ag, Au, Pd, Pt	(Schlitt and Richards, 1975)
Slag – Cu alloy	FeO_x-SiO_2-(CaO, MgO, Al_2O_3)	10^{-12} – 10^{-6}	1200	Pb, Bi, As, Sb	(Heo et al., 2012, Kim and Sohn, 1998)
Slag – Cu matte	FeOx-SiO_2-MgO	–	1250	Co	(Choi and Cho, 1997, Kho et al., 2006)
Slag – Cu alloy	FeO-Fe_2O_3-SiO_2-Al_2O_3	10^{-10} – 10^{-8}	1350	Co	(Derin and Yücel, 2002)]
Slag – Cu alloy	FeOx-SiO_2-MgO	10^{-11} – 10^{-6}	1300	As	(Chen and

					Jahanshahi, 2010)
Slag – Cu alloy	FeO_x-SiO_2	$10^{-9} – 10^{-5}$	1300	Pt, Pd	(Henao et al., 2006, Yamaguchi, 2013)
Calcium ferrite slag					
Slag – Cu alloy	CaO-FeO_x	$10^{-12} – 10^{-6}$	1250	Ag, Sn, Pb, As, Sb, Bi, Co	(Nakazawa and Takeda, 1983; Takeda et al., 1983; Yazawa et al., 1968, 1999
Slag – Cu alloy	CaO-FeO-Fe_2O_3-MgO	$10^{-12} – 10^{-6.8}$	1185 and 1250	Se, Te	(Johnston et al., 2010)
Slag – Cu matte	CaO-FeO_x	–	1250	Ag, Pb, Bi,Sb	(Roghani et al., 1996)
Slag – Cu alloy	FeO_x-CaO-MgO	$10^{-11} – 10^{-6}$	1300	As	(Acuna and Yazawa, 1987)
Ferrous calcium silicate slag					
Slag – Cu alloy	FeO_x-CaO-SiO_2	$10^{-6} – 10^{-8}$	1300	Sn, In	(Anindya et al., 2014, Anindya et al., 2013)
Slag – Pb alloy	FeO_x-CaO-SiO_2	$10^{-12} – 10^{-10}$	1200	In,	(Hoang and Swinbourne, 2007)
Slag – Cu alloy	FeO_x-CaO-SiO_2	10^{-6}	1300	Sb, Bi, Pb	(Kaur et al., 2009)
Slag – Ag alloy	FeO_x-CaO-SiO_2-MgO	$10^{-11} – 10^{-6}$	1300	As	(Chen and Jahanshahi, 2010)
Others slag system					
Slag – Cu alloy	CaF_2-CaO-MgO-SiO_2	–	1227	Sn, Sb	(Gortais et al., 1994)
Slag –Cu alloy	CaO-SiO_2-Al_2O_3	–	1350	Pb	(Matsuzaki et al., 2000, Heo et al., 2012)
Slag – Cu alloy	Cu_2O-CoO-SiO_2	–	1200 to 1300	Co	(Reddy and Healy, 1981)
Slag – Cu alloy	Na_2O_3-Na_2O-SiO_2	–	1250	As, Sb	(Riveros et al., 1987)

3.7 State of the art research tools and future challenges

Accurate measurement and meaningful data of elements distribution in phases rely on good experimental, characterisation and measurement techniques. Recent studies on the area emphasised on the use of equilibration and quenching technique to measure the distribution of valuable metals and understand their thermodynamic behaviour. During the equilibration, the multi-components in the system are let to equilibrate at certain conditions (e.g. p_{O_2} and temperature). It is important for the system to reach the true equilibrium. The checking of the true equilibrium condition can be done by carrying out experiments approaching equilibrium from different directions, for example from reducing and oxidising conditions.

Once the true equilibrium is achieved, a quenching of the sample is then carried out to preserve the conditions at a high temperature and allow the analysis at room temperature. It is important to carry out the quenching carefully as not to shift the equilibrium. The sample is then characterized and the elements distributions are then measured using different analysis methods, including XRD (X-Ray Diffraction), ICP-AES (Inductively Coupled Plasma-Atomic Emission Spectroscopy), EPMA (Electron Probe Micro Analyzer) as well as wet chemical analyses. EPMA measurement provides an accurate measurement of phases at the microscopic level. EPMA analysis, however, is not able to accurately measure concentration below 1 wt%. It cannot also be used to quantify accurately composition of sample with multivalent cation simultaneously exist, e.g. differing Fe_2O_3 and FeO, unless other techniques (such as wet chemical analysis) is used in conjunction

The challenges for future research include the understanding of the behaviour of volatile valuable metals, e.g. In, Ge and Sn. A novel experimental technique to limit the evaporation during equilibration is required. The choice of material for containing the sample is also a challenge as there may be a possibility of reaction between the sample and the material of the container. Some of the valuable metals have different state of valency; therefore, the oxidation state of metal in slag is another challenge to identify. Sometimes it is difficult to determine the slag composition using a single technique only, rather a multiple approach and techniques are required.

3.8 Summary

This chapter has highlighted the thermodynamic data of valuable trace elements in copper-slag systems to understand their partitioning behaviour in different phases in relation to oxygen partial pressure, temperature and slag composition. Kinetics also plays a role in different technologies which have not been considered here. The distributions of selected valuable elements have been investigated in different slag systems by previous researchers and the information is critically reviewed in the present study. Thermodynamic data of valuable elements in ferrous calcium silicate (FCS), which is relevant to secondary copper processing, is limited. Only data for Sn, In, Sb, Bi and As in selected operating conditions are available. Extending the thermodynamics knowledge in ferrous calcium silica (FCS) slag to understand the behaviour of remaining valuable trace elements such as Au, Ag, Pd, Te, Pt, Rh, Ru, Ge, In, Ga, Co and Ta would provide a more comprehensive information that can be used to develop more economical and eco-efficient high temperature routes for the recovery of all valuable metals and for an improved control of hazardous emission during the e-waste processing through primary and secondary copper production. There is still a lot of gap in the information and understanding, which requires further systematic research to develop, measure and generate a more comprehensive thermodynamics information.

Chapter 4 Methodology

4.1 Introduction

In the current study, combined thermodynamic assessmnet and experimental study were carried out. Thermodynamic assessment was employed to provide initial information about the effect of reactant composition, temperature and controlled atmosphere on the behaviour of any particular slag-metal equilibrium reaction and also to contribute to the design of the experimental study. The experimental study was carried out to understand the factors which affect the thermodynamic behaviour of valuable metals in a slag-metal equilibrium reaction. The aim of this chapter is to describe the thermodynamic calculation approach, selection of database and also discuss the limitation of databases for the thermodynamic assessment. This chapter also further explains the experimental methodology including the materials used, calibration of thermocouple and oxygen sensor, preparation of master alloys and slags, experimental techniques and post experimental samples analysis and characterization techniques. A summary of methodology adopted in the current study is shown in Figure 4.1.

4.2 Thermodynamic assessment and databases

The thermodymanic assessment in the context of current study refers to the careful analysis and calculation of equlibriums using a thermochemical package. Thermodynamic assessment was undertaken using thermochemical software FactSage 6.4 for understanding slag-metal equilibrium reactions for the ferrous and non-ferrous systems. There are a number of compound and solution databases in FactSage, i.e., FactPS, FToxide, FScopp, SGTE, etc., that can be used for calculations. The FactPS contains the database of pure substances which is mainly sourced from JANAF thermochemical tables. FToxide solution database contains oxides and liquid slag phases which are optimized with the quasichemical model. FScopp is a database for copper rich alloys and this database was used for the equilibrium calculation for the copper-rich alloy in the range of temperature 400-1600^o C (773-1873 K). SGTE is a database for the binary and ternary alloys. In SGTE database, the liquid phases are optimized using simple substitutional solution model.

FactSage also enables phase diagram, complex equilibria, viscosity and predominance diagram calculations. The equilibrium calculation is usually carried out using the ‘Equilib’ module of FactSage software with the appropriate databases. In this study thermodynamic

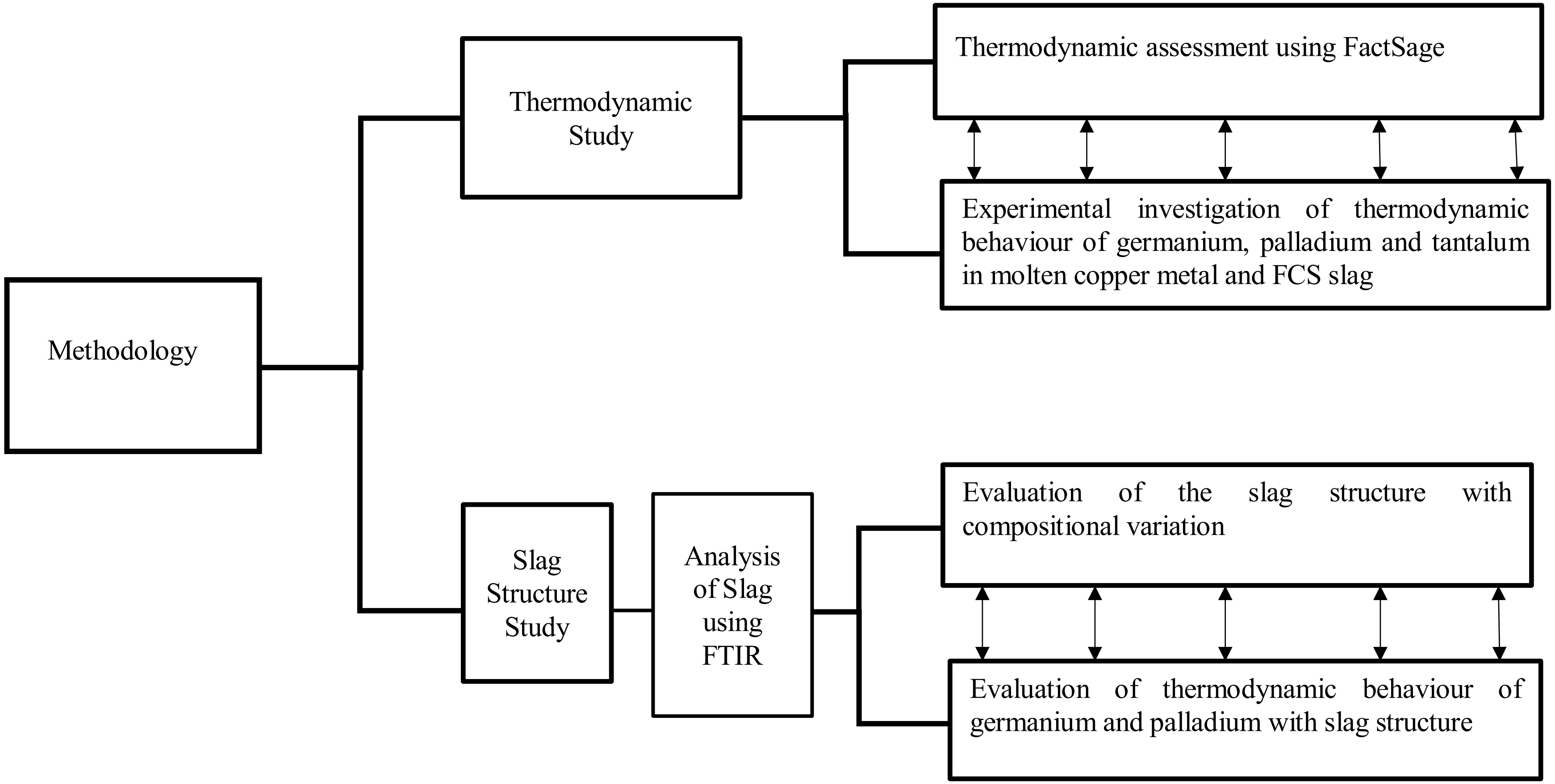

Figure 4.1: Summary of methodology used in the present study.

assessment was carried out to understand the general trend of the effect of process parameter on the distribution of precious metals in the different phases of the copper smelting process, i.e., metal, slag, and gas.

A predictive thermodynamic calculation will require optimized compound and solution databases. The databases will also need to include the relevant elements, e.g. in the context of the present study, they need to contain Ge, Pd, Ta, and Cu, and have been optimized for these elements. The author has investigated the existing databases in the FactSage software, and found that not all valuable elements of interest are included in them. Table 4.1 shows the summary of the availability of elements in the selected FactSage databases. It can be seen from the Table 4.1 that all the relevant databases (FactPS, FToxid, FScopp, SGTE) contain Ge. However, Ge has not been fully optimized over the range of conditions relevant to copper smelting. In the case of FToxid, the Ge has only been optimized for a simple GeO_2-SiO_2 binary system.

Table 4.1: Present of elements in different databases of FactSage

Element Database	Ag	Au	Ga	Ge	In	Pd	Pt	Ru	Se	Sn	Ta	Te	Ti	Y	RE
FactPS	√	√	√	√	√	√	√	√	√	√	√	√	√	√	√
FToxide	×	×	×	√	×	×	×	×	×	√	×	×	√	×	√
FScopp	√	√	√	√	√	√	√	×	√	√	×	√	√	√	√
SGTE	√	√	√	√	√	√	√	√	√	√	√	√	√	√	√

*√ means present in database; *× means not present in database
*RE means Rare Earth metals (Ce, Nd, Pr, Sm)

It was also found that Pd is not present in the FToxid database; while Ta is not present both in the FToxid and FScopp databases. Therefore, it is clear that predictive thermodynamic calculation involving the elements of Ta, and Pd cannot be carried out using FactSage. Equilibrium calculations involving Ge were carried in this study, but the results should taken as indicative.

The thermodynamic calculation carried out in this study is useful for evaluating the general trend and to help with experimental design. The thermodynamic package also used for the calculations of slag system FeO-Fe_2O_3-SiO_2-CaO-MgO-Cu_2O, in particular for determining the equilibrium composition (including Fe^{3+}/Fe^{2+} ratio, and activity of CaO). Further to this, viscosity of slag was calculated using ‘Viscosity’ module in FactSage.

4.3 Materials requirement

This section describes the powder materials used for the preparation of master alloy and master slag samples and other materials relevant to experimental study. It also reports about the gas specification and crucible dimensions and arrangement required for the experiments.

4.3.1 Powder materials

The chemicals used in the experiments in the current study were listed in Table 4.2. The master alloy samples were prepared from copper flakes and relevant metal powders, i.e., germanium, palladium and tantalum. The procedure is explained in more detailed in Section 4.6.12. The details of master slags preparation is also described in Section 4.6.21.

Table 4.2: Materials used in the present study

Materials	**Purity**	**Obtained from**
Copper Flake	99.99 %	Alfa Aesar
Germanium	99.999%	Sigma-Aldrich
Palladium	99.999%	Sigma-Aldrich
Tantalum	99.99%	Sigma-Aldrich
Silicon (IV) Oxide	99.5%	Alfa Aesar
Calcium Carbonate	99.5%	Alfa Aesar
Iron	99.9+%	Alfa Aesar
Iron (III) Oxide	99.99%	Alfa Aesar
Germanium Oxide	99.999%	Sigma-Aldrich
Palladium Oxide	99.99%	Sigma-Aldrich
Tantalum Oxide	99.99%	Sigma-Aldrich

4.3.2 Gases

High purity gas used for the experiments were supplied by Coregas. High purity argon gas was passed through a gas cleaning system before entering the furnace to ensure inside atmosphere has a low moisture and oxygen content. To control the oxygen partial pressure at a certain temperature a mixture of high purity carbon dioxide and carbon monoxide gases was used. The details of the gases used are given as followings:

- Carbon dioxide (CO_2), 99.995% purity, Grade 4.5.
- Carbon monoxide, (CO), 99.5% purity, Grade 2.5; the major impurity being nitrogen and carbon dioxide.
- Argon (Ar), 99.995% purity, Grade 5

4.3.3 Crucibles

Two sizes of high purity magnesia crucibles (97.4% MgO) were used in the experiments, supplied by Ozark Technical Ceramics, USA. The larger crucible, having an outside diameter of 51 mm with height of 51mm and wall thickness of 3mm, were used for master alloy and master slag samples preparation. The smaller crucibles of 18 mm outside diameter, 30 mm height and 2 mm wall thickness were used to perform the equilibrium experiments. Since the slag adhered to the walls of the crucible after an experiment, the slag was removed by breaking the crucible. Therefore, each of magnesia crucible was used for single experiment.

Two additional alumina crucibles were also used during the equilibrium experiments, one for containing of alumina powder and another for a cover crucible as shown in Figure 4.2. Louey et al. (1999) was successfully demonstrated a similar experimental technique. This technique is useful to minimise losses through volatilisation. The dimension of the base alumina crucible at the bottom was 45 mm in diameter and 20 mm in height. The cover cylindrical crucible was 30 mm in diameter and 45 mm in height. The purity of alumina crucibles was 99.8%, supplied by McDanel Advanced Ceramic Technologies, USA.

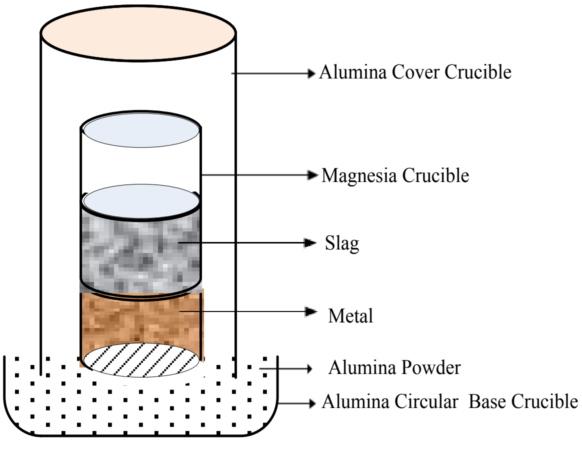

Figure 4.2: Arrangement of crucibles during the experiment.

4.4 Thermocouple calibration and temperature profile measurement

An R-type (Pt/ Pt- 13% Rh) reference thermocouple was used to calibrate the working thermocouple. Both thermocouples were placed inside the vertical tube furnace at temperature 1200°C (1473 K), 1250°C (1523 K), 1300°C (1573 K) and 1350°C (1623 K) and then the temperatures were recorded. The difference in the temperature reading at maximum temperature was 2 degrees between both thermocouples.

A temperature profile of vertical furnace tube furnace was measured using an external reference thermocouple. The measurements for temperature profile were carried out from the bottom part of the furnace in an upward direction with an increment of 2 cm at an interval of at least 5 minutes to ensure the thermal equilibration was attained. The isothermal zone of the vertical tube furnace was found to be 50 mm in the middle. It was also found that the actual temperature in the isothermal zone was recorded to be 39 degrees lower than the set temperature of 1300°C (1573 K) on the furnace controller. The temperature variation in the crucible system was less than 3 degrees. The temperature profiles at 1200°C (1473 K), 1250°C (1523K), 1300°C (1573 K) and 1350°C (1623 K) inside the furnace are shown in **Appendix A**. The calibration relationship of the actual temperature inside the furnace with controller temperature can also be found in **Appendix A**.

4.5 Oxygen partial pressure calculation, measurement and flow meter Calibration

The oxygen partial pressure inside the furnace was controlled chemically using a mixture of two gases, i.e. CO and CO_2. The flow rates of the CO-CO_2 gases for the required oxygen partial pressure at a fixed temperature were determined using the following relationship in Eq. (4.1) reported by Yazawa and Takeda (1982) from the thermodynamic data for reaction (4.2). The calculation of individual flow rate of each gas for an overall mixture flow rate of 400 mL/min is shown in **Appendix B.** The calculated value of CO_2 and CO gas flow rates for different oxygen partial pressure at 1300°C (1573 K) used during the experiments are presented in Table 4.3.

.

$$\log p_{\mathrm{O_2}} = 2\log\left(\frac{\mathrm{CO_2}}{\mathrm{CO}}\right) - \frac{29{,}510}{\mathrm{T}} + 9.05 \qquad (4.1)$$

$$2\ \mathrm{CO_{(g)}} + \mathrm{O_{2\,(g)}} \rightleftharpoons 2\mathrm{CO_{2\,(g)}} \qquad (4.2)$$

Table 4.3: Calculated flow rate of CO_2 and CO gas for required p_{O_2} at 1300°C (1573 K)

Required p_{O_2} (atm) at T =1300°C (1573 K)	$\frac{\mathbf{CO_2}}{\mathbf{CO}}$	**F_{CO_2} (ml/min)**	**F_{CO} (ml/min)**
1×10^{-7}	22.53	383	17
1×10^{-8}	7.33	352	48
1×10^{-9}	2.27	278	122
1×10^{-10}	0.72	167	233

A DS-type $SIRO_2$ C700+ solid zirconia electrolyte oxygen sensor supplied by Ceramic Oxide Fabricators, Australia was used to measure the p_{O_2} by inserting the probe from the top end of the furnace. A small pump was used to draw the reference air to the probe at a rate 10 cm^3/min through a flexible silicon tube. To prevent the oxygen diffusion from outside air, all seals and the connections were checked for leakage using a soapy liquid water before each experiment. Once proper sealing ensured then the EMF generated was measured by a high impedance digital voltmeter. The oxygen partial pressure was calculated using the Nernst equation as shown in Eq. (4.3) for the EMF value of oxygen sensor at a fixed temperature for the cell. The EMF reading from voltmeter was used to calculate p_{O_2} using Eq. (4.4) and the results are shown in Table 4.4.

$$\mathrm{E} = -\frac{RT}{nF}\, ln \frac{p_{O_2}}{p_{O_2}'} \tag{4.3}$$

Here,

E = Electromotive force (mV)

R = Gas constant = 8.314 J/mol. K

T = Temperature (in K)

n = number of charge

F = Faraday Constant = 96485.3329 A/mol

p_{O_2} = oxygen partial pressure

$p_{O_2}{}'$ = oxygen partial pressure of reference

After substituting all the relevant value and rearranging the Eq.(4.3) can be expressed as:

$$p_{O_2} = 0.209\exp(-\frac{46.42E}{T}) \tag{4.4}$$

Table 4.4: Calculation of measured p_{O_2} inside the furnace using oxygen sensor

Target p_{O_2} (atm)	**Temperature [^{0}C (K)]**	**Range of E (mV)**	**Mean E (mV)**	**Measured p_{O_2} (atm)**	**Error (%) ±**
10^{-7}	1300 (1573)	494 - 496	495	9.46×10^{-8}	5.35
10^{-8}	1200 (1473)	533 - 539	536	9.64×10^{-9}	3.55
10^{-8}	1250 (1523)	549-555	552	1.03×10^{-8}	3.12
10^{-8}	1300 (1573)	571 - 575	573	9.47×10^{-9}	5.28
10^{-8}	1350 (1623)	587 - 593	590	9.81×10^{-9}	1.93
10^{-9}	1300 (1573)	649 - 654	651.5	9.34×10^{-10}	6.59
10^{-10}	1300 (1573)	727 - 731	729	9.48×10^{-11}	5.13

The individual gas flow rate of CO_2 and CO was controlled with microprocessor driven digital mass flow controllers (DFC) supplied by Aalborg, USA. The mass flow controllers were connected to a digital command module (CM). The module allowed to mix up to four different types of gases. The digital mass flow controller (DFC) was calibrated with a reference gas rotameter. A manual gas rotameter (maximum flow rate of 500 mL/min) was used to calibrate each of the digital mass flow meter which was connected in between the digital mass flow controller and the gas cylinder. A number of data taken and plotted to obtain a calibration relationship between the flow rate of gas rotameter and digital mass flow controller. Similarly, the procedure was repeated for other gas. The plots between digital mass flow controller flow rate and manual gas rotameter flow rate for both gases are shown in **Appendix B**. The actual picture of the digital mass controller arrangement is shown in Figure 4.3

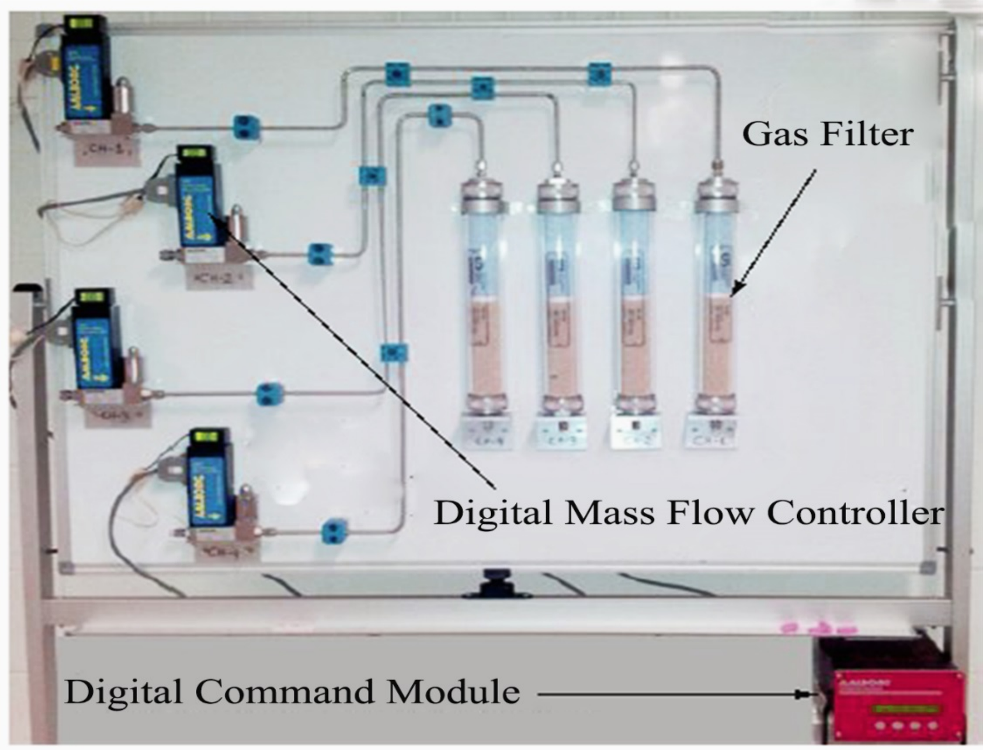

Figure 4.3: The arrangement of digital mass flow controller with command module.

4.6 Samples preparation

The preparation of master Cu-alloy and slag samples for the equilibrium experiments is described in this section. It also describes the melting procedure in the vertical tube furnace.

4.6.1 Master slags

Master slags were prepared from SiO_2 (99.5 pct purity), $CaCO_3$ (99.5 pct purity), Fe_2O_3 (99.99 pct purity), and Fe (99.9 pct purity) powders. $CaCO_3$ was dried to remove moisture at 500ºC (773 K) for 5 hours, followed by heating at 1100ºC (1373 K) for 4 hours in a high purity alumina tray inside a muffle furnace to produce CaO. The amount of powder was 50-60 g in each batch of master slag. The appropriate amount of iron, ferric oxide, silicon dioxide and calcium oxide (calcined $CaCO_3$) targeting selected Fe/SiO_2 ratios and CaO contents were weighed and mixed in a ball mill for 36 hours. The milled powders were then transferred to a high-density magnesia crucible (OD; 48mm, ID; 42mm, HT; 51mm) for melting to produce slags.

The melting of the mixtures was carried out in a vertical tube resistance furnace inside a crucible that was placed in the hot zone, suspended using an alumina (99.8 pct purity) rod.

At the beginning, the air inside this furnace was evacuated using an external vacuum pump before backfilled with high purity argon gas. The mixtures of powders were heated to 1300°C (1573 K) with a heating rate of 200°C/hour and pre-equilibrated for 6 hours at 1300°C (1573 K) under controlled CO-CO_2 atmosphere at p_{O_2}= 10^{-8} atm. After 6 hours of equilibration time, the liquid slag was then quenched rapidly by moving the system to the cool zone, and flowing high purity argon gas. The master slags were then recovered by carefully crushing the crucible containing the slags. The slag samples were analysed using inductively coupled plasma atomic emission spectroscopy technique to determine the final equilibrated composition (saturated amount). It was found that about 6.3 to 8.8 mass pct MgO is present in the slags due to the dissolution of the crucibles used for melting. The composition of master slags were used in the current study is shown in Table 4.5.

It was reported that the region of liquid zone stability of ferrous calcium silicate system is expanded sufficiently with increasing of temperature beyond 1200^0C (1473 K) and decreasing of oxygen partial pressure below 10^{-7} atm (Hidayat et al., 2012). Therefore, all master slags were prepared at 1300°C (1573 K) and p_{O_2}= 10^{-8} atm.

Table 4.5: Master slags composition used in the present study

	Fe_{Total} (%)	**SiO_2 (%)**	**CaO (%)**	**MgO (%)**
Batch MS#1	37.3	35.3	5.59	6.30
Batch MS#2	27.4	33.9	9.72	6.78
Batch MS#3	32.8	41.1	9.88	6.70
Batch MS#4	32.8	33.1	9.88	6.49
Batch MS#5	32.5	32.8	11.5	6.51
Batch MS#6	37.9	32.8	9.80	6.51
Batch MS#7	37.9	32.8	10.8	6.61
Batch MS#8	41.8	31.9	9.95	6.35
Batch MS#9	35.1	26.9	10.5	6.80
Batch MS#10	33.4	33.6	14.5	7.52
Batch MS#11	31.1	32.6	14.5	7.83
Batch MS#12	30.7	31.3	19.4	8.78

4.6.2 Master alloys

The master Cu-Ge alloy was prepared from copper flakes (99.99 pct purity, and germanium powder (99.999 pct purity). A mixture of copper flakes with 5 mass pct Ge was equilibrated for 6 hours in a high-density magnesia crucible (OD; 48mm, ID; 42mm, HT; 51mm) inside a vertical tube resistance furnace. At the beginning, the furnace was evacuated using an external vacuum pump before backfilled with high purity argon gas. The master alloy was then heated up to 1300°C (1573 K) with a heating rate of 200°C/hour under high purity argon gas at a rate 50 L/hour. The liquid master alloy was then cooled inside the furnace using the same cooling rate. The composition of the master alloy was confirmed using ICP-AES technique. It was found that approximately 1 mass pct of Ge was volatilized during the melting procedure. A trace amount of magnesium (< 0.005 mass pct) was found in the master alloy. A similar technique was applied in the second batch of master (Cu-Pd) alloy sample preparation from copper flakes (99.99 pct purity, and palladium powder (Pd) (99.999 pct purity). The aimed composition of palladium in the Cu-Pd master alloy was 6 mass pct. The melting practise was similar and less than 0.1 mass pct of palladium was lost from the system during the melting.

In the third batch, an attempt was taken to prepare the Cu-Ta master alloy sample from copper flakes (99.99 pct purity, and tantalum (Ta) powder (99.999 pct purity) with an aimed of 2 mass pct of tantalum. Tantalum is very refractory metal and it was difficult to prepare the alloy using a similar technique. Therefore, a number of approaches was taken for the preparation of Cu-Ta alloys. The master alloy was heated up to 1300°C (1573 K) and 1600°C (1873 K) with a heating rate of 200°C/hour equilibrated for 8 hours under high purity argon gas at a rate 50 L/hour in the vertical tube furnace. But, only very trace amount of tantalum was found in the copper alloy, since the formation of tantalum oxide is favourable due to having high negative value of Gibbs free energy in the condition. In the second approach, a muffle furnace was used for the preparation of the Cu-Ta master alloy with similarly aimed composition of Ta. A mixture of copper flakes with 2 mass pct Ta was equilibrated for 8 hours in two different high-density magnesia crucibles (OD; 48mm, ID; 42mm, HT; 51mm) in a muffle furnace at 1200°C (1473 K) with a heating rate of 200°C/hour. Once the time was reached, one crucible of liquid master Cu-Ta alloy was cooled inside the muffle furnace using the furnace cooling rate, while another crucible was taken out from the muffle furnace and quenched into water. The composition of cooled Cu-Ta alloys were confirmed using ICP-AES technique. Trace amount of tantalum is found in copper.

The third approach include melting of Cu-Ta mixture in a vertical tube furnace under controlled CO-CO_2 atmosphere at p_{O_2}= 10^{-16} atm and 1600°C (1873 K) for 24 hours of equilibration time. The mixture of copper flakes with 2 mass pct Ta (which was a mixture tantalum and tantalum powder) was equilibrated for 8 hours in a high density magnesia crucible (OD; 48mm, ID; 42mm, HT; 51mm) in the furnace at 1600°C (1873 K) with a heating rate of 200°C/hour. After 8 hours of holding time, the liquid alloy was then quenched rapidly in the cool zone using high purity argon gas to preserve the composition. The master Cu-Ta alloy was then recovered by carefully crushing the crucibles containing the master alloy and analysed using ICP-AES technique. Finally, Cu-Ta alloy was prepared with a 0.23 mass pct Ta. The final composition of all the master Cu- alloys used in the equilibrium experiments is shown in Table 4.6.

Table 4.6: Composition of master alloys used in the present study

Master Alloy	**Cu-Ge**		**Cu-Pd**		**Cu-Ta**	
Composition	Cu (%)	96	Cu (%)	94	Cu (%)	98.5
	Ge (%)	3.9	Pd (%)	5.90	Ta (%)	0.23

4.7 Experimental procedures

In this section, the detail of slag-metal equilibrium experiments conducted using master alloy and master slag samples at different experiment conditions are described. It also describes the techniques of analysis of the samples of post experiments using inductively coupled plasma atomic emission spectroscopy (ICP-AES), x-ray diffraction (XRD), Raman spectroscopy and Fourier transformation infrared (FTIR).

4.7.1 Main experimental program

A vertical tube furnace (Nabertherm RHTV 120-300/18) was used for the main experiments in the current study. A schematic diagram of the experimental apparatus is shown in Figure 4.4, including more details of the vertical tube furnace. The furnace was equipped with two open-ended tubes. One tube was an open-ended alumina tube with outer diameter of 80 mm, the wall thickness of 5 mm and height of 1.1 m. Another tube was the mullite sacrificial tube with outer diameter of 60 mm, wall thickness of 3 mm and height of 1 m. The ends of the large tube were sealed by flanges equipped with viton O-rings. A water cooling inlet was circulated through the flange at each end-cap to prevent the O-rings breaking down due to overheating. The furnace was equipped with vertical silicon molybdenum heating elements and was fitted with an alumina-sheathed platinum/platinum-13% rhodium thermocouple referred as the ‘internal thermocouple’, that was connected to a Nabertherm temperature controller. The heating elements were surrounded by foamed zirconia to provide insulation and protection. There was a gas inlet to pass gas into the furnace during the experiment and also a gas outlet to pass the off-gas. The actual picture of furnace with accessories is shown in Figure A.3 in **Appendix A**.

The furnace bottom end flange was designed in such a way that it is easy to raise or lower the crucible assembly. An alumina disc was attached using ceramic cement to the closed end of an alumina pedestal to support the crucible assembly. This assembly was then placed in the hot zone inside the furnace. The bottom part flange was sealed with an O-ring to prevent gas leakage and was fitted with an adjustable stainless steel fitting so that it was possible to move the alumina pedestal vertically.

For the equilibrium experiments, initially, the furnace chamber was evacuated using a vacuum pump at room temperature before backfilled with high purity argon gas. The furnace then heated up to the desired temperature before CO_2-CO gas mixture was flown into the furnace chamber. The desired oxygen partial pressure in the furnace at a particular temperature was achieved by flowing appropriate ratio of CO-CO_2 gas mixture considering Eq. (4.1) The individual gas flow of CO_2 and CO was regulated using a digital mass flow controller (DFC; Aalborg, USA). The gas mixture was introduced from the bottom of the furnace to minimize the effect of thermal segregation, and oxygen back diffusion from the air into the furnace was prevented using a gas bubbler before release to the exit line.

The overall flow rate of gas used in each experiment was 400 mL/min. To confirm the oxygen partial pressure an SIRO$_2$ C700+ zirconia ceramic electrolyte oxygen sensor (Ceramic Oxide Fabricators, Australia) was used to measure the actual oxygen partial pressure in the furnace. After the equilibrium time was achieved, the experiment was terminated by purging a high purity argon gas for 5 minutes and the crucible system was immediately quenched by lowering it to the cool zone at the bottom of the furnace. Once cooled down, the crucible system was collected and it was carefully crushed and the copper and slag were separated by physical means.

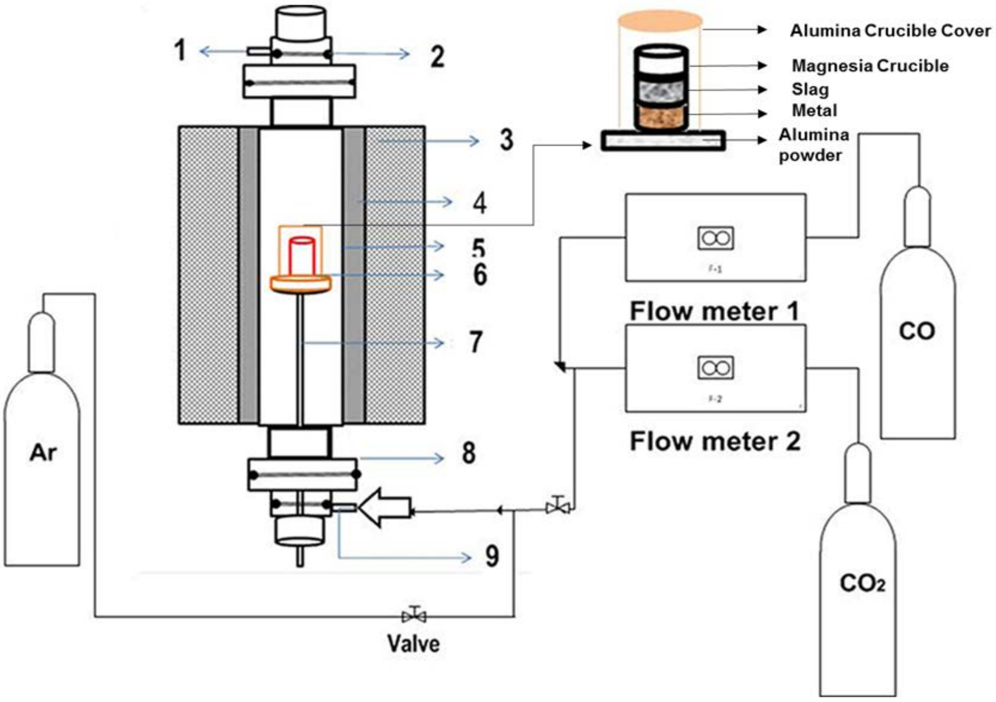

Figure 4.4: Schematic diagram of vertical tube furnace with experimental setup. (Legend: 1. Gas outlet, 2. Silicone O-ring, 3. MOSi_2 heating element, 4. Alumina Tube, 5. Mullite Tube, 6. Magnesia crucible, 7. Alumina pedestal, 8. Water Cooled Flange, 9. Gas Inlet)

4.7.2 ICP analysis

An inductively coupled plasma atomic emission spectrometry (ICP-AES) was used for analysis of the master alloys, master slags and all the equilibrated samples at Spectrometer Services Pty Ltd, Melbourne, Australia. Master slag samples were analysed for lime, total iron, silica, and magnesia. Metal samples were analysed for copper and minor elements, i.e., Ge, Pd, Ta. The equilibrated samples were analysed to get the valuable elements distribution in metal and slag phase and the amount of copper in the slag.

The preparation of the samples is described below:

Once the crucible system was cooled down, then it was carefully crushed and the copper alloy and slag were separated by physical means. The slag samples were ground into fine powder. For metal; the samples were cut into small pieces and then dissolved in hydrochloric acid which was further diluted in distilled water. The solution was transferred to a volumetric flask for the analysis of copper, germanium, palladium and tantalum concentration in the solution against multiple standard solutions. For slags; a finely ground slag sample was fused in sodium peroxide at high temperature, then the mixture was diluted with nitric acid. The diluted solution was analysed against multiple standard solutions.

4.7.3 XRD analysis

X-ray diffraction (XRD) patterns were obtained from the equilibrated slag samples using a Bruker AXS-D8 XRD which was equipped with Cu Kα (λ=1.5406 Å) radiation target. The diffraction patterns were collected over a 2θ range from 10^0 to 80° at a step size of 0.02°. The qualitative analysis of XRD data was performed using EVA software. The results enabled the identification of the phase of materials in the sample.

4.7.4 Raman analysis

Raman spectrometry analyses were carried out for the qualitative analysis of slag samples using a Raman spectroscope (inVia, Renishaw, UK) equipped with a Leica microscope. The raman spectra measurements were carried out using an excitation wavelength of 785 nm from an argon ion laser. For measurement, the samples were placed on a glass slide and the microscope was focused on the sample.

4.7.5 FTIR analysis

The infrared spectra were analysed using Fourier transform infrared (FTIR) technique using a Nicolet iD5 attenuated total reflection spectrometer ((Thermo Fisher Scientific, USA). It was equipped with a diamond crystal and ZnSe lens. The incident angle of the crystal was 42^0. The measured spectra of the slag samples were recorded at room temperature for 100 scans at a resolution of 4.0 cm^{-1} using the OMNIC software.

4.8 Error analysis

The error analysis of the current study are reported in **Appendix D**.

Chapter 5 Thermodynamics of Germanium in FeO_x-CaO-SiO_2-MgO Slag and Molten Copper

5.1 Introduction

Germanium (Ge) is a lustrous, grayish-white, brittle and scarce metalloid with a concentration in the earth crust of about 1.6 ppm (Moskalyk, 2004, Höll et al., 2007). The average concentration of Ge in sphalerite (Zn, Fe)S) ores is up to 0.3 mass pct. The main route for Ge production is through refining process of zinc, where Ge is recovered from zinc residue as a by-product (Bernstein, 1985). It is estimated that about 85 pct of Ge of the worldwide is used in fiber-optics, inferred optics, polymerization catalyst application, electronics and solar application (Guberman, 2015). The primary way of Ge production only replenishes 70 pct worldwide demand, the rest is fulfilled by recycling of Ge from alternative resources including end-of-life (eol) products and electronic waste (e-waste) (Guberman, 2015).

There has been a growing interest to recycle and recover trace valuable metals found in e-waste (including Ge) through black copper smelting, (a route of secondary copper smelting) (Anindya et al., 2013, Anindya et al., 2014). The details of black copper smelting have been described in Section 2.4. The process has a wide flexibility in which different variety of secondary copper resources (including e-waste) can be inputted into the process. This process can also be carried out for small to large scale operations. Unfortunately, no information and data are available in the literature on Ge distribution at conditions relevant to both primary and secondary copper smelting process.

The study presented in this chapter is part of a systematic investigation on the distribution-ratio and thermodynamic behaviour of minor elements in black copper smelting. This chapter mainly focuses on distribution behaviour of Ge in FeO_x-CaO-SiO_2-MgO slag and molten copper under conditions relevant to the black copper smelting. The distribution-ratio data obtained in this study is also vital to calculate the activity coefficient of germanium oxide and to determine the oxidation state of germanium in the slag.

5.2 Previous works on germanium distribution

There are only two experimental studies found in the open literature on the investigation of Ge behaviour during pyrometallurgical processing. Yan and Swinbourne (2003) investigated the Ge distribution at conditions relevant to zinc-lead smelting process. In this study, Pb and Ge were equilibrated with $CaO\text{-}SiO_2\text{-}FeO\text{-}Al_2O_3$ slag in an alumina crucible at oxygen partial pressures of $10^{-12.5}$ to 10^{-10} atm and temperatures of 1150 to 1250°C (1423 to 1523 K). In these conditions, they found that Ge is likely to go to the slag phase and present as GeO (Ge^{2+}). They also reported that temperature and slag composition have a small effect on the Ge distribution-ratio within the parameters studied. A highly reducing atmosphere was found to increase the loss of Ge into the gas phase rather than increasing the Ge concentration in the metal phase. It was also concluded in this study that there are little opportunities to reduce the Ge loss by controlling the lead smelting conditions.

Another study performed by Henao et al. (2010) examined the distribution-ratio of Ge in lead bullion and liquid slag $CaO\text{-}SiO_2\text{-}FeO\text{-}Fe_2O_3\text{-}MgO$ under oxygen partial pressures of 10^{-12} to 10^{-8} atm at 1200°C (1473 K). Henao et al. (2010) utilised electron probe X-ray microanalysis (EPMA) to analyse the quenched liquid slag. It was suggested that Ge presents in the slag as GeO_2 (Ge^{4+}) and that the slag composition enhances the partitioning of Ge to the lead phase. These discrepancies with the previous study of Yan and Swinbourne (2003) may be attributed to the different slag system (compositions) and crucible material used in their study. Henao et al. (2010) also carried out selected experiments at higher temperatures. However, due to excessive volatilization, Ge in the slag and metal was not detected (beyond the detection limit of EPMA technique).

The current study determines the distribution-ratio of Ge in copper-slag systems to contribute in understanding Ge thermodynamic behaviour and also compared with the previous data in lead-slag systems to resolve the discrepancy regarding the oxidation state of Ge in slag.

5.3 Experimental details

5.3.1 Sample preparation

The master Cu-Ge alloy and master FCS slag were used for the equilibrium experiments. The preparation of master Cu-Ge alloy and master slag samples have been described in Section 4.6.

5.3.2 Apparatus and procedure

The equilibration experiments were conducted in a vertical tube resistance furnace (Nabertherm, model: RHTV 120-300/18). Prior to experiments, the temperature profile measurement and calibration were carried out using an R-type (Pt/Pt-13 mass pct Rh) standard calibration thermocouple, to determine the hot zone and the actual temperature at locations along the length of the tube inside the furnace. The details of the furnace temperature profile measurement and calibration have been described in Section 4.4.

Two types of experiments were carried out in the current study, i.e. equilibration experiment approaching from reduced and oxidized conditions, respectively. Samples with approximately 3.5g of master slag, 2.8g of copper and 0.7g of master alloy (Cu-3.9 mass pct Ge) were used for experiments approaching equilibrium from reduced condition. For experiments approaching from oxidized condition, samples with 3.5g of copper, 3.45g of master slag and 0.05g of GeO_2 (99.999 pct, purity from Alfa Aesar) were used. These mixtures were placed in high-density magnesia crucibles (OD 18mm, ID 14mm, HT 30mm). It was expected that some Ge and its associated compound volatilized during equilibration experiments. There are not many data available on the vapour pressure of Ge and Ge oxides. Hultgren et al. (1973) reported a vapour pressure of Ge (g) over Ge (s) of 1.02×10^{-4} Pa at 927°C (1200 K). Swamy et al. (2003) interpolated data from Davydov (1957), and reported a vapour pressure of GeO_2 (g) over GeO_2 (s) of 1×10^{2} Pa at 1200°C (1473 K).

To reduce the Ge or GeO_2 losses, the crucible containing the sample was placed on top of a bed of alumina powder and covered with a bigger high purity alumina crucible in an upside down position, as shown in Figure 4.2 in Section 4.3.3. This technique to reduce volatilization has been successfully demonstrated by Louey et al. (1999). This assembly was then placed in the hot zone inside the furnace and supported with a high purity alumina pedestal rod. For the equilibration experiments, initially the furnace chamber was evacuated using a vacuum pump at room temperature before backfilled with high purity argon gas. The furnace then heated up to the desired temperature before CO_2-CO gas mixture was flown into the furnace chamber. The detailed of experimental procedure has been described in Section 4.7.1.

After the equilibrium time was achieved, the experiment was terminated by purging a high purity argon gas for 5 minutes and the crucible system was immediately quenched by lowering it to the cool zone at the bottom of the furnace. Once cooled down, the crucible system was collected and carefully crushed. The copper and slag were separated by physical means. In the current study, the effect of temperature, oxygen partial pressure and the different slag composition were investigated. Table 5.1 shows the experimental conditions studied.

Table 5.1: Experimental plan and parameters used in the present study

Temperature [°C (K)]	1200 (1473), 1250 (1523), 1300 (1573), 1350 (1623)			
Oxygen Partial Pressure (atm)	10^{-7}, 10^{-8}, 10^{-9}, 10^{-10}			
	Fe_{Total}	SiO_2	CaO	MgO
Slag Composition (mass pct)	37.3	35.3	5.59	6.3
	27.4	33.9	9.72	6.78
	32.8	33.1	9.88	6.49
	37.9	32.8	9.80	6.51
	41.8	31.9	9.95	6.35
	33.4	33.6	14.5	7.52
	31.1	32.6	14.5	7.83
	30.7	31.3	19.4	8.78

5.3.3 Chemical analysis and characterization

The separated slag and the metal samples were analysed using ICP-AES (inductively coupled plasma - atomic emission spectrometry) technique (Varian 730 ES: ICP-AES) to determine the bulk chemical compositions. The slag samples were also characterized using XRD (X-ray diffraction) technique (AXS-D8, Bruker) and Raman spectroscopy (inVia, Renishaw, UK) equipped with a Leica microscope. The details of characterization have been previously described in Section 4.7.2, 4.7.3 and 4.7.4, respectively.

5.3.4 Phase diagram of $FeO\text{-}SiO_2\text{-}CaO\text{-}MgO_{Sat}$ slag

The calculations of the phase diagrams of $FeO\text{-}SiO_2\text{-}CaO\text{-}MgO_{sat}$ slag were carried out using FactSage at a fixed oxygen partial pressure of 10^{-8} atm for different temperatures used during the actual experiments in the present study. The compositions of slag are represented in Figure 5.1 by open circles. It is seen from Figure 5.1 that at 1200°C (1473 K) and p_{O_2}= 10^{-8} atm, the fully liquid phase was surrounded by other primary phases such as Tridymite (SiO_2), Amonoxide [(Fe, Mg)O] and Wollastonite ($CaSiO_3$). The region of liquid zone was also found to be extended with increasing of temperature. The effect of p_{O_2} was found to be negligible on the liquid phase field at conditions studied. However, it has also been shown in the literature that the liquid phase field of the ferrous calcium silicate (FCS) system expands significantly with increasing of temperature beyond 1200^0C (1473 K) and decreasing of oxygen partial pressure below 10^{-7} atm (Hidayat et al., 2012). Therefore, the slags are in their liquid state (no solid crystals) for the equilibrium experiments.

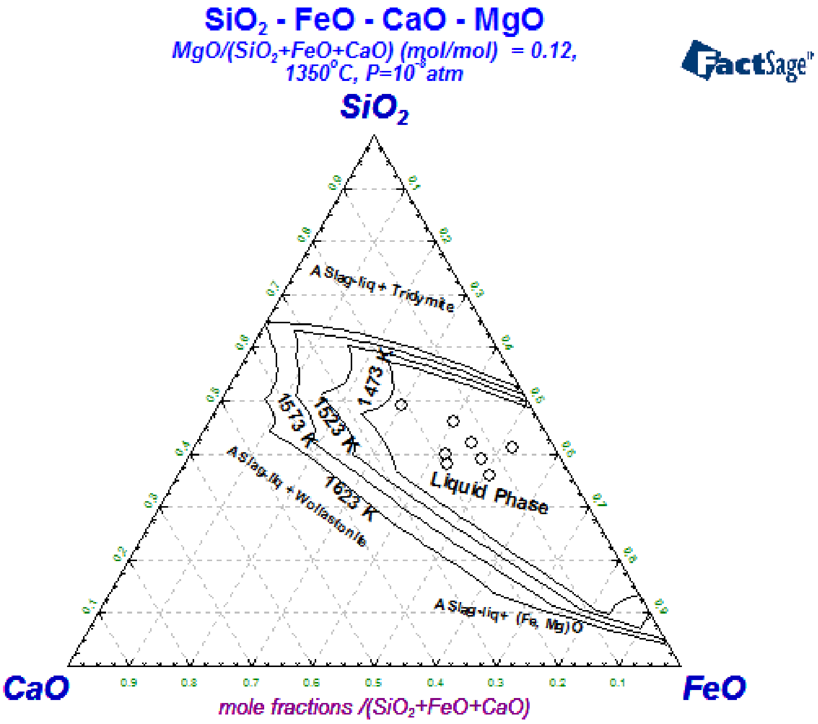

Figure 5.1: Liquidus isotherm diagram of FeO_x-CaO-SiO_2-$MgO_{Saturated}$ slag system calculated from FactSage and slag compositions of Ge study represented by the circle symbol at $p_{O_2} = 10^{-8}$ atm for different temperatures.

5.4 Checking of equilibrium and determination of minimum equilibration time

The attainment of equilibrium and the time to reach this condition were investigated by carrying out equilibration experiments approaching from an opposite direction, i.e. approaching from oxidized and reduced conditions. A slag having Fe/SiO_2 ratio (in weight) of 0.99 and CaO concentration of 14.5 mass pct was equilibrated with copper at oxygen partial pressure of 10^{-8} atm at 1300°C (1573 K). It has been mentioned that some of the MgO from the crucible entered into the slag. It was predicted by FactSage that this condition is in the liquid region of the FeO_x-CaO-SiO_2-MgO (FCS) slag system. A number of equilibration experiments were carried out with reaction time from 4 to 20 hours from both directions (approaching from oxidized and reduced conditions) to investigate the time required to reach equilibrium. Germanium is volatile in the conditions studied; to investigate the Ge loss by volatilization, mass balance coupled with bulk chemical analyses of copper and slag phase were carried out at different reaction time and the results are presented in Table 5.2. To avoid excessive Ge volatilization and re-shifting of equilibrium, it was necessary to determine the earliest time to reach equilibrium.

The data in Table 5.2 are plotted and presented in Figure 5.2. It can be seen that at p_{O_2}= 10^{-8} atm there are no significant differences in the distribution-ratio of Ge in slag and metal after 6 hours of equilibration approaching from both the oxidized and reduced conditions. It was also observed that with the increase of reaction time, more Ge is volatilized. Depending on the reaction time, about 20-55 mass pct Ge was found in copper metal, 21-49 mass pct in the slag and 2-60 mass pct volatilized.

Table 5.2: Distribution of Ge among slag, metal, gas as a function of equilibrium time at 1300°C (1573 K) and $p_{O_2} = 10^{-8}$ atm with a slag composition of Fe/SiO_2 = 0.96 and mass % CaO = 14.5

Equilibrium Time (Hours)	**Slag**		**Metal**		**Gas**	$L_{Ge}^{slag/metal}$
	Ge mass pct	**Distribution Pct**	**Ge mass pct**	**Distribution pct**	**Loss pct**	
Approaching from reduced condition						
4	0.33	42.31	0.43	55.13	2.56	0.77
6	0.37	47.44	0.35	44.87	7.69	1.06
8	0.34	43.59	0.33	42.31	14.10	1.03
16	0.27	34.62	0.25	32.05	33.33	1.08
20	0.24	30.77	0.22	28.21	41.03	1.09
Approaching from oxidized condition						
4	0.55	49.19	0.44	39.36	11.45	1.25
4	0.53	47.41	0.41	36.67	15.92	1.29
8	0.49	43.83	0.43	38.46	17.71	1.14
16	0.39	34.88	0.35	31.31	33.81	1.11
20	0.23	20.57	0.22	19.68	59.75	1.05

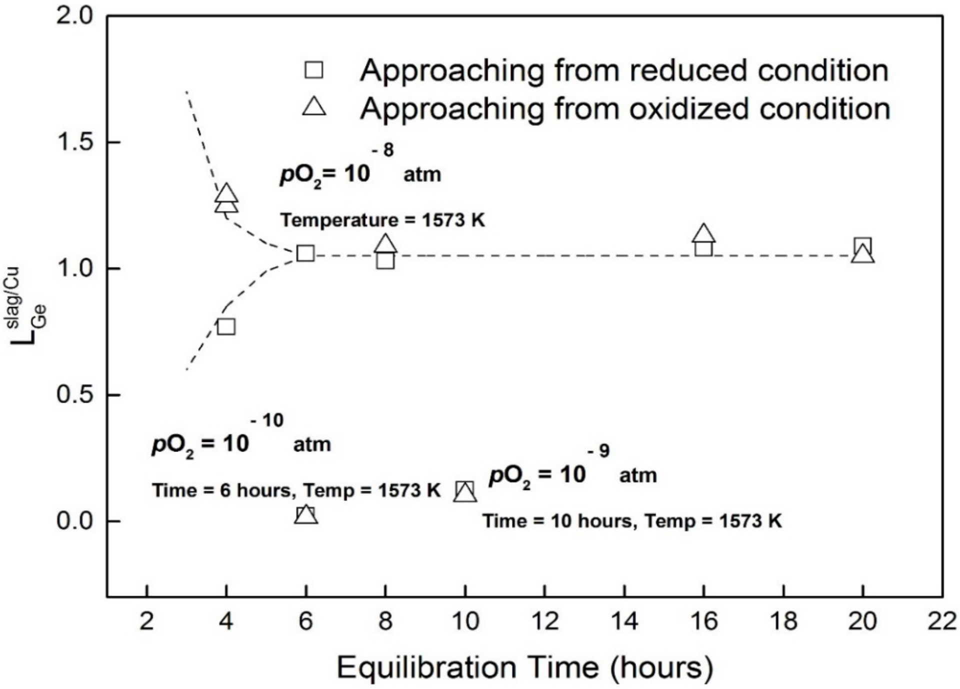

Figure 5.2: Germanium distribution-ratio in FeO_x-CaO-SiO_2-MgO slag and copper metal as a function of equilibration time at 1300ºC (1573 K).

To investigate further the appropriate minimum equilibration time, four additional experiments at different oxygen partial pressure were carried out. One set of experiments were carried out at 1300ºC (1573 K) and p_{O_2}= 10^{-10} atm for 6 hours equilibrium time and another set at 1300ºC (1573 K) and p_{O_2}= 10^{-9} atm for 10 hours from both directions. It can be seen from Figure 5.2 that at the indicated equilibration times, it was sufficient for the system to reach the equilibrium state at the two oxygen partial pressures. The data in Table 5.2 also show that the Ge loss to the gas phase was higher when the equilibrium is approached from oxidized condition. In this situation the Ge was added in the form of GeO_2 to the slag mixture at the beginning. This suggests that the Ge volatilization rate is higher when Ge was initially present in the slag phase as GeO_2 compared to when it was present as Ge in the Cu phase.

In addition to the Ge content, the Cu loss to the slag was also measured and tracked with time. Figure 5.3 shows the associated Cu loss to the slag as a function of time at temperature of 1300ºC (1573 K) and p_{O_2} of 10^{-8} atm. It was found that the loss of Cu to the slag is less than 2 mass pct in all experiments and levels at 1.6 mass pct at equilibrium. This finding is in agreement with previous results (Yazawa and Takeda, 1982, Yazawa et al.,

1999) which reported the copper content in FCS slags to be in the range of 2 to 3 mass pct.

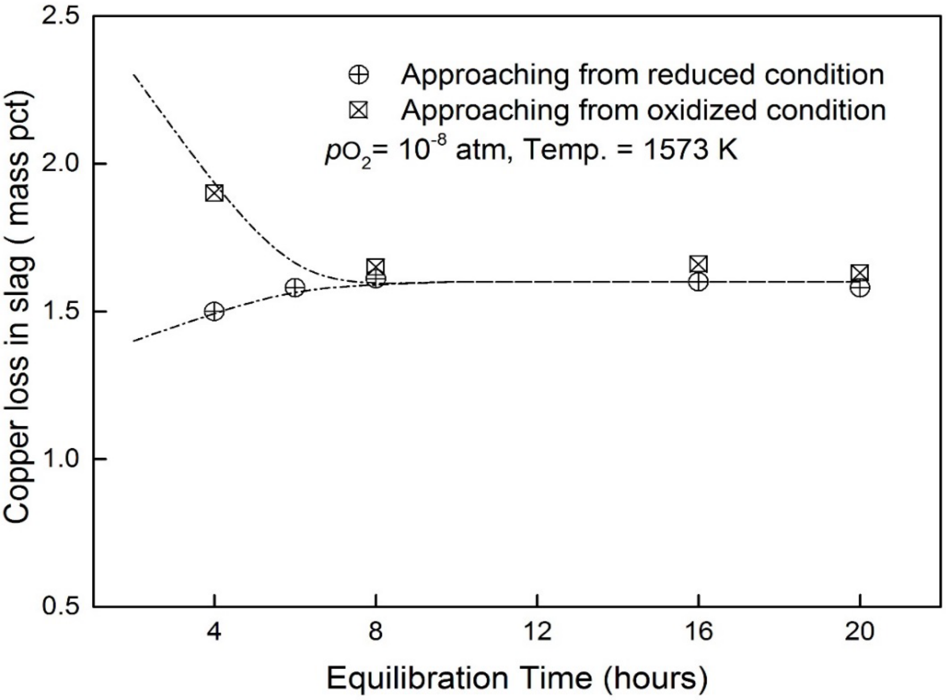

Figure 5.3: Copper loss in FeO_x-CaO-SiO_2-MgO slag as a function of reaction time at 1300°C (1573 K).

All the above results indicated that an equilibration time of 6 hours was sufficient for achieving equilibrium condition with minimum Ge loss to the gas phase. Therefore, further experiments were carried out using an equilibration time of 6 hours, unless otherwise stated.

5.5 Effect of oxygen partial pressure on the Ge distribution

The effect of oxygen partial pressure on the distribution-ratio of Ge, $L_{Ge}^{s/m}$, was investigated in the current study. The slag composition for this series of experiments was fixed at Fe/SiO_2 ratio of 0.96, and concentration of CaO and MgO of 14.5 mass pct and 7.8 mass pct, respectively. At high oxygen partial pressure, magnetite formation become easier. To avoid the magnetite formation, the experiments were performed in the range of oxygen partial pressure between 10^{-7} and 10^{-10} atm at 1300°C (1573 K).

The results from the experiments are given in Table 5.3 and are also plotted against oxygen partial pressure in a logarithmic form in Figure 5.4. For comparison, the previous published data of Ge distribution in lead smelting systems (Yan and Swinbourne, 2003, Henao et al., 2010) and the prediction distribution calculated using the FactSage^{TM} 6.4 (CRCT - Thermofact and GTT Technology, Canada) for similar types of slag and alloy composition at 1300°C (1573 K) are also presented in Figure 5.4. FactSage™ 6.4 is a commercial thermochemical software commonly used for multiphase gas–slag–metal equilibria calculations in both ferrous and non-ferrous systems (Bale et al., 2009). It should be noted that the slag oxide database FToxid in FactSage 6.4 and 7.0 (latest version) is not yet optimized for GeO_2 containing slags. Only the GeO_2-SiO_2 system has been evaluated over the entire composition range (FactSage, 2015) using the data selected by Swamy et al. (2003) for Ge-Si-O-Cl-H system. Therefore, the predicted results from FactSage as shown in Figure 5.4 should be taken as indicative.

Table 5.3: Distribution of Ge in slag, metal, gas at 1300°C (1573 K) with a slag composition of $Fe/SiO_2=0.96$, CaO=14.5 mass pct and MgO=7.8 mass pct and equilibrated for 6 hours

log p_{O_2}	**Slag**		**Metal**		**Gas**	**$L_{Ge}^{s/m}$**	**log $L_{Ge}^{s/m}$**
	Ge mass pct	**Distribution pct**	**Ge mass pct**	**Distribution pct**	**Loss pct**		
-7	0.65	83.33	0.105	13.46	3.21	6.19	0.79
-8	0.37	47.44	0.35	44.87	7.69	1.06	0.02
-9	0.08	10.26	0.63	80.77	8.97	0.13	-0.90
-10	0.014	1.79	0.73	93.58	4.63	0.02	-1.69

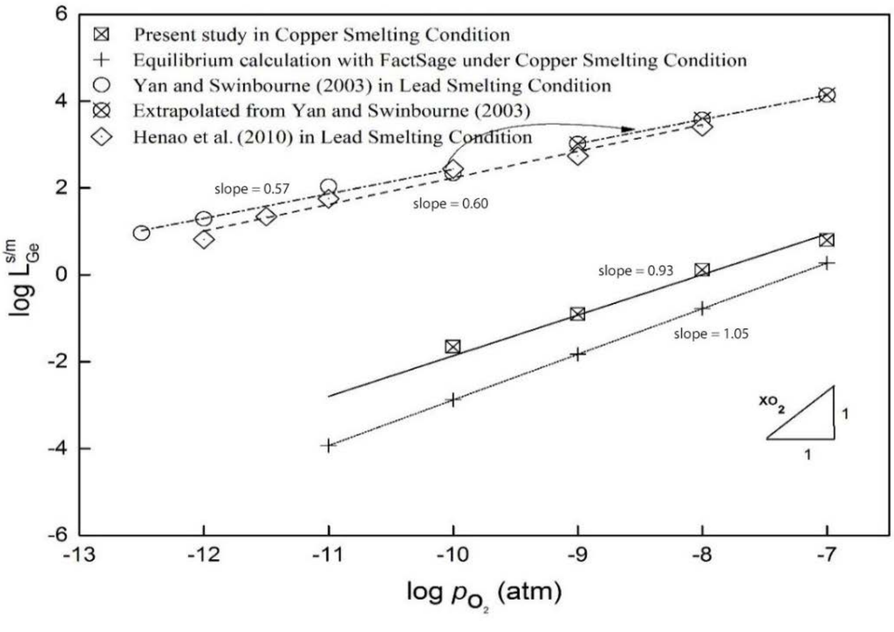

Figure 5.4: Germanium distribution-ratio in FeO_x-CaO-SiO_2-MgO slag and metal (copper and lead) as a function of oxygen partial pressure at 1300°C (1573 K).

The distribution-ratio of Ge ($\mathrm{L}_{\mathrm{Ge}}^{\mathrm{s/m}}$) in slag and metal can be expressed through Eq. (5.1) below:

$$\mathrm{L}_{\mathrm{Ge}}^{\mathrm{s/m}} = \frac{(mass\ pct\ \mathrm{Ge})_s}{[mass\ pct\ \mathrm{Ge}]_m} \tag{5.1}$$

where the subscript 's' denotes value in the slag and 'm' denotes value in the metal. The distribution-ratio can be presented in a different form which can provide information about the nature of the species in the slag; an approach which has been used by Takeda et al. (1983). As a first step to investigate the nature of the Ge in the slag (e.g. its oxidation state), the approach of Takeda et al. (1983) was adopted in the current study as described in the following paragraph.

Consider a general reaction for oxidation of germanium (Ge) as described in the following equation:

$$[\mathrm{Ge}] + \frac{\mathrm{v}}{2}\mathrm{O}_2 = (\mathrm{GeO}_{\mathrm{v}}) \tag{5.2}$$

Takeda et al. (1983) described that the oxide in the slag can be indicated in a monocation form (e.g. $GeO_{0.5}$ rather than Ge_2O), and thus the distribution-ratio can be expressed as

$$\mathrm{L}_{\mathrm{Ge}}^{\mathrm{s/m}} = \frac{K\ (n_T)[\,\gamma_{\mathrm{Ge}}^{o}]p_{\mathrm{O}_2}^{\mathrm{v}/2}}{[\,n_T](\,\gamma_{\mathrm{GeO}_{\mathrm{v}}}\,)} \tag{5.3}$$

Where K is the equilibrium constant for Reaction in Eq. (5.2), n_T is the total number of moles in constituents in the relevant phases, γ_{Ge} is the activity coefficient of Ge in the liquid metal, $\gamma_{\mathrm{GeO}_{\mathrm{v}}}$ is the activity coefficient of metal oxide $\mathrm{GeO}_{\mathrm{v}}$ in the slag and p_{O_2} is the oxygen partial pressure. The activity coefficient of metal and oxide can be assumed to be constant if their relative concentration is very small. Therefore, the Eq. (5.3) can be reformulated as

$$\log \mathrm{L}_{\mathrm{Ge}}^{\mathrm{s/m}} = \log B + \left(\frac{\mathrm{v}}{2}\right)\log p_{\mathrm{O}_2} \tag{5.4}$$

From the slope of the linear relationship between $\log \mathrm{L}_{\mathrm{Ge}}^{\mathrm{s/m}}$ and log p_{O_2} the degree of oxidation of solute Ge, $\frac{\mathrm{v}}{2}$ in the slag can be determined. Therefore, a slope of unity may indicate that the metal Ge is present in the slag as tetravalent Ge^{4+} (GeO_2), while a slope of 0.5 indicates the metal present as divalent Ge^{2+} (GeO).

Figure 5.4 shows that the oxygen partial pressure has a significant effect on the Ge distribution-ratio. It can be seen that the distribution-ratio increases with increasing oxygen partial pressure. Thus, more Ge is reporting to the slag as the oxygen partial pressure is increased. The experimental data from the current study can be fitted into a single straight line. The slope was found to be close to 1, i.e. 0.93. Similar line trend and gradient were observed from the FactSage prediction as shown in Figure 5.4. However, FactSage under predicted the Ge distribution-ratio by a factor of 10.

For comparison, previous studies on Ge distribution in a lead smelting system were also analysed. Yan and Swinbourne (2003) studied the Ge distribution-ratio in a lead (Pb)-slag (FeO-CaO-SiO_2-Al_2O_3) system at much lower oxygen partial pressure (10^{-10} to $10^{-12.5}$ atm). Their data were also plotted in Figure 5.4 and it can be seen that they can also be fitted in a straight line but with a smaller value of the slope, i.e. 0.57. They suggested in their study that Ge was present in the slag rather as divalent Ge^{2+} (GeO). Henao et al. (2010) reported a similar trend of the distribution-ratio of Ge (with a slope of 0.60) but suggested the tetravalent oxidation state of Ge in the slag. This conclusion was based on the EPMA measurement result of Ge-containing phase in the slag carried out in their study. It should be noted that in the lead-slag systems and the conditions studied by Henao et al. (2010) and Yan and Swinbourne (2003), the Ge concentration in the metal phase was very small which is likely to have contributed to the scatter of the reported data.

5.6 Characterization of slag with XRD and Raman analysis

To reconfirm further the oxidation nature of the Ge in the slag used in the current study, a further characterization that comprises of XRD and Raman spectrometry analyses were carried out on the quenched slag samples. The author was aware that analysing the quenched slag at room temperature is not an ideal approach, but believe that it can provide some insights on the possible nature of the slags at high temperature. The result of the XRD analysis of selected quenched slag sample is presented in Figure 5.5.

It can be seen that there were a number of crystallized phases present in the quenched slag, namely forsterite – $(Mg_{1.8}Fe_{0.2})(SiO_4)$, fayalite – $(Mg_{0.26}Fe_{1.74})SiO_4)$, diopside – $Ca0_{0.99}(Mg_{0.64}Fe_{0.34})(Si_{1.6}Fe_{0.42})O_6$, andradite – $Ca_3Fe_2(SiO_4)_3$, copper oxide – Cu_2O and germanium oxide – GeO_2. The same slag sample was also analysed using a Raman spectrometry to evaluate the molecular vibration of the compounds presence. Table 5.4 shows the typical Raman vibration frequency values of the phases identified using the Raman technique (Wang et al., 2009, Balkanski et al., 1969, Micoulaut et al., 2006, Handbook of Minerals Raman Spectra, 2015) while the result of the Raman spectrometry analysis of the quenched slag is presented in Figure 5.6. It can be seen in Figure 5.6 that

Raman shift spectrum confirms the presence of the forsterite, fayalite, diopside, andradite, Cu_2O as well as GeO_2. These results further support the idea that Ge present in the slag as tetravalent Ge^{4+} (or GeO_2).

Table 5.4: Raman vibration frequencies of phases present in the slag after equilibrium reaction

Phase	**Vibration Frequency (cm^{-1})**	**Ref.**
Cu_2O	220, 661	(Balkanski et al., 1969)
GeO_2	503, 593,701, 973	(Micoulaut et al., 2006)
Fayalite	284, 815, 841	(Handbook of Minerals Raman Spectra, 2015)
Andradite	452, 576, 995	(Handbook of Minerals Raman Spectra, 2015)
Forsterite	437, 610	(Handbook of Minerals Raman Spectra, 2015)
Diopside	182, 392, 560	(Handbook of Minerals Raman Spectra, 2015)

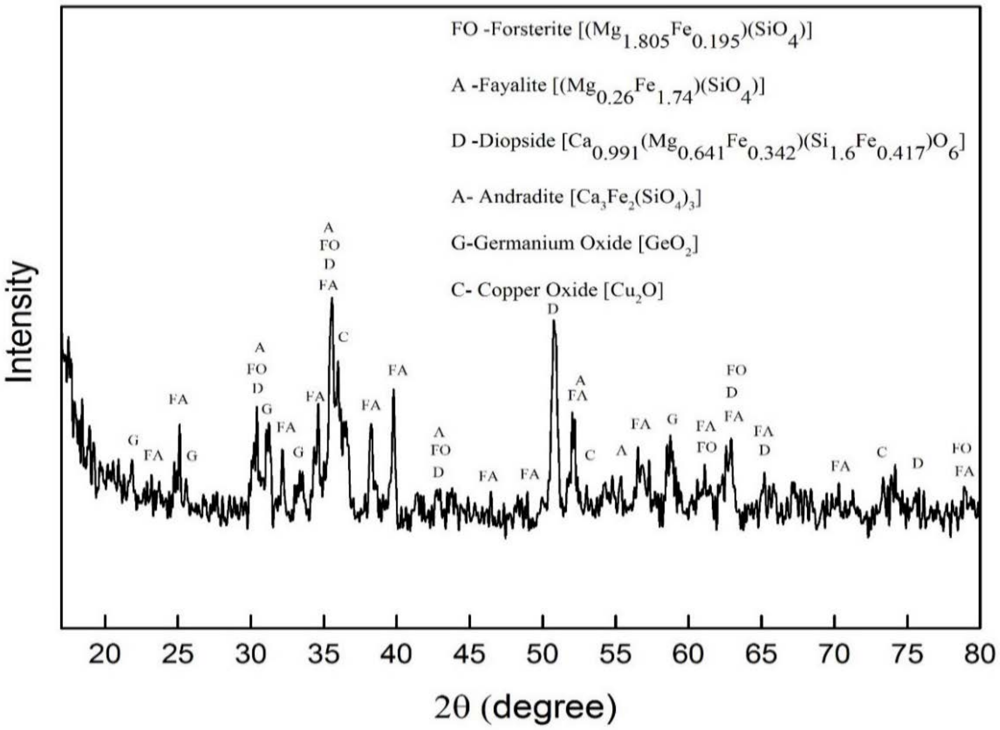

Figure 5.5: XRD spectrum of a quenched FeO_x-CaO-SiO_2-MgO slag containing GeO_2 equilibrated at (1300°C (1573 K) and $p_{O_2} = 10^{-8}$ atm for 6 hours.

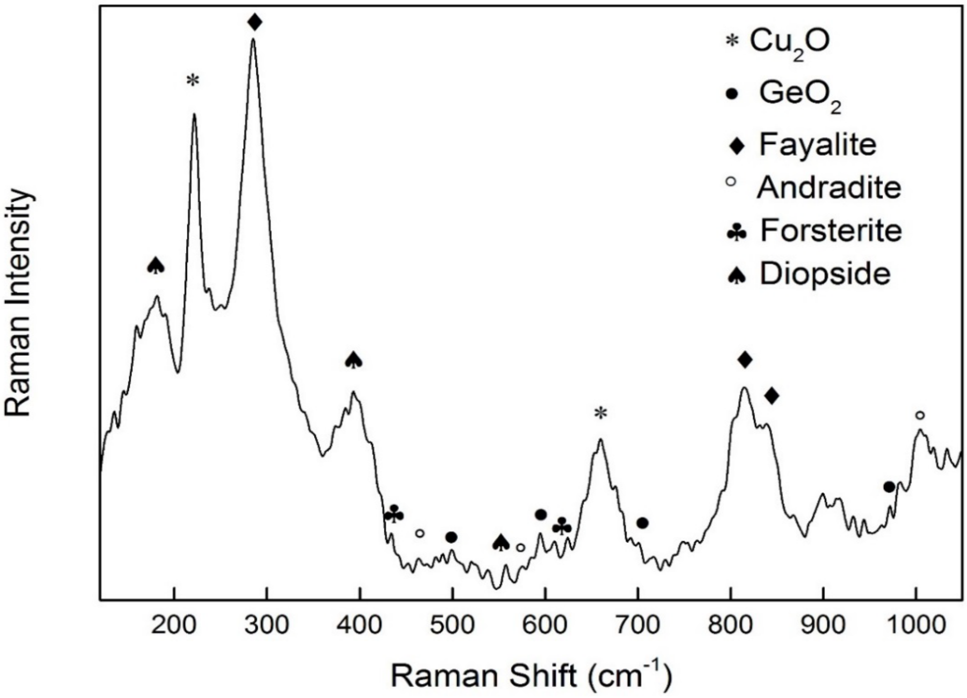

Figure 5.6: Raman shift spectrum of a quenched FeO_x-CaO-SiO_2-MgO slag containing GeO_2 equilibrated at 1300°C (1573 K) and $p_{O_2} = 10^{-8}$ atm for 6 hours.

5.7 Effect of oxygen partial pressure on Cu loss

The copper loss to the slag was also tracked in the current study. Figure 5.7 shows the copper loss to the slag at temperature 1300°C (1573 K) as function of oxygen partial pressure. The average copper content of the slag at high p_{O_2} as shown in Figure 5.7, is less than 2 mass pct, while at low p_{O_2}, about 1 mass pct copper is lost to the slag. Yazawa and Takeda (1982) developed the following Eq. (5.5) to estimate the copper losses to iron-silicate and calcium-silicate slags as a function of temperature and oxygen partial pressure:

$$\log(mass\ pct\ \mathrm{Cu}) = 0.221 \log p_{O_2} + \frac{2490}{T} + 0.455 \qquad (5.5)$$

The current results were found to follow a similar trend to those reported by (Yazawa and Takeda, 1982) as can be seen in Table 5.5. The copper loss at high oxygen partial pressure (p_{O_2}= 10^{-7}atm) obtained in the current study, however, was much lower compared to the value predicted using Eq. (5.5). It may be that different slag composition used in this study (containing MgO) contributed to the different in the copper losses. It is worth to mention that the slope of Figure 5.7 is about 0.1 which can be considered close to 1/4, which means that the stable oxidation state of copper in the slag is Cu^+, i.e., $CuO_{0.5}$. Moreover, it was also confirmed from XRD that the stable phase of Cu in equilibrated slag is Cu_2O.

Table 5.5: Comparison of copper loss to the slag between the current study and those from Yazawa and Takeda (1982) at 1300°C (1573 K).

log p_{O_2}	**Mass pct Cu in slag from Eq. (5.5)**	**Mass pct Cu in slag in the present study**
-10	0.7	0.97
-9	1.1	1.2
-8	1.9	1.6
-7	3.1	1.8

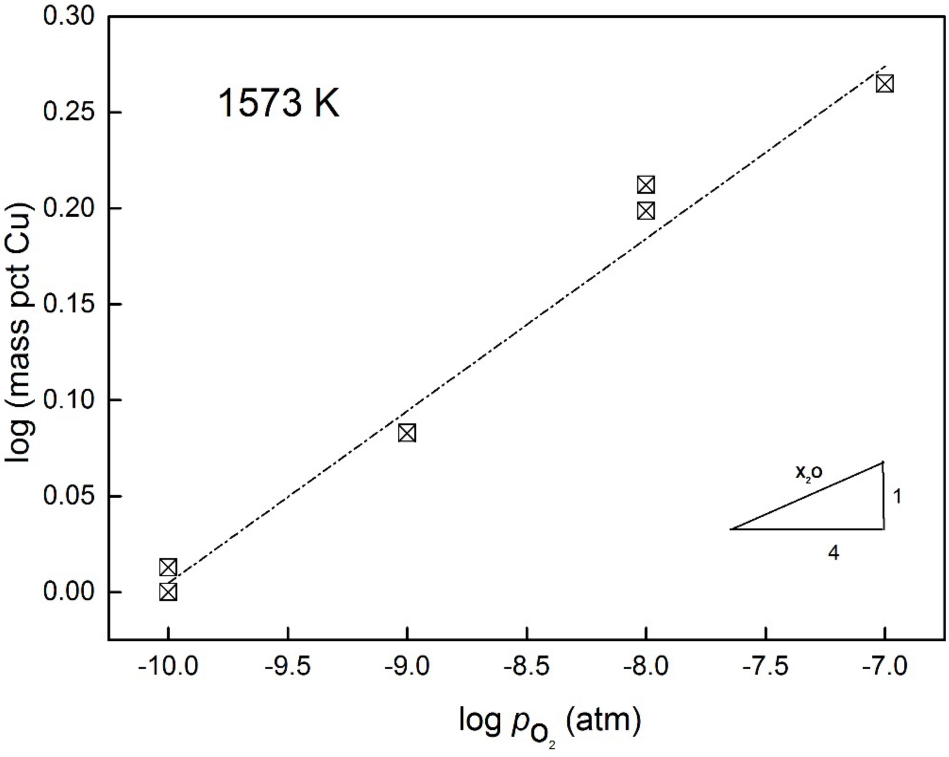

Figure 5.7: Copper loss to FeO_x-CaO-SiO_2-MgO slag as a function of oxygen partial pressure at 1300°C (1573 K).

5.8 Effect of temperature

The temperature dependence of Ge distribution-ratio in the FeO_x-CaO-SiO_2-MgO slag system (7 mass pct MgO) and copper is shown in Figure 5.8. This slag contained 9.8 mass pct of CaO with Fe/SiO_2 ratio of 0.99. It can be seen that the Ge distribution-ratio decreases with increasing temperature over the range 1200-1350°C (1473-1623 K) under an oxygen potential of 10^{-8} atm. Consider a reaction in Eq. (5.6), a similar reaction to Eq. (5.2):

$$Ge_{(l)} + O_{2(g)} = GeO_{2(l)} \qquad \Delta G^o = -562{,}000 + 180\ T\ (J/mol) \qquad (5.6)$$

The standard Gibbs free energy equation is shown in Eq. (5.6) was reported by Sreedharan et al. (1979). The value of equilibrium constant calculated using the above equation is very close to that of calculated using Factsage 6.4 thermochemical software. For example, the value of equilibrium constants of reaction in Eq. (5.6) at 1200ºC (1473 K), 1250ºC (1523 K), 1300ºC (1573 K) and 1350ºC (1623 K) are 33.8×10^4, 7.46×10^4, 1.82×10^4 and 4.83×10^3, respectively, as calculated using the "Reaction" module of FactSage 6.4. It can be seen here that the equilibrium constant value changes drastically with temperature. Therefore, the distribution-ratio would also change significantly, as expressed in Eq. (5.3). It can also be seen from Figure 5.8 that higher amount of Ge report to copper at higher temperatures. Moreover, the slag viscosity also decreases with increasing temperature that is also beneficial for slag separation during smelting. However, an opposite effect was observed for copper loss to the slag as shown in Figure 5.9. At fixed oxygen partial pressure, copper loss to the slag increases from 0.5 to 2.1 mass pct with increasing temperature. The percentage of copper loss to the FeO_x-CaO-SiO_2-MgO slag was found to be comparable to those reported in the previous studies (Johnston et al., 2007, Yazawa et al., 1999).

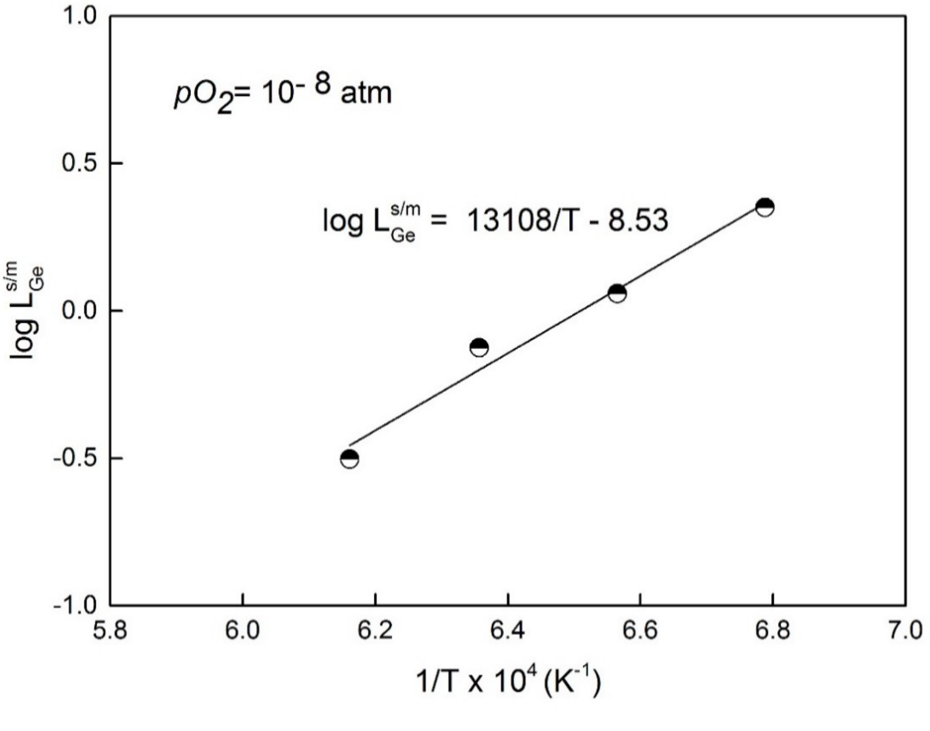

Figure 5.8: The effect of temperature on the Ge distribution-ratio in FeO_x-CaO-SiO_2-MgO slag and copper at $p_{O_2} = 10^{-8}$ atm equilibrated for 6 hours (Fe/SiO_2= 0.99, CaO = 9.8 mass pct).

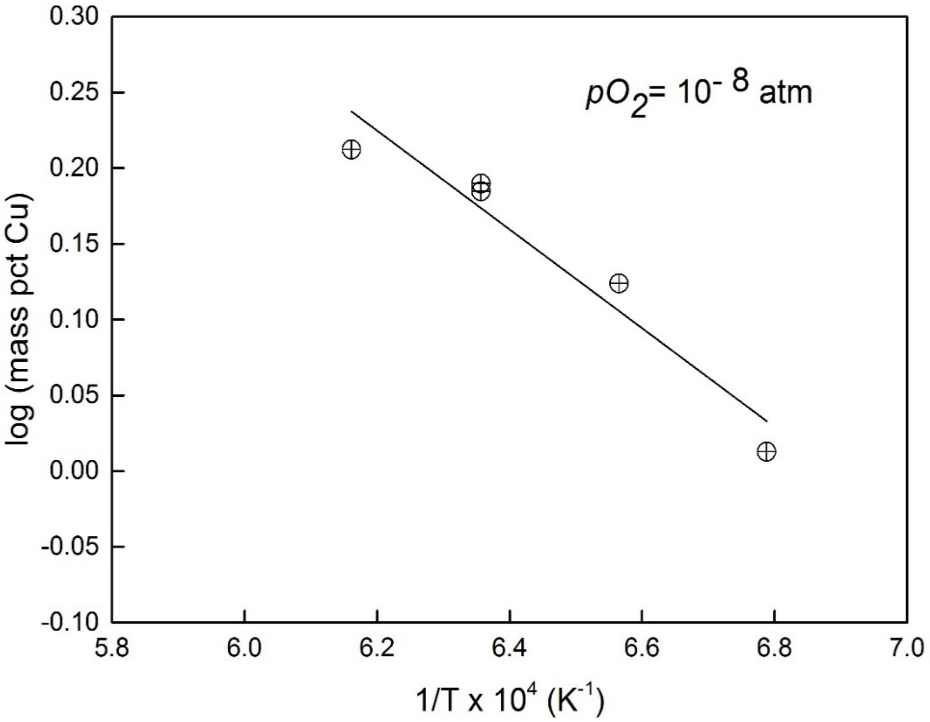

Figure 5.9: Copper loss in FeO_x-CaO-SiO_2-MgO slag as a function of temperature at p_{O_2} = 10^{-8} atm.

5.9 Effect of slag composition

The effect of slag composition, represented by the variation in the (CaO+MgO)/SiO_2 and Fe/SiO_2 ratios, on the Ge distribution-ratio was evaluated. Basicity and acidity of a slag can be represented by the ratio of acid and basic component of the slag component. In this study, the effect of the (CaO+MgO)/SiO_2 ratio, which represents the slag "basicity", on the Ge distribution-ratio in FeO_x-SiO_2-CaO-MgO slag and copper is shown in Figure 5.10. The partitioning of Ge into the copper metal (inverse of $L_{Ge}^{s/m}$) was found to decrease with increasing addition of lime to the FeO_x-SiO_2-CaO-MgO slag. The $L_{Ge}^{s/m}$ was observed to increase up to 5 times when more CaO is added to the slag within the composition range studied. It appeared that the GeO_2 behaves as acidic oxide, as the lime content in the slag was increased resulting in a more basic slag, more Ge report into the slag. The copper loss to the FeO_x-SiO_2-CaO-MgO slag, however, appeared to not change with the variation of (CaO+MgO)/SiO_2 ratio at a fixed ratio of Fe/SiO_2 ~ 1, as shown in Figure 5.11. It was found that the oxide of copper having neutral nature in the present FCS slag system. The maximum copper concentration in the slag was found to be about 1.6 mass pct, which is in a good agreement with the result of (Yazawa and Takeda, 1982). They reported a copper concentration of less than 2 mass pct in calcium ferrite slag at $p_{O_2}= 10^{-8}$ atm and 1300°C (1573 K). Therefore, within the range of the conditions studied, the copper loss to the slag appeared to be a function of oxygen partial pressure and temperature only.

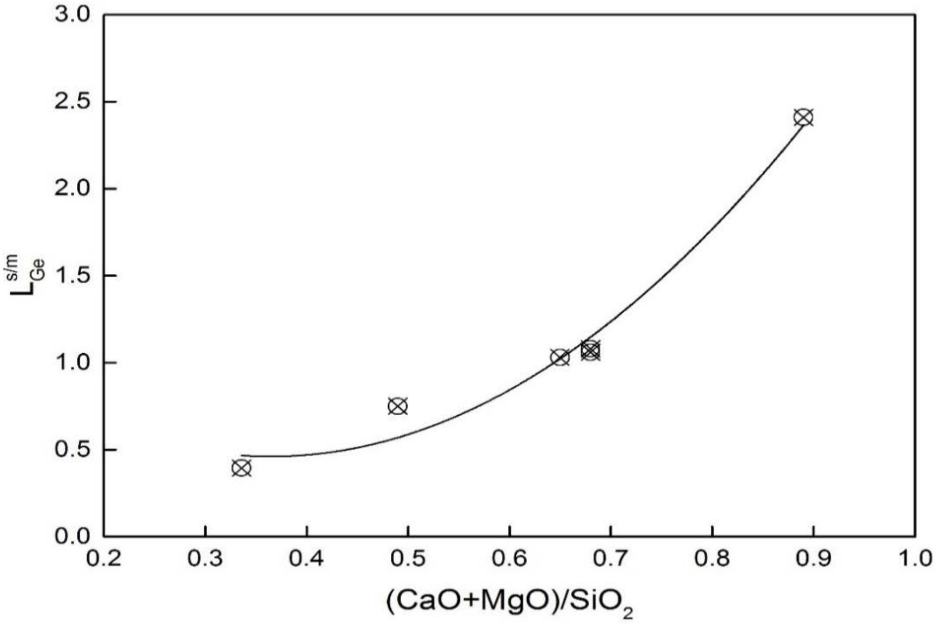

Figure 5.10: The effect of (CaO+MgO)/SiO_2 ratio on the Ge distribution-ratio in FeO_x CaO-SiO_2-MgO slag and copper at 1300°C (1573 K) and $p_{O_2}= 10^{-8}$ atm.

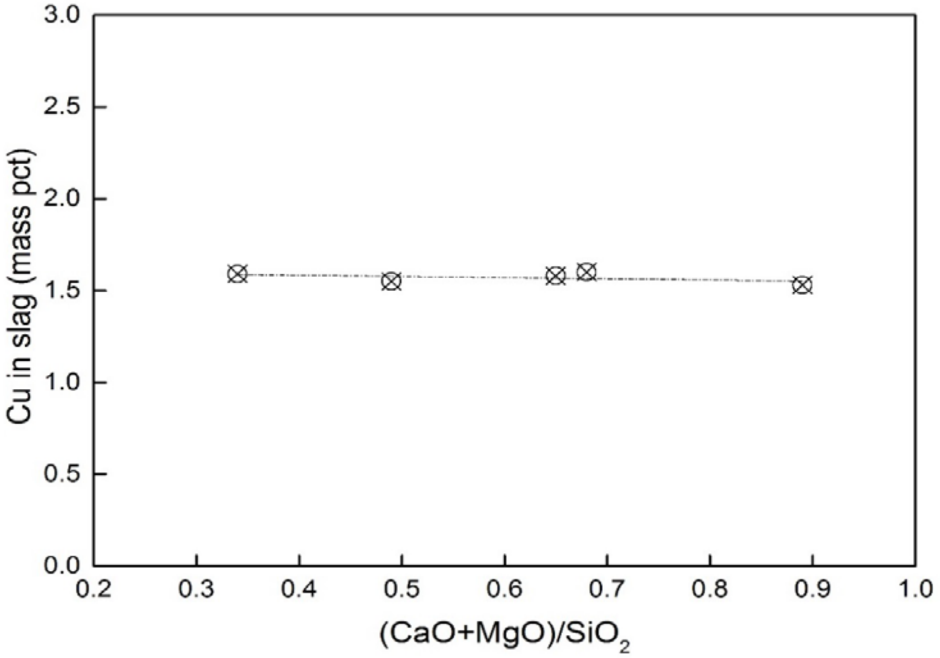

Figure 5.11: The effect of (CaO+MgO)/SiO_2 ratio on the copper loss to FeO_x-CaO-SiO_2-MgO slag at 1300°C (1573 K) and $p_{O_2}= 10^{-8}$ atm.

The effect of Fe/SiO2 ratio with fixed lime content on the Ge distribution-ratio is shown in Figure 5.12. The results show that the Ge distribution-ratio increases with increasing Fe/SiO2 ratio from 0.81 to 1.16. Beyond 1.16 no further increase in the Ge distribution-ratio was observed. It appeared that high silica content (i.e. low Fe/SiO2 ratio) was required to keep the Ge in the copper. This is also in line with the observation of the effect of (CaO+MgO)/SiO2 on the partitioning in Figure 5.10.

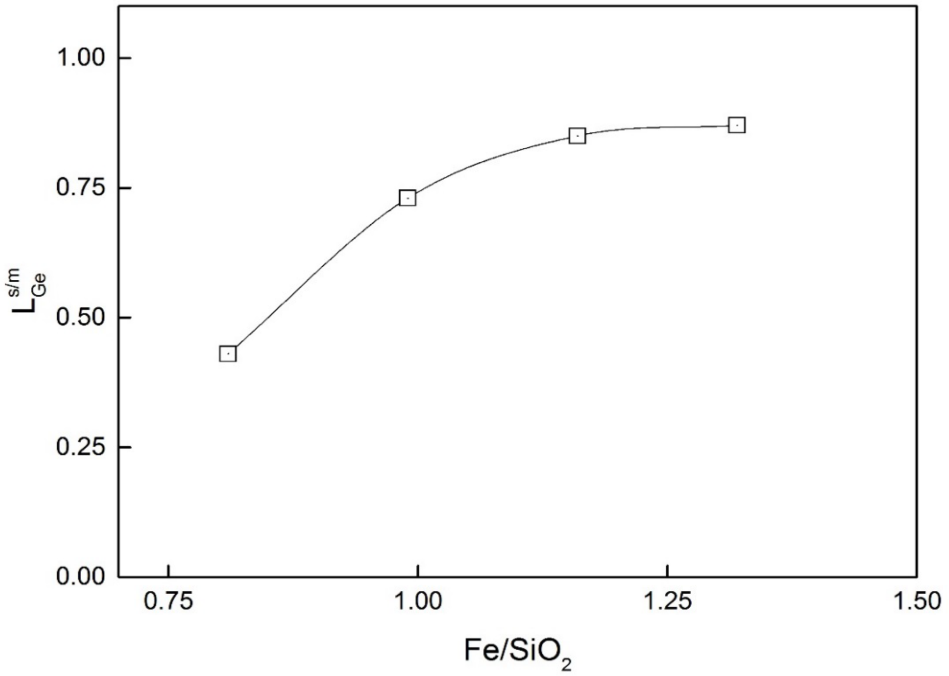

Figure 5.12: The effect of Fe/SiO2 ratio on the Ge distribution-ratio in FeO_x-CaO-SiO_2-MgO slag and copper at 1573 K (1300°C) and $p_{O_2} = 10^{-8}$ atm (CaO = 9.8 mass pct).

5.10 Effect of lime activity on the germanium distribution coefficient

The influence of the slag "basicity" may be explained in terms of free oxygen ion. As the activity of free oxygen ion cannot be measured experimentally, it was assumed that O^{2-} ion activity can be replaced by activity of CaO at fixed temperature and oxygen partial pressure, i.e. activity of CaO is proportional to O^{2-} ion. The activity of CaO in the different slag compositions studied was estimated using the FactSage 6.4 package. Figure 5.13 shows the linear relationship between the log of Ge distribution-ratio and the log a_{CaO}. Some experimental scatter was found in the present work. It was found that as the activity of CaO in slag decreases, the Ge distribution-ratio is also decreasing. Therefore, it can be suggested that, the less of O^{2-} ion presence in the slag, the more likely the Ge to report to metal phase.

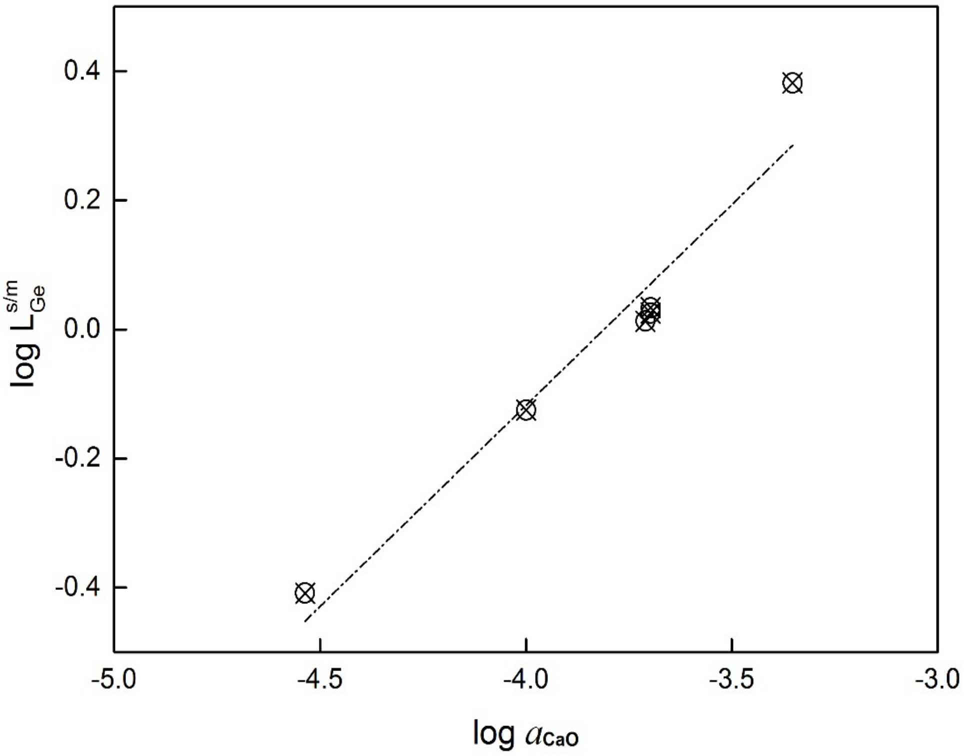

Figure 5.13: Dependency of CaO activity in FeO_x-CaO-SiO_2-MgO slag on the Ge distribution-ratio in slag and copper at 1300°C (1573 K) and p_{O_2}= 10^{-8} atm.

5.11 Activity coefficient of GeO_2 in the slag

The activity coefficient of GeO_2 in the slag can be calculated using the Eq. (5.3) utilising the information on the Ge distribution-ratio obtained in this study. Upon rearranging Eq. (5.3), the following Eq. (5.7) can be derived:

$$\gamma_{\mathrm{GeO_v}} = \frac{K\,(n_T)[\,\gamma^{o}_{\mathrm{Ge}}]p_{\mathrm{O_2}}^{\mathrm{v}/2}}{[\,n_T]\,\mathrm{L}^{\mathrm{s/m}}_{\mathrm{Ge}}} \tag{5.7}$$

Considering the reaction in Eq. (5.6), the value of equilibrium constant K can be calculated to be 1.82 × 10^4 at 1300°C (1573 K). The value of $[n_T]$ is 1.57 for 100g of copper, and (n_T) is between 1.94 to 2 for 100g of slag. The exponent "v/2" has a value of 1 for GeO_2 as shown in Figure 5.4. The value of limiting activity coefficients of Ge in copper obtained from different investigators are listed in Table 5.6. The values presented in the table were either taken from graph or calculated from the expressed relationship provided by the investigators.

Table 5.6: Activity coefficient of Ge γ_{Ge}^{o} in copper.

Temperature °C (K)	Sodeck et al. (1970)	Hager et al. (1973)	Sigworth and Elliott (1974)	Yazawa and Azakami (1969)
1525°C (1798 K)	0.03ǂ	0.03	-	-
1200°C (1473 K)	0.022ǂ	-	0.009*	0.02*

*estimated from previous experimental data
ǂ obtained at 1547°C (1820 K) and 1265°C (1538 K)

Sodeck et al. (1970) investigated the activity of Ge in copper in the temperature range between 1267°C (1540 K) and 1547°C (1820 K) using a Knudsen effusion cell and mass spectroscopy. Hager et al. (1973) also used a Knudsen effusion cell and mass spectroscopy technique to determine the activities of Ge in Cu-Ge alloy and found a good agreement with the results of Sodeck et al. (1970). Sigworth and Elliott (1974) reported a very small value of limiting activity coefficient of Ge as minor impurities in Cu alloy, but no detailed information had been provided. Azakami and Yazawa (1976) extrapolated the result of Alcock et al. (1970) to 1200°C (1473 K) by using the following relation $T.\ln\gamma^{o}$ = constant. Recently, Wang et al. (2010) assessed the Cu-Ge binary system using CALPHAD method through the Thermocalc® software and very good agreement was found between the calculated and the experimental data. There is no other information on the Ge activity coefficient and the effect of temperature, particularly at 1300°C (1573 K) The value of Ge activity coefficient used in the present study was interpolated from the finding of Hager et al. (1973) using the extrapolation relationship used by Yazawa and Azakami (1969). The calculated Ge activity coefficient in copper and its variation with temperature, extrapolated from data in Table 5.6, is presented in Figure 5.14. It can be seen from Figure 5.14 that the activity coefficient of Ge in copper increases with increasing temperature.

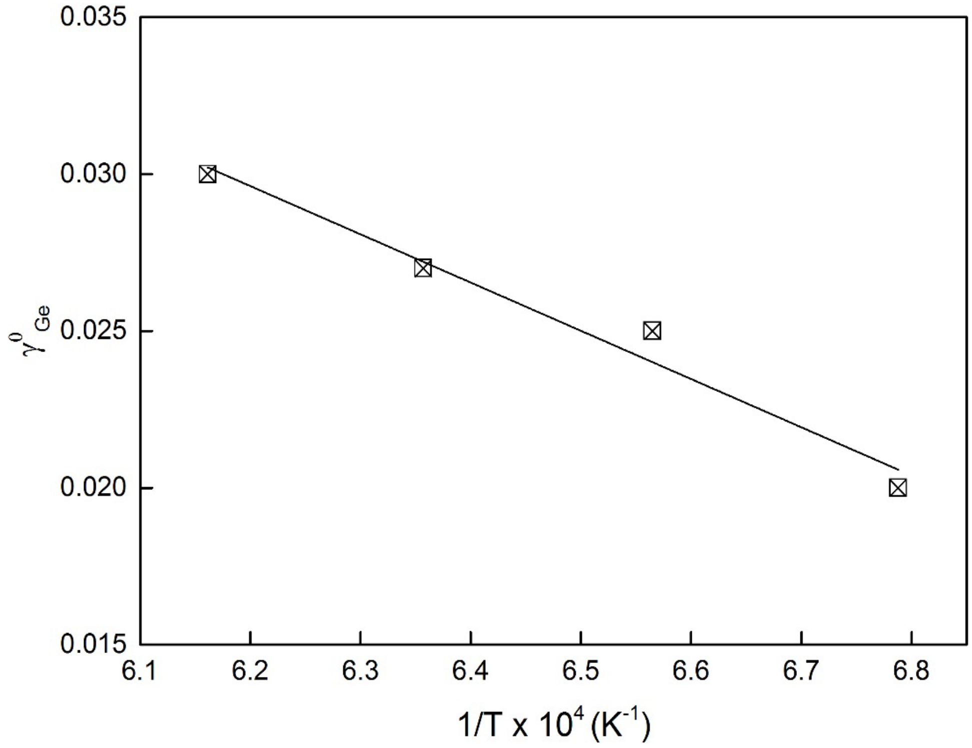

Figure 5.14: Activity of Ge in copper and its variation with temperature.

The activity coefficients of GeO_2 in the slag were then calculated by substituting all the relevant values into the Eq. (5.7), and the results are listed in Table 5.7 for different slag compositions. The effect of temperature and slag composition (represented using the (CaO+MgO)/SiO_2 ratio) on the GeO_2 activity coefficient are presented in Figures 5.15 and 5.16, respectively. It can be seen from Figure 5.15 that the activity coefficient GeO_2 in the FeO_x-CaO-SiO_2-MgO was found to decrease with increasing temperature. The reason behind the downward trend also relates to the Gibbs free energy and equilibrium constant values of reaction in Eq. (5.7). Both values decrease with increasing temperature due to the instability of GeO_2 at high temperature. The activity coefficient of GeO_2 in the FeO_x-SiO_2-CaO was also found to decrease with increasing (CaO+MgO)/SiO_2 ratio at fixed Fe/SiO_2 as shown in Figure 5.16. This also, again, suggests about the acidic nature of GeO_2 in the slag.

Table 5.7: Calculated activity coefficient of GeO_2 in slag and distribution-ratio of Ge in FeO_x-SiO_2-CaO-MgO slag and copper at 1300°C (1573 K) and $p_{O_2} = 10^{-8}$ atm

Slag Composition (mass pct)					n_T	$L_{Ge}^{s/m}$	γ_{GeO_2}
(CaO+MgO)/SiO_2	**Fe_{Total}**	**SiO_2**	**CaO**	**MgO**			
0.34	37.3	35.3	5.59	6.30	2.00	0.39	1.50
0.49	37.9	32.8	9.80	6.51	1.97	0.75	0.80
0.65	33.4	33.6	14.5	7.52	1.95	1.03	0.55
0.68	31.1	32.6	14.5	7.83	1.99	1.06	0.55
0.68	31.1	32.6	14.5	7.83	1.99	1.08	0.54
0.89	30.7	31.3	19.4	8.78	1.94	2.41	0.24

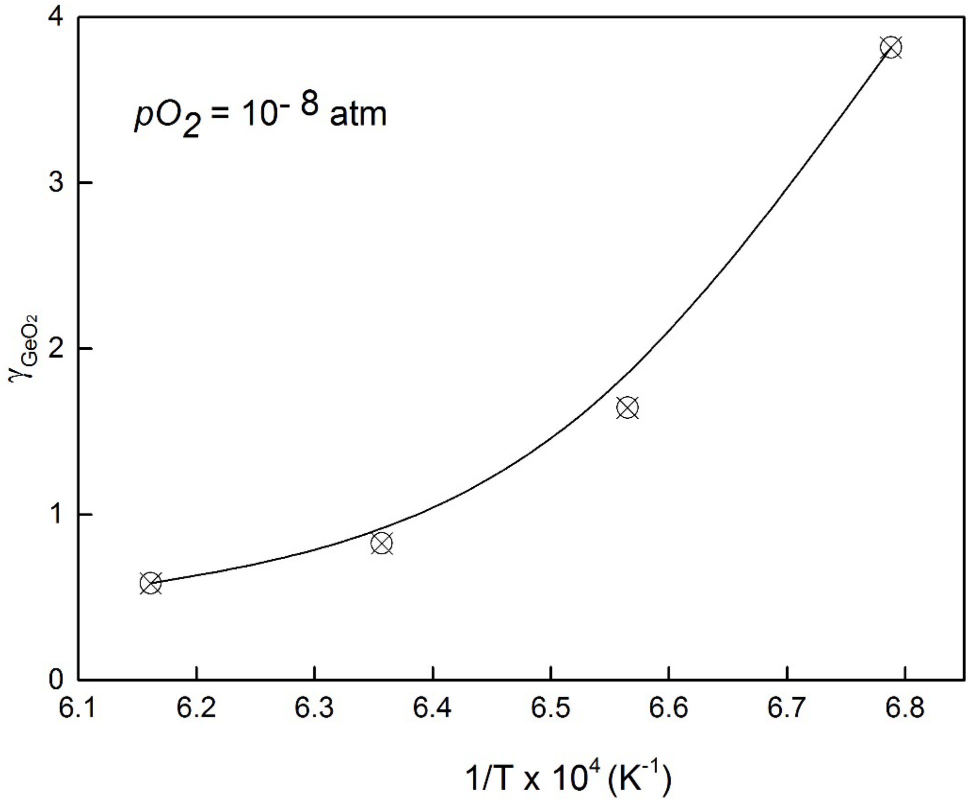

Figure 5.15: The effect of temperature on the activity coefficient of GeO_2 in FeO_x-CaO-SiO_2-MgO slag and copper at p_{O_2}= 10^{-8} atm (Fe/SiO_2= 0.99, CaO = 9.8 mass pct).

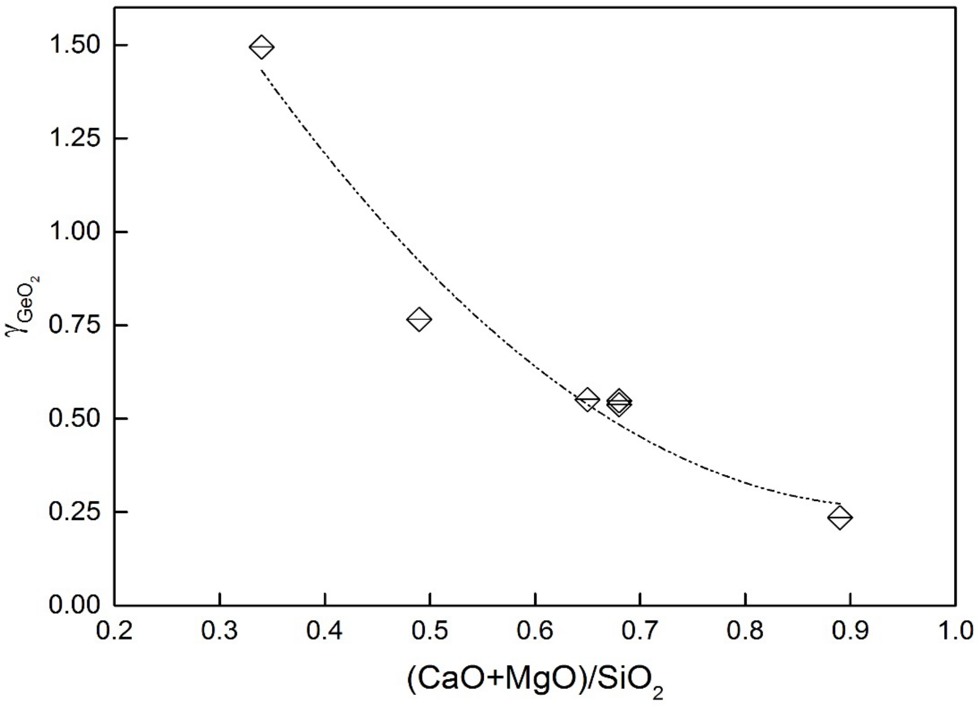

Figure 5.16 : The effect of (CaO+MgO)/SiO_2 ratio on the activity coefficient of GeO_2 in FeO_x-CaO-SiO_2-MgO slag and copper at 1300°C (1573 K) and $p_{O_2} = 10^{-8}$ atm.

5.12 Effect of optical basicity

In the discussion in the preceding paragraphs, the effect of slag composition on the behaviour of Ge (or GeO_2) was represented using the (CaO+MgO)/SiO_2 ratio. Another approach using an optical basicity to represent the variation of slag composition is adopted in this section. Optical basicity is a property of slag which was first suggested by Duffy and Ingram (1975) to understand the effect of metallurgical slag composition on its thermochemical properties (Duffy and Ingram, 1975, Duffy and Ingram, 1976, Duffy et al., 1978). The theoretical optical basicity values for pure oxides are given in Table 5.8.

Table 5.8: Theoretical optical basicity value for pure oxides

Oxide component	Theoretical optical basicity
Cu_2O	1.36
CaO	1
FeO	0.93
Fe_2O_3	0.77
SiO_2	0.48
MgO	0.78
GeO_2	0.61
PdO	1.19

The optical basicity of each molten slag used in the present study as listed in Table 5.1, can be calculated using Eq. (5.8)

$$\wedge_{melt} = \frac{\sum x_i \, n_i \wedge_i}{\sum x_i \, n_i} \tag{5.8}$$

where n_i, x_i, $\wedge_i$ are the number of oxygen in the oxide, the mole fraction, and the theoretical optical basicity of component *i*, respectively. The slags used in the present study contain Fe in the form of FeO and Fe_2O_3. A special wet chemical analysis to determine the ratio of percentage of FeO and Fe_2O_3 was not carried out, rather the slags' chemistry was only determined and analysed using ICP technique. Therefore, the equilibrium compositions of the slags (including the FeO and Fe_2O_3 concentrations) were determined by equilibrium recalculation using FactSage 6.4 considering the compositions in Table 5.7. The results on the recalculated equilibrium slag composition and the associated optical basicity are presented in Table 5.9.

Table 5.9: Equilibrium slag compositions recalculated using FactSage 6.4, associated optical basicity, distribution-ratio of Ge and activity coefficient of GeO_2 at 1300°C (1573 K) and $p_{O_2} = 10^{-8}$ atm

Recalculated equilibrium slag composition, mass pct						$\wedge_{melt}$	$\log L_{Ge}^{s/m}$	$\log \gamma_{GeO_2}$
FeO	Fe_2O_3	SiO_2	CaO	MgO	Cu_2O			
45.84	3.49	36.1	5.72	6.44	2.39	0.673	-0.408	0.17
44.15	4.79	32.67	9.76	6.48	2.14	0.692	-0.125	-0.11
38.36	4.55	33.28	14.36	7.45	2.00	0.694	0.012	-0.26
37.14	4.45	33.52	15.02	7.88	1.99	0.693	0.025	-0.26
37.14	4.45	33.52	15.02	7.88	1.99	0.693	0.033	-0.27
33.26	6.13	30.82	19.1	8.64	2.03	0.708	0.382	-0.63

The data in Table 5.9 were plotted and presented in Figure 5.17. It can be seen that the distribution-ratio of Ge decreases with decreasing optical basicity of the slag. It can also be seen from Figure 5.17 that the calculated activity coefficient of GeO_2 decreases with the increase of optical basicity. These observations are in line with the discussion on the effect of (CaO+MgO)/SiO_2 ratio on the Ge behaviour in the preceding Sections.

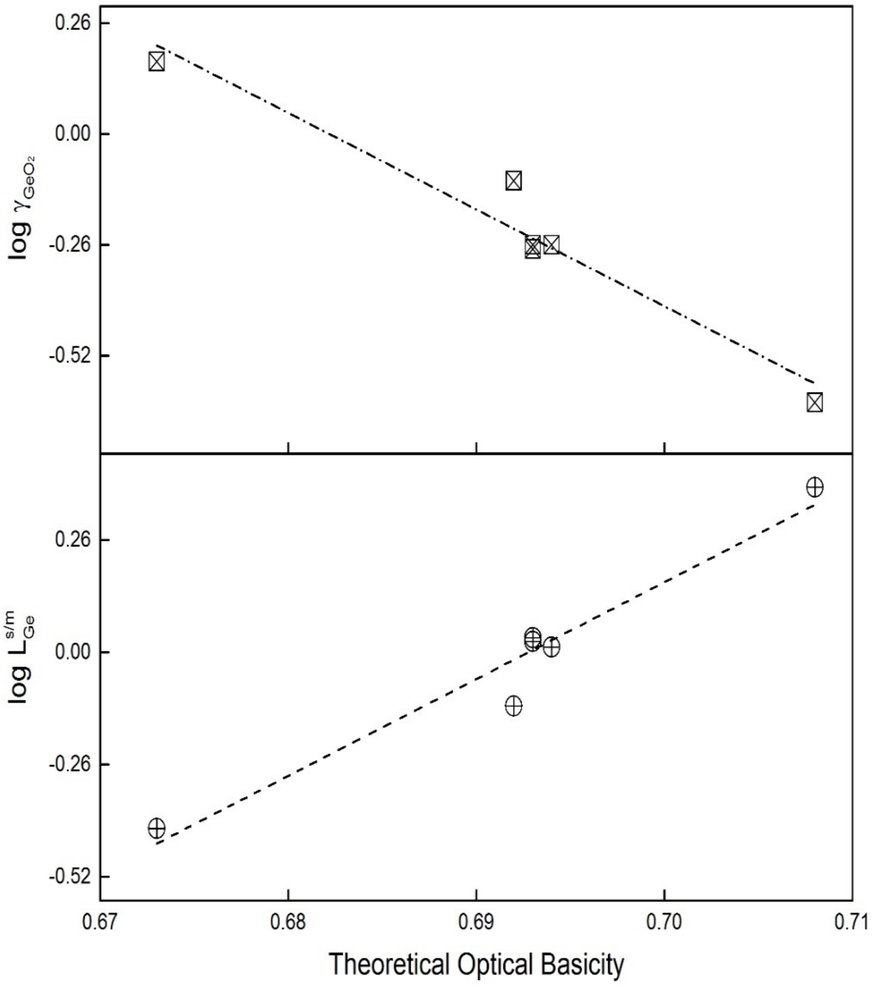

Figure 5.17: The effect of optical basicity on the Ge distribution-ratio and activity coefficient of GeO_2 in FeO_x-CaO-SiO_2-MgO slag at 1300°C (1573 K) and $p_{O_2}= 10^{-8}$ atm.

5.13 Nature of GeO_2 according to ionic theory

The results from the current study suggest that the nature of GeO_2 in the slag system studied is acidic. To clarify this notion, a calculation of ionic bond fraction of GeO_2 according to the ionic theory was carried out. The ionic theory suggests that a basic slag has free O^{2-} ion. This free O^{2-} ion can easily attack an acidic oxide which means that if the nature of the minor elements oxide is acidic then the elements will tend to report to the slag. In an acid slag, there are no free O^{2-} ions but it has high capacity to incorporate basic oxide to make a more complex structure. Gilchrist (1989) categorized the acid-basic nature of metal oxide through the ratio $z/_{a^2}$. Here, z is the charge of the metal ion and a is the sum of ionic radii of two ions ($r_{\text{cation}} + r_{\text{anion}}$). Gilchrist (1989) proposed the range 0.1- 0.35 for basic oxide, 0.39 - 0.90 for intermediate oxide and greater than 1 for acidic oxide. The ionic radii of Ge^{4+} and O^{2-} are 0.53 Å and 1.40 Å respectively and thus the value of $z/_{a^2}$ for GeO_2 is 1.07 which is in the range of acidic oxide (Ride, 2003). Pauling (1960) also provided a relationship of ionic bond fraction (IBF) as shown in Eq. (5.9) where he related the acidic-basic nature of oxide using the electronegativity of cation (x_b) and anion (x_a) of metal oxide.

$$\text{Ionic Bond Fraction (IBF)} = 1 - \exp^{-0.25\,(x_a\,-\,x_b)^2} \tag{5.9}$$

The values of x_a and x_b for GeO_2 are 3.44 and 2.01, respectively. Thus, the value of IBF for GeO_2 bond is calculated to be 0.40 which is close to Si-O bond indicated by Gilchrist (1989) All of these reconfirm the nature of GeO_2 as an acidic oxide.

5.14 Summary

The distribution-ratio and thermodynamic behaviour of Ge in magnesia saturated FeO_x-CaO-SiO_2 slag and molten copper have been investigated under the conditions relevant to the copper smelting processes. The following summary can be drawn from this chapter.

The Ge distribution-ratio, $L_{Ge}^{s/m}$, in FeO_x-CaO-SiO_2-MgO slag and molten copper was found to decrease with decreasing oxygen partial pressure at temperature 1300°C (1573 K) for a fixed slag composition. It was found that temperature have a significant effect on the Ge distribution-ratio at fixed oxygen potential. At higher temperature, significant amount of Ge reported to the copper, however, copper loss to the slag was also increased.

At 1300°C (1573 K) and p_{O_2} = 10^{-8} atm, the Ge distribution-ratio was found to be affected by the (CaO + MgO)/SiO_2 ratio or optical basicity. The Fe/SiO_2 ratio was also found to affect the Ge distribution-ratio but beyond 1.16 the effect is negligible. The activity coefficient of GeO_2 in FeO_x-CaO-SiO_2-MgO slag was calculated and found to be in the range of 0.24 to 1.50. Moreover, the Ge was suggested to be present in the FeO_x-CaO-SiO_2-MgO slag predominately as tetravalent Ge^{4+}, (GeO_2). GeO_2 is acidic, therefore it was suggested that a less-basic slag (or high SiO_2 content) and higher temperature with a reducing atmosphere are recommended to decrease the Ge deportment to the slag. However, higher temperature also means lower slag viscosity which promotes slag separation. Therefore, high silica content FeO_x-CaO-SiO_2-MgO slags can be used for high Ge recovery in the copper.

Chapter 6 Thermodynamics of Palladium and Tantalum in FeO_x-CaO-SiO_2-MgO Slag and Molten Copper

6.1 Introduction

Palladium (Pd), a member of the platinum group metals (PGMs), is a silvery white, dense, soft, ductile and scarce metal. The concentration of Pd in the earth's crust is 0.01 ppm which occurs naturally together along with platinum, copper and nickel ores (Allen, 1960, Kirk and Othmer, 1973). Palladium is widely used in electronic industries for the manufacture of the multi-layer ceramic capacitor (MLCC), hybrid integrated circuit (HIC), hydrogen storage material, connecting plating, gas sensor, and photovoltaic material (Omoto et al., 2000, Hesse, 2007, Ruhela et al., 2014). In 2012, one-sixth of globally produced Pd was accounted with electronic industries and the demand is significantly increased (Loferski, 2015). Tantalum (Ta) is another rare earth transition metal which is highly corrosion resistant, occurs naturally together along with iron, manganese and niobium. The chemical inertness property of Ta makes it valuable in chemical industry. Most of Ta produced in the world consumed every year mainly for capacitors due to superior capacitance characteristic for making the electronic equipment such as mobile phones, video game systems and computer (Spitczok von Brisinski et al., 2014). The total consumption of Ta had been increased three times for tantalum capacitors (TCs) in last decade, and about 42 pct of annual production of Ta is utilised for TCs in 2013 (Niu et al., 2016).

The high growing demand in global market and increasing depletion rate of Pd and Ta resources have redirected the industrial community to thinking about alternative of primary sources for these metals. These alternative sources are industrial, consumer and electronics and electrical equipment wastes (e-waste) (Worrell and Reuter, 2014). Among them, e-waste can be an important secondary source. E-waste is a highly generated waste but it contains metals which are precious and rare such as gold (Au), indium (In), germanium (Ge), tin (Sn), palladium (Pd), and tantalum (Ta). For example, one tonne of mobile phones scraps contains approximately 130 ppm of Pd, 140 g of Ta and 200 g of Au (Hagelüken, 2006, Hageluken, 2006, Usanov et al., 2013). This concentration is much higher than that of in the earth's crust which is one of the reasons why e-waste is a potential source for Pd and Ta.

In metal recycling industries, improved advance route of extractive metallurgy processes (combined with pyrometallurgy, hydrometallurgy and electrometallurgy) are used to recovery the precious metal from e-waste (Heukelem et al., 2004, Cui and Zhang, 2008, Khaliq et al., 2014). One of the industrial processes used for recovering the metals from Pd/Ta-containing e-waste is through the black copper smelting, a route of a secondary copper processing (Veldbuizen and Sippel, 1994, Lehner, 1998, Worrell and Reuter, 2014).

It has been found that the data of distribution-ratio, $\mathrm{L_M^{s/m}}$, of valuable elements is a very limited data not only primary copper smelting but also for secondary copper smelting. The present study mainly focuses on the examination thermodynamic behaviour of Pd and Ta in magnesia-saturated FeO_x-CaO-SiO_2 (FCS) slag and liquid copper at conditions pertinent to the black copper smelting.

6.2 Previous studies on palladium and tantalum distribution

The available thermodynamic data and study on the behaviour of Pd in the copper smelting process focus only the conditions applicable to primary copper processing, as explained below. The distribution-ratio of Pd between copper matte and iron silicate (FeO_x-SiO_2) slag was measured by Henao et al. (2006) using X-ray microanalysis techniques (EMPA) in magnesia crucible at 1300°C (1573 K) under a fixed p_{SO_2}. It was reported that the $\mathrm{L_{Pd}^{s/m}}$ increases with increasing copper matte grade beyond 60 pct. They reported a value of $\mathrm{L_{Pd}^{s/m}}$ of 10^{-3} which is similar to those reported by Yamaguchi (2010) in matte and iron silicate (FeO_x-SiO_2) slag at 1300°C (1573 K) and p_{SO_2}= 0.1 atm. Recently, Avarmaa et al. (2015) measured the distribution-ratio of precious metal including Pd using EMPA technique between silica saturated iron silicate (FeO_x-SiO_2) slag and copper matte at fixed oxygen, sulphur, and SO_2 partial pressure in the temperature range of 1250 to 1350°C (1523 to 1623K). They also reported similar trends to that described by Henao et al. (2006); however, the magnitude of $\mathrm{L_{Pd}^{s/m}}$ was reported to be three times higher. Avarmaa et al. (2015) also reported that the effect of temperature is less pronounced compared to the effect of grade of copper matte on the $\mathrm{L_{Pd}^{s/m}}$.

Yamaguchi (2013) measured the $\mathrm{L_{Pd}^{s/m}}$ in FeO_x-CaO slag and copper alloy at 1300°C (1573 K) at p_{O_2} of 10^{-9} to 10^{-5} atm. It was reported that $\mathrm{L_{Pd}^{s/m}}$ increases with increasing p_{O_2}, and a small quantity of Pd was lost in slag during the oxidation process. Nishijima and

Yamaguchi (2014) reported the effect of slag composition and p_{O_2} on PGMs distribution between Al_2O_3-CaO-SiO_2-Cu_2O-MgO slag and molten copper at p_{O_2} ranging from 10^{-10} to 10^{-5} atm and at 1450°C (1723 K). The $L_{Pd}^{s/m}$ increased with increasing of p_{O_2}, from which Pd was found to be present in the slag as Pd^{2+}. The activity coefficient of Pd oxide was also calculated and found to increase with increasing p_{O_2}. Two different compositional slags were used in the study of Nishijima and Yamaguchi (2014). On the basis of this, it was reported that slag composition has limited impact on the $L_{Pd}^{s/m}$. The influence of Al_2O_3 in slag on the $L_{Pd}^{s/m}$ was not reported (Nishijima and Yamaguchi, 2014).

Based on the literature review, the $L_{Pd}^{s/m}$ during copper processing is not only affected by p_{O_2} but also affected by temperature and slag chemistry. The limited previous studies on the Pd distribution described above focus on conditions relevant to primary copper smelting. No information available on Pd distribution in ferrous-calcium-silicate (FCS) slag at conditions pertinent to secondary copper processing.

Regarding the Ta metal, there is no thermodynamic information and distribution-ratio of Ta at conditions relevant to primary or secondary copper smelting processes. The study provides detailed thermodynamics insight of Pd and Ta in this chapter.

6.3 Experimental details

Experiments were carried out by equilibrating master slags and master alloy. The master Cu-Pd and Cu-Ta alloy were used to conduct the equilibrium experiments. The preparation of master alloys (i.e., Cu-Ge, Cu-Ta) and master slags have been described in Section 4.6.

The Pd equilibration experiments were carried out where the equilibrium was approached in both reduced and oxidized conditions. Experiments that approaching equilibrium from reduced condition were carried out using master slag (3.5 g), copper (2.8 g) and master alloy (Cu -5.9 mass pct Pd) (0.7 g). Copper (3.5 g), master slag (3.45 g) and PdO (99.99 pct purity) (0.05g) were used for experiments approaching from oxidized state. The Ta equilibration experiments were also carried out from two directions with equilibration times of 8 to 24 hours. In one set of experiments, master slag (3 g), master alloy (Cu - 0.23 mass pct Ta) (3 g) and tantalum powder (0.1g) were used, while other sets used master slag (3 g), Cu powder (3 g) and Ta_2O_5 (99.99 pct purity) (0.15 g).

The phase diagrams of FeO-SiO_2-CaO-MgO_{sat} slag were calculated using a similar technique described in Section 5.3.4 at a fixed oxygen partial pressure of 10^{-8} atm for different temperatures, in which the result is shown in Figure 6.1. The compositions of slag are represented in Figure 6.1 by open circles. Similar to Section 5.3.4, this means that the equilibrium experiments were carried out using fully liquid slags.

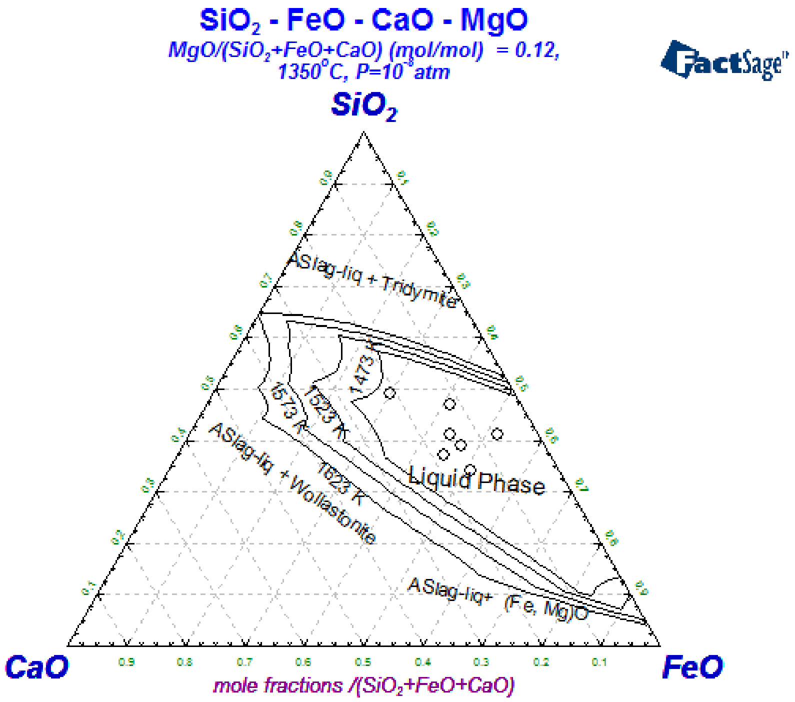

Figure 6.1: Liquidus isotherm diagram of FeO_x-CaO-SiO_2-$MgO_{Saturated}$ slag system calculated from FactSage and slag compositions of Pd study represented by the circle symbol at $p_{O_2} = 10^{-8}$ atm for different temperatures.

Table 6.1 shows the experimental conditions studied for palladium. To conduct the equilibrium experiments, samples were loaded into high purity magnesia crucible placed on alumina pedestal inside a vertical tube resistance furnace with six $MoSi_2$ heating elements. The details of experimental technique have been described in Section 4.7.1. The p_{O_2} inside the furnace at a particular temperature was controlled by flowing gas mixture with appropriate ratio of CO to CO_2. The gas flow rate used in the experiments was 400 mL/min. Mass flow controllers (DFC; Aalborg, USA) were used to control individual gas flow rate of CO_2 and CO. The p_{O_2} was reconfirmed by measuring directly inside the furnace using a $SIRO_2$ C700+ zirconia ceramic electrolyte oxygen sensor (Ceramic Oxide Fabricators, Australia). The details of oxygen partial pressure calculation and measurement have been described in Section 4.5.

Once the experiment was reached in equilibrium and immediately the crucible system purged with inert argon gas (99.99 pct purity). Then it was quickly extracted and lowering to the cooling zone of the furnace. After the crucible system cooled down, the equilibrium sample was collected, and metal and slag phases were physically separated. The slags were ground to powder. The equilibrated separated samples were fused and dissolved in sodium peroxide and acids (hydrochloric and nitric acid) respectively. The samples were finally analysed to determine the bulk composition by inductively coupled- atomic emission spectroscopy (Varian 730 ES: ICP-AES) at Spectrometer Service Pty Ltd, Coburg, Australia.

Table 6.1: Experimental parameters used in the present study for Pd

Temperature [°C (K)]	1200 (1473), 1250 (1523), 1300 (1573), 1350 (1623)			
Oxygen Partial Pressure (atm)	10^{-7}, 10^{-8}, 10^{-9}, 10^{-10}			
Slag Composition (mass pct)	Fe_{Total}	SiO_2	CaO	MgO
	37.3	35.3	5.59	6.30
	32.5	32.8	11.5	6.51
	32.8	41.1	9.88	6.70
	37.9	32.8	10.8	6.61
	35.1	26.9	10.5	6.80
	33.4	33.6	14.5	7.52
	30.7	31.3	19.4	8.78

6.4 Determination of equilibration time for Pd

Experiments with different time (4 to 20 hours; equilibrium approached from reduced and oxidized states) were carried to check the attainment of equilibrium and to determine the appropriate equilibration time. These experiments were conducted using a slag with Fe/SiO_2 ratio of 0.99 and 11.5 mass pct of CaO, and copper at p_{O_2} of 10^{-8} atm at 1300°C (1573 K). This condition was selected considering the liquidus temperature of the FeO_x-CaO-SiO_2-MgO slag system, predicted using FactSage thermochemical software. Magnesia (MgO) entered into the slag due to the dissolution of magnesia crucible during equilibration.

The results of chemical analysis of slag and copper phase from the experiments are plotted in Figure 6.2. The differences in the $L_{Pd}^{s/m}$ are not significant at p_{O_2} = 10^{-8} atm after

16 hours of equilibration approached from both reducing and oxidizing conditions. From analysis of mass balance at different reaction times, it was found that about 90-98 mass pct Pd report to copper metal, 1-3 mass pct in the slag and 0.3-6 mass pct lost to gas phase.

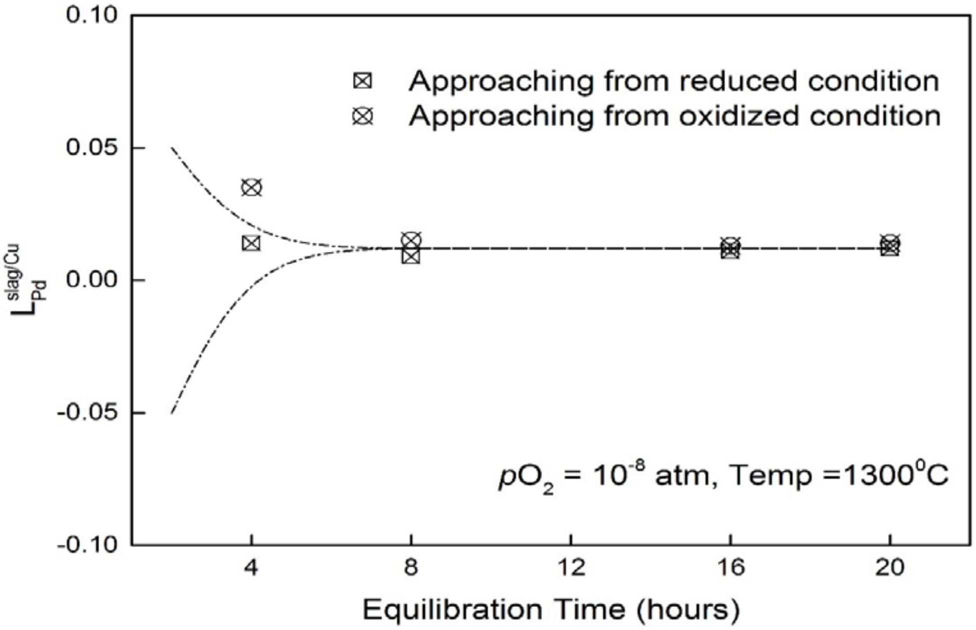

Figure 6.2: Distribution-ratio of Pd in FeO_x-CaO-SiO_2-MgO slag and copper metal as a function of equilibration time at 1300°C (1573 K).

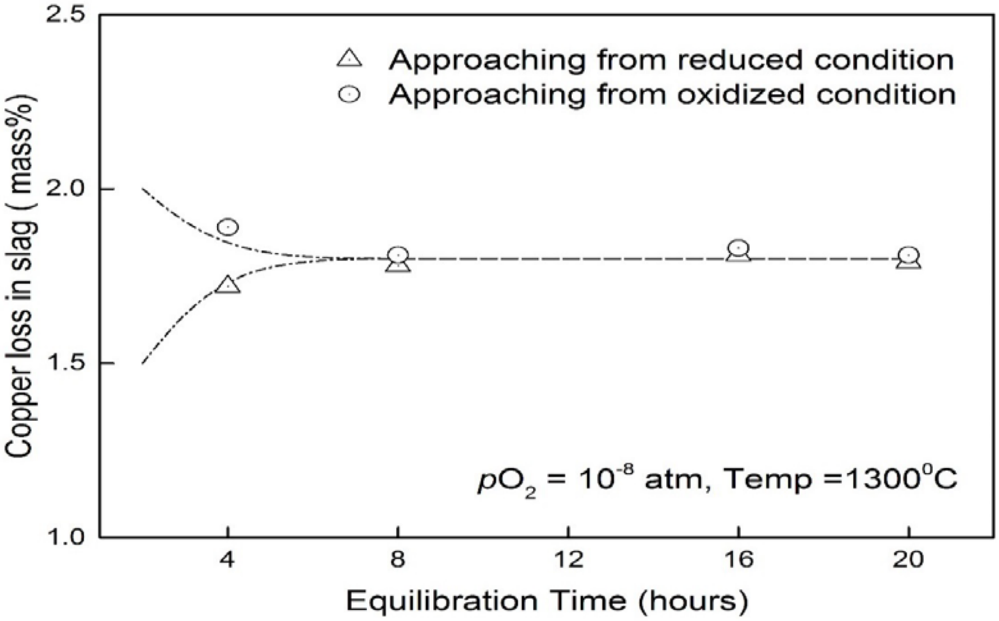

Figure 6.3: Copper loss in FeO_x-CaO-SiO_2-MgO slag as a function of equilibration time.

The losses of copper to the FeO_x-CaO-SiO_2-MgO slag were also measured with respect to the equilibration time at 1300°C (1573 K) and p_{O_2} of 10^{-8} atm, and are presented in Figure 6.3. The copper loss (approximately 1.8 mass pct) to the slag remained constant after 16 hours of equilibration for system equilibrated from both directions. The measured copper loss in previous study of Shuva et al. (2016b) on the distribution behaviour of Ge in FCS slag was slightly lower than the present study, i.e. 1.6 mass pct, which is mainly due to slightly different slag composition. Nevertheless, these values were within the range reported by Yazawa et al. (1999). Considering the above results, it can be said that 16 hours was sufficient to reach equilibrium. Therefore, an equilibration time of 16 hours was used for all the experiments, unless otherwise stated.

6.5 The influence of p_{O_2} on the Pd distribution

The influence of p_{O_2} (in the range 10^{-7} to 10^{-10} atm) on the distribution of Pd, $L_{Pd}^{s/m}$, in FeO_x-CaO-SiO_2-MgO slag and copper system was measured at 1300°C (1573 K). The results are listed in Table 6.2 and plotted in Figure 6.4 in the form of logarithm $L_{Pd}^{s/m}$ vs logarithm p_{O_2}.

Table 6.2: Pd distribution in slag, metal, gas at 1300°C (1573 K) equilibrated for 16 hours with a slag composition of Fe/SiO_2=0.99, CaO=11.5 mass pct and MgO=6.51 mass pct

log p_{O_2}	Slag		Metal		Gas	$L_{Pd}^{s/m}$	log $L_{Pd}^{s/m}$
	Pd mass pct	Distribution pct	Pd mass pct	Distribution pct	Loss pct		
-7	0.023	1.97	1.13	96.66	1.37	0.0169	-1.77
-8	0.013	1.05	1.12	98.33	0.61	0.011	-1.96
-9	0.002*	0.17	1.15	99.82	-	0.0017	-2.77
-10	0.006*	0.05	1.15	99.94	-	0.0005	-3.30

*Calculated by mass balancing

Similar to the analysis for Ge described in the Section 5.5, an approach by Takeda et al. (1983) can be adopted to investigate the oxidation state of species in a slag. The rationale behind this approach is explained briefly here. Consider the distribution-ratio of Pd ($L_{Pd}^{s/m}$) in two phases (e.g., slag and metal) as showed in Eq. (6.1).

$$L_{Pd}^{s/m} = \frac{(\text{mass pct Pd})_s}{[\text{mass pct Pd}]_m} \tag{6.1}$$

Where 's' and 'm' subscripts indicate value in the slag and metal, respectively. Now, consider an oxidation reaction of metal (e.g., palladium) as expressed by following:

$$[\mathrm{Pd}] + \frac{x}{2}O_2 = (\mathrm{PdO_x}) \tag{6.2}$$

When the oxide in the slag is presented as a monocation form (for example, $PdO_{0.5}$ in lieu of Pd_2O) the distribution-ratio can be expressed by the following equation:

$$\mathrm{L_{Pd}^{s/m}} = \frac{K\ (n_T)[\ \gamma_{\mathrm{Pd}}^{o}](p_{\mathrm{O_2}})^{x/2}}{[\ n_T](\ \gamma_{\mathrm{PdO_v}}\ )} \tag{6.3}$$

where $K, n_T, \gamma_{\mathrm{Pd}}$ and $\gamma_{\mathrm{PdO_x}}$ are the equilibrium constant for reaction in Eq. (6.2), total number of moles of constituent in the relevant phases, activity coefficient of Pd in the metal, activity coefficient of metal oxide $\mathrm{PdO_x}$ in the slag. If the relative concentration of solute is very small in metal and slag, then γ_{Pd} and $\gamma_{\mathrm{PdO_v}}$ can be assumed to be unity. Thus, Eq. (6.3) can be reformulation as

$$\log \mathrm{L_{Pd}^{s/m}} = \log B + \left(\frac{x}{2}\right) \log p_{\mathrm{O_2}} \tag{6.4}$$

Similar to the Section 5.5 using Eq. (6.4), the oxidation state of Pd can be determined from the slope. The linear relationship indicates the degree of oxidation of solute $\frac{x}{2}$ in the slag. The gradient of 1/2 may indicate the present of Metal Pd as divalent Pd^{2+} (PdO), while 1/4 represents as monovalent Pd^{+} (Pd_2O) in the slag.

Adopting the above approach, the oxidation state of Pd in the slag was investigated in the current study. Figure 6.4 shows that the p_{O_2} has a significant effect on the $\mathrm{L_{Pd}^{s/m}}$. The results indicated that the $\mathrm{L_{Pd}^{s/m}}$ increases linearly with increasing $p_{\mathrm{O_2}}$. Thus, more Pd is reporting to the slag as the $p_{\mathrm{O_2}}$ is increased. The effect of $p_{\mathrm{O_2}}$ on $\mathrm{L_{Pd}^{s/m}}$ in FeO_x-CaO slag and copper alloy is also shown in Figure 6.4 for comparison. The results of the present study are higher than the earlier result, particularly at higher oxygen pressure. The dependency of $\mathrm{L_{Pd}^{s/m}}$ on slag composition is the reason behind, which will be discussed in Section 6.7. But, it is interesting to note that the increasing trend of $\mathrm{L_{Pd}^{s/m}}$ with oxygen pressure is similar in both slag system. In the current study, a good linear relationship is found from the measured data with a slope, which is close to 1/2, i.e. 0.53. The results may suggest that the form (e.g. oxidation state) of Pd found in the FeO_x-CaO-SiO_2-MgO slag is in accord with those found in Al_2O_3-CaO-SiO_2-Cu_2O-MgO slag previously reported, that is as PdO (or Pd^{2+}) (Nishijima and Yamaguchi, 2014).

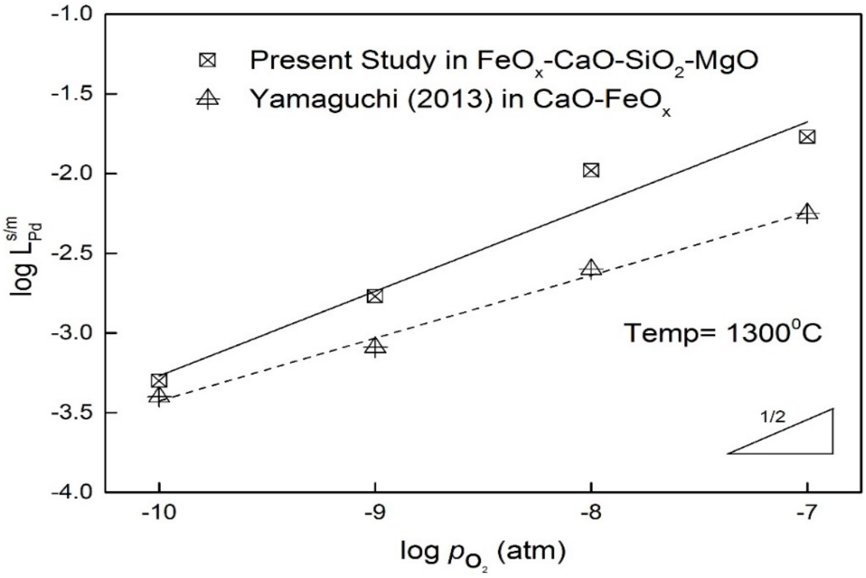

Figure 6.4: Pd distribution-ratio in FeO_x-CaO-SiO_2-MgO slag and copper as a function of p_{O_2} at 1573K (1300°C).

The copper loss to slag measured at 1300°C (1573 K) as a function of p_{O_2} is shown in Figure 6.5. The results were compared with the earlier results of copper loss for the case of Ge study in FCS slag having different slag composition (higher CaO concentration). The composition of slag in earlier study was $Fe/SiO_2 = 0.96$ with 14.5 mass pct CaO and 7.8 mass pct MgO. The results suggest that slight variation of slag composition, in particular basic oxide concentration, has an effect on the copper loss to the slag. The slope of Cu loss line in Figure 6.5 was found to be 0.15, which is considered close to the ¼. This also suggests that the oxidation state of Cu in the slag is 1+, i.e. Cu_2O.

The copper content of the slag was less than 3 mass pct at high p_{O_2}, while at low p_{O_2} the loss was about 1 mass pct as illustrated in Figure 6.5. Yazawa and Takeda (1982) reported a relationship of a copper loss as a function of temperature and p_{O_2} has shown in Eq. (5.5) in Section 5.7.

The copper loss observed in the Pd study, in the Ge study (presented in Chapter 5 and published in Shuva et al. 2016), and calculated using Eq. (5.5) are compared in Table 6.3. Although the increasing trend is similar, the exact Cu contents in the slags are different. This suggests that the Eq. (5.5) suggested by Yazawa and Takeda (1982) is insufficient to describe copper loss in a whole wide range of slag composition. There should be a parameter that also needs to be included in the equation to reflect the variation of slag composition, e.g. basicity or CaO concentration.

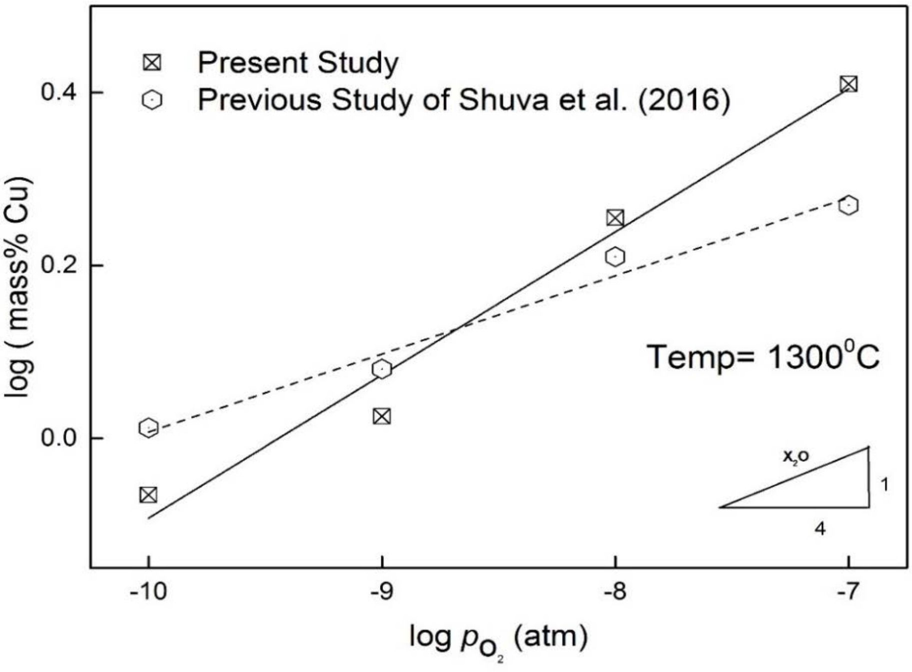

Figure 6.5: Copper loss to FeO_x-CaO-SiO_2-MgO slag as a function of p_{O_2} at 1300°C (1573 K).

Table 6.3: Comparison of the loss of copper to the slag between the present and previous study at 1300°C (1573 K).

log p_{O_2}	Mass % Cu in slag from Eq. (5.5)	Mass % Cu in slag in the Pd study	Mass % Cu in slag in the Ge study (Shuva et al., 2016 and presented in Chapter 5)
-10	0.7	0.86	0.97
-9	1.1	1.06	1.2
-8	1.9	1.8	1.6
-7	3.1	2.56	1.8

6.6 The effect of temperature on the Pd distribution

The effect of temperature on the $L_{Pd}^{s/m}$ in the FeO_x-CaO-SiO_2-MgO slag system and copper is illustrated in Figure 6.6. The concentration of CaO in the slag was 11.5 mass pct with Fe/SiO_2 ratio of 0.99 and 6.5 mass pct MgO. It can be observed from Figure 6.6 that over the temperature range 1200-1350°C (1473-1623 K), the $L_{Pd}^{s/m}$ decreases linearly with increasing temperature at a fixed p_{O_2} of 10^{-8} atm. To evaluate the effect of temperature on the $L_{Pd}^{s/m}$ one can consider a reaction in Eq. (6.5)

$$\mathrm{Pd_{(l)}} + 1/2\mathrm{O_{2(g)}} = \mathrm{PdO_{(l)}}, \quad \Delta G^{o} = -97910 + 87\,T\ (\mathrm{J/mol}) \qquad (6.5)$$

The standard Gibbs free energy equation as reported by Rastogi and Misra (2009) is also shown in Eq. (6.5). Similar to Section 5.8, equilibrium constant (K) can be calculated from Eq. (6.5) and FactSage 6.4 software. The equilibrium constant value at 1200°C (1473 K), 1250°C (1523 K), 1300°C (1573 K), and 1350°C (1623 K) are 8.75×10^{-2}, 6.57×10^{-2}, 5.03×10^{-2} and 3.92×10^{-2}, respectively (FactSage, 2015, Bale et al., 2009). The values of equilibrium constant change significantly with increasing temperature which actually indicates the instability of the oxides of Pd at high temperature. On that account, the $L_{\mathrm{Pd}}^{\mathrm{s/m}}$ would also change notably as represented in Eq. (6.3). Figure 6.6 also shows that the concentration of Pd reporting to slag is lower at higher temperature. Furthermore, the viscosity of slag is lower at higher temperature which is advantageous for the separation of slag during smelting. However, the loss of copper to the slag increased with increasing temperature, as shown in Figure 6.7. It can be observed that copper loss to the slag rises from 1.1 mass pct at 1200°C (1473 K) to 2.8 mass pct at 1350°C (1623 K) at a fixed $p_{\mathrm{O_2}}$.

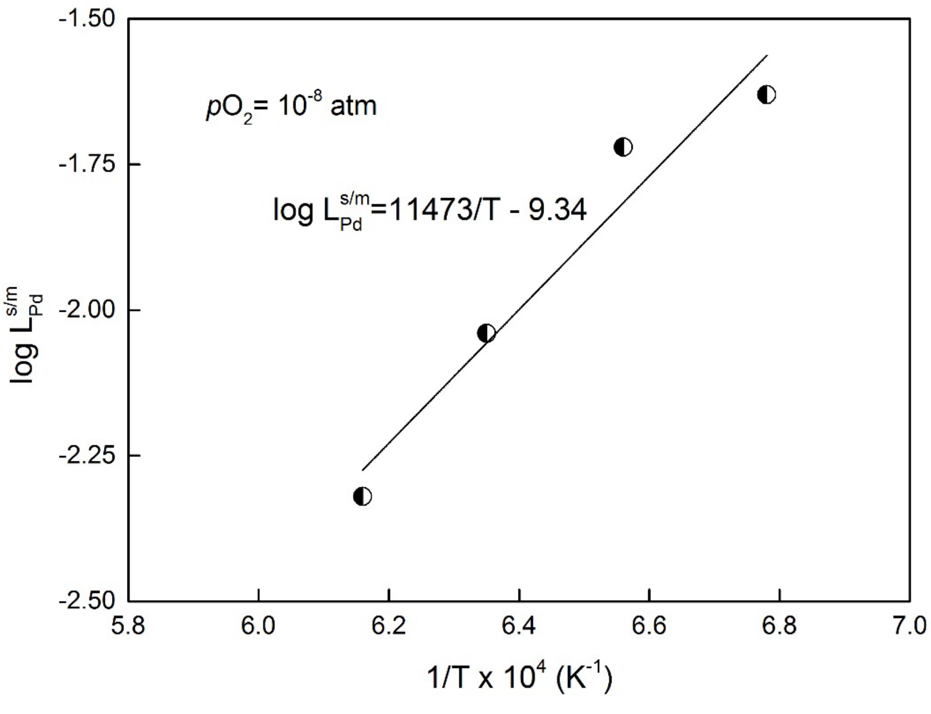

Figure 6.6: Pd distribution-ratio on temperature in FeO_x-CaO-SiO_2-MgO slag and copper at $p_{\mathrm{O_2}} = 10^{-8}$ atm equilibrated for 16 hours (Fe/SiO_2= 0.99, CaO = 11.5 mass pct).

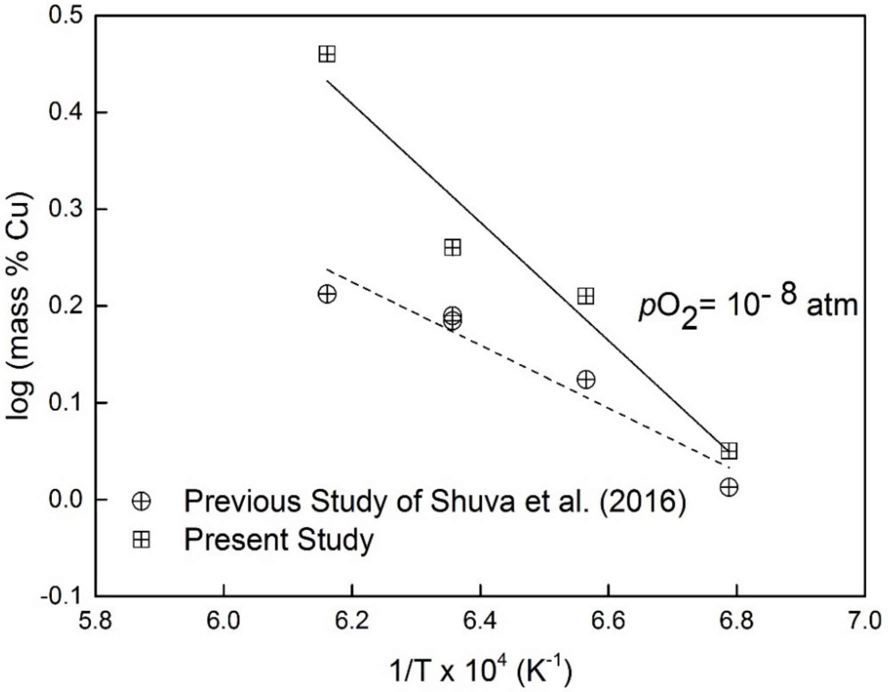

Figure 6.7: Copper loss in FeO_x-CaO-SiO_2-MgO slag as a function of temperature at p_{O_2}= 10^{-8} atm.

The results were compared to the previous results in Chapter 5 (Shuva et al., 2016) of copper loss in FCS slag having slightly different composition. It can be seen that the slag composition used in the Chapter 5, having slightly less basicity, was better to reduce the copper loss at high temperature. The copper loss to the magnesia-saturated FCS slag of both studies were found to be comparable to those illustrated in the earlier studies of Johnston et al. (2007) and Yazawa et al. (1999).

6.7 The effect of slag composition on the Pd distribution

Slag composition plays an important role, and the influence of slag composition on the $L_{Pd}^{s/m}$ in the FeO_x-CaO-SiO_2-MgO slag was evaluated by analysing the variation of (CaO+MgO)/SiO_2 and Fe/SiO_2. The effect of the (CaO+MgO)/SiO_2 (in mass pct) ratio on the $L_{Pd}^{s/m}$ at fixed Fe/SiO_2 ratio of ~1 and 1300ºC (1573 K) is shown in Figure 6.8. It can be seen that the distribution of Pd into the copper phase (inverse of $L_{Pd}^{s/m}$) was noticed increase with increasing of (CaO+MgO)/SiO_2. It was observed that $L_{Pd}^{s/m}$ decreases down by 5 times within the CaO composition range studied which may suggest that the PdO behaves as basic oxide in the slag. The addition of CaO to the slag resulted in a more basic slag and as a result, less Pd reported into the slag. The effect of slag composition can also be seen from the comparison of different slags presented in Figure 6.4. The results indicated that slag like CaO-FeO_x can be used to retain more Pd in the metal phase even at higher p_{O_2} compared to FCS slag of the present study. The maximum copper concentration from the current study in the slag was obtained about 1.96 mass pct which is similar to those reported by Yazawa and Takeda (1982), i.e., 2 mass pct to calcium ferrite slag at p_{O_2} = 10^{-8} atm and 1300°C (1573 K).

The parameter of Fe/SiO_2 (ratio of mass pct) can give some insight on the required amount of SiO_2 for economical fluxing for industry practice. The effect Fe/SiO_2 on the $L_{Pd}^{s/m}$ at a fixed lime content (~10%) and temperature of 1300°C (1573 K) is shown in Figure 6.9. The $L_{Pd}^{s/m}$ appeared to decrease initially with increasing Fe/SiO_2 until it reached a critical basicity level. No significant increase was observed beyond the ratio of Fe/SiO_2 0.99. These results also suggest the low silica region (i.e., high Fe/SiO_2 ratio) was important to keep more Pd in the copper phase. However, high Fe concentration can shift the slag composition to the magnetite phase field. The presence of magnetite crystals generally increases the viscosity of slag that could affect the operation of the process. It could also promote higher Cu loss to the slag due to the sticking of Cu droplets on the magnetite crystals. Thus, to maximize Pd, recovery through copper phase optimization of slag composition is required.

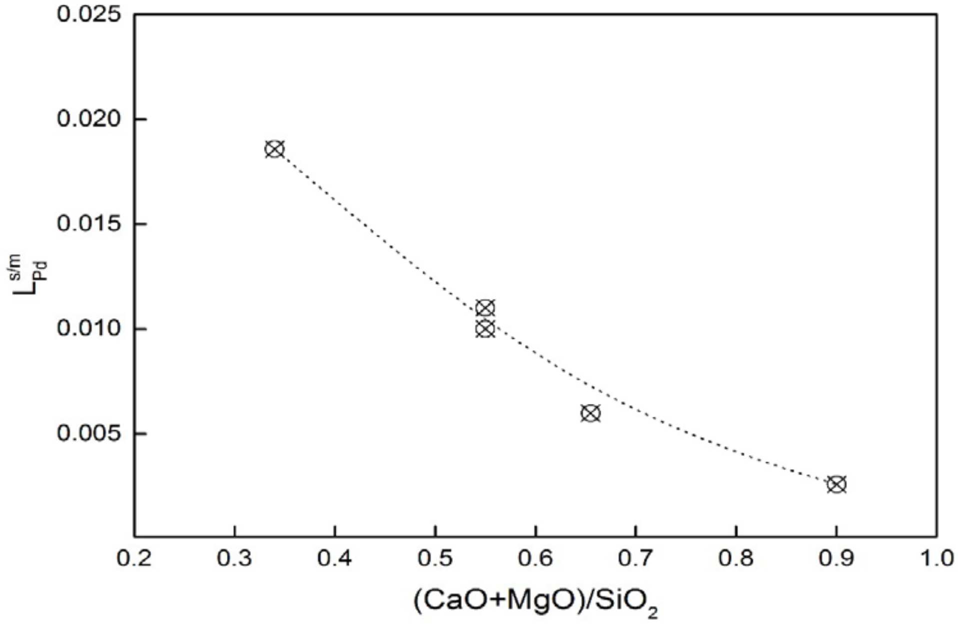

Figure 6.8: The effect of (CaO+MgO)/SiO_2 ratio on the Pd distribution-ratio in FeO_x-CaO-SiO_2-MgO slag and copper at 1573 K (1300°C) and p_{O_2} = 10^{-8} atm.

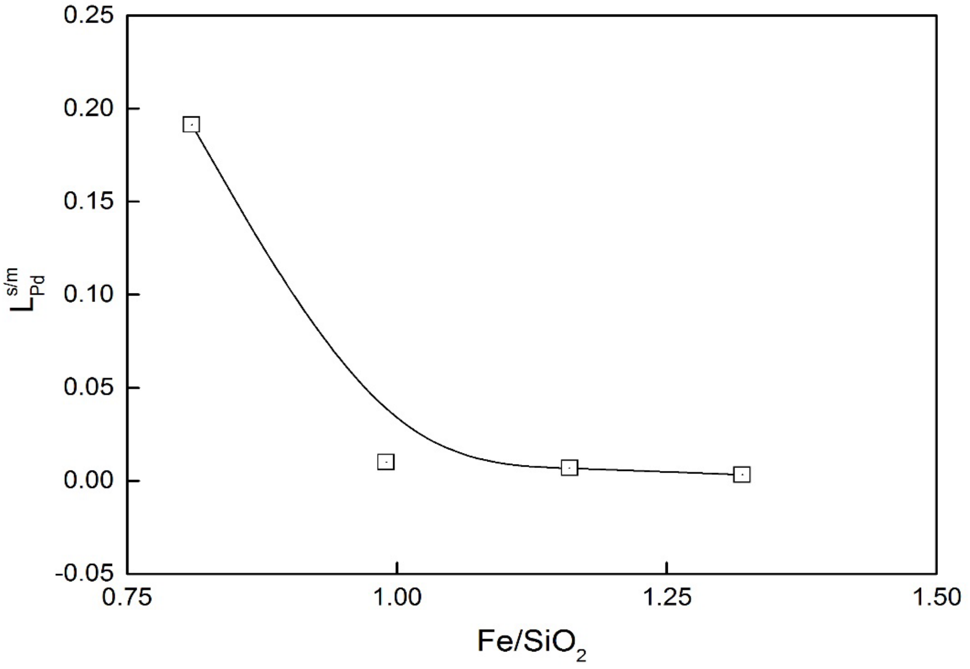

Figure 6.9: The effect of Fe/SiO$_2$ ratio on the Pd distribution-ratio in FeO$_x$-CaO-SiO$_2$-MgO slag and copper at 1300°C (1573 K) and $p_{O_2} = 10^{-8}$ atm (CaO ~ 10 mass pct).

6.8 Activity coefficient of PdO in the FeO$_x$-CaO-SiO$_2$-MgO slag

The activity coefficient of metal oxide (i.e. PdO) in FCS slag can be calculated using the results of the $L_{Pd}^{s/m}$ from Eq. (6.3). Therefore, Eq.(6.3) can be rearranged and written as the following:

$$\gamma_{PdO_x} = \frac{K\,(n_T)[\,\gamma_{Pd}^{o}](p_{O_2})^{x/2}}{[\,n_T]\,L_{Pd}^{s/m}} \tag{6.6}$$

where the value of K at 1300°C (1573 K) is 5.03×10^{-2} and $[n_T]$ is 1.54 for 100g of copper, while (n_T) is 1.94 to 2.02 for 100g of slag. From Figure 6.4, it was found that the value of exponent "$x/2$" is 1/2 for PdO. γ_M^0 is the Henrian activity coefficient for palladium in copper and was obtained from literature, as shown in Table 6.4.

Table 6.4: Activity coefficient of Pd (γ_{Pd}^{o}) in copper

Temperature, °C (K)	Sigworth and Elliott (1974)	Yazawa and Azakami (1969)	Li et al. (2008)
1600 (1873)	1.3*	-	-
1250 (1523)	-	-	0.0302**
1200 (1473)	-	0.06*	-

*Estimated from previous experimental data
**Obtained from optimization of previous experimental data

Sigworth and Elliott (1974) stated a limiting activity coefficient of Pd in liquid Cu alloy at 1600ºC (1873 K) of 1.3. They assumed the behaviour of minor impurities like Pd in liquid copper to be similar to that in the regular solution. Hultgren et al. (1973) attempted to assess the thermodynamic properties of Cu-Pd alloys using the experimental data from the available literature at that time. Yazawa and Azakami (1969) used the experimental result of Hultgren et al. (1973) and extrapolated activity coefficient of Pd at 1200ºC (1473 K) by employing the relation, $T\ln\gamma^{o}$ = constant. Li et al. (2008) optimized the thermodynamic properties of the Cu-Pd system using CALPHAD technique using the Thermo-calc® software. The information on the activity coefficient of palladium in copper, particularly at 1300ºC (1573 K) was not found in literature. Thus, activity coefficient of Pd (γ_{Pd}^{0}) was extrapolated at different temperature using the reported relationship of Yazawa and Azakami (1969) from the finding of Li et al. (2008). The calculated γ_{Pd}^{0} values with respective temperature are shown in Figure 6.10.

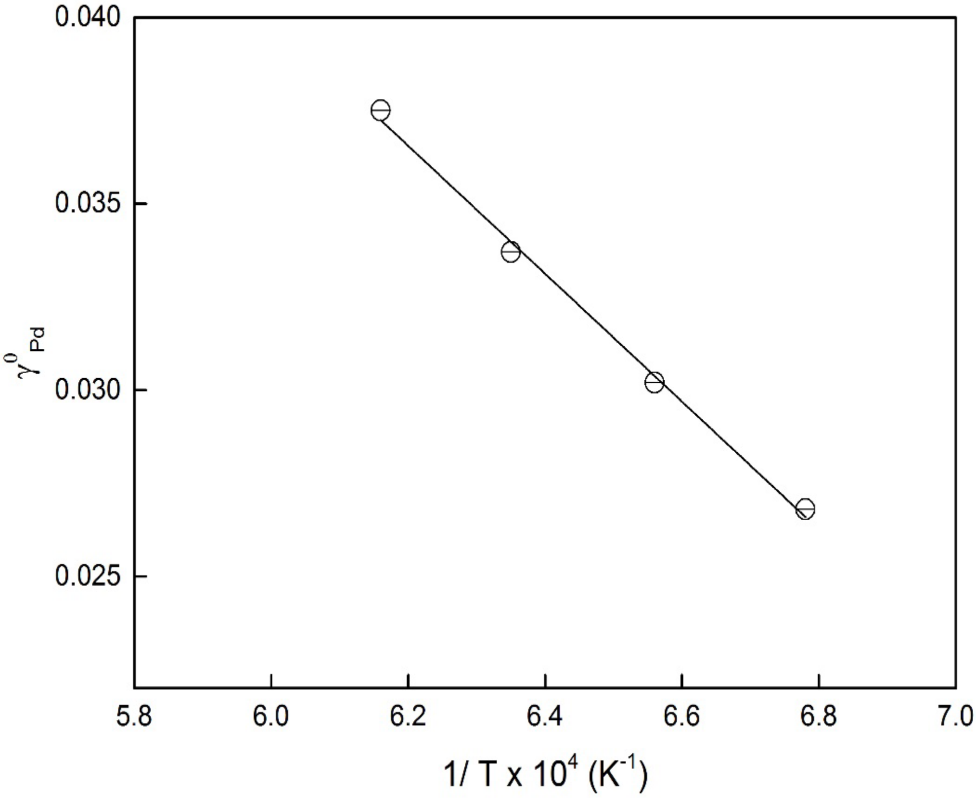

Figure 6.10: Activity of Pd in copper and its variation with temperature.

Table 6.5: Calculated activity coefficient of PdO in slag and distribution-ratio of Pd in FeO_x-CaO-SiO_2 -MgO slag and copper at 1573 K (1300°C) and $p_{O_2} = 10^{-8}$ atm

	Slag Composition (mass pct)				n_T	$L_{Pd}^{s/m}$	γ_{PdO}
(CaO+MgO)/SiO_2	Fe_{Total}	SiO_2	CaO	MgO			
0.34	37.3	35.3	5.59	6.30	2.00	0.018	3.89×10^{-3}
0.55	32.5	32.8	11.5	6.51	1.97	0.012	5.89×10^{-3}
0.55	32.5	32.8	11.5	6.51	1.95	0.011	6.32×10^{-3}
0.65	33.4	33.6	14.5	7.52	1.99	0.006	1.14×10^{-2}
0.90	30.7	31.3	19.4	8.78	1.94	0.003	2.63×10^{-2}

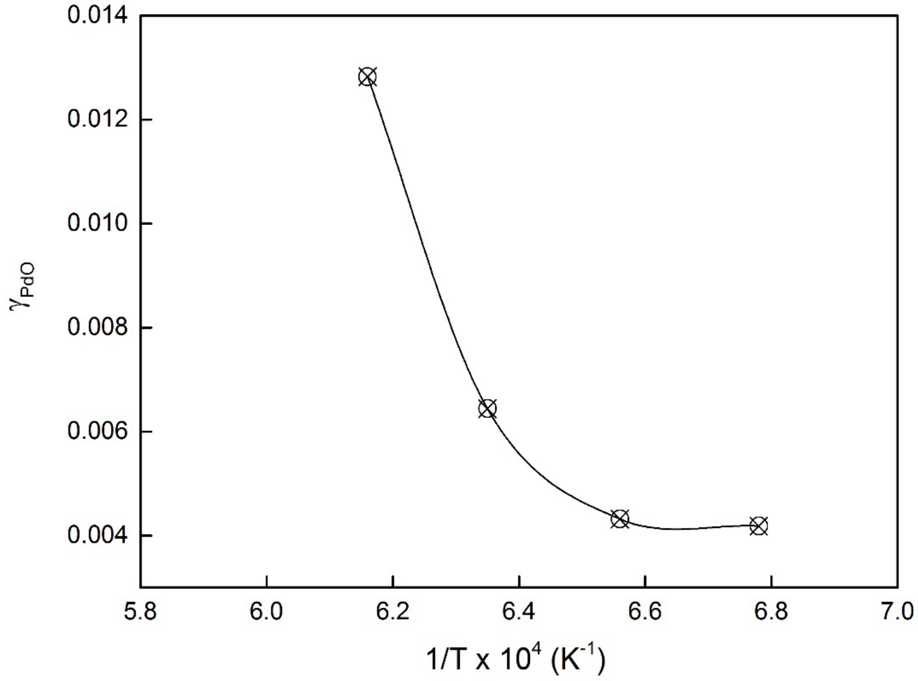

Figure 6.11: Influence of temperature on the activity coefficient of PdO in FeO_x-CaO-SiO_2-MgO slag and copper at p_{O_2} =10^{-8} atm (Fe/SiO_2= 0.99, CaO = 11.5 mass pct).

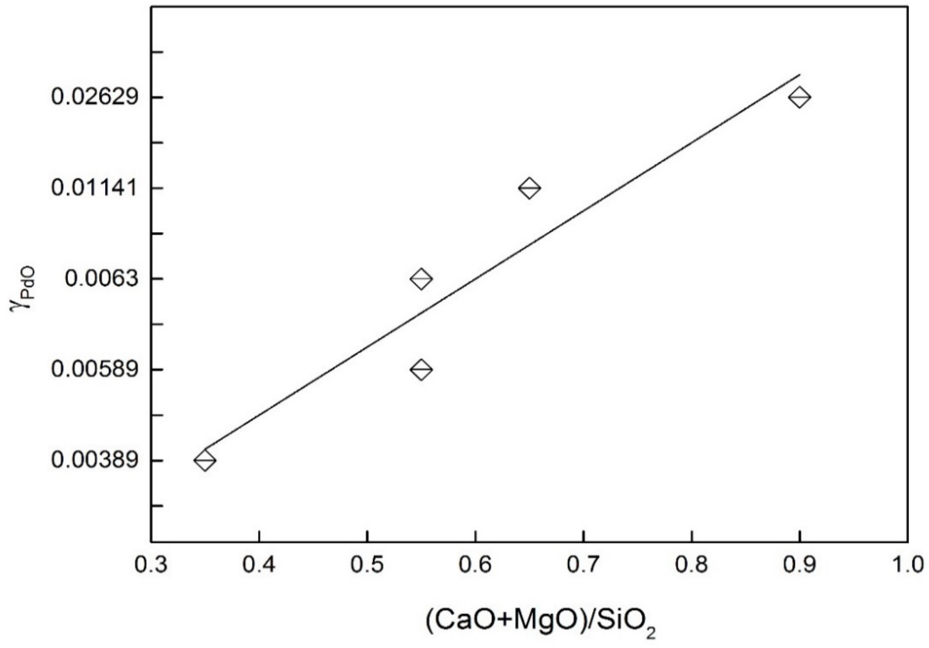

Figure 6.12: The relationship of (CaO+MgO)/SiO$_2$ ratio with the activity coefficient of PdO in FeO$_x$-CaO-SiO$_2$-MgO slag and copper at 1300°C (1573 K) and p_{O_2}= 10^{-8} atm.

All values were substituted into the Eq. (6.6) to determine the activity coefficients of PdO in the slag. Activity coefficient of PdO also calculated for different slag composition and temperature. The results for different slag compositions are also shown in Table 6.5. In Figure 6.11, the activity coefficient of PdO was plotted against the temperature at p_{O_2} =10-8 atm. The activity coefficient of PdO in the present slag system increases with increasing temperature, and it markedly increases at temperature above 1300^{0}C (1573 K). This means that the oxide of palladium is unstable at higher temperature according to the Gibbs energy in Eq. (6.5). The activity coefficient of PdO was also found to increase with increasing (CaO+MgO)/SiO$_2$ ratio in the present slag system at fixed Fe/SiO$_2$ as shown in Figure 6.12, which also supports the notion that the PdO in the slag behave as basic oxide.

6.9 The effect of optical basicity on the Pd distribution

Similar to Section 5.12 analysis, the effect of optical basicity on the Pd distribution was also investigated.

According to Section 5.12, the composition of slag recalculated through the 'Equilib' module of FactSage 6.4 to determine the equilibrium composition of each slag listed in Table 6.5. The recalculated equilibrium slag compositions and the optical basicity of each of slags are shown in Table 6.6.

Table 6.6: Equilibrium slag compositions recalculated using FactSage 6.4, associated optical basicity, Pd distribution-ratio and PdO activity coefficient at 1573 K and $p_{O_2} = 10^{-8}$ atm

Recalculated equilibrium slag composition, mass pct						Λ_{melt}	$\log L_{Pd}^{s/m}$	$\log \gamma_{PdO}$
FeO	Fe_2O_3	SiO_2	CaO	MgO	Cu_2O			
45.84	3.49	36.1	5.72	6.44	2.39	0.673	-1.74	-2.41
40.45	3.94	34.59	12.13	6.86	2.03	0.686	-1.92	-2.19
40.45	3.94	34.59	12.13	6.86	2.03	0.686	-1.96	-2.23
38.36	4.55	33.28	14.36	7.45	2.00	0.694	-2.22	-1.94
33.26	6.13	30.82	19.10	8.64	2.03	0.708	-2.52	-1.58

The data in Table 6.6 are graphically illustrated in Figure 6.13. As shown in Figure 6.13, the $L_{Pd}^{s/m}$ linearly decreases with increasing optical basicity of present slag system. The calculated activity coefficient of PdO linearly increases with the increase of optical basicity which can also be observed from Figure 6.13. The effect of (CaO+MgO)/SiO_2 ratio on the behaviour of Pd discussed in earlier section is in line with the observation regarding to optical basicity.

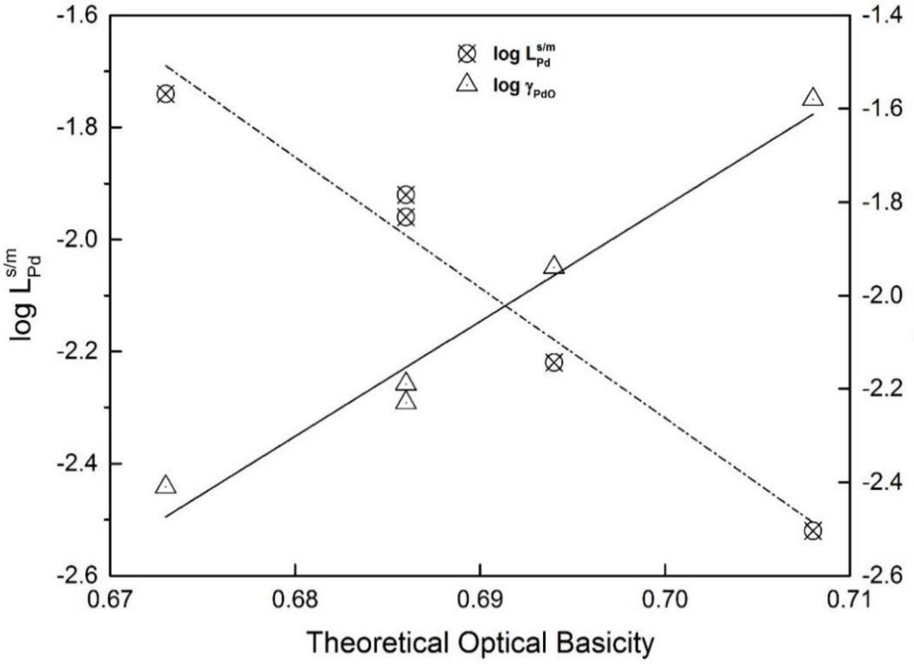

Figure 6.13: The effect of optical basicity on the $L_{Pd}^{s/m}$ and activity coefficient of PdO in FeO_x-CaO-SiO_2-MgO slag at 1300°C (1573 K) and p_{O_2} =10^{-8} atm.

The ionic bond fraction of PdO was calculated similarly to Section 5.13 using Eq. (5.9) to justify the observed behaviour. The values of x_a and x_b for PdO are 3.44 and 2.2, respectively. Thus, the value of IBF for PdO bond is calculated to be 0.32 which is close to Fe-O bond indicated by Gilchrist et al. (1989). This also reconfirms the nature of PdO as a mildly basic oxide in FeO_x-CaO-SiO_2-MgO slag.

6.10 Distribution of tantalum in slag and liquid copper

The author has taken an attempt to examine the thermodynamic behaviour of Ta in the present slag-copper system. A magnesia saturated ferrous calcium silicate slag was used in equilibration reaction which contains 9.8 mass pct CaO, 6.51 mass pct MgO and Fe/SiO_2 ratio of 1.16. The influence of p_{O_2} (in the range 10^{-12} to 10^{-16} atm) on the distribution of Ta, $L_{Ta}^{s/m}$, in FeO_x-CaO-SiO_2-MgO slag and copper system was measured at 1400°C (1673 K) for an equilibration period 8 hrs, and the results are presented in Table 6.7. From Table 6.7, it can be observed that Ta is mostly goes to slag phase. At 1400°C (1673 K), decreasing the oxygen potential from 10^{-12} to 10^{-16} atm did not appear to have an effect on Ta distribution. One additional investigation was carried at a higher temperature 1600°C (1873 K) and very reducing atmosphere (p_{O_2} = 10^{-16} atm) with longer equilibration time, i.e. 24 hrs. This condition is now more relevant to a steel making process condition. At this condition, a small amount of Ta (0.05 mass pct, $L_{Ta}^{s/m} = 1999$) was found to report to copper while majority reported to the slag phase. Different metal solvent system and conditions will be required to meaningfully recover Ta from secondary resources. Further investigation is required to find a suitable metal system.

Table 6.7: Ta distribution in slag-metal equilibrated reaction with slag composition of Fe/SiO_2 = 1.16, CaO = 9.8 mass pct and MgO=6.51 mass pct

Temperature, ° C (K)	p_{O_2}, atm	Equilibrium Time (h)	Cooling Method	Mass pct Ta (Distributed in Cu phase)	Mass pct Ta (Distributed in slag phase)	$L_{Ta}^{s/m}$
1400 (1673)	10^{-12}	8	Fast	0.005	99.995	19999
1400 (1673)	10^{-14}	8	Fast	0.005	99.995	19999
1400 (1673)	10^{-16}	8	Fast	0.005	99.995	19999
1600 (1873)	10^{-16}	24	Fast	0.05	99.95	1999

6.11 Minor elements distribution under black copper smelting condition

The black copper smelting route can be a suitable way for recovering precious metal from e-waste or other secondary resources. Recently, a number of investigations on the distribution of minors elements have been carried out at conditions relevant to the black copper smelting. The summaries of finding listed in the following Table 6.8. It was found that it can be a practical way for germanium (Ge), Pd (palladium) and Sn (tin) containing e-waste recycling can potentially be recovered with high partitioning to copper phase. Having said this, the suitable slag composition for recovery of Pd and Sn is different than those for Ge which is mainly due to the different nature of their oxide behaviour (i.e., basic *vs* acidic). Thus, optimization of the slag is required, and it may be that a multistage process needs to be developed to accommodate the different slag requirement for effective recovery of these metals.

One possible modification is to have a multi-stage black copper smelting that consists of two sub-process routes where one of the routes of the secondary copper resources are processed using basic slag and while in the other using acid slag. This proposed route is explained in more details in Figure 6.14. A single versatile reactor can be used to carry out the reduction and followed by oxidation operations using basic slag (top left). In this "basic" operation, copper scraps, e-waste, and coke are treated with basic slag and black copper is produced. The suitable conditions are p_{O_2}= 10^{-10} atm and temperature 1300°C (1573 K) for the reduction process. The precious metals and "basic" metals are partitioned into the copper phase (e.g. Au, Ag, Pd, In, Sn). The slag from this operation contains some valuable "acidic" elements, e.g. Ge, Se. Thus, the slags need to be re-used and processed further (reduction-oxidation reaction with copper scrap) in another reactor operating with an acid slag (bottom left).

The suitable conditions for the reduction are p_{O_2}= 10^{-10} atm and temperature 1300°C (1573 K). By doing this, the valuable "acidic" metals can also be enriched into the copper phase. The copper from both "basic" and "acidic" operation is then treated in anode furnace to produce anode copper and followed by electrorefining for rectifying the purity of copper. The valuable metals in the black copper (for example Ag, Pd, Ge, Sn, In, and Au) mainly goes to anode slime, a by-product of the electrorefining, which is processed further through hydrometallurgical route or precious metal refinery for their recover. Other valuable metals partitioned the gaseous phases (Zn, Pb, Cu) can also be further processed for their recovery. In case of volatile metal oxides (i.e., In_2O_3, GeO_2, etc.) to consider the type of reactor and its effect on the valuable metals partitioning to copper is vital.

Table 6.8: Distribution data of minor metals with condition favourable for black copper smelting

Target metal	Temperature, ° C (K)	p_{O_2} (atm)	Equilibrium time (hrs)	Suitable nature of slag	Maximum mass pct distributed in metal*	Maximum mass pct distributed in slag*	Ref.
Ge	1200 to 1350 (1473 - 1623)	10^{-7} -10^{-10}	6	Acidic	93.58	4.63	Present study
Ta	1400 to 1873 (1673-1873)	10^{-12} -10^{-16}	Up to 24	Acidic	0.05	99.95	Present study
In	1300 (1573)	10^{-6} -10^{-8}	16	Neutral	58.70	41.29	Anindya et al. (2014)
Pd	1200 to 1350 (1473-1623	10^{-7} -10^{-10}	20	Basic	99.94	0.05	Present study
Sn	1300 (1573)	10^{-6} -10^{-8}	16	Basic	88.29	11.70	Anindya et al. (2013)

*This is for equilibrium, not for different gas flows and operating conditions

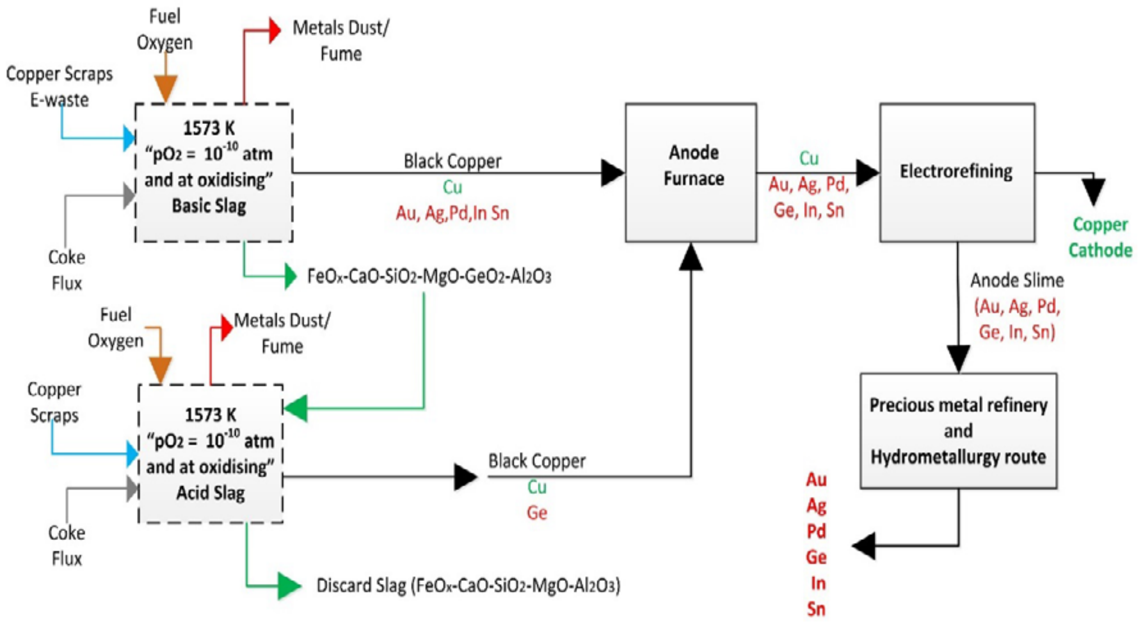

Figure 6.14: A conceptual route of e-waste recycling through black copper smelting.

It should also be pointed out that different types of slag will attack refractory lining in different ways. Each reactor is designed with appropriate refractory linings capable to handle a particular slag system. In industry, operation using different slag systems (acidic and basic) in a single reactor is difficult to implement because it is difficult to find a suitable refractory. Slag chemistry affects technological issues such as wear of refractory as replacement cost of refractory lining is very high. One of the possible solution is using copper cooling panels could mitigate this issue, allowing a more robust and flexible operation which can be tuned to the feed mix.

6.12 Summary

The thermodynamic behaviour and distribution-ratio of Pd and Ta in FeO_x-CaO-SiO_2-MgO slag and liquid copper have been studied at conditions relevant to the black copper smelting processes. A possible modification of black copper smelting operated using basic and acidic slag have also been discussed. The findings can be summarized as follows:

The $L_{Pd}^{s/m}$ was found strongly depend on the (CaO + MgO)/SiO_2 ratio and/or optical basicity at a fixed p_{O_2} and temperature 1300°C (1573 K). However, the ratio of Fe/SiO_2 affected the $L_{Pd}^{s/m}$ until the ratio value of 1, beyond that it is negligible. The $L_{Pd}^{s/m}$ in FeO_x-CaO-SiO_2-MgO slag and liquid copper was observed to linearly increase with increasing of p_{O_2} at a fixed temperature 1300°C (1573 K). Temperature has some contribution on the

$L_{Pd}^{s/m}$ at fixed p_{O_2}. The stability of PdO is less at higher temperature and mostly reported to metal phase as Pd metal. The activity coefficient of PdO in FeO_x-CaO-SiO_2-MgO slag was calculated to be in the range of 3.89×10^{-3} to 2.63×10^{-2}. The Pd was present in the magnesia saturated FeO_x-CaO-SiO_2 slag mostly as divalent $Pd^{2+,}$ (PdO). PdO is mildly basic, as a result, a less-acidic slag (or low SiO_2 content), and a reducing atmosphere with higher temperature is suggested to decrease the Pd deportment to the slag.

Tantalum is mostly reported to FeO_x-CaO-SiO_2-MgO slag. Further study is required to find suitable solvent system and conditions that promote Ta recovery.

Chapter 7 Analysis of the Slag Structure and its Correlation with Distribution-ratio

7.1 Introduction

Slag plays a vital role in the refining of liquid hot metal in metal production processes. The composition of slag controls the absorbance capacity of impurities from the liquid metal. The change of slag composition also has a dramatic influence both on the thermophysical and thermodynamic properties such as viscosity, surface tension, molar volume, sulphide capacity and mixing free energy of silicates (Park, 2013a, Halter and Mysen, 2004). These properties have a significant effect on the successful operation of metal production processes. Therefore, understanding the composition-structure-properties relationship is useful for designing a suitable slag for the processes. The structure-properties relationship of limited silicate slags system has been investigated extensively using spectroscopic techniques (Park, 2013a, Park and Min, 1999, Park et al., 2002, Mysen and Richet, 2005).

Silicate slag structure is primarily affected by the addition of network modifier metal oxides (e.g. Na_2O, CaO, MgO, Al_2O_3). The nature of these metal oxides, either acidic or basic, affects the polymerization of silicate containing slag by generating more free oxygen ions (O^{2-}) or providing bridging oxygen (O^0) in the silicate melt. It has been reported in Chapters 5 and 6 that the nature of oxides in slag and the slag composition have a strong influence on the distribution-ratio of minor elements. It would be useful to analyse the slag structure, through the investigation of silicate tetrahedra units using vibrational spectroscopy, and to evaluate their effect on the distribution-ratio. No information have been found in the literature on the correlation between the degree of polymerization and the distribution-ratio of solute elements.

In this chapter, a study on the analysis of the slag structure using FTIR (Fourier Transformed Intrared Spectrocopy) is presented. The effect of FeO_x-CaO-SiO_2-MgO slag composition, p_{O_2} and temperature on the degree of polymerization (DOP) was investigated. A semi-empirical relationship between the distribution-ratio with the degree of polymerization of the slag melt was developed using multiple regression analysis. Further to this, the speciation of three types of oxygen in slag was calculated using mass balance.

7.2 Previous studies on slag structure analysis using vibrational spectroscopy

There are numerous studies found in the open literature on the investigation of slag structure using vibrational spectroscopy techniques which have been shown in Table 2.4 in Chapter 2. Mysen et al. (1982) proposed that structural units of amorphous materials can be characterized in terms of non-bridging oxygen (NBO) in silicon per tetrahedron. The information can be acquired using a statistical approach using Gaussian functions and applying curve fitting to calculate non-bridging oxygen from Raman and infrared spectra obtained from the silicate slag samples (Mysen and Frantz, 1992, McMillan et al., 1992, McMillan, 1984, Park et al., 2002, Gao et al., 2014, Lee et al., 2004, Park, 2013b, Park, 2012). The validation of structure unit analysis has been also carried out by Schneider et al. (2003) where they measured the distribution of silicon species (Q^n) in different glass structures using nuclear magnetic resonance (NMR) and validated the measurements with thermodynamic model results. It indicates that thermodynamic properties could be determined from the structure analysis of silicate slag.

The effect of slag melt structure on the physical properties was examined by Mills (1993). It was mentioned that the primary factor which affects the physical properties is the depolymerization of silicate slag structure. However, cations only have a secondary effect on the depolymerization of slag. He did not provide any information about the influence of P and Ti on the relative concentration of anionic structures. Recently, Sun et al. (2015) investigated the $CaO-SiO_2-P_2O_5$ and $CaO-SiO_2-P_2O_5-TiO_2$ slag structure to evaluate the effect of phosphorus and titanium oxide on the silicate structure. They used different spectroscopy techniques such as FTIR, Raman and NMR, and found consistent results. They found that the addition of P_2O_5 increases Q^3 (NBO/Si= 1) fraction. The results interpreted that phosphorous incorporate them into four-fold coordination and act a role of network former hence, the degree of polymerization (DOP) increases. TiO_2 also acts as network former and resulted more complex structure in the $CaO-SiO_2-P_2O_5-TiO_2$ slag.

The structure aspects of $CaO-SiO_2$ and $CaO-SiO_2-CaF_2$ slags were studied by Park et al. (2002) using FTIR. They found that the addition of CaO split up silicate tetrahedra bands in the $CaO-SiO_2$ binary system and their relative intensities increase through the formation of Ca-O complexes. The network breaker oxide (i.e., CaO), therefore, decreases the DOP. Similar results were presented by Lee et al. (2004) and they observed adding CaO in the silicate melts can bind the dissociated silicate anions with increased Ca^{2+}, and the intensity of the IR bands also increased. The effect of fluorine and oxygen ions on the structure were also studied by Park et al. (2002). They found that to maintain similar level of DOP, it required higher concentration of F^{-}ion in the $CaO-SiO_2-CaF_2$ ternary system compared to the O^{2-} in the $CaO-SiO_2$ binary system.

In another study, Park (2012) reported the relative abundance of silicates unit in the $CaO-SiO_2-MnO$ using micro-Raman spectroscopy and observed that thermophysical properties are significantly affected by the degree of polymerization. Correlations with viscosity and slag structure were also reported by Wang et al. (2017) to understand the effect of chlorine in $CaO-SiO_2-CaCl_2$ system. They observed that role of chlorine in the slag is network modifier and therefore, the degree of polymerization and viscosity decrease with increasing the content of $CaCl_2$ at a fixed temperature.

An investigation was carried out by Park (2013a) to determine a relationship between thermochemical properties and structure using the distribution of silicate units and chemical species of oxygen (i.e., O^{2-}, O^{0}, O^{-}) in $CaO-SiO_2-MgO$ and $CaO-SiO_2-MnO$ slags. It was revealed that the excess free energy of oxides in slag (CaO, MgO, MnO) is strongly dependent on the silicon anionic units which was also elucidated further with ionization potential (Z/a^2). Park (2013a) also reported that an increasing mole fraction of silica decreases the NBO and linked with increases of $[SiO_4]^{4-}$ tetrahedral form in large silicate anions. The activity of manganese oxide (MnO) in $CaO-SiO_2-MnO$ slag was measured by Eom et al. (2016) and they correlated it with the oxygen fraction present in the slag. It was found that the activity of MnO increases with slag basicity as represented by $(CaO+MgO+FeO)/SiO_2$, because of the increasing of free O^{2-} ions. Mn^{2+} cation was found to behave as network modifier (up to 30 mole pct concentration) and balanced the charge of Q^2 corner shared O^{-} ions in the silicate structure.

A study using FTIR-RAS (Fourier transform infrared reflection absorption spectroscopy) and Raman spectroscopy was carried out by Mohassab and Sohn (2015). They investigated complex ironmaking slag system (i.e.$CaO-SiO_2-MgO-MnO-Al_2O_3-FeO-FeS-Ca_2P_2O_7$) to understand the effect of water vapour content in the gas mixtures. They reported that presence of water in the gas mixture could affect the degree of polymerization (DOP) and therefore, increases DOP with increasing of water content in the gas mixtures. The dissolution characteristic of hydrogen was investigated by Park et al. (2012). They found that hydrogen reacts with bridged oxygen in acidic slag and increase the depolymirezation. However, hydrogen provides free hydroxyls reacting with free oxygen in the highly basic slag increases the DOP.

Gao et al. (2014) investigated a complex slag structure of SiO_2-CaO-MgO-9 mass pct Al_2O_3 and also measured the viscosity of the slag. They found that the complex slag structure transforms into a simpler structure with increasing basicity or MgO, and therefore, the viscosity and the activation energy of viscous flow also decreased. It is also reported by Řeháčková et al. (2015) that viscosity is determined by the internal slag structure. They measured the dynamic viscosity of the CaO-SiO_2-Al_2O_3 ternary system to assess the effect of temperature and basicity and correlated them with slag structure spectra obtain from FTIR. They found that viscosity decreases with increasing of basicity as a result of the destruction of silicate bond and achieve a minimum point for the critical concentration of CaO. However, beyond the critical concentration of CaO, the dynamic viscosity of the slag increases which indicates the structure complex of silicate structures from the spectra of FTIR. Non-bridging oxygen (NBO) and bridging oxygen (BO) can be used to evaluate the silicate slag structure and physical properties of slag. It is revealed by Kong et al. (2013) that NBO/BO ratio increases with the addition of $CaCO_3$ in the SiO_2-Al_2O_3-CaO-FeO slag because of increasing Si-O which also changes the viscosity behaviour.

Although there have been a number of studies in different slag system, there is still lack of information on the structure of FeO_x-CaO-SiO_2-MgO, particularly at conditions relevant to black copper smelting practise (low oxygen potential).

7.3 Experimental details

Ferrous calcium silicate (FCS) master slags were used in the study. The details of preparation of the slag have been described in Section 4.6.1. Equilibrated slags from Ge and Pd experiments were also used for the study. The procedure of equilibrium experiments have been described previously in Sections 5.3 and 6.3, respectively. The bulk composition of master slags were determined using ICP-AES. The details of analysis technique have been described in Section 4.7.2.

The infrared spectra of the slag samples were collected using Fourier transform infrared (FTIR) technique using a Nicolet iD5 attenuated total reflection spectrometer (Thermo Fisher Scientific, USA). It was equipped with a diamond crystal and ZnSe lens.

The incident angle of the crystal was 42°. The measured spectra of the slag samples were collected at room temperature in the frequency range of 200 to 1600 cm^{-1} for 100 scans at a resolution of 4.0 cm^{-1} and the spectra were recorded using the OMNIC software. Gaussian functions were used and fitted to deconvolve the spectra using PeakFit V4.12 software. The relative abundance of the Q^n units were calculated from area fraction of the fitted Gaussian curves at a different frequency of silicate units.

It is worth to mention here that the samples were cooled by purging of argon and followed by lowering to the cooler zone of the furnace. However, it was found in the literature that there has no significant difference between the spectra of quenched sample and in-situ at high temperature (Mysen, 1990a, Virgo et al., 1980, Mysen et al., 1980, Mysen and Richet, 2005, Mysen and Frantz, 1992).

7.4 Structure analysis of the FeO_x-CaO-SiO_2-MgO (FCS) master slags

The IR spectra of magnesia saturated ferrous calcium silicate (FCS) master slags were recorded to investigate the effect of compositional variation on anionic structure units and determine the degree of polymerization. The details of analysis are described in the following section.

7.4.1 Effect of Fe/SiO_2 on the structure of FCS slag

The FTIR results of FeO_x-CaO-SiO_2-MgO (FCS) master slag samples are shown in Figure 7.1 as a function of the wavenumbers with varying Fe/SiO_2 ratio. Characteristic spectra of the FTIR are typically focused in the wavenumber range of 700 cm^{-1} to 1500 cm^{-1} which represents mainly symmetric stretching vibration bands of the [SiO_4] tetrahedral. As can be seen in Figure 7.1, the peaks of high frequency band ~ 1100 cm^{-1} (Q^3) and low frequency band ~ 850 cm^{-1} (Q^0) are shifted towards low wavenumber region with increasing Fe/SiO_2 ratio. The intensity of high frequency absorbance band ~ 1100 cm^{-1} (Q^3) shortens in depth indicates a depolymerization of the slag structure as suggested in the literature (Mysen, 1990b, Park et al., 2002). The peak shifting of spectra of silicate melts also indicates an increase in the number of NBO per silicon tetrahedra. The increase of NBO in silicate melts also support the notion that the depolymerization of slag increases with increasing Fe/SiO_2 ratio from 0.81 to 1.16.

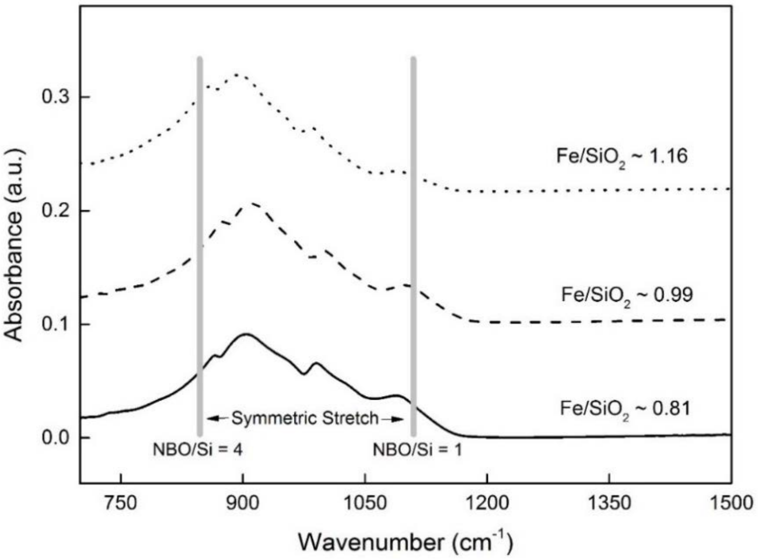

Figure 7.1: FTIR spectra of FCS master slags containing Fe/SiO$_2$ ratio from 0.81 to 1.16 ($p_{O_2} = 10^{-8}$ atm and T= 1300°C).

The measured IR spectra data of the master slags with different Fe/SiO$_2$ were deconvolved by fitting Gaussian functions to obtain the relative abundance of Q^0 (SiO_4^{4-}- monomer), Q^1 ($Si_2O_7^{6-}$- dimer), Q^2 ($Si_2O_4^{4-}$- chain) and Q^3 ($Si_2O_5^{2-}$- sheet) units at the frequency for the symmetric stretching. The results obtained from the deconvolution of IR spectra of master slags with different Fe/SiO$_2$ ratios are listed in Table 7.1 and shown in Figure 7.2.

Table 7.1: FTIR shift position and peak area ratio obtained from deconvolution of FTIR spectra for master FCS slags of different Fe/SiO$_2$ ratio

	Peak Position (cm^{-1})				Best Fitted Gaussian Peak Area (pct)				
Fe/SiO$_2$	Q^0	Q^1	Q^2	Q^3	Q^0	Q^1	Q^2	Q^3	Q^3/Q^2
0.81	856	912	990	1088	0.208	0.343	0.281	0.168	0.59
0.99	849	917	1003	1100	0.216	0.420	0.232	0.131	0.56
1.16	851	905	989	1090	0.321	0.426	0.191	0.062	0.32

Composition of slag (mass pct)
Fe$_T$ = 27.4 %, SiO$_2$= 33.9 %, CaO = 9.72 %, MgO = 6.78% (Fe/SiO$_2$ = 0.81)
Fe$_T$ = 32.8 %, SiO$_2$= 33.1 %, CaO = 9.88 %, MgO = 6.49 % (Fe/SiO$_2$ = 0.99)
Fe$_T$ = 37.9 %, SiO$_2$= 32.8 %, CaO = 9.80 %, MgO = 6.51% (Fe/SiO$_2$ = 0.99)

Figure 7.2, shows that the envelope of Q^3 and Q^2 silicate units in the FCS slag decrease with increasing Fe/SiO$_2$. The relative fraction of the silicate units obtained from the deconvolution of IR spectra are plotted in Figure 7.3 as a function of Fe/SiO$_2$. It was found that, the fraction of Q^1 (Si_2O_7-dimer) unit is dominant in the master slag. The Q^0 (SiO_4-monomer) unit did not show significant increase with increasing Fe/SiO_2 ratio from 0.81 to 0.99. Therefore, silicates structure mainly transformed from highly polymerized Q^3 (Si_2O_5-sheet) and Q^2 (SiO_3-chain) units into depolymerized Q^1 (Si_2O_7-dimer) unit as Fe/SiO_2 increases from 0.81 to 0.99. It is also noticeable that the fraction of Q^0 unit increases significantly as Fe/SiO_2 ratio increases from 0.99 to 1.16, while Q^3 and Q^2 units decrease drastically. It indicates that silicate structure transformed from highly polymerized Q^3 (Si_2O_5-sheet) and Q^2 (SiO_3-chain) units depolymerized into Q^0 (SiO_4-monomer) silicates units as Fe/SiO_2 ratio increases beyond 0.99.

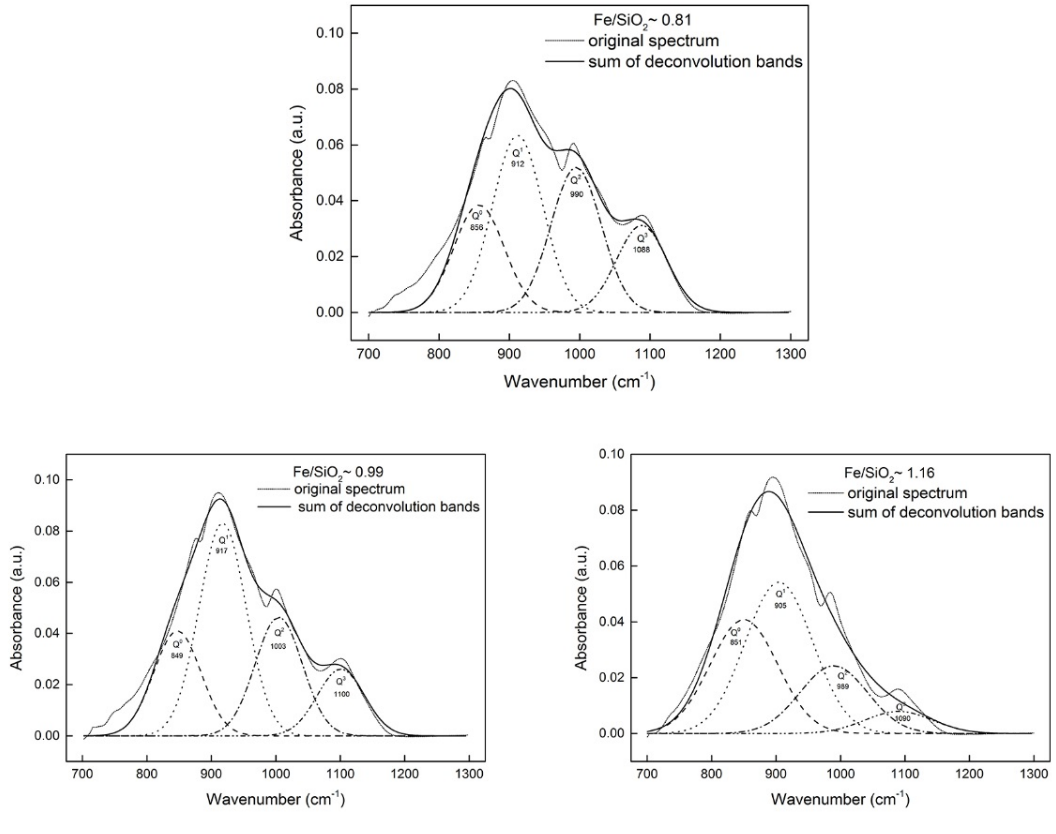

Figure 7.2: Deconvolution results of FTIR spectra of FCS master slags with different Fe/SiO_2 ratio ($p_{O_2} = 10^{-8}$ atm and T= 1300°C).

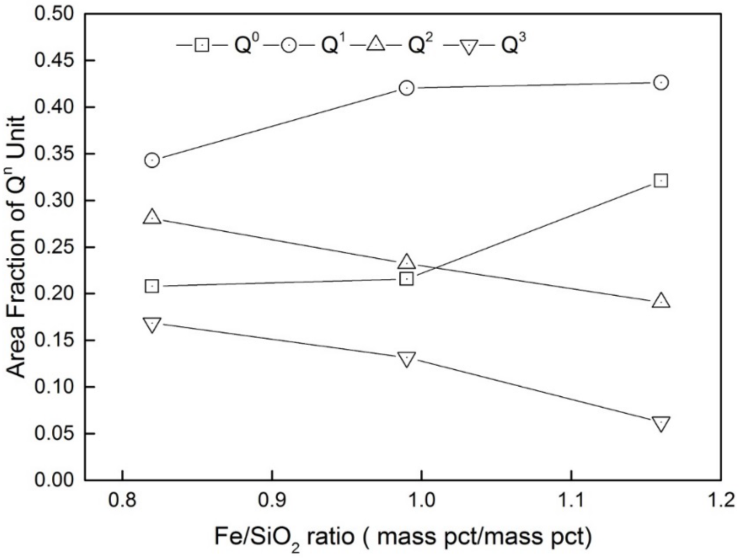

Figure 7.3: Abundance of structural units in FCS slag as a function of Fe/SiO_2 ratio ($p_{O_2} = 10^{-8}$ atm and T= 1300°C).

In Figure 7.4, the Q^3/Q^2 ratio of FCS master slag (Fe/SiO_2 = 0.81- 1.16) was plotted as a function of Fe/SiO_2. Here, the Q^3/Q^2 of silicate network was proposed as a degree of polymerization index based on the following reaction in Eq. (7.1) (Mysen, 1990b, Mysen and Dubinsky, 2004, Mysen and Richet, 2005).

$$[\mathrm{Si_2O_5}]^{2-} \leftrightarrow [\mathrm{Si_2O_6}]^{4-} + [\mathrm{SiO_2}] \tag{7.1}$$

The equilibrium constant (K) of equilibrium reaction of Eq. (7.2) at a given temperature can be written as

$$\mathrm{K} = \frac{[\mathrm{Si_2O_6}]^{4-}.\ [\mathrm{SiO_2}]}{[\mathrm{Si_2O_5}]^{2-}} = \frac{\mathrm{Q^2.\ Q^4}}{\mathrm{Q^3}} \tag{7.2}$$

It was assumed that the equilibrium constant (K) is independent to slag composition. Thus the concentration of highly polymerized (Q^4) unit is in proportion to the concentration ratio of Q^3 to Q^2 at a given temperature.

$$\frac{\mathrm{Q^3}}{\mathrm{Q^2}} \propto \text{Degree of polymerization } (\mathrm{Q^4}) \tag{7.3}$$

It can be seen from Figure 7.4 that the degree of polymerization (Q^3/Q^2) of the FeO_x-SiO_2-CaO-MgO (FCS) master slag system decreases with increasing Fe/SiO_2 ratio from 0.81 to 1.16, which suggests that Fe^{2+} acts as a role of network modifier in the silicate tetrahedra of FCS slag to increase the depolymerization. The slags used in the present study was prepared at particular oxygen potential and contain Fe in the form of FeO and Fe_2O_3.

Fe^{2+} cation units can essentially modify the slag structure by incorporated themselves in the tetrahedral coordinate of silicate network units (Mysen and Dubinsky, 2004, Mysen, 1990b). The ionization potential of Fe^{3+} ($Z/r^2 = 9.9$) is almost twice of Fe^{2+} ($Z/r^2 = 5.4$). Therefore, Fe^{3+} can adopt both four-fold (IV) and six-fold (VI) coordination. Four-fold coordination suggests cations will work as network former while six-fold coordination suggests network breaker. It was reported that role of Fe^{3+} depends on particularly $Fe^{3+}/(Fe^{2+}+Fe^{3+})$ ratio in the slag (Mysen, 1990b, Mills, 1993, Virgo et al., 1980). Fe^{3+} act as a network former and network breaker when the ratios are > 0.5 and <0.3, respectively.

It has been mentioned in Chapter 5 that an appropriate wet chemical analysis is required to determine the ratio of percentage of FeO and Fe_2O_3. This analysis was not carried out, rather the bulk slag chemistry (total Fe) was determined and analysed using ICP technique. Therefore, the compositions of the slags (including the FeO and Fe_2O_3 concentrations) were determined by equilibrium recalculation using FactSage 6.4 considering the bulk composition obtained from ICP analysis. The results are also given in Figure 7.4. It was found that Fe^{3+} ion increases with increasing Fe/SiO_2 ratio. But, the $Fe^{3+}/(Fe^{2+}+Fe^{3+})$ ratio is still far less than 0.3 as shown in Figure 7.4, which suggests that the Fe^{3+} contributes as a network breaker.

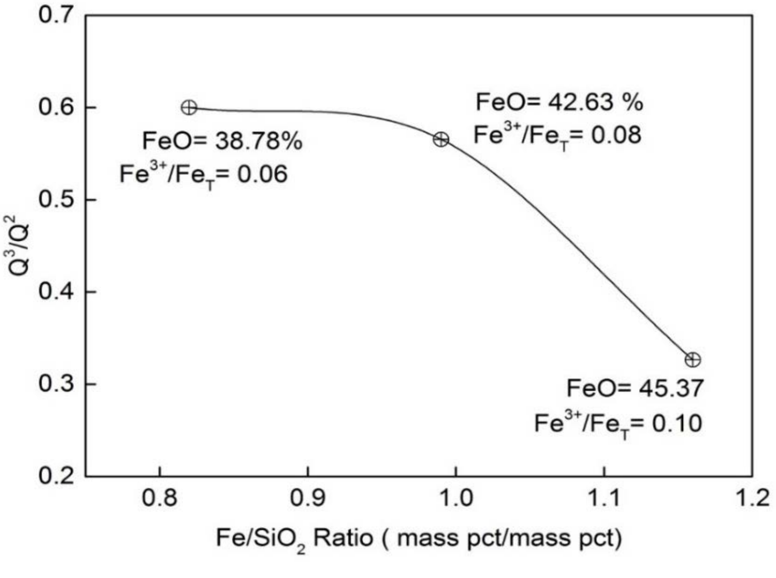

Figure 7.4: Relationship between Fe/SiO_2 ratio and Q^3/Q^2 ratio of FCS slag ($p_{O_2} = 10^{-8}$ atm and T = 1300°C).

7.4.2 Effect of basicity on the structure of FCS slag

The FTIR results of FeO_x-CaO-SiO_2-MgO (FCS) master slag samples are shown in Figure 7.5 as a function of the wavenumbers range 700 to 1500 cm^{-1} for different basicity values. Here the basicity is defined as (mass pct CaO + mass pct MgO)/ (mass pct SiO_2). As can be seen in Figure 7.5, the relative intensity of high frequency (1100(±10) cm^{-1}) peaks decreases in height with increasing basicity. It also seems a weak shoulder in main silicate envelope at basicity of 0.89. Similar to the case for different Fe/SiO_2 the depth of low frequency (850(±5) cm^{-1}) peak increase and the peaks slightly shift towards low wavenumber region with increasing basicity. It indicates that depolymerization of slag increases with increasing basicity from 0.49 to 0.89.

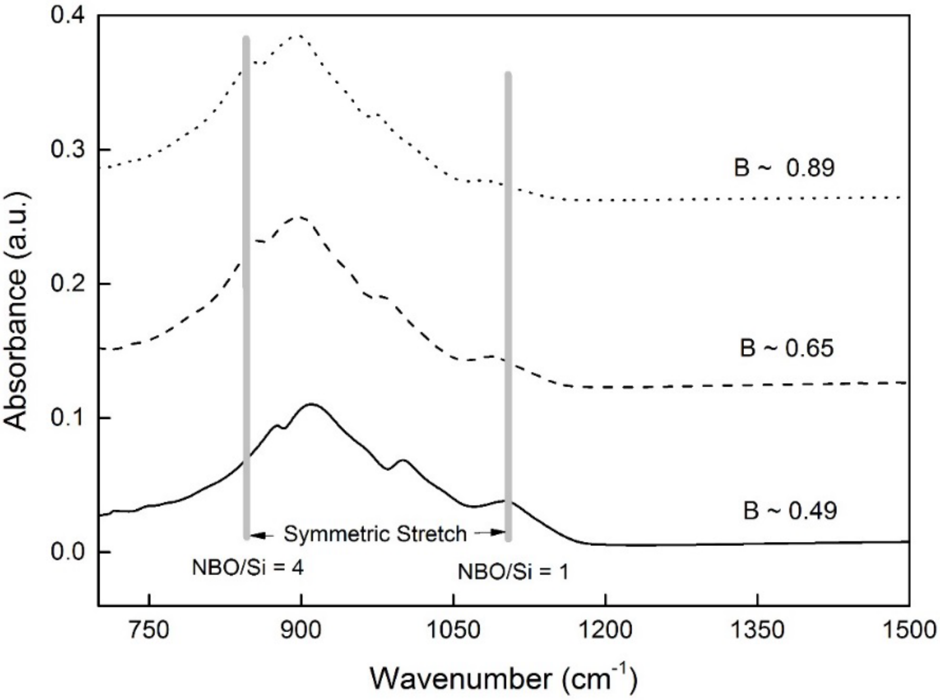

Figure 7.5: FTIR spectra of FCS master slags of basicity 0.49 to 0.89 ($p_{O_2} = 10^{-8}$ atm and T = 1300°C).

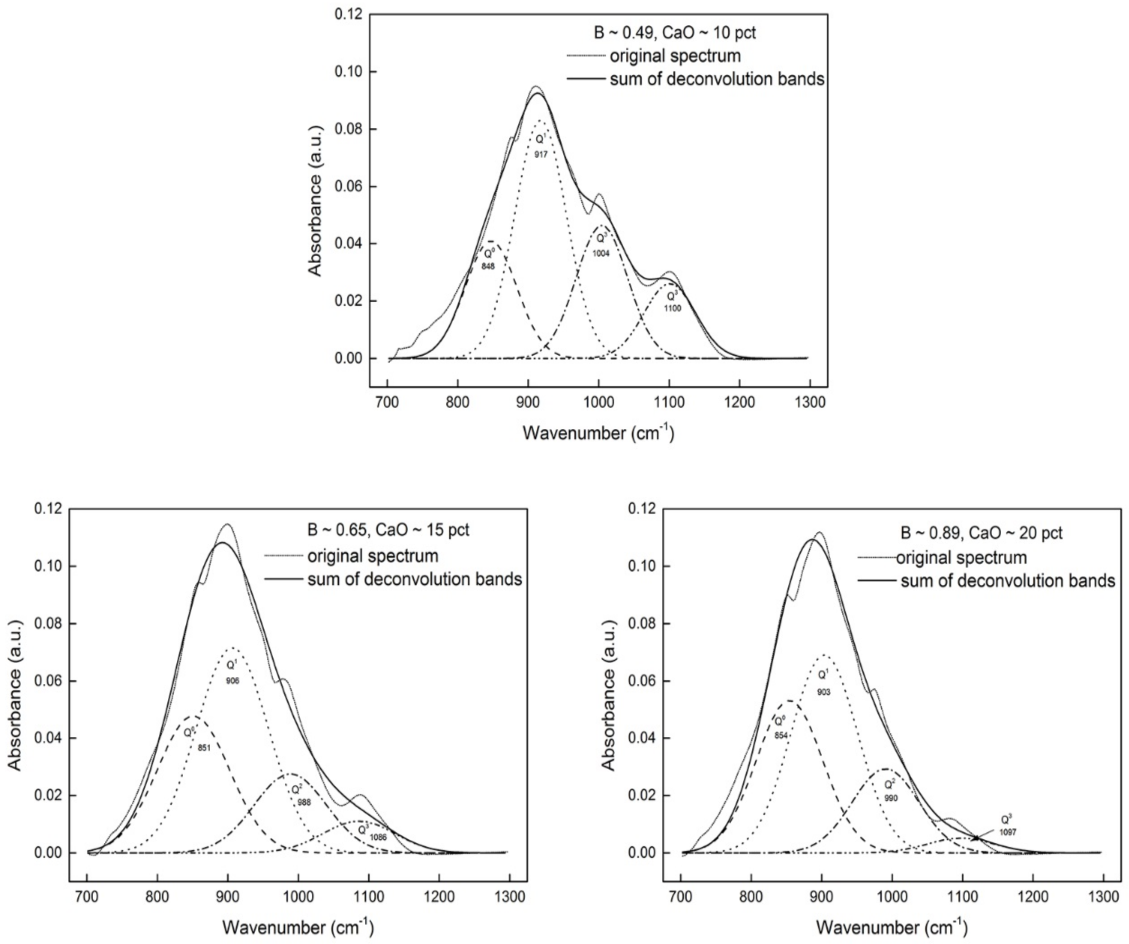

Figure 7.6: Deconvolution results of FTIR spectra of FCS master slags of different basicity ($p_{O_2} = 10^{-8}$ atm and T = 1300°C).

The results obtained from deconvolution based on Gaussian functions of IR spectra of master slags with varied basicity are shown in Figure 7.6 and listed in Table 7.2. Figure 7.6, shows the envelope of Q^3 and Q^2 silicates units in the FCS slag decrease, while Q^1 increases with increasing basicity. The relative fractions of the silicate units obtained from the deconvolution of IR spectra are plotted as a function of basicity in Figure 7.7.

Table 7.2: FTIR shift position and peak area ratio obtained from deconvolution of FTIR spectra of master FCS slags for different basicity

Basicity	Peak Position (cm^{-1})				Best Fitted Gaussian Peak Area (pct)				
	Q^0	Q^1	Q^2	Q^3	Q^0	Q^1	Q^2	Q^3	Q^3/Q^2
0.49	848	917	1004	1100	0.216	0.420	0.232	0.131	0.565
0.65	851	906	988	1086	0.303	0.453	0.174	0.070	0.402
0.89	854	903	990	1097	0.339	0.441	0.187	0.033	0.176

Composition of slag in mass pct
Fe_T = 32.8 %, SiO_2 = 33.1 %, CaO = 9.88 %, MgO = 6.49% (B = 0.49)
Fe_T =33.4 %, SiO_2 = 33.6 %, CaO = 14.5 %, MgO = 7.52% (B = 0.65)
Fe_T = 30.7 %, SiO_2 = 31.3 %, CaO = 19.4 %, MgO = 8.78% (B= 0.89)

As can be seen in Figure 7.7, the fractions of Q^3 and Q^2 units decrease with increasing basicity in the magnesia saturated FCS slag system, while Q^1 units do not change significantly. It indicates that silicates structure mainly depolymerized from highly polymerized Q^3 (Si_2O_5-sheet) and Q^2 (SiO_3-chain) units into Q^0 (SiO_4-monomer) unit as basicity increases from 0.49 to 0.89.

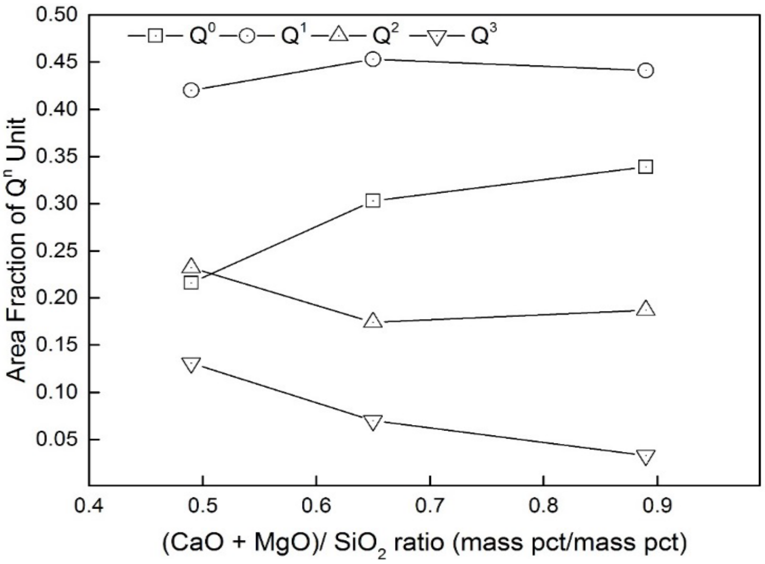

Figure 7.7: Abundance of structural units in FCS master slag as a function of basicity ($p_{O_2} = 10^{-8}$ atm and T= 1300°C).

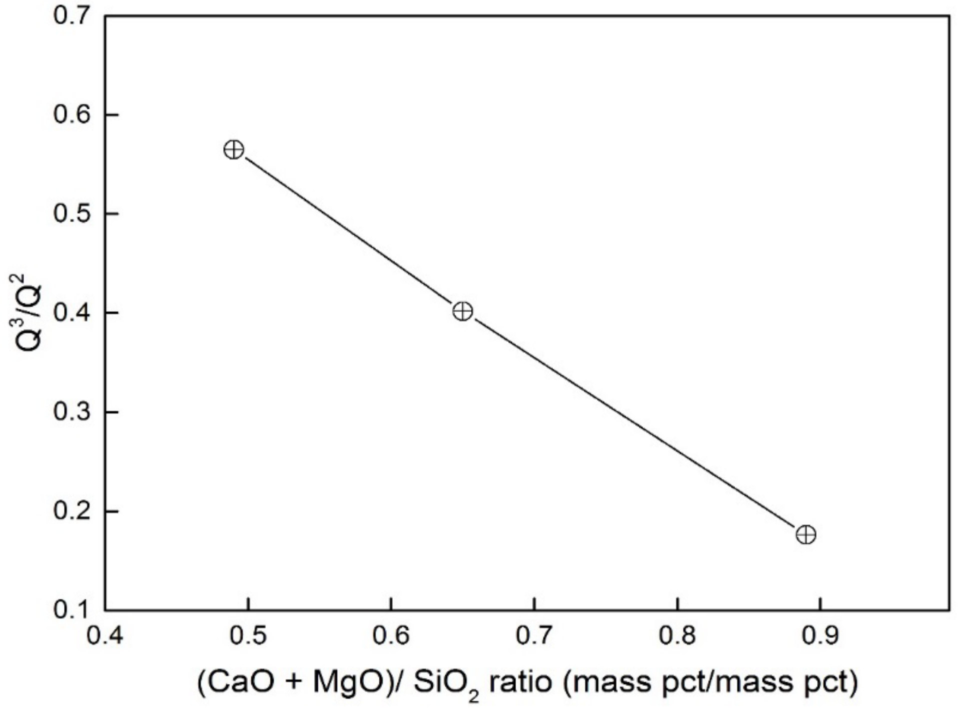

Figure 7.8: Relationship between Q^3/Q^2 ratio and basicity of FCS master slag ($p_{O_2} = 10^{-8}$ atm and T= 1300°C).

In Figure 7.8, the Q^3/Q^2 ratio of FCS master slag is plotted as a function of basicity range from 0.49 to 0.89. It can be seen from Figure 7.8 that the degree of polymerization (Q^3/Q^2) of the FeO_x-SiO_2-CaO-MgO (FCS) master slag system decreases with increasing basicity, which suggests that Ca^{2+} and Mg^{2+} both cations act as a role of network modifier in the silicate tetrahedra of FCS slag to increase the depolymerization. It is worth noting that the variation of the Q^3/Q^2 with basicity is highly linear. This suggests that the parameter Q^3/Q^2 is highly relevant to basicity. In fact, the Q^3/Q^2 is more suitable parameter to represent "basicity" of the slag compared to the simple ratio of (CaO+MgO)/SiO_2 as it represents directly the structure of the slag and can also be directly measured.

The ionization potential of Mg^{2+} ($Z/r^2 = 3.9$) is much higher than Ca^{2+} ($Z/r^2 = 2$) and the ability of MgO to offer O^{2-} is considered to be weaker than CaO. Thus, the polarizing power of Mg^{2+} is stronger than that of Ca^{2+}, and Mg^{2+} have a strong electrostatic interaction with another ion in the presence of Ca^{2+} in slag melts. Therefore, CaO has higher ability to act as network modifier compared to MgO in the FCS slag system.

The parameter of average bridging oxygen can also be used to characterize the degree of depolymerization of silicate melt, which can be represented by the Si-O structural units as in Eq. (7.4).

$$\mathrm{BO} = 0 \times Q^0 + 1 \times Q^1 + 2 \times Q^2 + 3 \times Q^3 \tag{7.4}$$

It is generally known that degree of polymerization would decrease with basicity, which could be confirmed by decreasing from average bridging oxygen in the silicate units of slag. The relationship with slag basicity and average bridging oxygen (BO) is shown in Figure 7.9. It can be noticed that average bridging oxygen in the FCS master slag system decreases with increasing basicity.

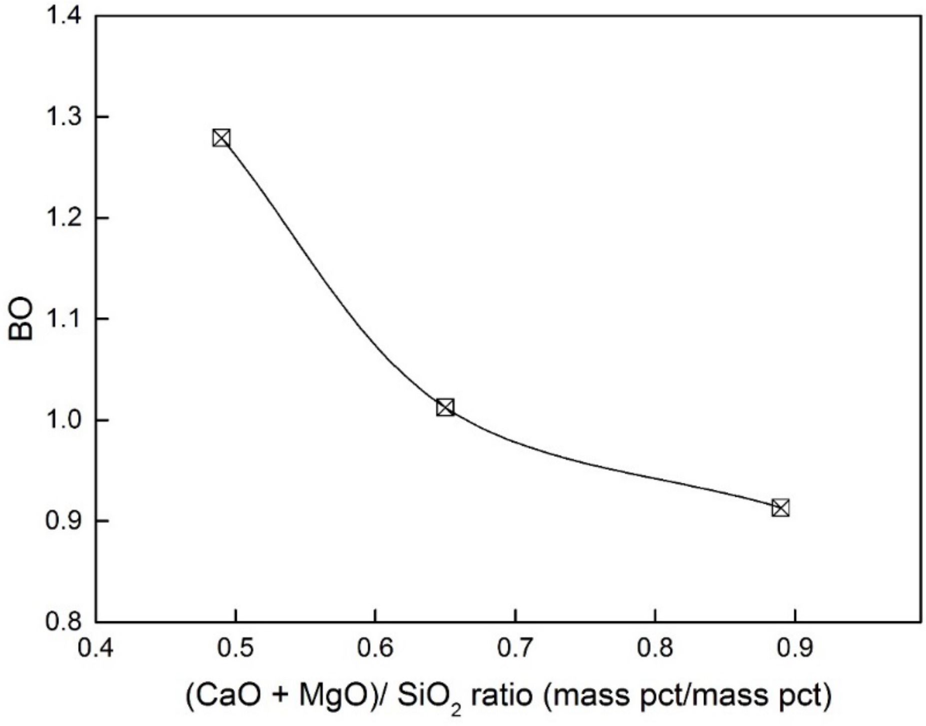

Figure 7.9: Relationship between basicity and bridging oxygen (BO) of FCS slag ($p_{O_2} = 10^{-8}$ atm and T = 1300°C).

7.5 Structure analysis of the equilibrated FeO$_x$-CaO-SiO$_2$-MgO-Cu$_2$O-GeO$_2$ and FeO$_x$-CaO-SiO$_2$-MgO-Cu$_2$O-PdO slag

The FTIR spectra of equilibrated FeO$_x$-CaO-SiO$_2$-MgO-Cu$_2$O-GeO$_2$ and FeO$_x$-CaO-SiO$_2$-MgO-Cu$_2$O-PdO slags from the study as explained in Chapters 5 and 6 were analysed to evaluate the effect of oxygen potential, temperature and compositional variation on anionic structure units and the degree of polymerization. The details of results are described in the following section.

7.5.1 Effect of oxygen potential

The FTIR analyses results of the equilibrated FeO_x-CaO-SiO_2-MgO-Cu_2O-(GeO_2/PdO) slag samples are shown in Figure 7.10 as a function of the wavenumbers ranges 700 to 1500 cm^{-1} for different oxygen partial pressure. Figure 7.10 (a) and Figure 7.10 (b) shows the results of equilibrium slag from germanium (Ge) and palladium (Pd) studies at varied p_{O_2}, respectively.

As can be seen in Figure 7.10 (a), the relative intensity of low-frequency Q^1 (915(±10) cm^{-1}) peak decreases, while the intensity of high-frequency Q^3 (1100(±10) cm^{-1}) band increases with increasing p_{O_2}. The peak of ~980 cm^{-1} band (Q^2) shifts significantly with increasing p_{O_2} which suggests that polymerization of equilibrated slag increases with increasing p_{O_2}. It is also seen from Figure 7.10 (b) that the spectra does not show any significant changes with decreasing pressure in the equilibrated slags of Pd study. Even no siginificant differnces can be seen from the spectra at lower p_{O_2} of Ge study. However, only differene was found in spectra at higher $p_{O_2} = 10^{-7}$ atm. It indicates that increasing p_{O_2} results in the polymerization of the silicate network because of the formation new bonds in the tetradehra units, and therefore, it increases the rate of polymerization.

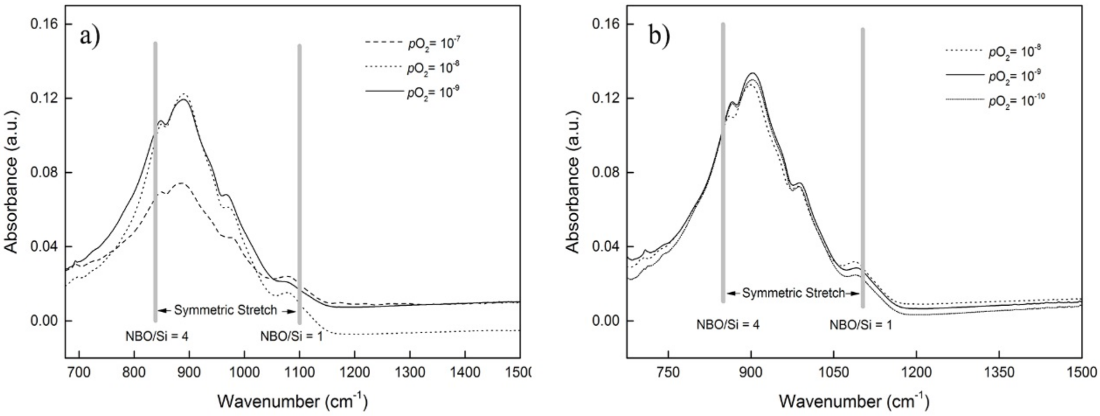

Figure 7.10: FTIR spectra of equilibrated FeO_x-CaO-SiO_2-MgO-Cu_2O- (GeO_2/PdO) slags with varied oxygen partial pressure at 1300°C from a) Ge, and b) Pd study

All the results obtained from deconvolution IR spectra of the FeO_x-CaO-SiO_2-MgO-Cu_2O- (GeO_2/PdO) slags with varied p_{O_2} are shown in **Appendix C**.

The degree of polymerization (Q^3/Q^2) of the FeO_x-CaO-SiO_2-MgO-Cu_2O-(GeO_2/PdO) slags from germanium and palladium studies with varied p_{O_2} and their relevant distribution-ratios are plotted at 1300°C (1573 K) in Figure 7.11 (a) and (b), respectively.

It can be seen in Figure 7.11 (a) that the degree of polymerization (Q^3/Q^2) of the slags and the distribution-ratio both increase with increasing p_{O_2}, which suggests that oxygen potential from the gas phase can incorporate oxygen atom into the tetradehral coordinate of silicate network units and help the formation of new bond in silicon tetrahedra units. Therefore, the polymerization of slag increases with increasing oxygen partial pressure at a fixed temperature. On the other side in Figure 7.11 (b) does not show any significant particularity after p_{O_2}=10^{-9} atm, which is in line with the results found in Figure 7.10 (b)

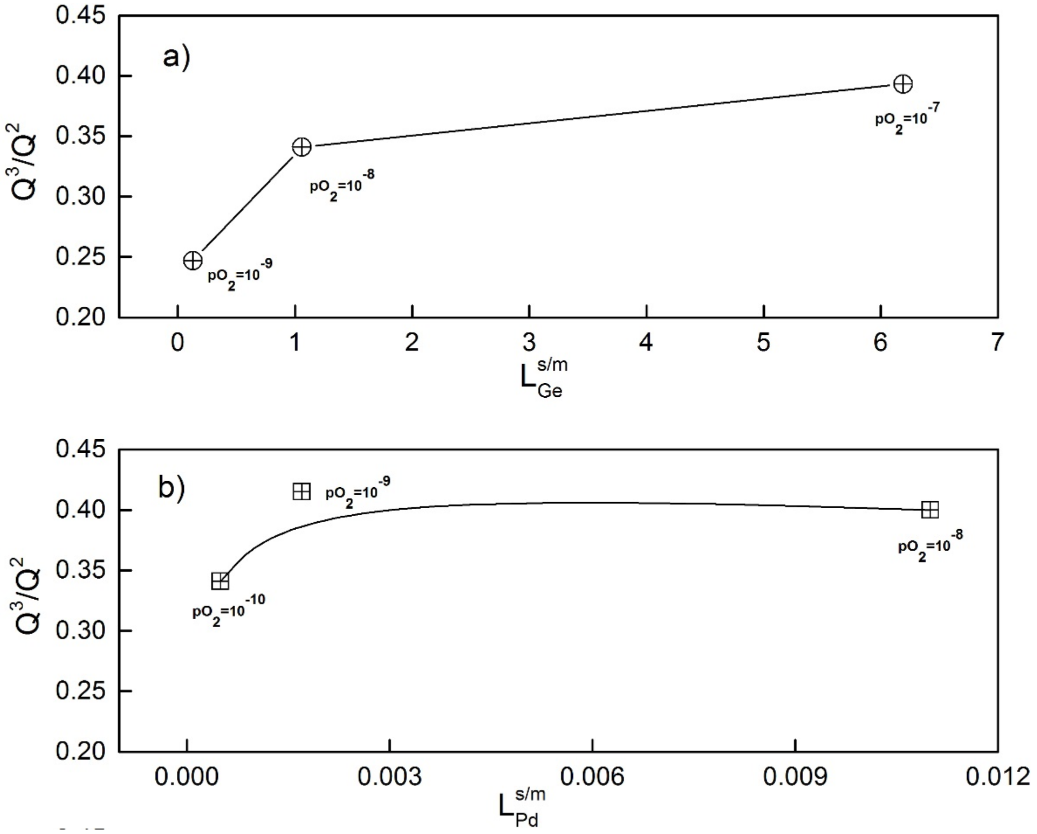

Figure 7.11: Relationship of the Q^3/Q^2 ratio and distribution-ratio at different oxygen partial pressure in the FeO_x-CaO-SiO_2-MgO-Cu_2O-(GeO_2/PdO) from a) Ge study, and b) Pd study (T =1300°C).

7.5.2 Effect of temperature

The FTIR results of the equilibrated slag samples are shown in Figure 7.12 as a function of the wavenumbers from 700 to 1500 cm^{-1} for different temperatures. Figure 7.12 (a) and Figure 7.12 (b) show the results from the Ge and Pd studies, respectively.

As can be seen in Figure 7.12 (a), the frequency of both ~1100 cm^{-1} band (Q^3) and ~980 cm^{-1} band (Q^2) peaks slightly shift toward lower values with increasing temperature. The intensity of peak near ~980 cm-1 band (Q^2) also increases as a function of temperature. The peak near ~910 cm^{-1} (Q^1) of spectra of silicate melts does not shift significantly. Increasing of intensity and shifting of the absorbance bands to lower frequency indicate a depolymerization of the slag structure as suggested in the literature (Mysen and Frantz, 1992). The increasing temperature results in the depolymerization of silicate network because of the increased kinetic energy of atoms make it easier to breaks the silicon tetrahedral units. It can also be seen from Figure 7.12 (b) that the slags from the Pd study show similar trends to the slags from the Ge study.

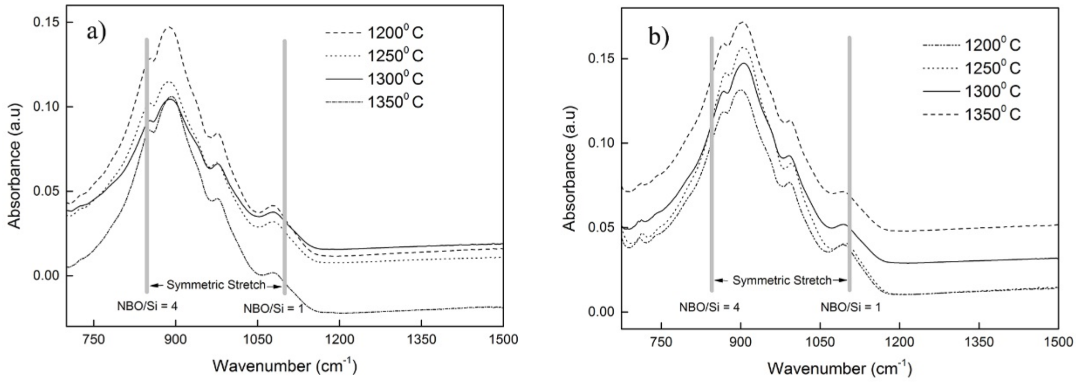

Figure 7.12: FTIR spectra of equilibrated FeO_x-CaO-SiO_2-MgO-Cu_2O-(GeO_2/PdO) slag with different temperatures from a) Ge, and b) Pd study ($p_{O_2} = 10^{-8}$ atm).

The results obtained from deconvolution of IR spectra of equilibrated slags at different temperatures including the silicate units are shown in **Appendix C**. The degree of polymerization (Q^3/Q^2) of the equilibrated FeO_x-CaO-SiO_2-MgO-Cu_2O-(GeO_2/PdO) slags and their relevant distribution-ratios are plotted as a function temperature at a fixed p_{O_2} in Figure 7.13 (a) and (b), respectively.

It can be seen from Figure 7.13 (a) and (b) from that the degree of polymerization (Q^3/Q^2) of the slag and distribution-ratio both decrease with increasing temperature, which suggests that high temperature can help to modify the slag structure by breaking the tetrahedral coordinate of silicate network units. Consequently, as the depolymerization of slag increases with increasing temperature, and more Ge and Pd deport to metal phase.

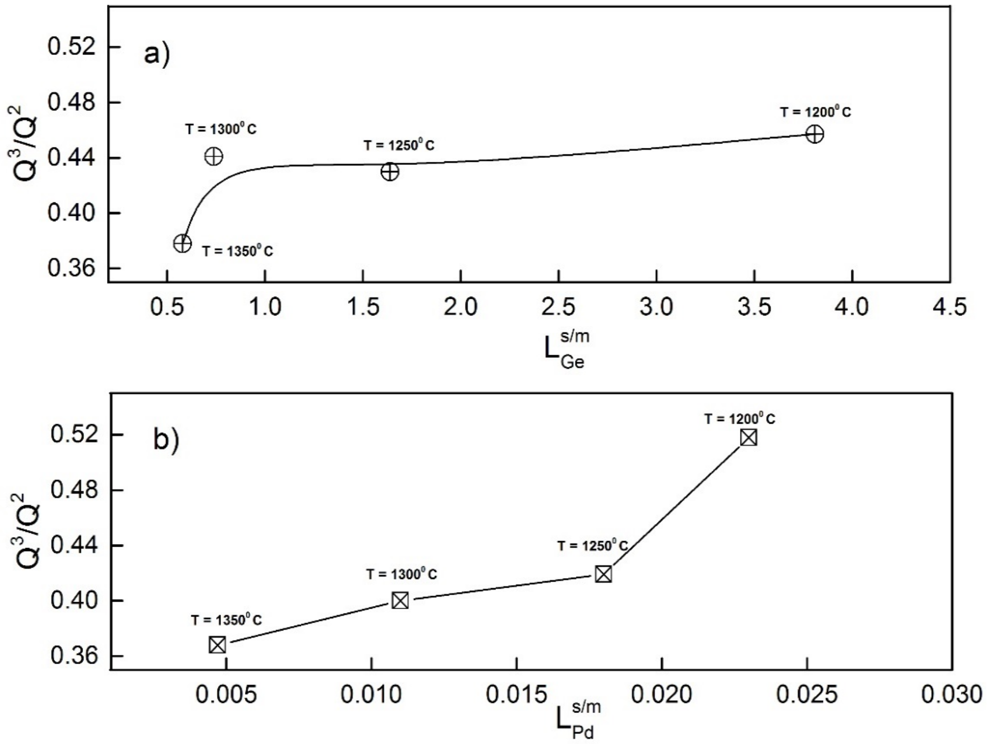

Figure 7.13: Relationship of the Q^3/Q^2 and distribution-ratio a) Ge study, and b) Pd study for different temperatures ($p_{O_2} = 10^{-8}$ atm).

7.5.3 Effect of slag composition

The FTIR results of the equilibrated FeO_x-CaO-SiO_2-MgO-Cu_2O-(GeO_2/PdO) slags samples are shown in Figure 7.14 as a function of the wavenumbers from 700 to 1500 cm^{-1} for varied Fe/SiO_2 ratio. Figure 7.14 (a) and (b) shows the results of equilibrated slag from Ge study, and Pd study respectively at varied Fe/SiO_2 ratio. As can be seen in Figure 7.14 (a) and (b), the relative intensity of frequency 980(±10) cm^{-1} (Q^2) peak and high-frequency Q^3 (1100(±10) cm^{-1}) band decrease with increasing Fe/SiO_2. The peak of ~880 cm^{-1} band (Q^0) shifts significantly with increasing Fe/SiO_2, which suggests that polymerization of equilibrated FCS slag increase with increasing Fe/SiO_2.

The results obtained from deconvolution of IR spectra of FeO_x-CaO-SiO_2-MgO-Cu_2O-(GeO_2/PdO) slags with different Fe/SiO_2 are shown in **Appendix C**. The relative fraction of the silicate units obtained from the deconvolution of IR spectra are plotted in Figure 7.15 as a function of Fe/SiO_2. Similar to Section 7.4.1, it is noticed that silicates structure mainly transformed from highly polymerized Q^3 (Si_2O_5-sheet) and Q^2 (SiO_3-chain) units into depolymerized Q^0 (SiO_4-monomer) unit as Fe/SiO_2 ratio increases in the equilibrated slag from 0.8 to 0.99.

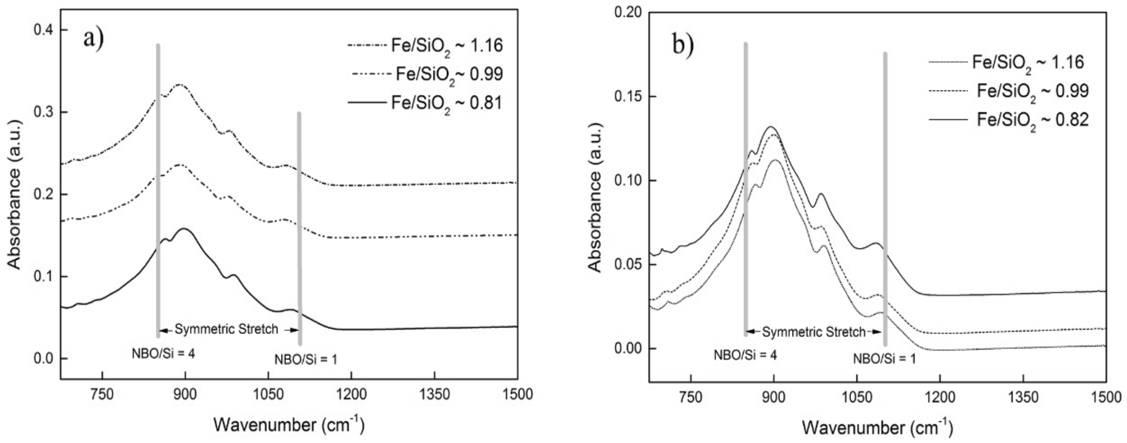

Figure 7.14: FTIR spectra of FeO_x-CaO-SiO_2-MgO-Cu_2O-(GeO_2/PdO) equilibrated slags a) Ge, and b) Pd study with different Fe/SiO_2 (p_{O_2}= 10^{-8} atm and T =1300°C).

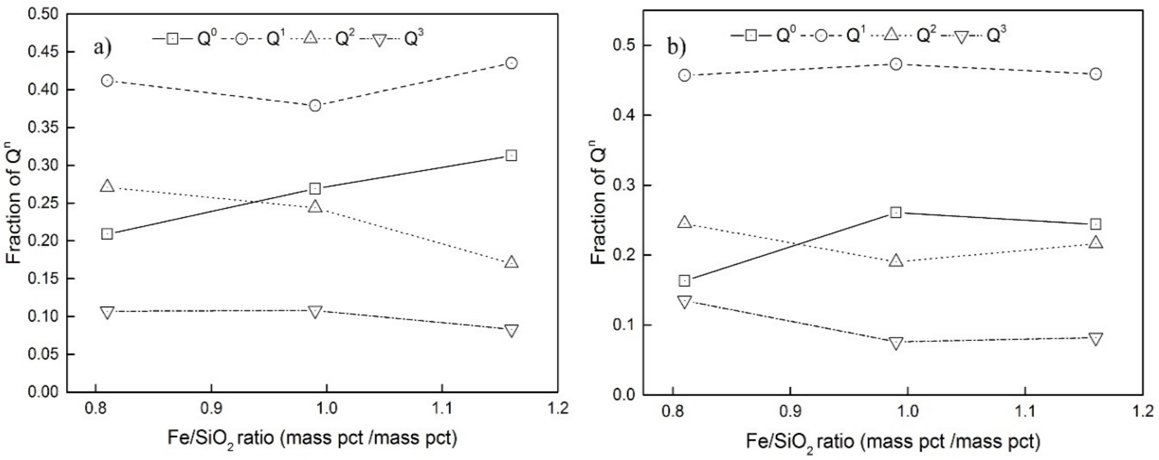

Figure 7.15: Abundance of structural units in FeO_x-CaO-SiO_2-MgO-Cu_2O-(GeO_2/PdO) equilibrated slag from a) Ge, and b) Pd study as a function of Fe/SiO_2 ratio ($p_{O_2} = 10^{-8}$ atm and T= 1300°C).

The degree of polymerization (Q^3/Q^2) of the FeO_x-CaO-SiO_2-MgO-Cu_2O-(GeO_2/PdO) slags and their relevant distribution-ratios are plotted in Figure 7.16 (a) and (b), respectively, as a function of Fe/SiO_2 ratio at a fixed temperature and p_{O_2}.

It can be seen from Figure 7.16 (a) that the degree of polymerization (Q^3/Q^2) of the slag system and $L_{Ge}^{s/m}$ increase with increasing Fe/SiO_2 ratio from 0.81 to 1.16. It shows the opposite trend compared to that shown in Figure 7.4 for master FCS slags. It suggests that Ge^{4+} cation act as a network former in the slag and increase the degree of polymerization. The ionization potential of Ge^{4+} ($z/r^2 = 26$) is higher than Si^{4+} ($z/r^2 = 25$) and can adopt four-fold (IV) coordination. However, the concentration of Ge^{4+} in the slag is very small, and it was difficult to find the intensity of this tetrahedral in IR spectra over silicon tetrahedra.

On the other hand, Figure 7.16 (b) shows that the degree of polymerization (Q^3/Q^2) decreases as Fe/SiO_2 ratio increases. The decreasing of the Q^3/Q^2 also indicates the decrease of $L_{Pd}^{s/m}$ and then less Pd goes to slag phase.The small concentration of Pd in slag does not have any significant effect on the Q^3/Q^2. Although, the ionization potential of Pd^{2+} (z/r^2 =5.4) is much lower than Ge^{4+} (z/r^2 =26) and it should act as a network modifier.

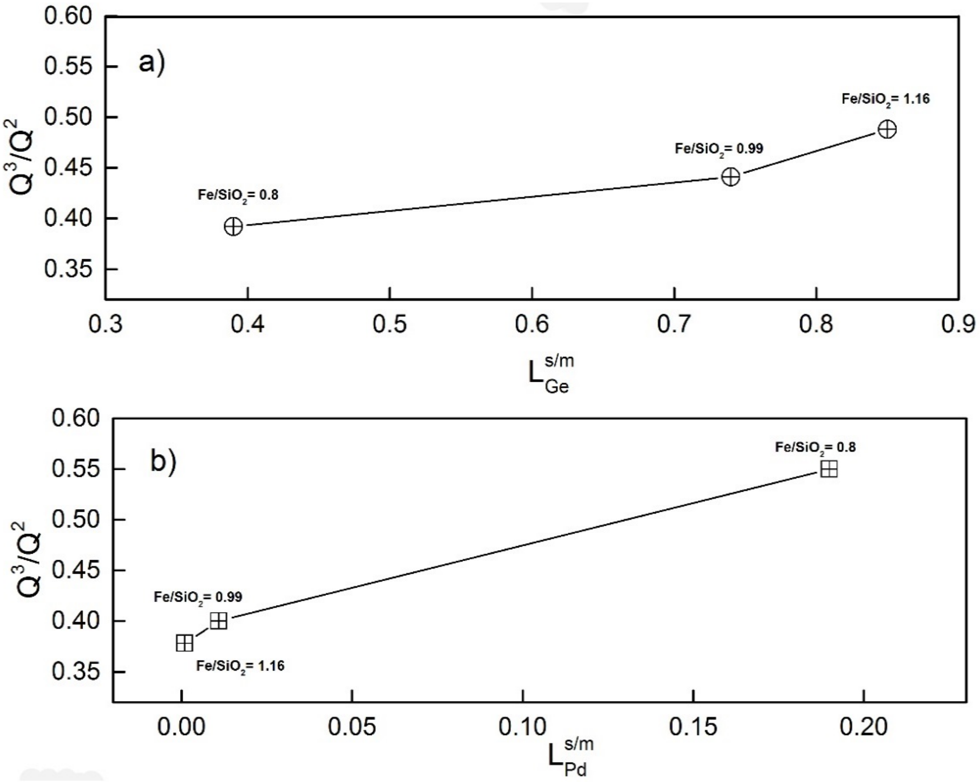

Figure 7.16: Relationship of the Q^3/Q^2 and distribution-ratio a) Ge study, and b) Pd study with different Fe/SiO_2 ratio in FeO_x-CaO-SiO_2-MgO-Cu_2O-(GeO_2/PdO) slag (p_{O_2}= 10^{-8} atm and T =1300ºC)

The FTIR results of FeO_x-CaO-SiO_2-MgO-Cu_2O-(GeO_2/PdO) slag samples are shown in Figure 7.17 (a) and (b) as a function of the wavenumbers from 700 to 1500 cm^{-1} for different basicity.

As can be seen in Figure 7.17 (a) and (b), the relative intensity of frequency 910(±10) cm^{-1} (Q^1) peak increases and high-frequency Q^3 (1100(±10) cm^{-1}) band decreases with increasing basicity. The peak of ~880 cm^{-1} (Q^0), ~920 cm^{-1} (Q^1) and ~980 cm^{-1} bands (Q^2) shift significantly with increasing basicity, which suggests that polymerization of equilibrated FCS slag increases with increasing basicity.

The results obtained from deconvolution based on Gaussian functions of IR spectra of FeO_x-CaO-SiO_2-MgO-Cu_2O-(GeO_2/PdO) slags with different basicity are shown in **Appendix C**. The relative fraction of silicate units from the deconvolution of IR spectra are plotted in Figure 7.18. It indicates that silicates structure mainly transformed from highly polymerized Q^3 (Si_2O_5-sheet) and Q^1 (Si_2O_7-dimer) units into depolymerized Q^0 (SiO_4-monomer) and Q^2 (SiO_3-chain) units as basicity increases in the slag beyond 0.6. However, at lower basicity Q^3 (Si_2O_5-sheet) and Q^2 (SiO_3-chain) depolymeirized into Q^1 (Si_2O_7-dimer).

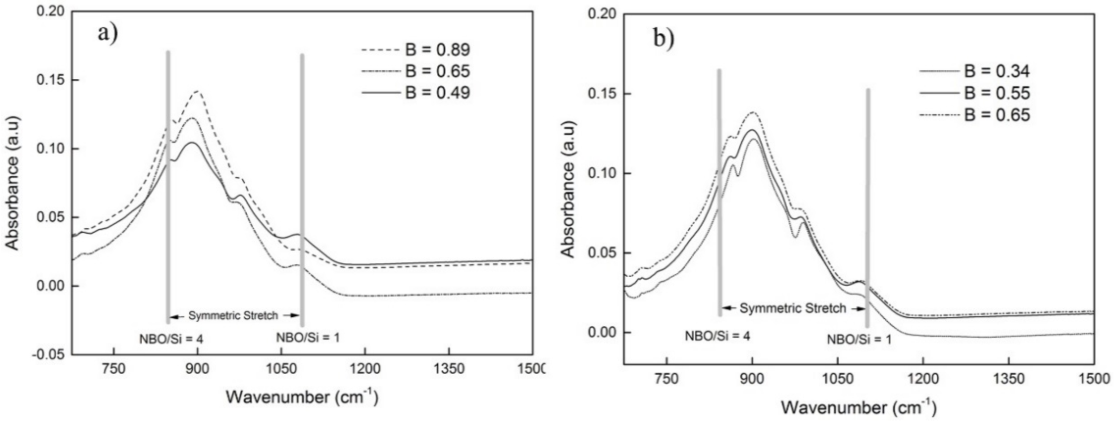

Figure 7.17: FTIR spectra of FeO_x-CaO-SiO_2-MgO-Cu_2O-(GeO_2/PdO) slags a) Ge, and b) Pd study with different basicity (p_{O_2}= 10^{-8} atm and T =1300°C).

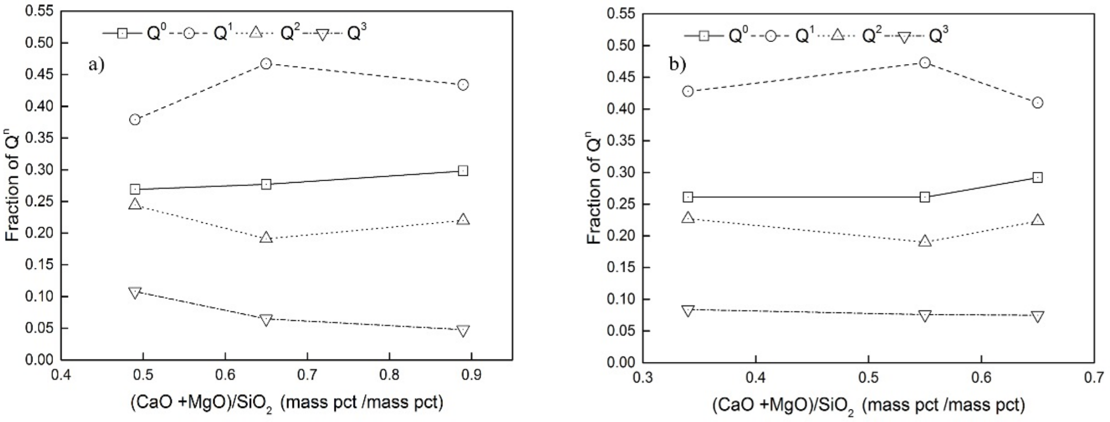

Figure 7.18: Abundance of structural units in FeO_x-CaO-SiO_2-MgO-Cu_2O-(GeO_2/PdO) equilibrated slag from a) Ge, and b) Pd study as a function of basicity (p_{O_2} = 10^{-8} atm and T= 1300°C).

The degree of polymerization (Q^3/Q^2) of the FeO_x-CaO-SiO_2-MgO-Cu_2O-(GeO_2/PdO) slag of Ge and Pd study and their relevant distribution-ratios are plotted in

Figure 7.19 (a) and (b), respectively, as a function of basicity at a fixed temperature and p_{O_2}.

It can be seen from Figure 7.19 (a) that the degree of polymerization (Q^3/Q^2) of the slag decreases with increasing basicity. It is also found that $L_{Ge}^{s/m}$ increases with decreasing of the Q^3/Q^2 and more germanium deported to the slag. As can be seen from Figure 7.19 (b), the degree of polymerization (Q^3/Q^2) decreases as basicity increases. Therefore, it can be recalled again according to Chapters 5 and 6 that basic slag (slag having the lower Q^3/Q^2) is better for Pd partitioning, whereas acidic slag (slag having the higher Q^3/Q^2) allow less Ge to deport in the slag which is also shown in Figure 7.19 (a) and (b).

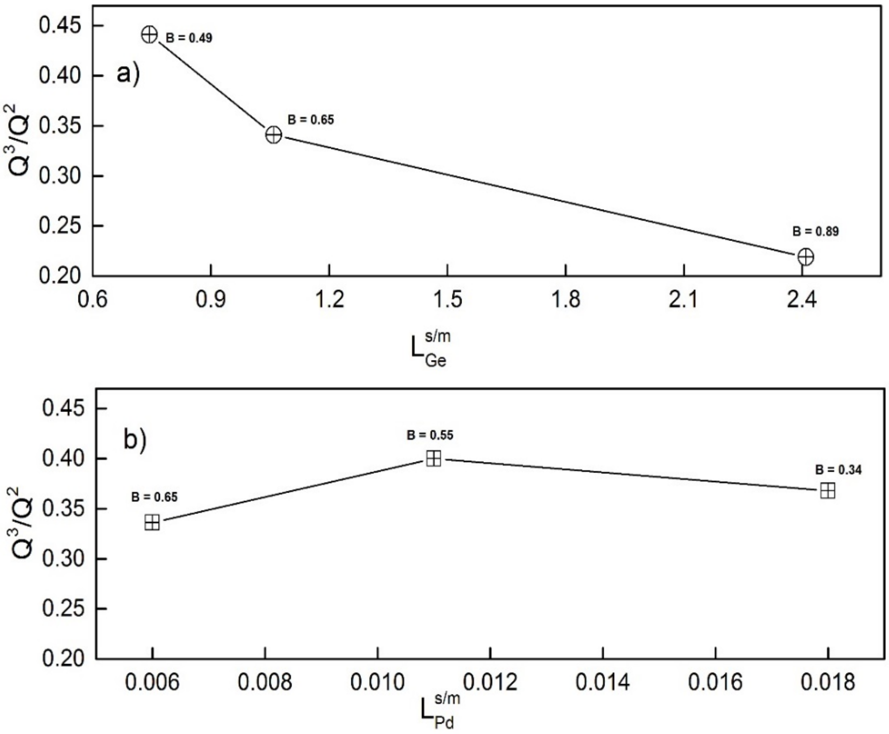

Figure 7.19: Relationship of the Q^3/Q^2 and distribution-ratio a) Ge, and b) Pd study for different basicity (p_{O_2}= 10^{-8} atm and T =1300°C).

7.6 Relationship between degree of polymerization, composition and partitioning ratio

An attempt has been taken in the current study to develop a correlation between the slag structure and experimental parameters that have been studied. The slag structure is expressed using an index of the degree of polymerization (Q^3/Q^2). The multiple regression analysis methods was used to develop the relationships. A relationship was were established, by combining the results of Ge study and Pd study, and are shown in Eq. (7.5). The percentage of GeO_2, PdO and Cu_2O have not been accounted for in the Eq. (7.5) because of having small concentrations in the slag.

$$\frac{Q^3}{Q^2} = \frac{4}{73} log\, p_{O_2} + \frac{1665}{\mathrm{T}} - \frac{1}{217}\,\mathrm{CaO}\ (\mathrm{pct}) - \frac{6}{49}\,\mathrm{MgO}\ (\mathrm{pct}) + \frac{1}{57}\mathrm{SiO_2}\ (\mathrm{pct}) - \frac{1}{751}\,\mathrm{Fe_T}\ (\mathrm{pct}) - \frac{3}{53} \tag{7.5}$$

The calculated values from Eq. (7.5) was compared with the relevant measured values and then the results are plotted and is shown in Figure 7.20 (a) and (b) respectively. A very good correlation (R^2 = 0.861 (for Ge) and R^2 = 0.65 (for Pd)) was found between the calculated value and measured value. This equation can be used to calculate the degree of polymerization of relevant slag system at any temperature, p_{O_2} and slag composition.

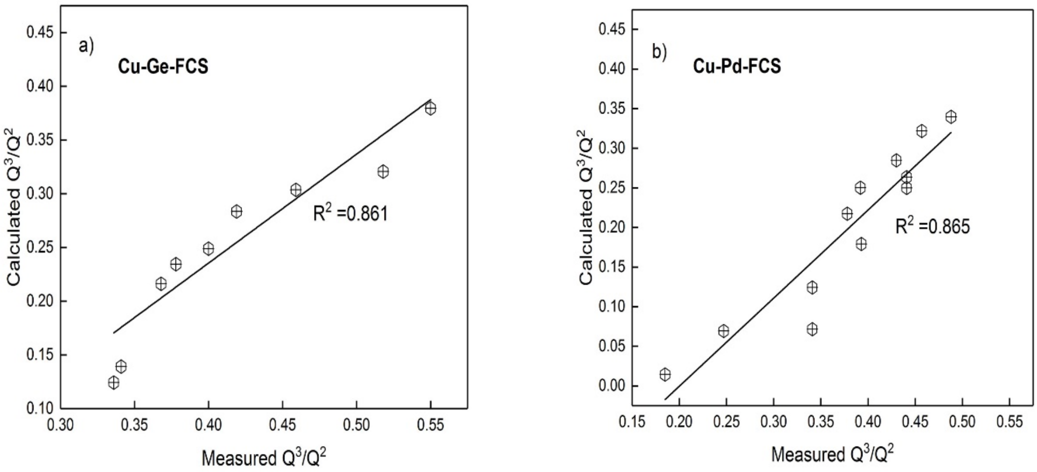

Figure 7.20: Comparison of calculated and measured value of the Q^3/Q^2 for a) Ge, and b) Pd study.

It was reported that Gibbs free energy, and thermodynamic properties can be correlated to the slag structure units (Halter and Mysen, 2004). In the present study, a relationship between the distribution-ratio of Ge and Pd, and the degree of polymerization was established using the linear regression analysis, which is presented in Eq. (7.6) and (7.7).

$$\mathrm{L}_{\mathrm{Ge}}^{\mathrm{S/m}} = \frac{181}{75}\log p_{O_2} + \frac{61422}{\mathrm{T}} - \frac{365}{36}\ {Q^3}\!/{Q^2} - \frac{115}{8} \tag{7.6}$$

$$\mathrm{L}_{\mathrm{Pd}}^{\mathrm{S/m}} = \frac{74}{9999}\log p_{O_2} - \frac{724}{T} + \frac{8}{21}\ {Q^3}\!/{Q^2} + \frac{2}{5} \tag{7.7}$$

The calculated values from Eq. (7.6) and (7.7) were compared with the relevant measured values and then the results are plotted and shown in Figure 7.21 (a) and (b) respectively. It is noticeable the values are scattered in the both plots. It might be the reason of partial crystalline structure formation during the cooling and limitation of quenching in experimental technique. The correlation (R^2 = 0.754 and R^2 = 0.751) is found between the calculated and measured values to be taken as an indicative which is required further modification. Further modification including the changing quenching technique (i.e., quench in water), analysis the slag with other spectroscopic techniques and extend the number of experiments in a wide range of parameters in the present slag-metal system. The modified equation may be used to calculate the $\mathrm{L}_{\mathrm{X\,(Ge,Pd)}}^{\mathrm{s/m}}$ of relevant slag system at any temperature and p_{O_2}.

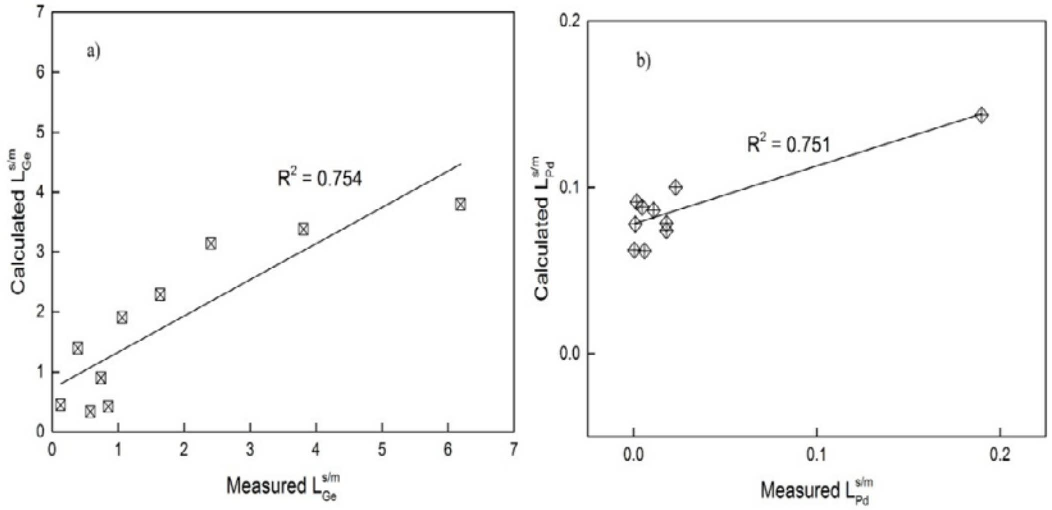

Figure 7.21: Comparison of calculated and measured value of the $\mathrm{L}_{\mathrm{X\,(Ge,Pd)}}^{\mathrm{s/m}}$ a) Ge, and b) Pd study.

The possible of stoichiometric reactions between cations present in the equilibrated slag and silicate units are shown in Eq. (7.8) to Eq. (7.31).

Here, $\mathrm{Q}^0 = \mathrm{SiO}_4^{4-}$, $\mathrm{Q}^1 = \mathrm{Si_2O}_7^{6-}$

$\mathrm{Q}^2 = \mathrm{Si_2O}_6^{4-}$, and $\mathrm{Q}^3 = \mathrm{Si_2O}_5^{2-}$

$$2Ca^{2+} + Q^0 = Ca_2Q^0 \tag{7.8}$$

$$3Ca^{2+} + Q^1 = Ca_3Q^1 \tag{7.9}$$

$$6Ca^{2+} + 3Q^2 = Ca_6Q_3^2 \tag{7.10}$$

$$Ca^{2+} + Q^3 = CaQ^3 \tag{7.11}$$

$$2Mg^{2+} + Q^0 = Mg_2Q^0 \tag{7.12}$$

$$3Mg^{2+} + Q^1 = Mg_3Q^1 \tag{7.13}$$

$$6Mg^{2+} + 3Q^2 = Mg_6Q_3^2 \tag{7.14}$$

$$Mg^{2+} + Q^3 = MgQ^3 \tag{7.15}$$

$$2Fe^{2+} + Q^0 = Fe_2Q^0 \tag{7.16}$$

$$3Fe^{2+} + Q^1 = Fe_3Q^1 \tag{7.17}$$

$$6Fe^{2+} + 3Q^2 = Fe_6Q_3^2 \tag{7.18}$$

$$Fe^{2+} + Q^3 = FeQ^3 \tag{7.19}$$

$$4Fe^{3+} + 3Q^0 = Fe_4Q_3^0 \tag{7.20}$$

$$2Fe^{3+} + Q^1 = Fe_2Q^1 \tag{7.21}$$

$$4Fe^{3+} + 3Q^2 = Fe_4Q_3^2 \tag{7.22}$$

$$2Fe^{3+} + 3Q^3 = Fe_2Q_3^3 \tag{7.23}$$

$$Ge^{4+} + Q^0 = GeQ^0 \tag{7.24}$$

$$3Ge^{4+} + 2Q^1 = Ge_3Q_2^1 \tag{7.25}$$

$$Ge^{4+} + Q^2 = GeQ^2 \tag{7.26}$$

$$Ge^{4+} + 2Q^3 = GeQ_2^3 \tag{7.27}$$

$$2Pd^{2+} + Q^0 = Pd_2Q^0 \tag{7.28}$$

$$3Pd^{2+} + Q^1 = Pd_3Q^1 \tag{7.29}$$

$$6Pd^{2+} + 3Q^2 = Pd_6Q_3^2 \tag{7.30}$$

$$Pd^{2+} + Q^3 = PdQ^3 \tag{7.31}$$

The above reactions free energy can be calculated considering an ideal mixing which was successfully used by Halter and Mysen (2004) in the Na_2O- SiO_2 binary system. They reported thermodynamic properties of the species can be determined from speciation data collecting by the spectroscopic technique. Other thermodynamic information such as enthalpy, heat capacity and entropy can also be determined. It is expected that as the slag become more complex, the behaviour will deviate from ideal mixing. Further modification such as using a quasichemical solution model can also be applied for a more complex system. This will be required in future work.

7.7 Speciation of three types oxygen from IR spectra

Park et al. (2002, 2012, 2013a, 2013b) described about the estimation of NBO/Si values in the slag using a mass balance of Si and O atom. In this study, similar technique to measure and calculate NBO/Si using following Eq. (7.32) and Eq. (7.33) was adopted (Park et al., 2002, Park, 2013a, Park, 2013b, Park, 2012).

$$\frac{\mathrm{NBO}}{\mathrm{Si}}(\mathrm{means.}) = \sum_{n=1}^{4} n \times f_{Q^{4-n}} \tag{7.32}$$

where $f_{Q^{4-n}}$ represents the area fraction of silicate structure units.

The theoretical NBO/Si (cal) of silicates can be obtained from Eq. (7.33)

$$\mathrm{NBO/Si\ (calc.)} = \frac{\sum 2\, X_{MO}}{X_{SiO_2}} \tag{7.33}$$

where X_{MO} is the mole fraction of oxide MO (M = Ca, Mg, and Fe). The FeO_x-CaO-SiO_2-MgO-Cu_2O-(GeO_2/PdO) slag compositions were determined through the approach mentioned in Chapters 5 and 6 and then calculated value of NBO/Si was determined according to Eq.(7.33).

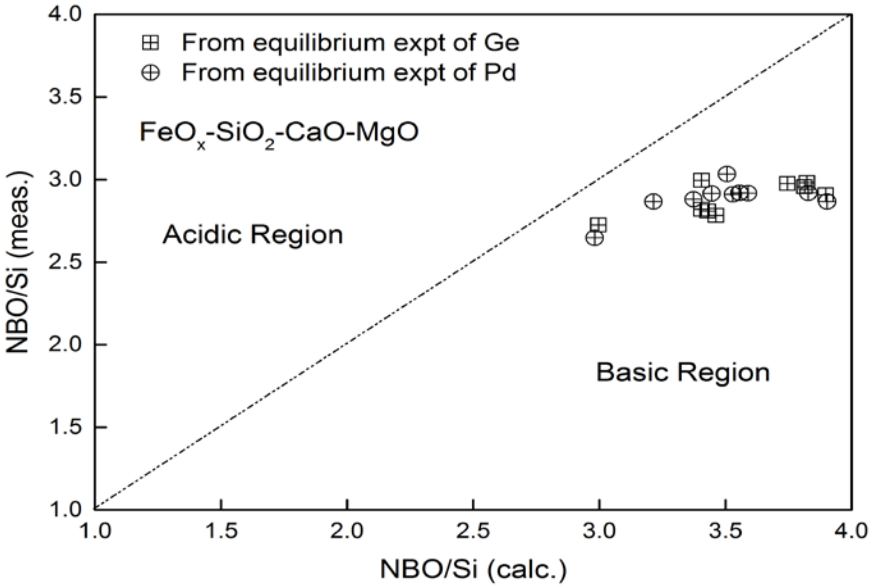

Figure 7.22: Relationship between the measured and calculated value of NBO/Si.

The relationship between the measured and calculated value of non-bridging oxygen (NBO) per silicon tetrahedra of equilibrated FCS slag is shown in Figure 7.22. The graph is divided into two region, the 'Acidic Region' in which the measured NBO/Si is greater than the calculated NBO/Si and vice versa for 'Basic Region' (Park, 2013a, Park, 2013b, Park, 2012). It can be seen from Figure 7.22 that the calculated value of NBO/Si is significantly greater than measured NBO/Si. The overestimated value of NBO/Si (calc.) suggests that silicon network is not perfectly depolymerized. Therefore, free oxygen (O^{2-}) interact with M^{2+} cations and formed a weak ionic bond rather than reach in an equilibrium state according to Eq.(7.34) with non-bridging and bridging oxygen.

$$O^0 + O^{2-} = 2O^- \tag{7.34}$$

$$K = \frac{[O^-]^2}{[O^o].[O^{2-}]} \tag{7.35}$$

Where is K the equilibrium constant of Eq. (7.34).

The measured value of the NBO/Si is lower than the calculated value of the NBO/Si, which suggests there is free network modifier from the depolymerization reaction, is called 'excess base'. The mole fraction of oxygen species in the slag can be estimated from simple mass balance. The fraction of three types of oxygen speciation in the slag can be calculated from Eq. (7.36) to Eq. (7.39) (Park et al., 2002, Park, 2013a, Park, 2013b, Park, 2012).

$$X_{O^{2-}} = \frac{excess\ base}{2SiO_2 + \sum X_{MO}} \tag{7.36}$$

$$\text{excess base} = \sum X_{MO} - \sum_{n=1}^{4} n \times f_{Q^{4-n}}.X_{SiO_2} \tag{7.37}$$

$$X_{O^{-}} = (1 - X_{O^{2-}}).\frac{NBO/Si\,(meas)}{NBO/Si\,(meas) + \sum_{n=1}^{n=4} \frac{(4-n)}{2} \times f_{Q^{4-n}}.} \tag{7.38}$$

$$X_{O^{0}} = (1 - X_{O^{2-}}).\frac{\sum_{n=1}^{n=4} \frac{(4-n)}{2} \times f_{Q^{4-n}}}{NBO/Si\,(meas) + \sum_{n=1}^{n=4} \frac{(4-n)}{2} \times f_{Q^{4-n}}.} \tag{7.39}$$

The calculated oxygen fraction of free and bridging oxygen in the FeO_x-CaO-SiO_2-MgO-Cu_2O-(GeO_2/PdO) slags as a function of mole fraction SiO_2 and CaO at fixed p_{O_2} =10^{-8} atm and 1300° C are shown in Figure 7.23 and Figure 7.24, respectively.

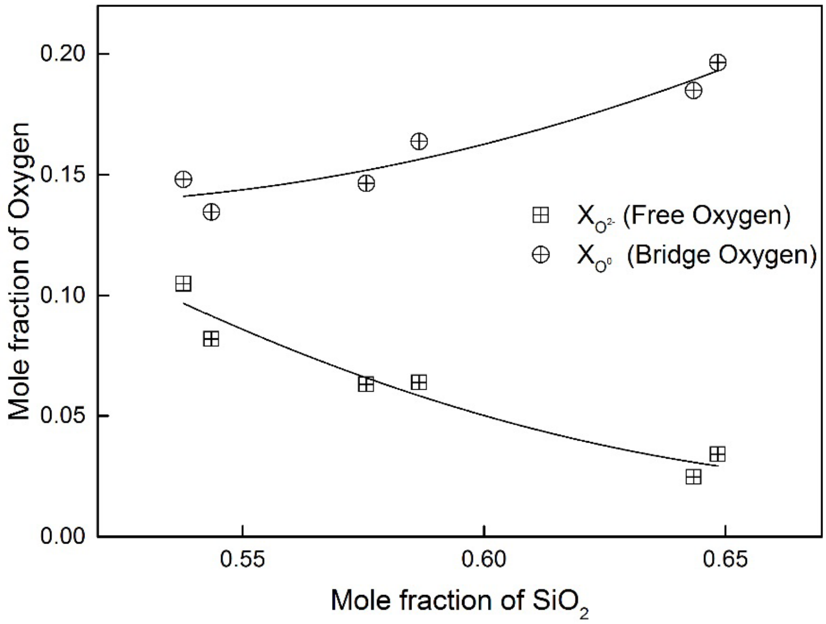

Figure 7.23: Mole fraction of oxygen as a function of mole fraction of SiO_2 in the FeO_x-CaO-SiO_2-MgO-Cu_2O-(GeO_2/PdO) slag (p_{O_2}= 10^{-8} atm and T =1300°C).

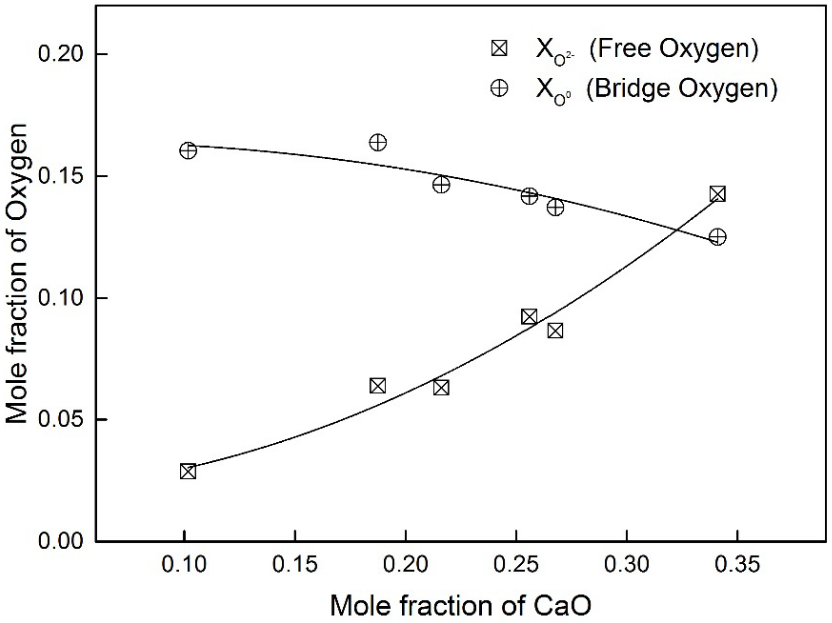

Figure 7.24: Mole fraction of oxygen as a function of mole fraction of CaO in the FeO_x-CaO-SiO_2-MgO-Cu_2O-(GeO_2/PdO) slag (p_{O_2}= 10^{-8} atm and T =1300°C).

In Figure 7.23, the relative concentration of free oxygen decreases while bridging oxygen increases with increasing silica contents and it will disappear when silica contents exceed a certain composition. It suggests that the formation of large silicate anions network structure by linking $[SiO_4]^{4-}$ tetrahedra units together (Zhang and Jahanshahi, 1998) when it reaches that critical composition.

On the other hand, it is seen from Figure 7.24 that the fraction of free oxygen increases, while bridging oxygen decreases with increasing CaO contents. It suggests that the breaking of large silicate anions network structure by introducing more Ca^{2+} cations will break the $[SiO_4]^{4-}$ tetrahedra units. Thus, the analysis of the structure of silicate melts is an important investigation not only the structure change but also determine the concentration of free oxygen ions.

7.8 Effect of Q^3/Q^2 on the viscosity

Viscosity is widely affected by the addition of alkali or alkaline earth metal oxides (e.g. Na_2O, CaO, MgO) to silica containing slags. Previous studies showed that thermophysical properties such as viscosity could also be correlated with the relative fractions of silicate structure units (Park, 2013b, Park, 2012, Mills, 1993). In this study, the viscosity of FeO_x-CaO-SiO_2-MgO slags of different Fe/SiO_2 and basicity at a fixed temperature and p_{O_2}= 10^{-8} atm was calculated using viscosity module of FactSage, and is plotted in Figure 7.25 as a function of the Q^3/Q^2. It was found that the viscosity of the FeO_x-CaO-SiO_2-MgO slag decreases with decreasing the degree of polymerization in slags.

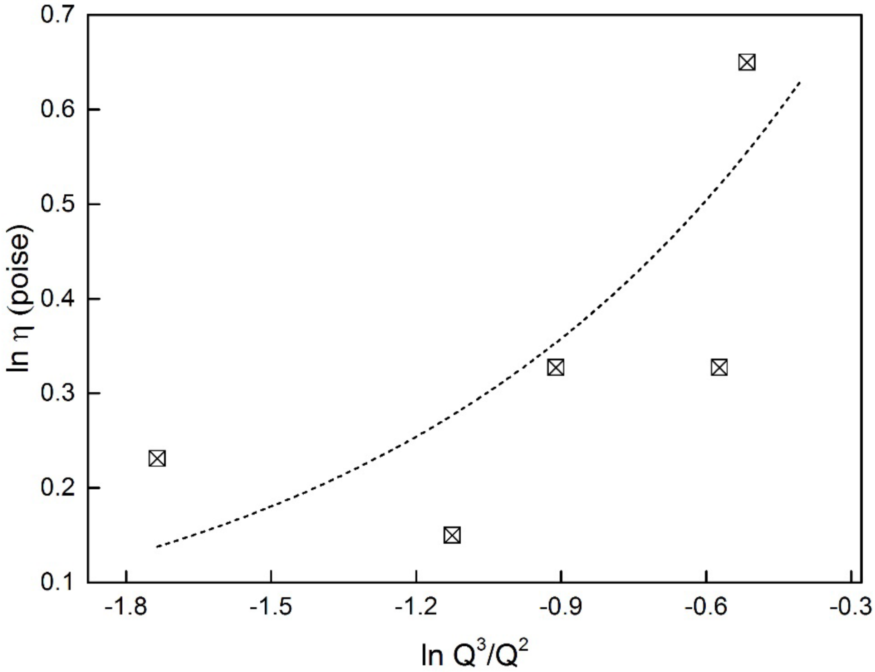

Figure 7.25: Relationship between the Q^3/Q^2 and viscosity of the FeO_x-CaO-SiO_2-MgO slag (p_{O_2}= 10^{-8} atm and T =1300°C).

The relationship between the viscosity of the FeO_x-CaO-SiO_2-MgO-Cu_2O-(GeO_2/PdO) slags and Q^3/Q^2 is shown in Figure 7.26. Similar to the FeO_x-CaO-SiO_2-MgO slag, the viscosity of the FeO_x-CaO-SiO_2-MgO-Cu_2O-(GeO_2/PdO) slags linearly decrease with increasing the depolymerization. Therefore, the viscosity of the both types of slag decrease as the degree of polymerization decreases at a fixed temperature and p_{O_2}, which is in good agreement with previous studies (Park, 2012, Park et al., 2002).

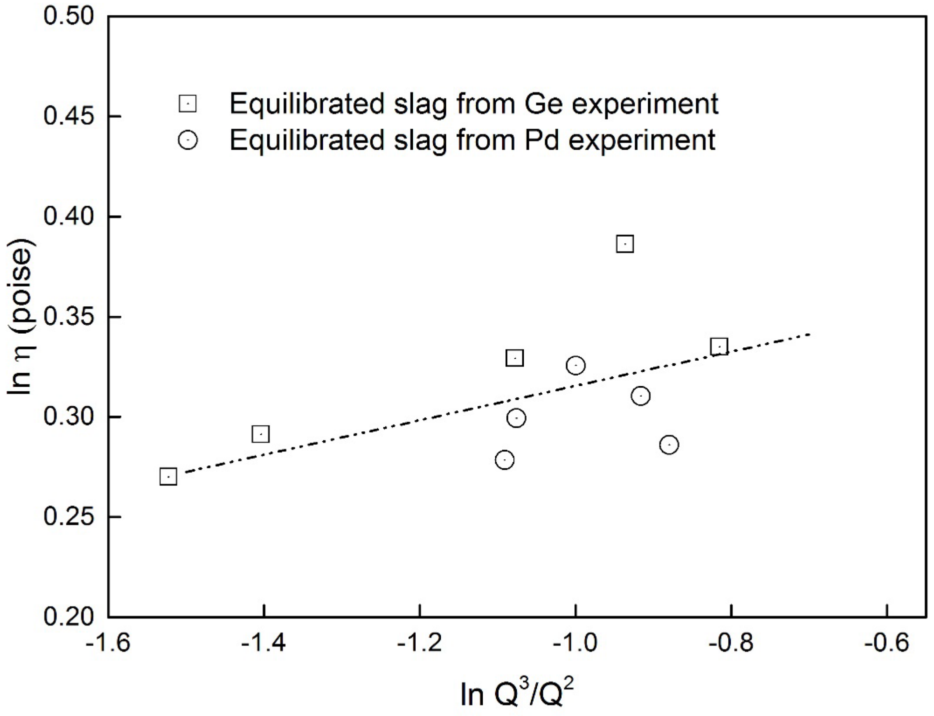

Figure 7.26: Relationship between the Q^3/Q^2 and viscosity of the FeO_x-CaO-SiO_2-MgO-Cu_2O-(GeO_2/PdO) slag (p_{O_2}= 10^{-8} atm and T =1300°C).

7.9 Summary

The FTIR spectra of the FeO_x-CaO-SiO_2-MgO and FeO_x-CaO-SiO_2-MgO-Cu_2O-(GeO_2/PdO) slags were measured to investigate the effect of temperature, oxygen partial pressure and slag composition on the silicate structure. The spectra of slags were interpreted on the basis of silicon tetrahedra units with various NBO/T. Furthermore, an empirical relationship was also developed between the degree of polymerization and distribution-ratio. The summary of the study is explained below:

1) The relative intensity of both high-frequency band ~ 1100 cm^{-1} (Q^3) and low-frequency band ~ 850 cm^{-1} (Q^0) of IR spectra of FeO_x-CaO-SiO_2-MgO master slag was affected by Fe/SiO_2 ratio and basicity. The degree of polymerization was found to decrease with increasing Fe/SiO_2 ratio and basicity.
2) The relative intensity of high-frequency band ~ 1100 cm^{-1} (Q^3) and low-frequency band ~ 850 cm^{-1} (Q^0) of IR spectra of FeO_x-CaO-SiO_2-MgO-Cu_2O-(GeO_2/PdO) slag was mainly affected by increasing oxygen potential, temperature and slag composition. The degree of polymerization was found to decreases with increasing temperature and decreasing p_{O_2}.

3) Semi-empirical equations have been developed using multiple regression analysis. A very good correlation was found between the degree of polymerization and temperature, p_{O_2} and slag compositions. This correlation can be used to predict the degree of polymerization of magnesia saturated ferrous calcium silicate slag, within the range of compositions investigated.
4) A correlation between the degree of polymerization and distribution-ratio, $\mathrm{L}_{\mathrm{X\ (Ge,Pd)}}^{\mathrm{s/m}}$ has been developed and this can be used to predict the partitioning ratio of Ge, and Pd in present slag system investigated.
5) The speciation of oxygen was calculated in the FeO_x-CaO-SiO_2-MgO-Cu_2O-(GeO_2/PdO) slag system. It can be said that slag structure analysis can be used to calculate three types of oxygen in the slag a fixed temperature and oxygen pressure.
6) The viscosity was calculated for the FeO_x-CaO-SiO_2-MgO-Cu_2O-(GeO_2/PdO) slag system and found to be decreased with increasing the NBO/Si (meas).

The summary of the present study suggests that Q^3/Q^2 are strongly related with thermochemical and thermophysical properties. The quantitative slag structure analysis can be used to determine the distribution-ratio in a wide range of composition. Moreover, Q^3/Q^2 is a good candidate for practical measurement of the degree of networking that relates slag structure to thermodynamics and properties.

Chapter 8 Conclusions and Recommendations

The study presented in this thesis was carried out to contribute to the knowledge of thermodynamics of valuable trace elements at conditions relevant to the black copper processing. In Chapters 5 and 6, the results on the study of thermodynamic behaviour of germanium (Ge), palladium (Pd) and tantalum (Ta) have been discussed. The effect of experimental parameters and reducing conditions on the distribution-ratios of Ge, Pd and Ta have also been investigated. The results suggested that high temperature and low oxygen partial pressure promote the partitioning of Ge and Pd into the copper phase. The suitable slag chemistry was found to be opposite for high recovery of Ge and Pd. It was also found that the recovery of Ge to the copper phase is less than 80 percent with an acidic slag at p_{O_2}= 10^{-8} atm and 1300°C (1573 K). On the other hand, more than 95 percent of Pd was recovered to the copper phase with a basic slag at the same oxygen potential and temperature. Moreover, the study found that the typical conditions of the black copper (high temperature and reducing atmosphere) were not favourable for the partitioning of Ta into copper phase. Further studies are therefore necessary to investigate the partitioning of tantalum (Ta) in different solute systems.

A conceptual multi-stage black copper smelting route using two different slag systems (acidic and basic) has also been suggested in Chapter 6 considering the nature of Ge and Pd. This concept can potentially be implemented to maximise the partitioning of both acidic and basic valuables elements to the copper phase.

The analyses of slags structure have been carried out and the results have been presented in Chapter 7. The effect of experimental conditions (relevant to black copper smelting) on the slag structure has been investigated. The finding suggests that the degree of polymerization is not affected by lowering the oxygen potential. Empirical correlations between the degree of polymerization and the experimental parameters were developed for the FeO_x-CaO-SiO_2-MgO-Cu_2O-(GeO_2/PdO) slags; these include the correction between Q^3/Q^2 and the distribution-ratio of Ge and Pd.

The present study has provided insights into Design for Resource Efficiency (DfRE) and Design for Recycling (DfR) which could contribute significantly to create Circular Economy (CU).

The detailed conclusions drawn from this study are as follows:

1. For the high temperature equilibrium experiments the equilibrium was approached from both oxidized and reduced conditions. No significant difference was found from both approach after 6 hours of equilibration time. Therefore, to minimize the volatilization of Ge, the sufficient time to achieve equilibrium was determined to be 6 hrs.
2. In the temperature range studied, the Ge distribution-ratio was found to decrease with increasing temperature at fixed oxygen potential. At higher temperature, significant amount of Ge was reported to the copper, however, copper loss to the slag was also increased.
3. The partitioning of Ge into the metal phase was found to increase from 13.5% to 93.5% with decreasing oxygen partial pressure at temperature 1300°C (1573 K) for a fixed slag composition.
4. The oxidation state of Ge was found predominately to be a tetravalent Ge^{4+}, (GeO_2) in the FeO_x-CaO-SiO_2-MgO slag.
5. The effect of the slag composition on $L_{Ge}^{s/m}$ was investigated. The results show that the Ge distribution-ratio is affected by the (CaO + MgO)/SiO_2 ratio or optical basicity at 1300°C (1573 K) and $p_{O_2} = 10^{-8}$ atm. The Fe/SiO_2 ratio was also found to affect the Ge distribution-ratio but beyond 1.16, the effect is negligible.
6. The $L_{Ge}^{s/m}$ data was used to calculate the activity coefficient of GeO_2 in FeO_x-CaO-SiO_2-MgO slag. The activity coefficient was found to be in the range of 0.24 to 1.50. The activity of GeO_2 was also found to decrease with increasing temperature and slag basicity.
7. Considering the findings from the experiments, a less-basic slag (or high SiO_2 content) and higher temperature with a reducing atmosphere are recommended to decrease the Ge deportment to the slag. Higher temperature also lowers slag viscosity which promotes slag separation. Therefore, high silica content FeO_x-CaO-SiO_2-MgO slags can be used for high Ge recovery in the copper.
8. The results of equilibrium time determination of Pd study suggest that the equilibrium time of 20 hours is required (from either direction).
9. The $L_{Pd}^{s/m}$ was found to be strongly dependant on the (CaO + MgO)/SiO_2 ratio and optical basicity at a fixed p_{O_2} and temperature 1300°C (1573 K). The ratio of Fe/SiO_2

was found to affect the $L_{Pd}^{s/m}$ until the ratio value of 1, beyond this, the effect is negligible.

10. In the oxygen partial pressure range studied, the $L_{Pd}^{s/m}$ in FeO_x-CaO-SiO_2-MgO slag and liquid copper was observed to linearly increase with increasing of p_{O_2} at a fixed temperature 1300°C (1573 K).
11. The stability of PdO was found to decrease with increasing temperature and mostly report to copper phase at a fixed oxygen potential.
12. The activity coefficient of PdO in FeO_x-CaO-SiO_2-MgO slag was calculated to be in the range of 3.89×10^{-3} to 2.63×10^{-2} and found to increase with increasing temperature and slag basicity.
13. The results suggest that Pd is present in the magnesia saturated FeO_x-CaO-SiO_2 slag mostly as divalent $Pd^{2+,}$ (PdO).
14. Considering the nature of PdO, a less-acidic slag (or low SiO_2 content), and a reducing atmosphere with higher temperature are suggested.
15. Tantalum was found mostly to report to FeO_x-CaO-SiO_2-MgO slag. Further study is required to find suitable solvent system and conditions that promote Ta recovery.
16. The relative intensity of both high-frequency band ~ 1100 cm^{-1} (Q^3) and low-frequency band ~ 850 cm^{-1} (Q^o) of IR spectra of FeO_x-CaO-SiO_2-MgO slag was found to be affected by Fe/SiO_2 ratio and basicity. The degree of polymerization was found to decrease with increasing Fe/SiO_2 ratio and basicity.
17. The relative intensity of high-frequency band (Q^3) and low-frequency band (Q^o) of IR spectra of FeO_x-CaO-SiO_2-MgO-Cu_2O-(GeO_2/PdO) slag was mainly affected by increasing oxygen potential, temperature and slag composition. The degree of polymerization was found to decrease with increasing temperature and decreasing p_{O_2}.
18. Semi-empirical equations were developed using multiple regression analysis between the degree of polymerization and temperature, p_{O_2} and slag compositions. These equations potentially can be used to predict the degree of polymerization of magnesia saturated ferrous calcium silicate slag within the range of compositions investigated.
19. Furthermore, the correlations between the degree of polymerization and distribution-ratio, $L_{X\,(Ge,Pd)}^{s/m}$ were developed and these can also potentially be used to predict the

partitioning ratio of Ge, and Pd in present slag system investigated.

20. The speciation of oxygen was calculated in the present slag system using silicate structure units and mass balance. The results suggest that mole fraction of oxygen species (i.e., O^{2-}, O^{o}) in FeO_x-CaO-SiO_2-MgO-Cu_2O-(GeO_2/PdO) were affected by mole fraction of SiO_2 and CaO a fixed temperature and oxygen partial pressure.
21. At 1300°C (1573 K) and $p_{O_2} = 10^{-8}$ atm, the viscosity of the FeO_x-CaO-SiO_2-MgO and FeO_x-CaO-SiO_2-MgO-Cu_2O-(GeO_2/PdO) slags were calculated using the FactSage to evalute the effect of Q^3/Q^2 on the thermophysical properties. The results show that the viscosity was found to decrease with decreasing Q^3/Q^2.

    Finally, the results from slags analysis suggest that Q^3/Q^2 is an important parameter to correlate the structure and thermochemical and thermodynamic properties.

The following recommendations are suggested for the future study:

- Expand the study to the other valuable elements found in e-waste, e.g., Ruthenium (Ru), Platinum (Pt), Gallium (Ga), etc.
- Develop a more rigorous model to correlate the structure with solution thermodynamic model
- To investigate the suitable solvent system (other than Cu) and conditions that promote Ta recovery using high temperature route
- To investigate the thermodynamic behaviour of Ge, Pd and Ta in other slag systems (i.e., FeO_x-SiO_2-Al_2O_3)

References

Australian Bureau of Statistics, 2013. Waste account, Australia, experimental estimates, Available from: http://www.abs.gov.au/ausstats/abs@.nsf/mf/4602.0.55.005 (accessed 13.06.16).

ABE, T., SUNDMAN, B. & ONODERA, H. 2006. Thermodynamic assessment of the Cu-Pt system. *Journal of Phase Equilibria and. Diffusion,* 27**,** 5-13.

ACUNA, C. & YAZAWA, A. 1987. Behaviours of arsenic, antimony and lead in phase-equilibria among copper, matte and calcium or barium ferrite slag. *Transactions of the Japan Institute of Metals,* 28**,** 498-506.

ALCOCK, C. B., SRIDHAR, R. & SVEDBERG, R. C. 1970. A thermodynamic study of the liquid alloy systems copper+gallium and copper+germanium. *The Journal of Chemical Thermodynamics,* 2**,** 255-263.

ALLEN, C. C. 1960. The Platinum Metals. Canada: Mineral Resources Division, Ottawa.

ALLIBERT, M. 1995. *Slag Atlas*, Edited by Verein Deutscher Eisenhuttenletute, Verlag Stahleisen GmbH.

ALVEAR, G. R., KANAI, T., FUKUYAMA, H., FUJISAWA, T. & YAMAUCHI, C. 1994. Thermodynamic considerations for elimination of Te and Se from molten copper by using Na_2CO_3 slag. *Materials Transactions, JIM,* 35**,** 508-515.

ANINDYA, A., SWINBOURNE, D. R., REUTER, M. A. & MATUSEWICZ, R. W. 2013. Distribution of elements between copper and FeO_x–CaO–SiO_2 slags during pyrometallurgical processing of WEEE: part 1- tin. *Mineral Processing and Extractive Metallurgy,* 122**,** 165-173.

ANINDYA, A., SWINBOURNE, D. R., REUTER, M. A. & MATUSEWICZ, R. W. 2014. Distribution of elements between copper and FeO_x–CaO–SiO_2 slags during pyroprocessing of WEEE: part 2 - indium. *Mineral Processing and Extractive Metallurgy,* 123**,** 43-52.

AVARMAA, K., O'BRIEN, H., JOHTO, H. & TASKINEN, P. 2015. Equilibrium distribution of precious metals between slag and copper matte at 1250–1350 C. *Journal of Sustainable Metallurgy,* 1**,** 216-228.

AWASTHI, A. K. & LI, J. 2017. Management of electrical and electronic waste: A comparative evaluation of China and India. *Renewable and Sustainable Energy Reviews,* 76**,** 434-447.

AZAKAMI, T. & YAZAWA, A. 1976. Activity measurements of liquid copper binary alloys. *Canadian Metallurgical Quarterly,* 15**,** 111-122.

BALE, C., BÉLISLE, E., CHARTRAND, P., DECTEROV, S., ERIKSSON, G., HACK, K., JUNG, I.-H., KANG, Y.-B., MELANÇON, J. & PELTON, A. 2009. FactSage thermochemical software and databases—recent developments. *Calphad,* 33**,** 295-311.

BALKANSKI, M., NUSIMOVICI, M. & REYDELLET, J. 1969. First order Raman spectrum of Cu_2O. *Solid State Communications,* 7**,** 815-818.

BERNSTEIN, L. R. 1985. Germanium geochemistry and mineralogy. *Geochimica et Cosmochimica Acta,* 49**,** 2409-2422.

BINNEMANS, K., JONES, P. T., BLANPAIN, B., VAN GERVEN, T. & PONTIKES, Y. 2015. Towards zero-waste valorisation of rare-earth-containing industrial process residues: a critical review. *Journal of Cleaner Production,* 99**,** 17-38.

BINNEMANS, K., JONES, P. T., BLANPAIN, B., VAN GERVEN, T., YANG, Y., WALTON, A. & BUCHERT, M. 2013. Recycling of rare earths: a critical review. *Journal of Cleaner Production,* 51**,** 1-22.

BISWAS, A. K. & DAVENPORT, W. G. 2013. *Extractive Metallurgy of Copper: International Series on Materials Science and Technology,* Elsevier.

CABRI, L. J. 1992. The distribution of trace precious metals in minerals and mineral products. *Mineralogical Magazine,* 56**,** 289-308.

CHASKAR, V., RICHARDS, G. G. & MCCAMMON, C. A. 1993. A mössbauer study of the behaviour of iron cations in iron oxide-containing melts at 1400°C. *Metallurgical Transactions B,* 24**,** 101-111.

CHEN, C. & JAHANSHAHI, S. 2010. Thermodynamics of arsenic in FeO_x-CaO-SiO_2 slags. *Metallurgical and Material Transactions B,* 41**,** 1166-1174.

CHEN, C., ZHANG, L. & JAHANSHAHI, S. Review and thermodynamic modelling of CoO in iron silicate-based slags and calcium ferrite-based slags. Proceedings of the 7th International Conference on Molten Slags, Fluxes and Salts, 2004. 509-515.

CHI, X., WANG, M. Y. & REUTER, M. A. 2014. E-waste collection channels and household recycling behaviours in Taizhou of China. *Journal of Cleaner Production,* 80**,** 87-95.

CHIPMAN, J. & CHANG, L.C. 1949. The ionic nature of metallurgical slags. simple oxide systems. *Transactions of the Metallurgical Society of AIME,* 185**,** 191-197.

CHOI, N. & CHO, W. D. 1997. Distribution behaviour of cobalt, selenium, and tellurium between nickel-copper-iron matte and silica-saturated iron silicate slag. *Metallurgical and Material Transactions B,* 28**,** 429-438.

CUI, J. & ZHANG, L. 2008. Metallurgical recovery of metals from electronic waste: A review. *Journal of Hazardous Materials,* 158**,** 228-256.

DAVENPORT, W. G., KING, M. J., SCHLESINGER, M. E. & BISWAS, A. K. 2002. *Extractive metallurgy of copper*, Elsevier.

DAVYDOV, V. 1957. Izuchenie ravnovesnykh uprugostei para dvuokisi germaniya. *Russian Journal of Inorganic Chemistry* (*Zhurnal Neorganicheskoi Khimii),* 2**,** 1460-1466.

DEGTEROV, S. A. & PELTON, A. D. 1999. Thermodynamic modeling of lead distribution among matte, slag, and liquid copper. *Metallurgical and Material Transactions B,* 30**,** 1033-1044.

DERIN, B. & YÜCEL, O. 2002. The distribution of cobalt between Co-Cu alloys and Al_2O_3-FeO-Fe_2O_3-SiO_2 slags. *Scandinavian Journal of Metallurgy,* 31**,** 12-19.

DORAN, M. 2014. Researchers worried precious metals lost in e-waste recycling. *ABC,* Available from http://www.abc.net.au/news/2013-06-13/researchers-worried-precious-metals-lost-in-e-waste-recycling/4750774 (accessed 10.05.16).

DUFFY, J. & INGRAM, M. 1975. Physics and Chem. *Glasses,* 16**,** 119.

DUFFY, J. A. & INGRAM, M. D. 1976. An interpretation of glass chemistry in terms of the optical basicity concept. *Journal of Non-Crystalline Solids,* 21**,** 373-410.

DUFFY, J. A., INGRAM, M. D. & SOMMERVILLE, I. D. 1978. Acid–base properties of molten oxides and metallurgical slags. *Journal of the Chemical Society, Faraday Transactions 1: Physical Chemistry in Condensed Phases,* 74**,** 1410-1419.

EEROLA, H., JYLHA, K. & TASKINEN, P. 1984. Thermodynamics of impurities in calcium ferrite slags in copper fire-refining conditions. *Transactions of the Institute of Mining and Metallurgy,* C193-C199.

EMSLEY, J. 2001. *Nature's Building Blocks: An A-Z Guide to the Elements* [Online]. Availiable:http://books.gggolge.com.au/books?id=jXu07p3cKwC&printsec=frontcover &hl=en#onepage&q&f=false.

EOM, C.H., LEE, S.H., PARK, J.G., PARK, J.H. & MIN, D.J. 2016. Thermodynamic behaviour of manganese oxide in lime-based manganese smelting slags. *ISIJ International,* 56**,** 37-43.

EU 2002/96/EC, Directive 2002/96/EC of the European Parliament and of the Council of 27 January 2003 on waste electrical and electronic equipment (WEEE). *Official Journal of the European Union*, *L37*, 24–38.

EU 2012/19/EU, Directive 2012/19/EU of the European Parliament and of the Council of 4 July 2012 on waste electrical and electronic equipment (WEEE). *Official Journal of the European Union*, *L197*, 38–71.

European Union. Communication from the Commission to the European Parliament, the Council, the European Economic and Social Committee of the Regions. 2015. Closing the loop—An EU Action Plan for the Circular Economy. http://eur-lex.europa.eu/ legal-content/EN/TXT/PDF/?uri=CELEX:52014DC0398&from =EN, 2015. Accessed 10 December 2016

FACTSAGE. 2015. *FactSage^{TM} 6.4*. Available: www. Factsage.com.

FANG, L. & LYNCH, D. 1987. Evaluation of the behaviour of selenium in silicate slag. *Metallurgical Transactions. B,* 18**,** 181-187.

FOUNTAIN, C. R., COULTER, M. D. & EDWARDS, J. S. 1991. Minor element distribution in the copper Isasmelt process. *Pyrometallurgy of Copper (Cobre 91).* Toronto, Canada.

FURUKAWA, T., FOX, K. E. & WHITE, W. B. 1981. Raman spectroscopic investigation of the structure of silicate glasses. III. Raman intensities and structural units in sodium silicate glasses. *The Journal of Chemical Physics,* 75**,** 3226-3237.

GAO, Y.-M., WANG, S.-B., HONG, C., MA, X.-J. & YANG, F. 2014. Effects of basicity and MgO content on the viscosity of the SiO_2-CaO-MgO-9wt%Al_2O_3 slag system.

International Journal of Minerals, Metallurgy, and Materials, 21**,** 353-362.

GEORGE, D. B. Continuous copper converting-A perspective and view of the future. Sulfide Smelting 2002, Proceedings of a Symposium held during the TMS Annual Meeting, 2002. TMS Warrendale, PA, 17-21.

GILCHRIST, J. D. 1989. *Extraction metallurgy,* Oxford, UK.

GOONAN, T. G. 2010. Copper recycling in the United States, Retrieved from http://pubs.er.usgs.gov/publication/cir1196X (accessed 10.06.16).

GORTAIS, J., HODAJ, F., ALLIBERT, M. & WELTER, J. M. 1994. Equilibrium distribution of Fe, Ni, Sb, and Sn between liquid Cu and a CaO-rich slag. *Metallurgical and Material Transactions B,* 25**,** 645-651.

GÖTZE, R. & ROTTER, V. S. Challenges for the recovery of critical metals from waste electronic equipment-A case study of indium in LCD panels. Electronics Goes Green 2012. IEEE, 1-8.

GRAEDEL, T., BERTRAM, M., FUSE, K., GORDON, R., LIFSET, R., RECHBERGER, H. & SPATARI, S. 2002. The contemporary European copper cycle: the characterization of technological copper cycles. *Ecological Economics,* 42**,** 9-26.

GRIMSEY, E. & TOGURI, J. 1988. Cobalt in silica saturated fayalite slags. *Canadian Metallurgical Quarterly,* 27**,** 331-333.

GRIMSEY, E. J. & LIU, X. The effect of silica, alumina calcia and magnesia on the activity coefficient of cobalt oxide in iron silicate slags. Molten Slags, Fluxes & Salts Conference, 1997. Iron & Steel Institute, 709-718.

GUBERMAN, D. E. 2015. 2013 Minerals Yearbook: Germanium [Advance Release]. *In:* SURVEY, U. S. G. (ed.).

HAGELUKEN, C. 2006. Recycling of electronic scrap at umicore's integrated metals smelter and refinery. *World of Metallurgy-ERZMETALL,* 59**,** 152–161.

HAGELÜKEN, C. 2006. Improving metal returns and eco-efficiency in electronics recycling. *Int. Symposium on Electronics and the Environment (IEEE).*

HAGER, J. P., HOWARD, S. M. & JONES, J. H. 1973. Thermodynamic properties of the liquid Ge-Cu and Ge-Au systems by mass spectrometry. *Metallurgical Transactions,* 4**,** 2383-2388.

HALTER, W. E. & MYSEN, B. O. 2004. Melt speciation in the system $Na_2O–SiO_2$. *Chemical Geology,* 213**,** 115-123.

HAN, Y. S. & PARK, J. H. 2015. Thermodynamics of indium dissolution behaviour in FeO-bearing metallurgical slags. *Metallurgical and Material Transactions B,* 46**,** 235-242.

HAN, Y. S., SWINBOURNE, D. R. & PARK, J. H. 2015. Thermodynamics of gold dissolution behaviour in CaO-SiO_2-Al_2O_3-MgO_{sat} slag system. *Metallurgical and Material Transactions B,* 46**,** 2449-2457.

HANDBOOK OF MINERALS RAMAN SPECTRA 2015. (website: http://www.ens-lyon.fr/LST/Rama)

HENAO, H., HAYES, P. & JAK, E. Research on indium and germanium distributions between lead bullion and slag at selected process conditions. Lead-Zinc 2010, 2010 Vancouver, Canada. TMS, 1145-1160.

HENAO, H. M., YAMAGUCHI, K. & UEDA, S. Distribution precious metals between copper metal and iron silicate slag at 1573K. TMS Fall Extraction & Processing: Sohn International Symposium, 2006 San Diego, California, USA. 723-729.

HEO, J. H., PARK, S.-S. & PARK, J. H. 2012. Effect of slag composition on the distribution behaviour of Pb between Fe_tO-SiO_2 (-CaO, Al_2O_3) slag and molten copper. *Metallurgical and Material Transactions B,* 43**,** 1098-1105.

HESSE, R. W. 2007. *Jewelrymaking through history: An encyclopaedia*, Greenwood Publishing Group.

HEUKELEM, A., REUTER, M. & HUISMAN, J. 2004. Eco-efficient optimization of pre-processing and metal smelting in Electronics goes green 2004: driving forces for future. *Electronics***,** 657-661.

HIDAYAT, T., HAYES, P. C. & JAK, E. 2012. Experimental Study of Ferrous Calcium Silicate Slags: Phase Equilibria at pO_2 Between 10^{-8} atm and 10^{-9} atm. *Metallurgical and Material Transactions B,* 43**,** 27-38.

HOANG, G. & SWINBOURNE, D. 2007. Indium distribution between $FeO–CaO–SiO_2$ slags and lead bullion at 1200° C. *Mineral Processing and Extractive. Metallurgy,* 116**,** 133-138.

HÖLL, R., KLING, M. & SCHROLL, E. 2007. Metallogenesis of germanium- A review. *Ore Geology Reviews,* 30**,** 145-180.

HULTGREN, R., DESAI, P. D., HAWKINS, D. T., GLEISER, M. & KELLEY, K. K. 1973. Selected values of the thermodynamic properties of binary alloys. DTIC Document.

JIMBO, I., GOTO, S. & OGAWA, O. 1984. Equilibria between silica-saturated iron silicate slags and molten Cu-As, Cu-Sb, and Cu-Bi Alloys. *Metallurgical Transactions B,* 15**,** 535-541.

JOHNSON, E. 1983. Laboratory investigations on the behaviour of accessory elements in lead blast furnace smelting. *United State Department of Interior***,** 21.

JOHNSTON, M., JAHANSHAHI, S., ZHANG, L. & LINCOLN, F. 2010. Effect of slag basicity on phase equilibria and selenium and tellurium distribution in magnesia-saturated calcium iron silicate slags. *Metallurgical and Material Transactions B,* 41**,** 625-635.

JOHNSTON, M. D., JAHANSHAHI, S. & LINCOLN, F. J. 2007. Thermodynamics of selenium and tellurium in calcium ferrite slags. *Metallurgical and Material Transactions B,* 38**,** 433-442.

KASHIMA, M., EGUCHI, M. & YAZAWA, A. 1978. Distribution of impurities between crude copper, white metal and silica-saturated slag. *Transactions of the Japan Institute of Metals,* 19**,** 152-158.

KAUR, R., SWINBOURNE, D. & NEXHIP, C. 2009. Nickel, lead and antimony distributions between ferrous calcium silicate slag and copper at 1300°C. *Mineral Processing and Extractive Metallurgy,* 118**,** 65-72.

KAUR, R., SWINBOURNE, D., WADSLEY, M. & NEXHIP, C. 2011. Comparison of ferrous calcium silicate slag and calcium ferrite slag interactions with magnesia-chrome refractories. *Metallurgical and Material Transactions B,* 42**,** 451-459.

KHALIQ, A., RHAMDHANI, M. A., BROOKS, G. & MASOOD, S. 2014. Metal extraction processes for electronic waste and existing industrial routes: a review and Australian perspective. *Resources,* 3**,** 152-179.

KHO, T., SWINBOURNE, D. & LEHNER, T. 2006. Cobalt distribution during copper matte smelting. *Metallurgical and Material Transactions B,* 37**,** 209-214.

KIM, D. W., JANG, S. T. & CHOI, S. R. 2011. A Study on the recovery of Sn and Ni from the steel ball scraps for barrel plating. *Journal of the Korean Institute of Resources Recycling.,* 20**,** 46-51.

KIM, H. & SOHN, I. 2011. Effect of CaF_2 and Li_2O additives on the viscosity of CaO–SiO_2–Na_2O slags. *ISIJ International.,* 51**,** 1-8.

KIM, H. G. & SOHN, H. Y. 1998. Effects of CaO, Al_2O_3, and MgO additions on the copper solubility, ferric/ferrous ratio, and minor-element behaviour of iron-silicate slags. *Metallurgical and Material Transactions B,* 29**,** 583-590.

KIRK, R. E. & OTHMER, D. F. 1973. Encyclopaedia of Chemical Technology. *Encyclopaedia of Chemical Technology.* 3rd ed.: Wiley Publications.

KO, K. Y. & PARK, J. H. 2011. Dissolution behaviour of indium in CaO-SiO_2-Al_2O_3 slag. *Metallurgical and Material Transactions B,* 42**,** 1224-1230.

KO, K. Y. & PARK, J. H. 2012. Dissolution mechanism of indium in CaO-Al_2O_3-SiO_2 slag at low silica region. *Metallurgical and Material Transactions B,* 43**,** 440-442.

KOIKE, K. & YAZAWA, A. 1994. Thermodynamic studies of the molten Cu_2S-FeS-SnS systems. *Journal of the Mining and Materials Processing Institute of the Japan.,* 110**,** 43-47.

KONG, L., BAI, J., BAI, Z., GUO, Z. & LI, W. 2013. Effects of $CaCO_3$ on slag flow properties at high temperatures. *Fuel,* 109**,** 76-85.

KUBIŠTA, J. & VŘEŠT’ÁL, J. 2000. Thermodynamics of the liquid Co-Cu system and calculation of phase diagram. *Journal of Phase Equilibria,* 21**,** 125-129.

LEE, Y. S., MIN, D. J., JUNG, S. M. & YI, S. H. 2004. Influence of basicity and FeO content on viscosity of blast furnace type slags containing FeO. *ISIJ International,* 44**,** 1283-1290.

LEHNER, T. Integrated recycling of non-ferrous metals at Boliden Ltd. Ronnskar smelter. Electronics and the Environment, Proceedings of IEEE International Symposium, 1998. 42-47.

LEHNER, T. 2003. E&HS aspects on metal recovery from electronic scrap. *Electronics and the Environment, IEEE International Symposium*

LI, M., DU, Z., GUO, C. & LI, C. 2008. A thermodynamic modeling of the Cu–Pd system. *Calphad,* 32**,** 439-446.

LI, M., DU, Z., GUO, C. & LI, C. 2009. Thermodynamic optimization of the Cu–Sn and Cu–Nb–Sn systems. *Journal of Alloys and Compounds,* 477**,** 104-117.

LIDE, D. 2003. *Handbook of chemistry and physics, vol. 84*, CRC Press.

LOFERSKI, P. J. 2015. USGS Mineral Commodity Summaries—Platinum Group Metals. *In:* SURVEY, U. S. G. (ed.).

LOUEY, R., SWINBOURNE, D. R. & LEHNER, T. Silver and tin distribution between copper matte and fayalite slag. AusIMM Proceedings, 1999. The Australian Institute of Mining and Metallurgy, 31-36.

LU, X., NAKAJIMA, K., SAKANAKURA, H., MATSUBAE, K., BAI, H. & NAGASAKA, T. 2012. Thermodynamic estimation of minor element distribution between immiscible liquids in Fe–Cu-based metal phase generated in melting treatment of municipal solid wastes. *Waste Management,* 32**,** 1148-1155.

MACKEY, P. 1982. The physical chemistry of copper smelting slags—a review. *Canadian Metallurgical Quarterly,* 21**,** 221-260.

MATSUZAKI, K., ISHIKAWA, T., TSUKADA, T. & ITO, K. 2000. Distribution equilibria of Pb and Cu between $CaO-SiO_2-Al_2O_3$ melts and liquid copper. *Metallurgical and Material Transactions B,* 31**,** 1261-1266.

MCCAMMON, C., CHASKAR, V. & RICHARDS, G. 1991. A technique for spatially resolved Mossbauer spectroscopy applied to quenched metallurgical slags. *Measurement Science and Technology.,* 2**,** 657.

MCMILLAN, P. 1984. A Raman spectroscopic study of glasses in the system $CaO-MgO-SiO_2$. *American Mineralogist,* 69**,** 645-659.

MCMILLAN, P. F., WOLF, G. H. & POE, B. T. 1992. Vibrational spectroscopy of silicate liquids and glasses. *Chemical Geology,* 96**,** 351-366.

MENIKPURA, S., SANTO, A. & HOTTA, Y. 2014. Assessing the climate co-benefits from Waste Electrical and Electronic Equipment (WEEE) recycling in Japan. *Journal of Cleaner Production,* 74**,** 183-190.

MICOULAUT, M., CORMIER, L. & HENDERSON, G. 2006. The structure of amorphous, crystalline and liquid GeO_2. *Journal of Physics: Condensed Matter,* 18**,** R753.

MILLS, K. C. 1993. The Influence of structure on the physico-chemical properties of slags. *ISIJ International,* 33**,** 148-155.

MOHASSAB, Y. & SOHN, H. Y. 2015. Analysis of slag chemistry by FTIR-RAS and Raman Spectroscopy: effect of water vapor content in H_2-H_2O- CO-CO_2 mixtures relevant to a novel green ironmaking technology. S*teel Research Internation,* 86**,** 740-752.

MOSKALYK, R. 2004. Review of germanium processing worldwide. *Minerals Engineering,* 17**,** 393-402.

MOSKALYK, R. R. & ALFANTAZI, A. M. 2003. Review of copper pyrometallurgical practice: today and tomorrow. *Minerals Engineering,* 16**,** 893-919.

MWEMA, M. D., SEGERS, L. & WINAND, R. Behaviour of cobalt in copper smelting processes. Copper 95–Cobre 95 International Conference, 1995. The Metallurgical Society of CIM, 451-462.

MYSEN, B. O. 1990a. Effect of pressure, temperature, and bulk composition on the structure and species distribution in depolymerized alkali aluminosilicate melts and quenched melts. *Journal of Geophysical Research: Solid Earth,* 95**,** 15733-15744.

MYSEN, B. O. 1990b. Relationships between silicate melt structure and petrologic processes. *Earth-Science Review,* 27**,** 281-365.

MYSEN, B. O. 1990c. Role of Al in depolymerized, peralkaline aluminosilicate melts in the systems Li_2O-Al_2O3-SiO_2, Na_2O-Al_2O_3-SiO_2, and K_2O-Al_2O_3-SiO_2. *American. Mineralogist,* 75**,** 120-134.

MYSEN, B. O. & DUBINSKY, E. V. 2004. Melt structural control on olivine/melt element partitioning of Ca and Mn. *Geochimica et Cosmochimica Acta,* 68**,** 1617-1633.

MYSEN, B. O., FINGER, L. W., VIRGO, D. & SEIFERT, F. A. 1982. Curve-fitting of Raman spectra of silicate glasses. *American Mineralogist,* 67**,** 686-695.

MYSEN, B. O. & FRANTZ, J. D. 1992. Raman spectroscopy of silicate melts at magmatic temperatures: Na_2O-SiO_2, K_2O-SiO_2 and Li_2O-SiO_2 binary compositions in the temperature range 25–1475° C. *Chemical Geology,* 96**,** 321-332.

MYSEN, B. O. & RICHET, P. 2005. *Silicate glasses and melts: properties and structure*, Elsevier.

MYSEN, B. O., VIRGO, D. & SCARFE, C. M. 1980. Relations between the anionic structure and viscosity of silicate melts—a Raman spectroscopic study. *American Mineralogist* 65**,** 690-710.

NAGAMORI, M., MACKEY, P. & TARASSOFF, P. 1975a. Copper solubility in FeO-Fe_2O_3-SiO_2-Al_2O_3 slag and distribution equilibria of Pb, Bi, Sb and As between slag and metallic copper. *Metallurgical Transactions B,* 6**,** 295-301.

NAGAMORI, M., MACKEY, P. & TARASSOFF, P. 1975b. The distribution of As, Sb, Bi, Se, and Te between molten copper and white metal. *Metallurgical and Material Transactions B,* 6**,** 197-198.

NAGAMORI, M. & MACKEY, P. J. 1977. Distribution equilibria of Sn, Se and Te between FeO-Fe_2O_3-SiO_2-Al_2O_3-$CuO_{0.5}$ slag and metallic copper. *Metallurgical Transactions B,* 8**,** 39-46.

NAGAMORI, M. & MACKEY, P. J. 1978. Thermodynamics of copper matte converting: part II. distribution of Au, Ag, Pb, Zn, Ni, Se, Te, Bi, Sb and As between copper, matte and slag in the noranda process. *Metallurgical Transactions B,* 9**,** 567-579.

NAKAJIMA, K., TAKEDA, O., MIKI, T., MATSUBAE, K. & NAGASAKA, T. 2011. Thermodynamic analysis for the controllability of elements in the recycling process of metals. *Environmental Science and Technology,* 45**,** 4929-4936.

NAKAMURA, S., IWASAWA, K., MORITA, K. & SANO, N. 1998. The influence of basicity on the solubility of platinum in oxide melts. *Metallurgical and Material Transactions B,* 29**,** 411-414.

NAKAMURA, S. & SANO, N. 1997. Solubility of platinum in molten fluxes as a measure of basicity. *Metallurgical and Material Transactions B,* 28**,** 103-108.

NAKAZAWA, S. & TAKEDA, Y. 1983. Distribution behaviour of various elements in copper smelting systems. *Advances in Sulfide Smelting.* Warrendale, PA, USA: TMS-AIME.

NELEN, D., MANSHOVEN, S., PEETERS, J. R., VANEGAS, P., D'HAESE, N. & VRANCKEN, K. 2014. A multidimensional indicator set to assess the benefits of WEEE material recycling. *Journal of Cleaner Production,* 83**,** 305-316.

NISHIJIMA, W. & YAMAGUCHI, K. 2014. Effects of slag composition and oxygen potential on distribution ratios of platinum group metals between Al_2O_3-CaO-SiO_2-Cu_2O slag system and molten copper at 1723 K. *Journal of the Japan Institute of Metals,* 78**,** 267-273.

NIU, B., CHEN, Z. & XU, Z. 2016. A method for recycling tantalum from waste tantalum capacitors by chloride metallurgy. *ACS Sustainable Chemistry and Engineering,* 5, 1376-1381

OGUCHI, M., MURAKAMI, S., SAKANAKURA, H., KIDA, A. & KAMEYA, T. 2011. A preliminary categorization of end-of-life electrical and electronic equipment as secondary metal resources. *Waste Management,* 31**,** 2150-2160.

OMOTO, A., MORIYA, K. & KARASAWA, H. 2000. Hydrogen management and overpressure protection of the containment for future boiling water reactors. *Nuclear Engineering and Design,* 197**,** 281-299.

PARK, J. H. 2012. Structure–property correlations of CaO-SiO_2-MnO slag derived from Raman spectroscopy. *ISIJ International,* 52**,** 1627-1636.

PARK, J. H. 2013a. Effect of silicate structure on thermodynamic properties of calcium silicate melts: Quantitative analysis of Raman spectra. *Metals and Materials International,* 19**,** 577.

PARK, J. H. 2013b. Structure–property relationship of CaO-MgO-SiO_2 slag: quantitative analysis of Raman spectra. *Metallurgical and Material Transactions B,* 44**,** 938-947.

PARK, J. H. & MIN, D. J. 1999. Quantitative analysis of the relative basicity of CaO and BaO by silver solubility in slags. *Metallurgical and Material Transactions B,* 30**,** 689-694.

PARK, J. H. & MIN, D. J. 2000. Solubility of silver in MO (M_2O)–B_2O_3 (M= Ca, Ba and Na) slags. *Material Transactions, JIM,* 41**,** 425-428.

PARK, J. H., MIN, D. J. & SONG, H. S. 2002. FT-IR spectroscopic study on structure of CaO-SiO_2 and CaO-SiO_2-CaF_2 slags. *ISIJ International,* 42**,** 344-351.

PARK, J. Y., PARK, S. J., CHANG, W. S. & SOHN, I. 2012. Effect of FeO_t content and CaO/SiO_2 ratio on hydrogen dissolution in CaF_2–CaO–SiO_2-based welding fluxes.

Journal of the American Ceramic Society, 95**,** 1756-1763.

PAULINA, L., SWINBOURNE, D. & KHO, T. 2013. Distribution of bismuth between copper and FeO_x–CaO–SiO_2 slags under copper converting conditions. *Mineral Processing and Extractive Metallurgy,* 122**,** 79-86.

PAULING, L. 1960. *The nature of the chemical bond and the structure of molecules and crystals: an introduction to modern structural chemistry*, Cornell University Press.

PICKLES, C. A., HARRIS, C. & PEACEY, J. 2011. Silver loss during the oxidative refining of silver–copper alloys. *Minerals Engineering,* 24**,** 514-523.

PUCKETT, J., BYSTER, L., WESTERVELT, S., GUTIERREZ, R., DAVIS, S., HUSSAIN, A. & DUTTA, M. 2002. Exporting harm: the high-tech trashing of Asia. basel action network and silicon valley toxics coalition. *Retrieved from: http://ban.org/E-waste/technotrashfinalcomp.pdf.*

RASTOGI, R. & MISRA, R. 2009. *Introduction to Chemical Thermodynamics*, Vikas Publishing House Pvt Ltd.

REDDY, R. G. & HEALY, G. W. 1981. The Solubility of cobalt in Cu_2O-CoO-SiO_2 Slags in equilibrium with liquid Cu-Co alloys. *Canadian Metallurgical Quarterly,* 20**,** 135-143.

ŘEHÁČKOVÁ, L., ROSYPALOVÁ, S., DUDEK, R., KUKUTSCHOVÁ, J. & DOBROVSKÁ, J. 2015. Effect of CaO/SiO_2 ratio on viscosity and structure of slag. *Metalurgija,* 54**,** 455-458.

REUTER, M. & KOJO, I. V. 2014. Copper: a key enable of resource efficiency. *World of Metallurgy-Erzmetall,* 67**,** 5-12.

REUTER, M. A., HUDSON, C., HAGELÜKEN, C., HEISKANEN, K., MESKERS, C. & VAN SCHAIK, A. 2013. Metal recycling: opportunities, limits, infrastructure. *UNEP.*

RIDE, D. R. 2003. *Handbook of Chemistry and Physics,* Boca Raton, FL, CRC Press.

RIVEROS, G., PARK, Y.-J., TAKEDA, Y. & YAZAWA, A. 1987. Distribution equilibria of arsenic and antimony between Na_2CO_3–Na_2O–SiO_2 melts and liquid copper. *Transactions of the Japan Institute of Metals,* 28**,** 749-756.

ROBINSON, B. H. 2009. E-waste: An assessment of global production and environmental impacts. *Science of the Total Environment,* 408**,** 183-191.

RODRIGUEZ, C. P., MCCLOY, J. S., SCHWEIGER, M. J., CRUM, J. V. & WINSCHELL, A. E. 2011. *Optical basicity and nepheline crystallization in high alumina glasses*, Pacific Northwest National Laboratory.

ROGHANI, G., FONT, J. C., HINO, M. & ITAGAKI, K. 1996. Distribution of minor elements between calcium ferrite slag and copper matte at 1523 K under high partial pressure of SO_2. *Materials Transactions, JIM,* 37**,** 1574-1579.

ROGHANI, G., HINO, M. & ITAGAKI, K. 1997a. Phase equilibrium and minor element distribution between SiO_2-CaO-FeO_x-MgO and copper matte under high partial pressures of SO_2. *Proceedings of 5th International Conference on Molten Slags, Fluxes and Salts.* Warrendale, USA: Iron Steel Soc.

ROGHANI, G., HINO, M. & ITAGAKI, K. 1997b. Phase equilibrium and minor elements distribution between SiO_2–CaO–FeO_x–MgO slag and copper matte at 1573 K under high partial pressures of SO_2. *Materials Transactions, JIM,* 38**,** 707-713.

ROUESSAC, F. & ROUESSAC, A. 2013. *Chemical analysis: modern instrumentation methods and techniques*, John Wiley & Sons.

RUHELA, R., SINGH, A., TOMAR, B. & HUBLI, R. 2014. Separation of palladium from high level liquid waste–A review. *RSC Advances,* 4**,** 24344-24350.

SANO, N., KATAYAMA, H., SASABE, M. & MATSUOKA, S. 1998. Research activities on removal of residual elements from steel scrap in Japan. *Scandinavian Journal of Metallurgy,* 27**,** 24-30.

SAURAT, M. & BRINGEZU, S. 2008. Platinum group metal flows of Europe, part 1. *Journal of Industrial Ecology,* 12**,** 754-767.

SCHLESINGER, M. E., KING, M. J., SOLE, K. C. & DAVENPORT, W. G. 2011. Chapter 3 - Production of High Copper Concentrates – Introduction and Comminution. *Extractive Metallurgy of Copper (Fifth Edition).* Oxford: Elsevier.

SCHLITT, W. & RICHARDS, K. 1975. The distribution of silver, gold, platinum and palladium in metal-matte systems. *Metallurgical Transactions B,* 6**,** 237-243.

SCHNEIDER, J., MASTELARO, V. R., ZANOTTO, E. D., SHAKHMATKIN, B. A., VEDISHCHEVA, N. M., WRIGHT, A. C. & PANEPUCCI, H. 2003. Qn distribution in stoichiometric silicate glasses: thermodynamic calculations and 29Si high resolution

NMR measurements. *Journal of Non-Crystalline Solids,* 325**,** 164-178.

SHUVA, M. A. H., RHAMDHANI, M. A., BROOKS, G. A., MASOOD, S. & REUTER, M. A. 2016. Thermodynamics behavior of germanium during equilibrium reactions between FeOx-CaO-SiO2-MgO slag and molten copper. *Metallurgical and Material Transactions B,* 47**,** 2889-2903.

SIGWORTH, G. K. & ELLIOTT, J. F. 1974. The thermodynamics of dilute liquid copper alloys. *Canadian Metallurgical Quarterly,* 13**,** 455-461.

SODECK, G., ENTNER, P. & NECKEL, A. 1970. Mass spectrometric determination of thermodynamic activities: the liquid system copper-germanium. *High Temperature Science,* 2**,** 311-321.

SOHN, I. & MIN, D. J. 2012. A review of the relationship between viscosity and the structure of calcium-silicate-based slags in ironmaking. S*teel Research International,* 83**,** 611-630.

SPITCZOK VON BRISINSKI, L., GOLDMANN, D. & ENDRES, F. 2014. Recovery of metals from tantalum capacitors with ionic liquids. *Chemie Ingenieur Technik,* 86**,** 196-199.

SREEDHARAN, O., ATHIAPPAN, E., PANKAJAVALLI, R. & GNANAMOORTHY, J. 1979. The free energy of formation of GeO_2 (hex) by emf measurements. *Journal of the Less Common Metals,* 68**,** 143-152.

StEP Initiative. 2014. One global definition of e-waste. Available: http:step-initianltinr.ogr/files/sept/documents

STREET, S. J., COLEY, K. S. & IRONS, G. A. 2001. Tin solubility in CaO-bearing slags. *Scandinavian Journal of Metallurgy,* 30**,** 358-363.

SUN, Y., ZHANG, Z., LIU, L. & WANG, X. 2015. FTIR, Raman and NMR investigation of CaO–SiO_2- P_2O_5 and CaO–SiO_2–TiO_2–P_2O_5 glasses. *Journal of Non-Crystalline Solids,* 420**,** 26-33.

SWAMY, V., DECTEROV, S. A. & PELTON, A. D. 2003. Thermodynamic assessment of the Ge-Si-O-Cl-H system. *Glass Science and Technology,* 76**,** 62-70.

SWINBOURNE, D., BARBANTE, G. & SHEERAN, A. 1998. Tellurium distribution in copper anode slimes smelting. *Metallurgical and Material Transactions B,* 29**,** 555-562.

SWINBOURNE, D., YAN, S. & SALIM, S. 2005. The solubility of gold in metallurgical slags. *Mineral Processing and Extractive Metallurgy,* 114**,** 23-29.

TAKEDA, Y., ISHIWATA, S. & YAZAWA, A. 1983. Distribution equilibria of minor elements between liquid copper and calcium ferrite slag. *Transactions of the Japan Institute of Metals,* 24**,** 518-528.

TAKEDA, Y. & ROGHANI, G. Distribution equilibrium of silver in copper smelting system. First International Conference on Processing Materials for Properties, 1993. 357-360.

TAKEDA, Y. & YAZAWA, A. Dissolution loss of copper, tin and lead in FeO_n-SiO_2-CaO slag. Productivity and Technology in the Metallurgical Industries, 1989. 227-240.

TEAGUE, K., SWINBOURNE, D. & JAHANSHAHI, S. 2001. A thermodynamic study on cobalt containing calcium ferrite and calcium iron silicate slags at 1573 K. *Metallurgical and Material Transactions B,* 32**,** 47-54.

TEPPO, O., NIEMELÄ, J. & TASKINEN, P. 1990. An assessment of the thermodynamic properties and phase diagram of the system Bi-Cu. *Thermochimica Acta,* 173**,** 137-150.

USANOV, A., DE RIDDER, M., AUPING, W., LINGEMANN, S., ESPINOZA, L. T., ERICSSON, M., FAROOKI, M., SIEVERS, H. & LIEDTKE, M. 2013. *Coltan, Congo and Conflict*, The Hague Centre for Strategic Studies.

VEIT, H. M. & BERNARDES, A. M. 2015. *Electronic waste: generation and management*, Springer.

VELDBUIZEN, H. & SIPPEL, B. 1994. Mining discarded electronics. *Industry and Environment,* 17**,** 7-14.

VIRGO, D., MYSEN, B. & KUSHIRO, I. 1980. Anionic constitution of 1-atmosphere silicate melts: Implications for the structure of igneous melts. *Science,* 208**,** 1371-1373.

WANG, C., NAGASAKA, T., HINO, M. & BAN-YA, S. 1991. Activities of tin and antimony in liquid Fe-S alloy saturated with carbon. *ISIJ International,* 31**,** 1336-1344.

WANG, C., ZHANG, J., LIU, Z., JIAO, K., WANG, G., YANG, J. & CHOU, K. 2017. Effect of chlorine on the viscosities and structures of CaO-SiO_2-$CaCl_2$ slags. *Metallurgical and Material Transactions B,* 48**,** 328-334.

WANG, J., JIN, S., LEINENBACH, C. & JACOT, A. 2010. Thermodynamic assessment of the Cu–Ge binary system. *Journal of Alloys and Compounds,* 504**,** 159-165.

WANG, X., DUAN, L., DONG, G., WEI, P., WANG, W., WANG, L. & QIU, Y. 2009. Synthesis and characterization of nano/micro-structured crystalline germanium dioxide with novel morphology. *Chinese Science Bulletin,* 54**,** 2810-2813.

WIRASERANEE, C., OKABE, T. H. & MORITA, K. 2013a. Dissolution behaviour of rhodium in the Na_2O-SiO_2 and CaO-SiO_2 slags. *Metallurgical and Material Transactions B,* 44**,** 584-592.

WIRASERANEE, C., YOSHIKAWA, T., OKABE, T. & MORITA, K. 2013b. Effect of Al_2O_3, MgO and CuO_x on the dissolution behaviour of rhodium in the Na_2O-SiO_2 slags. *Journal of Mining and Metallurgy B: Metallurgy,* 49**,** 131-138.

WIRASERANEE, C., YOSHIKAWA, T., OKABE, T. H. & MORITA, K. 2014. Dissolution behaviour of platinum in Na_2O–SiO_2-based slags. *Materials Transactions, JIM,* 55**,** 1083-1090.

WOOD, J., CREEDY, S., MATUSEWICZ, R. & REUTER, M. A. Secondary copper processing using Outotec Ausmelt TSL technology. Proceedings of MetPlant, 2011. 460-467.

WORRELL, E. & REUTER, M. 2014. *Handbook of Recycling: state-of-the-art for practitioners, analysts, and scientists*, Newnes.

WYPARTOWICZ, J. 1995. Thermodynamic properties of copper-arsenic liquid solutions. *Journal of Alloys and Compounds,* 227**,** 86-92.

YAMAGUCHI, K. Distribution of precious metals between matte and slag and precious metal solubility in slag. Proceedings of Copper, 2010. 1287-1295.

YAMAGUCHI, K. Distribution ratios of platinum and palladium between Iron oxide slags and molten copper Proceedings of Copper, 2013 Chile. 775-784.

YAN, S. & SWINBOURNE, D. 2003. Distribution of germanium under lead smelting conditions. *Mineral Processing and Extractive Metallurgy,*112, 75-80

YAZAWA, A. 1974. Thermodynamic considerations of copper smelting. *Canadian Metallurgical Quarterly,* 13**,** 443-453.

YAZAWA, A. 1980. Nonferrous Extractive Metallurgy, Japan Institute of Metals.

YAZAWA, A. & AZAKAMI, T. 1969. Thermodynamics of removing impurities during copper smelting. *Canadian Metallurgical Quarterly,* 8**,** 257-261.

YAZAWA, A. & TAKEDA, Y. 1982. Equilibrium relations between liquid copper and calcium ferrite slag. *Transactions of the Japan Institute of Metals,* 23**,** 328-333.

YAZAWA, A., TAKEDA, Y. & NAKAZAWA, S. 1968. Distribution behaviours of various elements in copper smelting system. *Copper 68-Copre 68 International Conference.*

YAZAWA, A., TAKEDA, Y. & NAKAZAWA, S. Ferrous calcium silicate slag to be used for copper smelting and converting. Copper 99-Copre 99 International Conference, 1999. 587-597.

ZENG, X., SONG, Q., LI, J., YUAN, W., DUAN, H. & LIU, L. 2015. Solving e-waste problem using an integrated mobile recycling plant. *Journal of Cleaner Production,* 90**,** 55-59.

ZHANG, L. & JAHANSHAHI, S. 1998. Review and modeling of viscosity of silicate melts: Part I. Viscosity of binary and ternary silicates containing CaO, MgO, and MnO. *Metallurgical and Material Transactions B,* 29**,** 177-186.

ZHAO, Y. & IRONS, G. 1997. The kinetics of selenium removal from molten copper by powder injection. *Metallurgical and Material Transactions B,* 28**,** 1039-1051.

Appendix A : Temperature Profile and Picture of Vertical Furnace

The temperature profile inside the furnace and the calibration curve with controller temperature and actual furnace temperature are shown as follows:

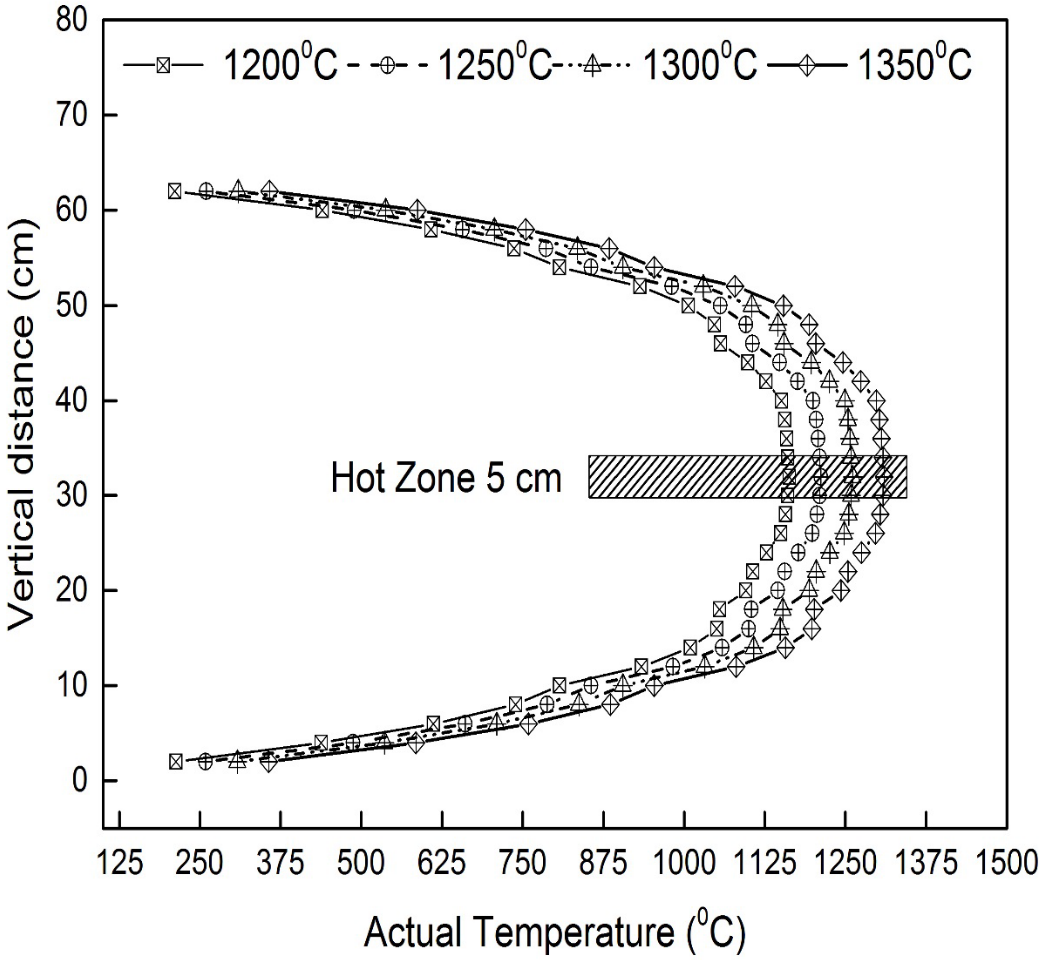

Figure A.1: Temperature profiles inside furnace for the controller temperature of 1200°C, 1250°C, 1300°C and 1350°C.

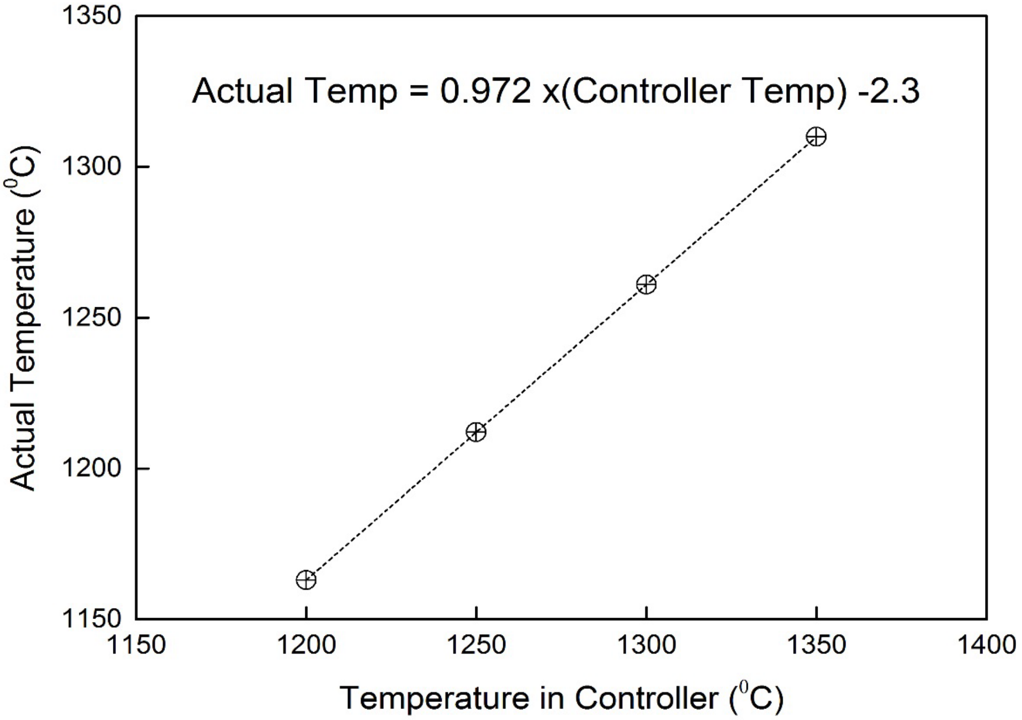

Figure A.2: Calibration of actual temperature inside furnace with controller temperature of 1200°C, 1250°C, 1300°C and 1350°C.

Figure A.3: Vertical tube furnace with controller temperature equipped with vacuum pump.

Appendix B : Flow Rate Calculation and Calibration

The calculation of flow rate of CO and CO_2 can be found from following calculation.

Using Eq. 4.1 the ratio of CO/CO_2 can be calculated at T = 1300°C (1573 K) for a desired $p_{O_2}=10^{-8}$ atm as following

$$\log 10^{-8} = 2\log\left(\frac{CO_2}{CO}\right) - \frac{29{,}510}{1573} + 9.05$$

or, $CO_2/CO = 7.16$

The overall flow is 400 ml/min, then

$$\text{Flow rate of } CO_2\text{, } F_{CO2} = \frac{CO_2}{CO+CO_2} \text{ x } 400 \text{ ml/min}$$

$$= \frac{7.16\ CO}{CO+7.16\ CO} \text{ x } 400 \text{ ml/min}$$

$$= 351 \text{ ml/min}$$

Therefore, the flow rate of CO, F_{CO} is (400-351) ml/min or 49 ml/min.

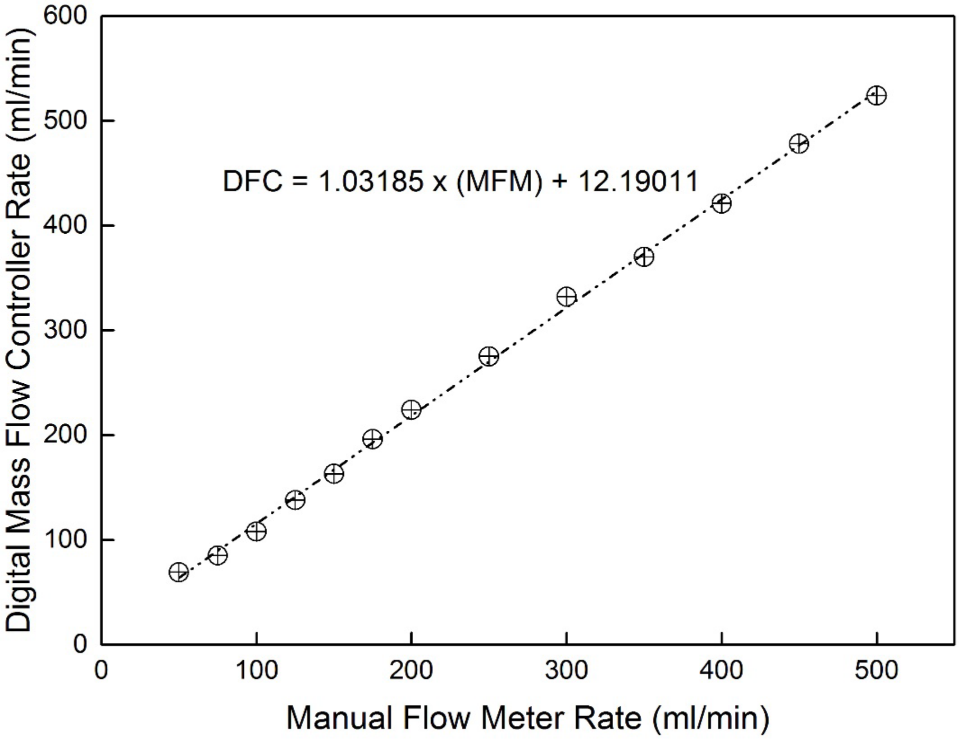

Figure B.1: Calibration of digital mass flow controller (DFC) with manual gas rotameter for CO gas.

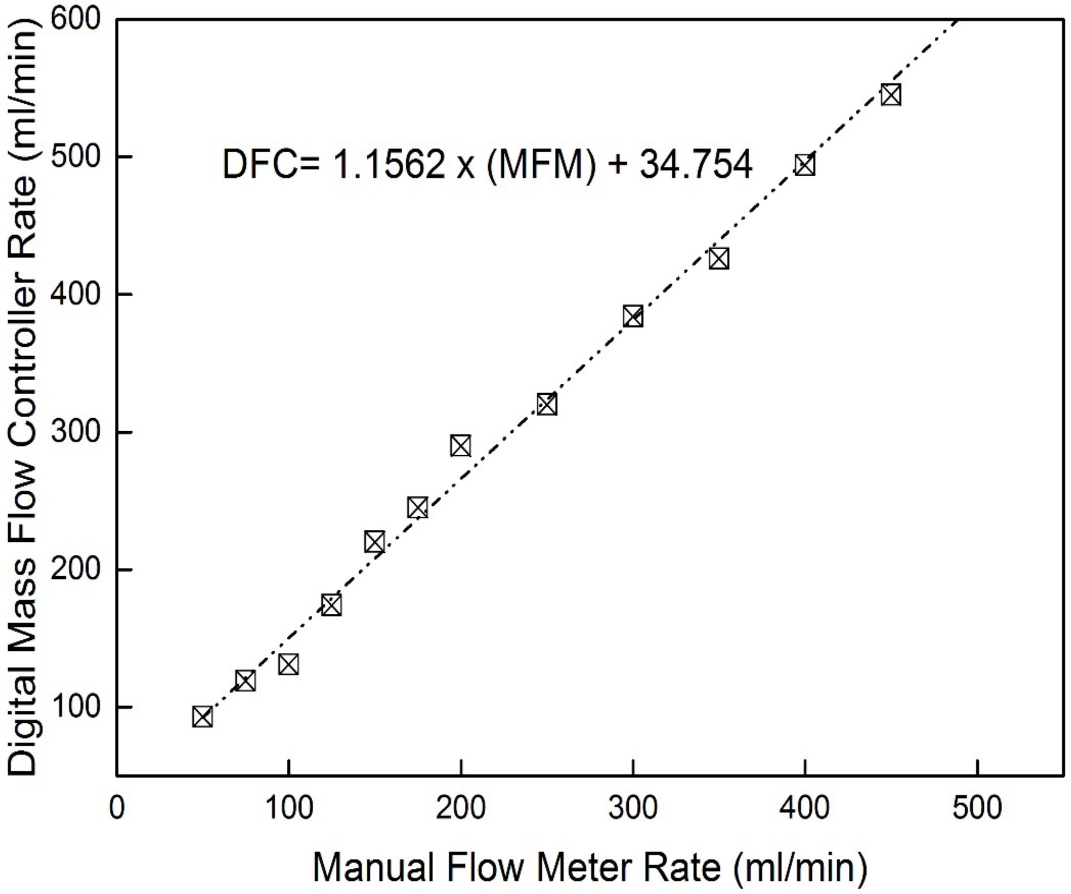

Figure B.2: Calibration of digital mass flow controller (DFC) with manual gas rotameter for CO_2 gas.

Appendix C : Curve Fitting on IR Spectra of Slags

The results obtained from the deconvolution of FTIR spectra of FeO_x-CaO-SiO_2-MgO-Cu_2O-GeO_2 slags with different experimental parameters are shown in Figures C.1, C.2, C.3, and C4.

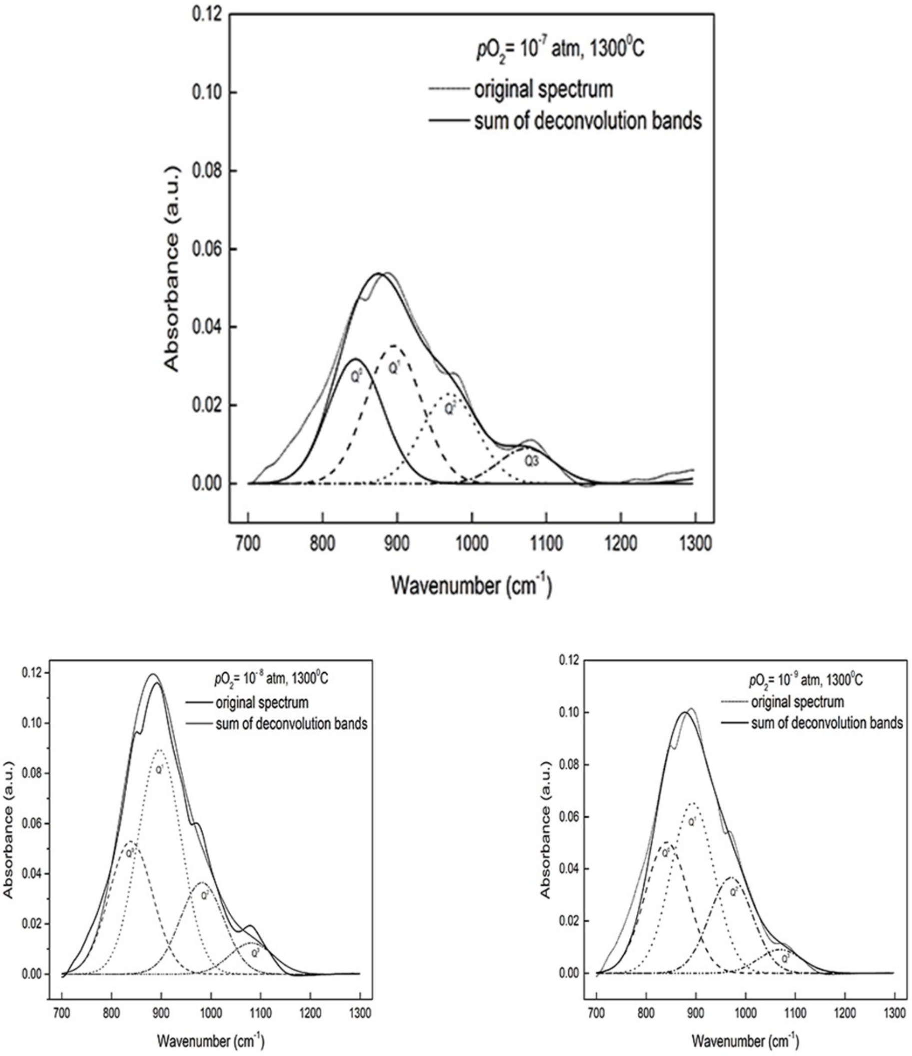

Figure C.1: Deconvolution results of FTIR spectra of FeO_x-CaO-SiO_2-MgO-Cu_2O-GeO_2 slag at different p_{O_2} (T= 1300°C).

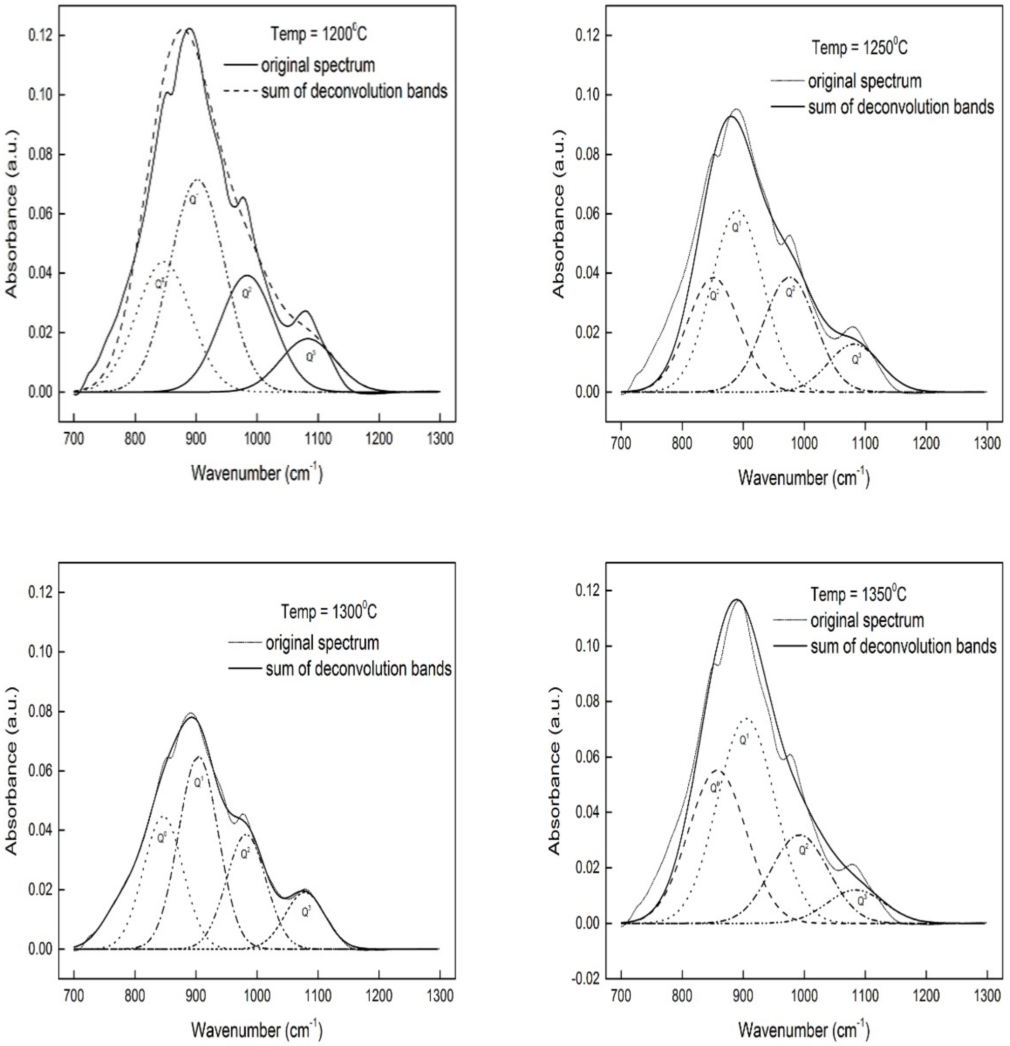

Figure C.2: Deconvolution results of FTIR spectra of FeO_x-CaO-SiO_2-MgO-Cu_2O-GeO_2 slag at different temperatures ($p_{O_2} = 10^{-8}$ atm).

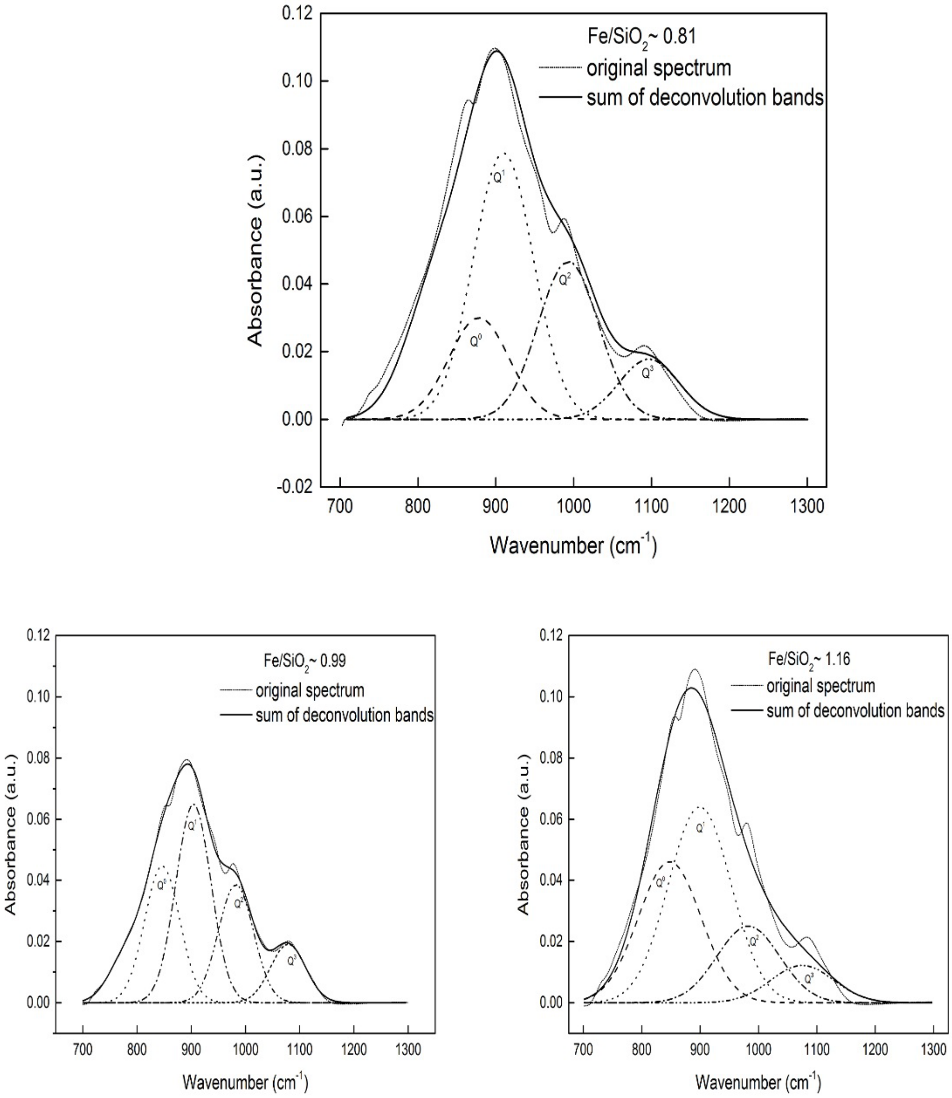

Figure C.3: Deconvolution results of FTIR spectra of FeO_x-CaO-SiO_2-MgO-Cu_2O-GeO_2 slag at different Fe/SiO_2 ($p_{O_2} = 10^{-8}$ atm and T= 1300°C).

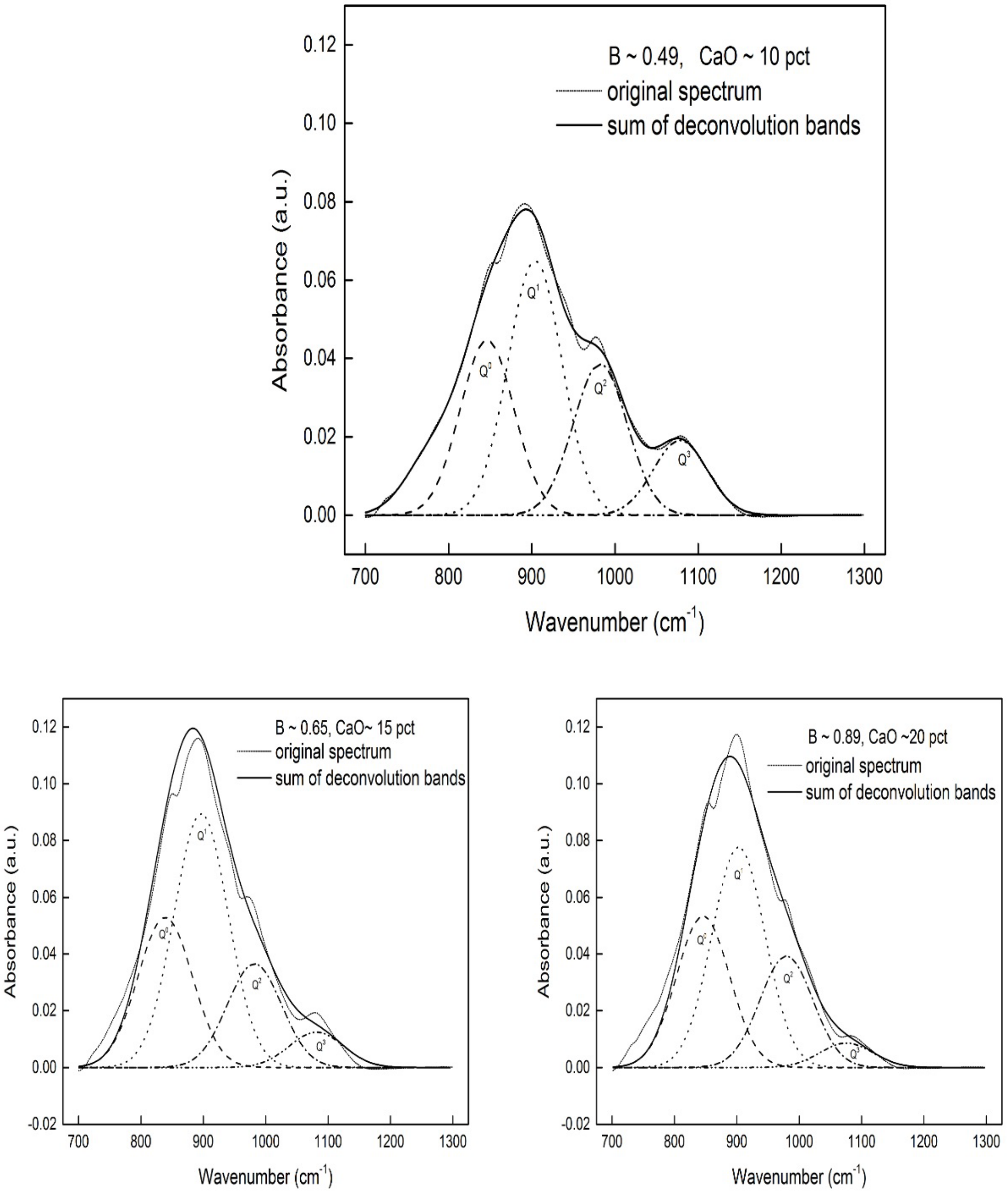

Figure C.4: Deconvolution results of FTIR spectra of FeO_x-CaO-SiO_2-MgO-Cu_2O-GeO_2 slag at different basicity ($p_{O_2} = 10^{-8}$ atm and T= 1300°C).

The results obtained from the deconvolution of FTIR spectra of FeO_x-CaO-SiO_2-MgO-Cu_2O-PdO slags with different experimental conditions are shown in Figures C.5, C.6, C.7, and C.8.

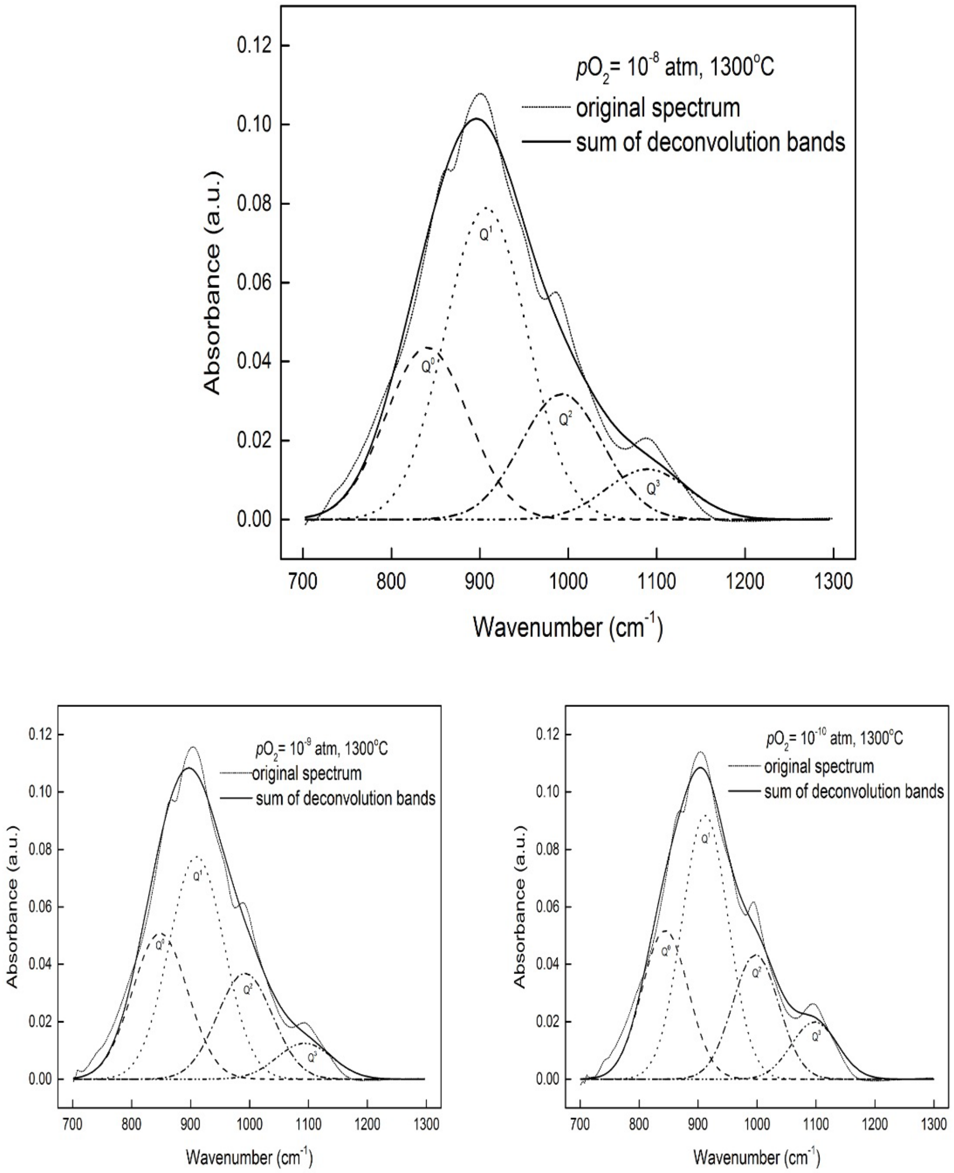

Figure C.5: Deconvolution results of FTIR spectra of FeO_x-CaO-SiO_2-MgO-Cu_2O-PdO slag at different p_{O_2} (T= 1300°C).

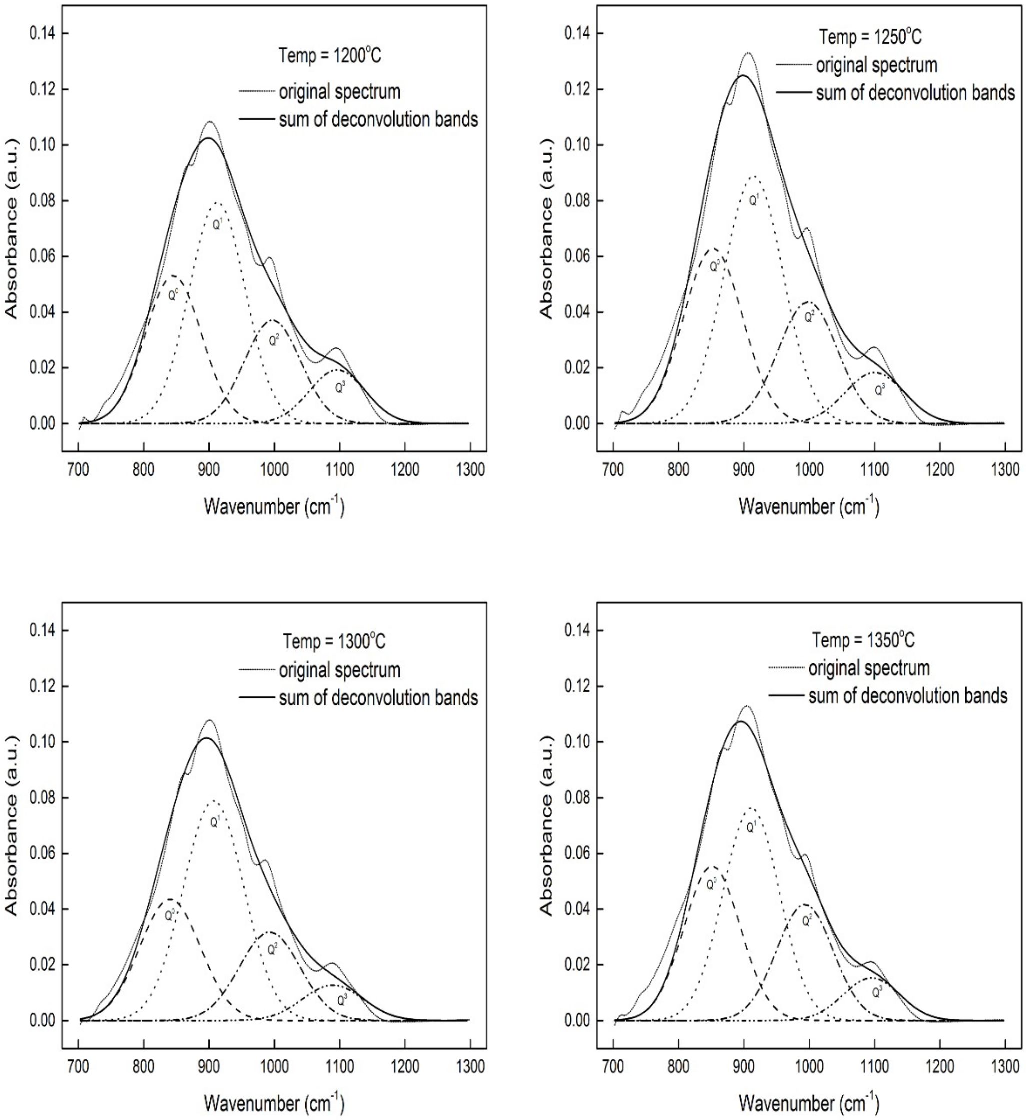

Figure C.6: Deconvolution results of FTIR spectra of FeO_x-CaO-SiO_2-MgO-Cu_2O-PdO slag at different temperatures ($p_{O_2} = 10^{-8}$ atm).

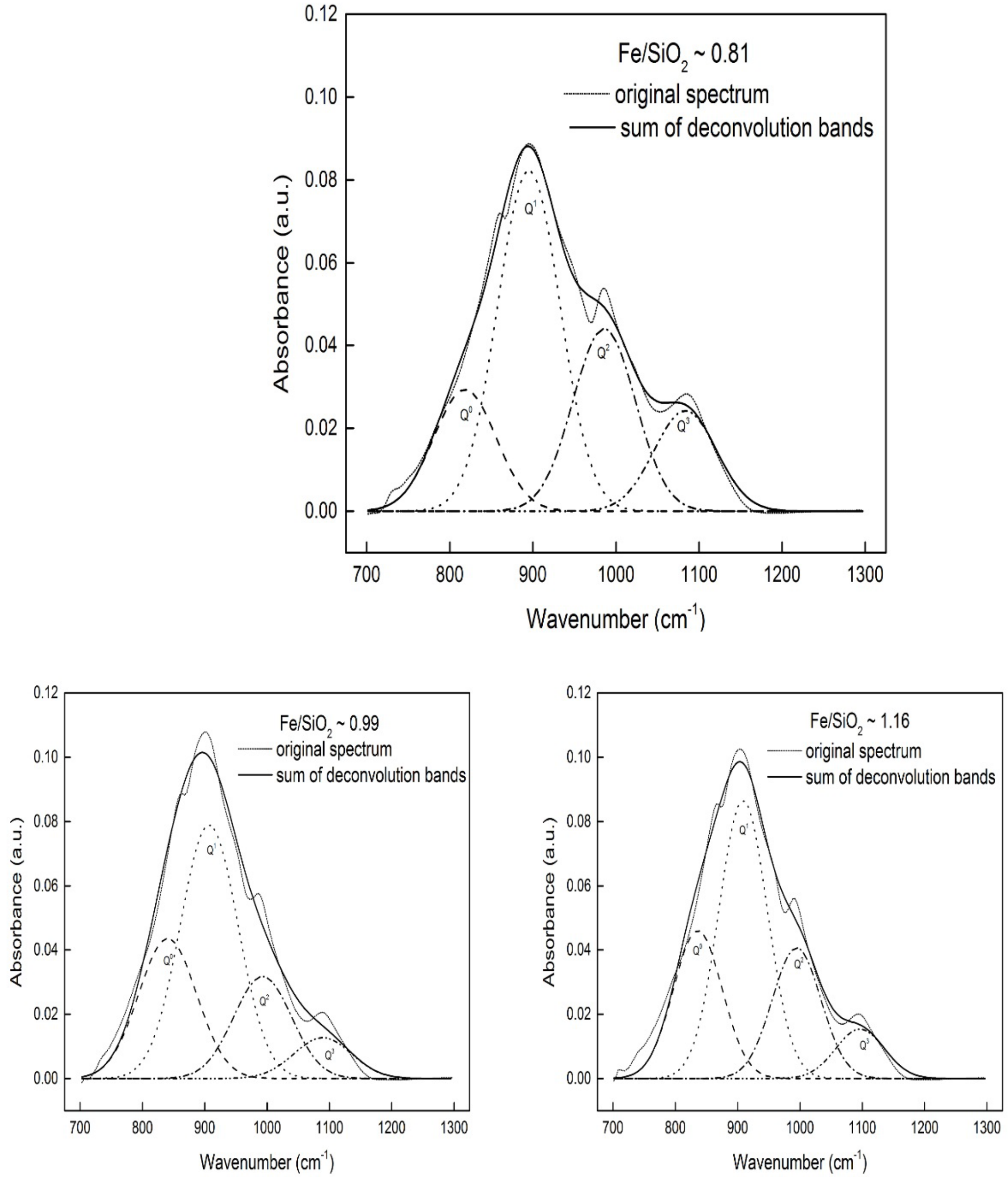

Figure C.7: Deconvolution results of FTIR spectra of FeO$_x$-CaO-SiO$_2$-MgO-Cu$_2$O-PdO slag at different Fe/SiO$_2$ ($p_{O_2} = 10^{-8}$ atm and T= 1300°C).

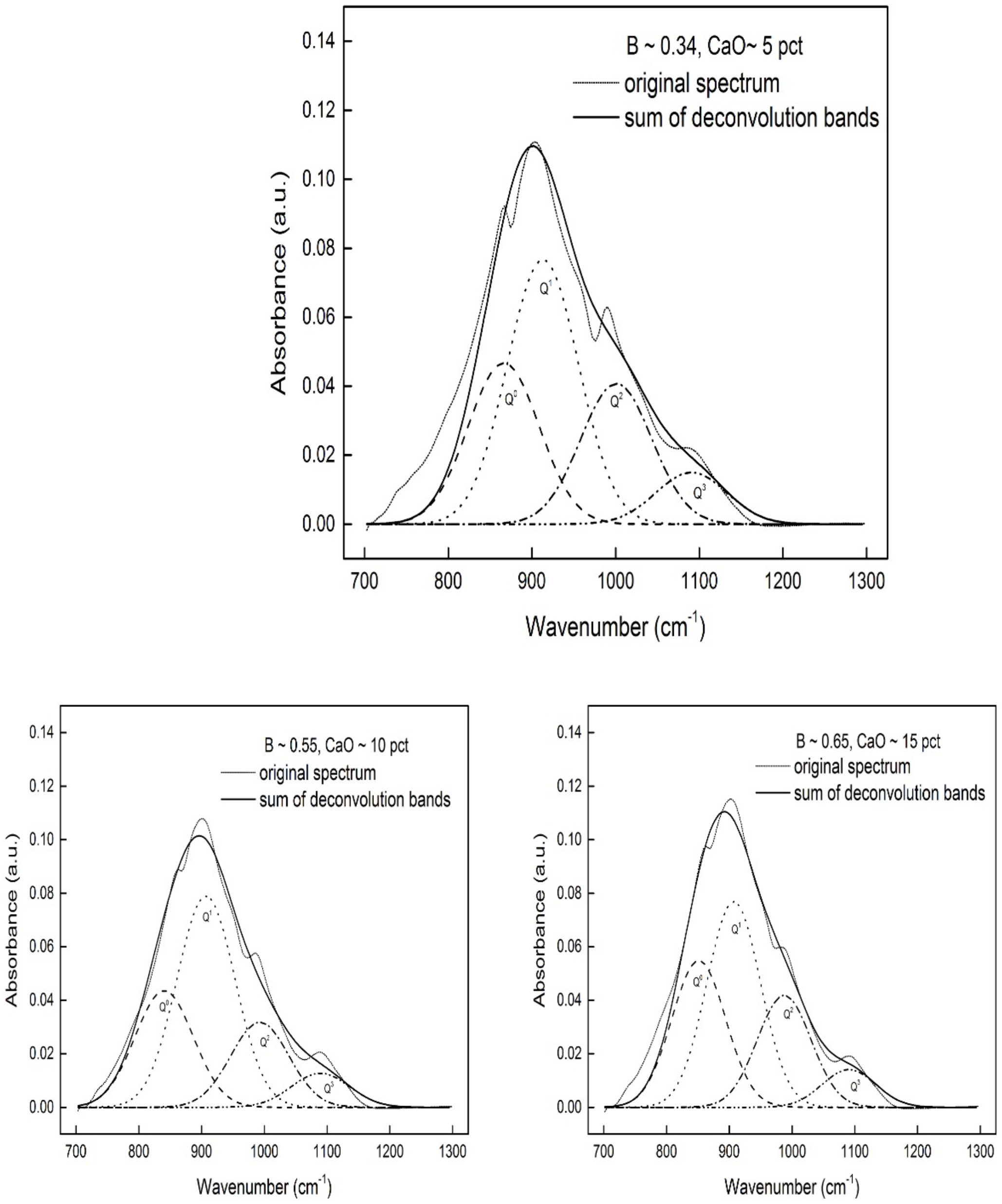

Figure C.8: Deconvolution results of FTIR spectra of FeO_x-CaO-SiO_2-MgO-Cu_2O-PdO slag at different basicity ($p_{O_2} = 10^{-8}$ atm and T= 1300°C).

Appendix D : Error Analysis

The error associated in the current study is outlined in this appendix. The difference between the actual and measured values of a physical quantity from the experiment is known as error. For the experimental study, the final results of any physical quality is associated with some error. Most of this error are relevant to systematic error and random error. Systematic errors are instrumental error due to minor design and calibration fault which is difficult to figure out even after the several repetition of experiments. Random errors are generated from the fluctuation of a physical data during the repetition of the process. This category of error is uncertain and does not show any particular trend. Therefore, statistical analysis is required to minimise the random errors by repeating the experiments. The statistical analysis can be done by using the repetition of observed value and calculating average, mean and standard deviation. The general formula is written as:

$$\bar{Y} = \frac{1}{N}\sum_{i=1}^{N} y_i = \frac{1}{N}\left(y_1 + y_2 + y_3 + \cdots + y_N\right) \tag{D.1}$$

Where, N is the number of repeated measurement from similar type of experiment of y

Standard deviation (S) is statistic technique for characterizing both the variation and dispersion of measured set of physical values from the mean value of that set of data. It is denoted as S and the general formula is given as following:

$$S = \sqrt{\frac{1}{N-1}\sum_{i=1}^{N}(y_i - \bar{Y})^2}$$

$$= \sqrt{\frac{1}{N-1}[(y_1 - \bar{Y})^2 + (y_2 - \bar{Y})^2 + (y_3 - \bar{Y})^2 + \cdots + (y_N - \bar{Y})^2} \tag{D.2}$$

Considering the errors, the final results will be:

The Final result = Average Value ± Standard deviation (D.3)

The experimental results throughout the thesis were carried by minimizing the errors. There are some experimental errors and post experimental errors which were also described in the following sections.

D.1 Error in experimental procedure

D.1.1 Sample weight measurement

An electronic balance was used to measure the powder materials. The accuracy of the electric balance was ± 0.0001 g. The final calculation was not differ with the small variation of sample weight measurement.

D.1.2. Temperature measurement

A temperature profile and furnace temperature for the vertical tube furnace was carried out using an R-type thermocouple. The reading of temperatures were recorded with a digital temperature controller. The reading of temperatures were taken from the bottom part of the furnace with equal upward shifting of 2 cm and the error relevant of the positioning was assumed to be ±3mm.The length of uniform heating zone was 50 mm approximately with temperature variation about ±3 ^{0} C. The temperature profile for the vertical tube furnace has shown in Figure A.1 in **Appendix A**. It was also assumed that the temperature variation inside the crucible arrangement was less than 3 ^{0}C.

From Figure A.2 in **Appendix A**, it was found that the actual temperature inside the furnace was approximately 39 degree lower than the set temperature from the furnace controller. It was a systematic error which was minimized by recalculating the controller temperature using the reaction with actual temperature and the set up temperature has shown in Figure A.2 in in **Appendix A.**

D.1.3 Sample position inside furnace

The position of the crucible arrangement inside the furnace was approximately at uniform heating zone (50 mm). The position was adjusted with the alumina pedestal rod from the bottom of the furnace. The sample position error was measure to be ± 3 mm.

D.1.4 Flow rate

A manual gas rotameter was used to calibrate the digital mass flow meter and the calibration results have presented graphically with the correlation in Appendix B. The error estimated error was ±5 mL/min associated with gas rotameter for the parallax error and the systematic error of digital mass flow controller was ±3 mL/min.

D.2 Error in Analysis techniques

D.2.1 ICP analysis

The composition of master alloys, master slags and the distribution of germanium, palladium and tantalum in slag and metal phase of the equilibrated samples were determined using ICP-AES technique. The error of the instrument was carried out by repeating similar type of experiments. The solid sample was dissolved in hydrochloric acid and nitric acid for analysis. The error was estimated from the repeated experiments to be 1%. The error also associated with other sources, i.e., manual handling, dissolution process and weighting the samples could also contribute in the final result of ICP techniques and therefore final error to be within ± 6%.

D.2.2 XRD analysis

In XRD analysis, the resulted spectra may be associated with errors. It may be the reason of sample displacement in the holder, misalignment of the equipment, scattering and absorbing of the peak. In the current study, XRD spectra was used as a tool to identify the phase and errors were not inevitable to consider. The systemic error XRD estimated to be within ± 5%.

D.2.3 Raman analysis

The errors associated with Raman analysis may be caused by improper focus of sample under the microscope, wrong wavelength of laser, misalignment of the instrument, scattering and absorption of characteristic wavelengths. In this current study, the measurement from the Raman spectroscopy was used to identify the phase. Therefore, the error was considered less important and the estimated error to be within ± 5%.

D.2.4 FTIR analysis

The master slag and equilibrated slag samples were analysed using FTIR spectrometry equipped with an attenuated total reflection technique. The possible source of error in FTIR may be caused by expiring of calibration of the instrument, scattering and absorption of wavelengths, different background spectra. The average error propagation of the FTIR equipment was estimated to be within ± 5%.